Wisconsin Highway Research Program

Fatigue Risks in the Connections of Sign Support Structures Phase 1

SPR # 0092-08-14

Christopher M. Foley, PhD, PE; Baolin Wan, PhD; Mathew Weglarz; Matthew Hellenthal; Jordan Komp; Andrew Smith; and Joseph P. Schmidt

Department of Civil & Environmental Engineering
Marquette University

December 2008

WHRP 08-05

Technical Report Documentation Page

1. Report No. WHRP 08-05	2. Government Accession No	3. Recipient's Catalog No
4. Title and Subtitle Fatigue Risks in the Connections of Sign Support Structures: Phase 1		5. Report Date December 2008 6. Performing Organization Code Wisconsin Highway Research Program
7. Authors Christopher M. Foley, PhD, PE; Baolin Wan, PhD; Mathew Weglarz; Matthew Hellenthal; Jordan Komp; Andrew Smith; Joseph P. Schmidt		8. Performing Organization Report No.
9. Performing Organization Name and Address Department of Civil & Environmental Engineering Marquette University, Milwaukee, WI		10. Work Unit No. (TRAIS) 11. Contract or Grant No. WisDOT SPR #0092-08-14
12. Sponsoring Agency Name and Address Wisconsin Department of Transportation Division of Business Services Research Coordination Section 4802 Sheboygan Ave. Rm 104 Madison, WI 53707		13. Type of Report and Period Covered Final Report, 2007-2008 14. Sponsoring Agency Code
15. Supplementary Notes		

16. Abstract

Wisconsin sought to assess the risk of fatigue-induced fracture in its existing sign support structures designed before the latest AASHTO specifications that included fatigue design. A framework for assessing fatigue-induced fracture risk is developed and detailed synthesis of fatigue testing of connections is conducted. Statistical analysis of tests conducted since 1970 is made and models for characterizing uncertainty in the fatigue life of these connections are proposed. Recommendations regarding further fatigue testing (specimen configuration, number and stress range) are given. Statistical models for wind speed and direction are developed using historical records obtained through the National Climatic Data Center for eight cities within the state of Wisconsin. Nonlinear finite element analysis of a typical mast-arm-to-plate connection with octagonal mast arm is conducted using various configurations of bolt pretension. Recommendations regarding the impact of loose bolts on the distribution of normal stress within octagonal mast arms are provided and comparison to AASHTO design specification procedures is made.

17. Key Words Fatigue-Induced Fracture, Wind-Speed Variability, Reliability-Based Fatigue Evaluation, Statistical Analysis, Fatigue Testing, Finite Element Analysis, Mast-Arm Connections		18. Distribution Statement No restriction. This document is available to the public through the National Technical Information Service 5285 Port Royal Road Springfield VA 22161	
19. Security Classification (of this report) Unclassified	19. Security Classification (of this page) Unclassified	20. No. of Pages 205	21. Price

Form DOT F 1700.7 (8-72) Reproduction of completed page authorized

NOTICE:

This research was funded through the Wisconsin Highway Research Program by the Wisconsin Department of Transportation and the Federal Highway Administration under Project #0092-08-14. The contents of this report reflect the views of the authors who are responsible for the facts and accuracy of the data presented herein. The contents do not necessarily reflect the official views of the Wisconsin Department of Transportation or the Federal Highway Administration at the time of publication.

Table of Contents

ACKNOWLEDGEMENTS

The authors would like to acknowledge the support and help from the following individuals at the Wisconsin Department of Transportation: Travis McDaniel, Bruce Karow, Joel Alsum, Kent Bahler, and Thomas Heydel. The authors would also like to acknowledge fruitful discussions with Marquette University colleagues Robert Stango, PhD, and Piyush Khullar, MS.

EXECUTIVE SUMMARY

Wisconsin recently encountered problems with the connections contained in, and the in-service performance of, several cantilevered mast-arm sign support structures. In one case, it was discovered that recently installed bolts were loose, which may have led to premature fatigue failure. In a second case, a routine inspection discovered a welded tube to plate connection that exhibited cracking over 50% of its circumference since the last scheduled inspection. The latest edition of the AASHTO design specifications has provisions for fatigue design. However, many structures presently in service were designed before fatigue provisions were part of the design specifications.

The objectives of the research effort are: (a) implement state-of-the-art fatigue reliability analysis and current knowledge regarding fatigue lives of connections in a systematic assessment of fatigue-induced fracture risk in WisDOT's sign support structures; (b) recommend the most effective retrofit strategies in instances where fatigue-induced fracture is likely; and (c) assign inspection cycle frequencies for these structures and their components.

The objectives of the present phase in the research effort outlined in this report are as follows. Identify details and structures that are currently seeing fatigue-related problems and identify details that may be problematic in the future. Present a detailed national and international literature review and synthesis to learn what has been done, what is currently being done, and what is likely to be done in the near future related to fatigue-induced failure of critical connection details in sign structures and potential retrofit measures that are being evaluated and/or employed. Assemble all pertinent fatigue testing data into a form that is suitable for evaluating its sufficiency for predicting risk of fatigue-induced fracture of WisDOT's sign support structures. Synthesize the data available for ultrasonic impact treatment (UIT) and gusset stiffening retrofit measures to determine if it is sufficient to justify using it to predict the likelihood of fatigue-induced failure once these retrofit measures are in place. Expand the database of statistical information related to wind speed and direction and use this new informational source to select regions within the State that may be fruitful for field acquisition of data for sign and signal support structures. This database of wind speed and direction models can also be used for fatigue-life simulation using reliability-based engineering methodologies. Finally, the research report seeks to provide objective evaluation retrofit measures that have been implemented and tested in previous research and investigate novel retrofit techniques that may be worthy of future in-depth evaluation.

Details related to collection and synthesis of fatigue testing data completed to date for connection details similar to those found in Wisconsin's cantilever signal and sign support structures are provided. Fatigue testing that has been conducted since 1970 on connection details that are similar to those found in cantilever sign and signal support structures in Wisconsin are reviewed and these tests are synthesized using accepted methods of statistical analysis. The review also includes fatigue testing of connections involving ultra-sonic impact treatment (UIT) and mechanical (hammer) peening. Recommendations related to additional fatigue testing to be conducted in phase 2 are made. Collection and synthesis of wind speed and direction data for southern Wisconsin is described. The collected wind speed data is also synthesized through established statistical analysis procedures. Recommendations for candidate cities suitable for in-field monitoring of sign support structures are made and information needed to include uncertainty (*i.e.* variability) in demand within the analysis procedures that facilitate assessment of fatigue-induced fracture risk is generated. The project kick-off meeting stressed the need to evaluate the impact of loose bolts on the fatigue performance of mast-arm to plate

connections within the structures considered in this research effort. To this end, finite element analysis was undertaken to evaluate the variation in stress distribution around the perimeter of a typical mast-arm tubular cross-section with various patterns of loose bolts present. Comparison of the FEA results with stress magnitude predictions made using traditional specification-based procedures are provided and the impact of loose (non-pretensioned) bolts on the stress distribution around an octagonal mast arm is quantified.

The Kolmogorov-Smirnov goodness of fit test indicated that the variability in all fatigue tests conducted to date can be modeled using lognormal cumulative distribution functions (CDFs) and the corresponding probability density function. In the case of gusset-stiffened mast arm connections, a normal CDF appeared to be a better model for the sample experimental data, but a lognormal CDF was suitable. It should be emphasized that there is a need to be sensitive to the fatigue lives that are likely to occur at low stress ranges. The experimental testing done to date follows a long-known trend with regard to variability in fatigue life: as the stress range is reduced, the variability in fatigue life increases. The next phase in the present research effort may not be able to include the number of tests at the low stress ranges needed to achieve targeted mean interval estimates because the testing duration may be too great (number of stress cycles required to initiate fatigue failure may be too large). This issue will require detailed evaluation as testing recommendations and protocols are finalized.

The statistical analysis conducted indicates that two-minute wind speeds are fairly consistent throughout the eight cities in southern Wisconsin considered. The present research effort confirmed findings of previous research efforts: wind speed and direction are statistically dependent events. The statistical analysis of the wind speed data collected suggests that lognormal probability density and cumulative distribution functions are acceptable models for wind speed variability once a direction has been defined. As a result, there is the possibility to define a continuous random variable model for wind speed given each of the eight cardinal directions considered. If a sign structure in the field is identified and the orientation of its signal or signage is known, a probability model for the two-minute average wind speed distribution can be used for reliability analysis.

The finite element analysis conducted indicates that the normal stresses in the mast-arm wall can be affected by loose bolts. It should be noted that the analysis included a single bi-directional bending moment condition. However, given the analysis limitations, loose bolts can account for a 7% increase in normal stresses in the mast-arm wall. Furthermore, mast-arm-plate flexibility and the discrete load paths resulting from the bolted connection arrangement can conspire to create significant amplification of normal stress around the perimeter of the octagonal mast arm that is not currently included in the analysis recommendations found in the design specifications. It should be noted that these amplifications are indirectly included in the fatigue detail category constant amplitude fatigue limits and the stress-life curves.

The statistical analysis of the fatigue testing suggests that further testing be conducted. It is recommended that additional un-stiffened mast arm connections be tested at stress ranges of 15-ksi and at 6-ksi. All the recommended tests may or may not be feasible, and discussions with the testing contractor will need to occur. However, if the recommended tests are conducted at these two stress ranges, there will be significant enhancement in the understanding

of uncertainty in the fatigue life of un-stiffened mast arm connections that will provide a very sound foundation for the risk assessment to be conducted in phase 3 of the research effort. It is expected that the present research effort will not be able to address risk of fatigue-induced fracture in pole-base connections. Future research efforts should address these connections as they are integral to characterizing fatigue performance of the entire signal or sign support structural system. It should be noted that pole-base connections have not exhibited premature fracture in sign supports (at least in Wisconsin).

There are very few tests that have been conducted on retrofitted connections (*e.g.* hammer peening, UIT). Therefore, it is recommended that additional fatigue life testing be conducted for a single retrofit measure. At this point, hammer peening appears to be a more reliable method to improve fatigue life. In addition, there is a relatively new tool used for surface preparation (corrosion product removal) that may serve beneficial as a result of its ability to mildly peen the surface of steel. The tool is the MBX® Bristle Blaster. The research team became aware of this tool through conversation with colleagues at Marquette University in the mechanical engineering department. The MBX® Bristle Blaster tool appears to be a portable means with which to mechanically peen the surface of base metal in the vicinity of weld toes with potential to smooth the geometric discontinuities normally present at these locations within welded components. Therefore, it is recommended that this tool be considered as a potential retrofit measure in the present research effort.

The statistical analysis of wind speed and direction indicates that Green Bay and Milwaukee are two cities that make good candidates for field instrumentation as a result of their relatively high mean two-minute average wind speeds and the frequency from which these higher speeds come from a large number of cardinal directions.

The finite element analysis conducted suggests that inspection protocols include examination of bolt pretension in mast-arm connections and that all bolts have pretension in them. While a lower-bound magnitude of pretension was not established in the present effort, the analysis clearly indicates that lack of pretension in bolts around the mast-arm connection can result in elevated states of normal stress in the mast arm. Therefore, if bolts are found loose in these connections, they should be tightened to establish contact at the faying surfaces of the connecting plates. This will help to alleviate unforeseen concentration of stress resulting from the loose condition. The FEA conducted also confirms the importance of plate flexibility in the fatigue testing to be conducted in phase 2 of the research effort. It is therefore recommended that any fatigue testing include a specimen configuration with this flexibility to more accurately include these effects.

Chapter 1
Introduction

INTRODUCTION

Wisconsin recently encountered problems with the connections contained in, and the in-service performance of, several cantilevered mast-arm sign support structures. In one case, a structure was taken down because of excessive mast-arm deflections. After detailed inspection, it was discovered that recently installed bolts were loose, which may have led to premature fatigue failure. In a second case, a routine inspection discovered a welded tube to plate connection that exhibited cracking over 50% of its perimeter since the last scheduled inspection. The latest edition of the AASHTO design specifications (AASHTO 2001) has provisions for fatigue design. However, many structures presently in service were designed before fatigue provisions were part of the design specifications. As a result, Wisconsin undertook a research effort designed to assess the risk of fatigue-induced fracture in its existing sign support structures that were designed before these latest AASHTO specification revisions.

The proposed research effort contains two phases. The first phase includes data collection and planning, while the second will be undertaken in the manner recommended by the results of the first. In Phase 1, in-service structural systems are reviewed to select typical connections and structure configurations in use throughout the state for further detailed examination. Bolted and welded components of the connections in these structures are evaluated. A literature review is conducted to find fatigue-related research for similar types of connections including the effectiveness of potential retrofit measures (*e.g.* ultrasonic impact treatment – UIT). Completion of Phase 1 will lay the ground work for Phase 2 whereupon additional testing is recommended to achieve the ultimate goals and deliverables of the total effort.

The objectives of the multi-phase research effort are: (a) implement state-of-the-art fatigue reliability analysis and current knowledge regarding fatigue lives of connections in a systematic assessment of fatigue-induced fracture risk in WisDOT's sign support structures; (b) recommend the most effective retrofit strategies in instances where fatigue-induced fracture is likely; and (c) assign inspection cycle frequencies for these structures and their components.

There are very clear benefits to the proposed research effort. First and foremost, there is an unknown probability of future failures in mast-arm-to-pole connections typical of sign support structures in Wisconsin. This research will result in guidelines for inspection cycles, retrofit measures, or other changes in inspection

or maintenance policy to assure the safety of the traveling public. Application of the results of the effort will reduce inconvenience to the motoring public through establishing rational inspection intervals for these structures. Furthermore, these relatively innocuous structures are sources of relatively severe failure consequences and regular short-interval inspection cycles to mitigate this risk have economic impact and the results of the present research effort will foster better use of public funds for ancillary structure inspection.

FRAMEWORK FOR ASSESSING FATIGUE-INDUCED FRACTURE RISK

When one discusses risk and recommendations of inspection cycles for structural systems, there is a natural migration toward uncertainty. With regard to sign, signal and luminaire supports, there are a very large number of parameters used to define performance that contain uncertainty including: statistical scatter in the basic fatigue data; the equations used to describe fatigue crack growth under random stresses; weld fabrication issues (*e.g.* undercut severity vary tremendously); wind speeds and direction defining the loading; expressions used to migrate wind speed to pressures for structural analysis; equations used to conduct detailed stress analysis at the joints in these structures (*e.g.* stress concentration factors, stress intensity factors); ability of inspection tools (*e.g.* visual inspection, dye penetrant, magnetic particle) to detect cracks; and environmental conditions (*e.g.* corrosion, reduced material toughness). Therefore, if one were to definitively quantify risk, these uncertainties must be modeled. Fully probabilistic (reliability-based) procedures for predicting the fatigue lives of offshore structures have been proposed (Kirkemo 1988; Wirsching 1988), but they rely on highly detailed probabilistic models for the uncertainties previously described that aren't complete for the structures considered as part of the proposed research effort.

The proposed research effort will be somewhat forced into several simplifying assumptions to make the effort tractable (Foley *et al.* 2004), but will also consider implementation of the probabilistic approach used extensively in the offshore industry (Wirsching 1984). As a result, risk of fatigue-related fracture can be quantified and inspection cycles can be established. A brief review of a procedure for risk assessment is prudent as it sets the foundation for the manner in which the literature review and synthesis will be carried out. It will also justify additional testing that may be required to carry the procedure through to completion.

The fatigue life of a welded joint when subjected to constant amplitude loading is characterized using the well-known S-N (or stress life) diagram defined by (AASHTO 2001);

$$N \cdot S^m = A \tag{1}$$

where $m = 3$ for joints composed of structural steel. The value of A defines the detail category and therefore establishes the fatigue life, N, for a given stress range, S. Fatigue damage resulting from a stress range applied over a defined number of cycles in a time period is widely characterized using an accumulation model (Miner 1945);

$$D = \frac{n_T}{N} = \frac{n_T}{A/S^m} = \frac{n_T}{A} \cdot E\left(S^m\right) \tag{2}$$

where n_T is the applied number of cycles at the expected value of S^m defined as $E(S^m)$ that occur during the time period, T .

Uncertainty in modeling is assumed to manifest itself in the stress range defined for the damage analysis through an adjustment (Wirsching 1984) leading to the definition of an actual stress range;

$$S_{act} = B \cdot S \tag{3}$$

The random variable, *B*, is defined as: $B = B_M \cdot B_N \cdot B_H$. The components then describe uncertainty in: fabrication and assembly, B_M ; nominal member loads, B_N ; and estimation of stress concentration (hot spot) factors, B_H . The median and coefficient of variation for the modeling error can be expressed as,

$$\tilde{B} = \prod_i \tilde{B}_i = \tilde{B}_M \cdot \tilde{B}_N \cdot \tilde{B}_H$$

$$COV_B = \sqrt{\prod_i \left(1 + COV_i^2\right) - 1}$$

Therefore, uncertainty in modeling (*i.e.* member dimensions, computation of loads, stress concentrations) can be quantified. The frequency of stress cycles occurring over a time period, T , is (Wirsching 1984);

$$f_o = \frac{n_T}{T}$$

Damage can now include passage of time and modeling uncertainty (Wirsching 1984),

$$D = \frac{n_T}{A} \cdot \left[B^m E\left(S^m\right)\right] = \frac{T \cdot B^m}{A}\left[f_o E\left(S^m\right)\right] = \frac{T \cdot B^m}{A} \cdot \Omega \tag{4}$$

The stress parameter, Ω, allows the expected number of stress cycles to be defined using a deterministic method, a spectral (probabilistic) method, or a Weibull modeling approach (Wirsching 1984).

If damage resulting from blocks of constant amplitude stress cycles is assumed (*i.e.* the deterministic method is employed), the fatigue damage during a time period can be expressed as (Wirsching 1984),

$$D = \frac{T \cdot B^m}{A} \cdot \left[f_o \cdot \sum_i \zeta_i S_i^m\right] \tag{5}$$

where: f_o is now defined as the average frequency of stress ranges; S_i is a constant amplitude stress range; and ζ_i is the fraction of total stress ranges for which S_i acts. Wirsching (1984) describes a probabilistic method within the context of spectral (frequency domain) analysis. In this case, the cumulative fatigue damage in an offshore platform is written as (Wirsching 1984);

$$D = \frac{T \cdot B^m}{A} \cdot \left[\lambda(m)\left(2\sqrt{2}\right)\Gamma\left(1 + \frac{m}{2}\right) \cdot \sum_i \gamma_i f_i \sigma_i^m\right] \tag{6}$$

where: $\Gamma(\cdot)$ is the gamma function; $\lambda(m)$ is a rainflow counting correction factor (Wirsching 1984); γ_i is the fraction of time for the *i*th sea state; f_i is the frequency of wave loading for the *i*th sea state; and σ_i is the root mean square of the stress process for the *i*th sea state.

Ginal (2003) and Foley *et al.* (2004) used a slightly different formulation of equation (6) and based their fatigue damage estimates upon probabilistic estimates of wind speed, direction, simulation of turbulent wind time-histories with 5-second averaging times, and rain flow counting of fatigue stress cycles. Using this procedure, equation (6) was re-cast into the following form (Foley *et al.* 2004; Ginal 2003);

$$D = \frac{T \cdot B^m}{A} \cdot \left[n_{5-\sec/\,year} \sum_j \sum_i P\left[\bar{V}_{5-\sec} = v_j\right] \cdot P\left[D = d \,|\, \bar{V}_{5-\sec} = v_j\right] \cdot \left(S_i^m\right)_{v_j} \right] \tag{7}$$

where: $n_{5-\sec/\,year}$ is the number of 5-second intervals in the given time period (one year in this former effort); $P\left[\bar{V}_{5-\sec} = v_j\right]$ is the probability that the 5-second averaged wind speed will be the user-defined magnitude, v_j; and $P\left[D = d \,|\, \bar{V}_{5-\sec} = v_j\right]$ is the probability that the wind speed is in a user-defined direction, d, (taken as direction perpendicular to sign face) given the 5-second averaging time is equal to the user-defined magnitude; and $\left(S_i\right)_{v_j}$ is the *i*th stress cycle magnitude for a given 5-second wind speed, v_j. It should be noted that modeling uncertainty was ignored (*i.e.* $B^m = 1$) and five-second wind speeds were taken as 5, 10, 15, 20, 25, 30, 35, 40, 45, and 50 mph.

Equations (6) and (7) are very similar to one another. Their difference arises from the structural analysis that is carried out and the load modeling. In the spectral method, equation (6), frequency domain analysis is used and in the method describe in equation (7), time-history simulation is implemented.

It has been recommended that failure be defined as $D \geq \Delta$ where Δ is a random variable describing accumulated damage at failure. With this definition, equation (4) can be re-written to define the time to fatigue-induced cracking or failure (Wirsching 1984),

$$D = \frac{T \cdot B^m}{A} \cdot \Omega = \Delta \quad \Rightarrow \quad T = \frac{A \cdot \Delta}{B^m \cdot \Omega} \tag{8}$$

where A, B, and Δ are random variables and the time to failure is therefore a random variable. The uncertainty in many quantities in structural engineering has been successfully modeled using lognormal random variables. Peronto (2003) confirmed that the number of cycles to failure for a welded pipe or CHS joint follows lognormal probability density functions. Foley *et al.* (2004) used these and other lognormal models to predict fatigue lives of sign and luminaire support structures. Wirsching (1984) recommended that A, B, and Δ be modeled using lognormal random variables.

If the service life for a detail (and therefore structural system) is defined as T_s, the probability of fatigue failure at the detail (or joint) is defined by,

$$p_f = P\left[T \le T_s\right]$$

With lognormal random variable modeling, the probability of the fatigue life being less than the intended service life can be computed using (Wirsching 1984);

$$p_f = \Phi\left[-\frac{\ln\left(\tilde{T}/T_s\right)}{\sigma_{\ln T}}\right] \tag{9}$$

where: $\tilde{T}$ is the median of the random variable describing the time to fatigue failure; $\Phi(\cdot)$ denotes the standard normal cumulative distribution function; and $\sigma_{\ln T}$ denotes the standard deviation of the natural logarithm of the time to failure. The median time to failure is given by,

$$\tilde{T} = \frac{\tilde{A}\cdot\tilde{\Delta}}{\tilde{B}^m\cdot\Omega} \tag{10}$$

The tildes denote median (or bias) of each random variable. The standard deviation is written as (Wirsching 1984);

$$\sigma_{\ln T} = \ln\left[\left(1+COV_\Delta^2\right)\left(1+COV_A^2\right)\left(1+COV_B^2\right)^{m^2}\right]^{1/2} \tag{11}$$

where *COV* denotes the coefficient of variation of each random variable. The probability of failure defined in equation (9) provides useful relative measures of the safety of the structural system with regard to fatigue-related fracture.

The previous discussion outlines a systematic methodology for including uncertainty in fatigue life predictions and therefore, establishes a formal methodology for assessing risk of fatigue-related fracture in cantilevered mast arm signal and sign support structures. Equation (9) allows probabilities to be attached to service lives given median estimates of the time to fatigue-induced crack. For example, if the median time to fatigue-induced failure is 15 years, the probability of not meeting 10-year, 25-year and 30-year service lives can be computed using equation (9). These probabilities of not meeting target service lives can also be used to establish rational inspection cycles. As an example, consider the following hypothetical scenario. Suppose the wind loading and detail categories present in a single mast-arm sign support suggest the median time to fatigue-induced failure is 15 years. The procedure laid out and discussed previously would suggest that the probability of *not* meeting 15 years of service is 50%. The probability of *not* seeing a 17-year service life may be on the order of 84% and the probability of *not* seeing a 12-year service life would be on the order of 40%. An inspection scenario can be formulated using this information: (a) conduct first field inspection at 12 years; (b) conduct second inspection at 15 years; (c) conduct the third inspection two years later; and (d) conduct annual inspections thereafter unless a retrofit measure is employed. The procedure can also be used

to red-flag problem structures. For example, assume the median time to fatigue failure is 15 years. If the structure has been in service for 17 years, there is an 84% probability that a fatigue-induced crack is present. Therefore, inspection should be done immediately and at regular intervals thereafter until a retrofit measure can be employed.

REPORT OUTLINE AND OBJECTIVES

As alluded to in the previous discussion, the ability to quantify risk depends heavily on having statistical information available for modeling all pertinent random variables including those affecting demand and capacity. There is a need to ascertain if sufficient information is available to apply the risk assessment procedure previously discussed for the sign support structures considered; and if not, recommend additional targeted testing and data collection to fill in the necessary blanks. Statistical information related to the demand placed on the details within the structural systems must also be gathered. This information includes wind speed and direction probabilities. All efforts undertaken in this phase of the research effort and outlined in this research report are targeted towards assembling the information needed to employ the framework for assessing fatigue-induced fracture risk outlined in the immediately preceding section.

The phase of the present research effort outlined in this report includes data collection, synthesis and recommendations to move forward into phases 2 and 3 of the research effort. The objectives of the present phase are as follows. Identify details and structures that are currently seeing fatigue-related problems and identify details that may be problematic in the future. Present a detailed national and international literature review and synthesis to learn what has been done, what is currently being done, and what is likely to be done in the near future related to fatigue-induced failure of critical connection details in sign structures and potential retrofit measures that are being evaluated and/or employed. Assemble all pertinent fatigue testing data into a form that is suitable for evaluating its sufficiency for predicting risk of fatigue-induced fracture of WisDOT’s sign support structures. Synthesize the data available for ultrasonic impact treatment (UIT) and gusset stiffening retrofit measures to determine if it is sufficient to justify using it to predict the likelihood of fatigue-induced failure once these retrofit measures are in place. Expand the database of statistical information related to wind speed and direction previously generated (Foley *et al.* 2004; Ginal 2003) and use this new informational source to select regions within the State that may be fruitful for field acquisition of data for sign and signal support structures. Finally, the research report seeks to provide objective evaluation retrofit measures that have been implemented and tested in previous research and investigate novel retrofit techniques that may be worthy of future in-depth evaluation.

The report is broken down into four parts that follow this introductory chapter. The first chapter provides details related to collection and synthesis of fatigue testing data completed to date for connection details similar to those found in Wisconsin's cantilever signal and sign support structures. It should be noted that this

chapter relies very heavily on the fatigue testing information included in appendices A through I of the research report. These appendices include details regarding fatigue testing that has been conducted since 1970 on connection details that are similar to those found in cantilever sign and signal support structures in Wisconsin. This chapter concludes with recommendations related to additional fatigue testing to be conducted in phase 2.

The procedures used to collect and synthesize wind speed and direction data for southern Wisconsin are outlined in chapter 3 of the report. Appendices J through Q of the report include the collected wind speed data and its synthesis through established statistical analysis procedures. The chapter concludes with a description of the expanded database of wind speed and direction information and recommendations regarding candidate cities for in-field monitoring of sign support structures. The chapter also includes information needed to include uncertainty (*i.e.* variability) in demand within the analysis procedures that facilitate assessment of fatigue-induced fracture risk.

The project kick-off meeting stressed the need to evaluate the impact of loose bolts on the fatigue performance of mast-arm to plate connections within the structures considered in this research effort. Loose bolts are often found in many of these structures during regular inspections and there was concern that non-tightened fasteners may lead to reduced fatigue life in these connections. To this end, finite element analysis was undertaken to evaluate the variation in stress distribution around the perimeter of a typical mast-arm tubular cross-section with various patterns of loose bolts present. Chapter 4 in the report outlines this finite element analysis in detail. Comparison of the FEA results with stress magnitude predictions made using traditional specification-based procedures are provided and the impact of loose (non-pretensioned) bolts on the stress distribution around an octagonal mast arm is quantified.

The research report concludes with Chapter 5, which summarizes the research conducted, assembles conclusions that can be drawn from the research effort and then proceeds to provide recommendations for phases 2 and 3 of the effort.

REFERENCES

AASHTO. (2001). *Standard Specifications for Structural Supports for Highway Signs, Luminaires and Traffic Signals, 4th Edition with 2006 Interim Revisions*, American Association of State Highway and Transportation Officials, Washington, D.C.

Foley, C. M., Ginal, S. J., Peronto, J. L., and Fournelle, R. A. (2004). "Structural Analysis of Sign Bridge Structures and Luminaire Supports." *WHRP 04-03*, Wisconsin Highway Research Program, Madison, WI.

Ginal, S. J. (2003). "Fatigue Performance of Full-Span Sign Support Structures Considering Truck-Induced Gust and Natural Wind Pressures," MS Thesis, Marquette University, Milwaukee, WI.

Kirkemo, F. (1988). "Applications of Probabilistic Fracture Mechanics to Offshore Structures." *Applied Mechanics Reviews*, 41(2), American Society of Mechanical Engineers, 61-84.

Miner, M. A. (1945). "Cumulative Damage in Fatigue." *Transaction of the ASME, Journal of Applied Mechanics*, 67, A159-A164.

Peronto, J. L. (2003). "High-Cycle Constant Amplitude Fatigue Life Variability of Welded Round HSS Y-Joints," MS Thesis, Marquette University, Milwaukee, WI.

Wirsching, P. H. (1984). "Fatigue Reliability for Offshore Structures." *Journal of Structural Engineering*, 110(10), American Society of Civil Engineers, 2340-2356.

Wirsching, P. H. (1988). "Probability-Based Fatigue Design for Marine Structures." *Marine Structures*, 11(1), 23-45.

Chapter 2
Fatigue Test Data Synthesis

INTRODUCTION

The fatigue performance of mast-arm sign and signal support structures has remained an active area of research since the first FWHA sponsored effort in the early 1980's (Fisher et al. 1981). On the one hand, it is disconcerting that such a simple structural system requires such advanced and sustained research efforts. However, it must also be understood that these simple structural systems involve fabrication procedures that can result in fatigue-sensitive details with significant uncertainty in their fatigue life. The systems are also subjected to highly variable and chaotic loading resulting from natural wind, which then results in high levels of uncertainty in the loading demand as well. Assessing the risk of fatigue induced failure in these structures is a daunting challenge and adequately assessing this risk requires more thorough understanding of both the uncertainty in the fatigue life of typical details and the uncertainty in loading demand.

The present chapter in the report seeks to provide direction for future fatigue testing targeted toward developing a more comprehensive understanding of the fatigue life variability of details typically used in mast-arm signal and sign support structures in Wisconsin. To this end, current Wisconsin Department of Transportation practice related to design and fabrication of mast-arm signal and sign support structures is reviewed. A comprehensive literature review of all pertinent fatigue testing completed from 1970 through the present is conducted including review of the connection details tested, the testing apparatus utilized and the results obtained. A synthesis of this past research is provided and this synthesis is used in a subsequent chapter of the report to make recommendations for the research to be undertaken in phases 2 and 3.

WISDOT MATERIALS, SUPPLIERS AND TYPICAL DETAILS

The usual practice of signal and sign support construction in the state of Wisconsin includes the Wisconsin Department of Transportation providing a series of detailing and design standards along with material specifications to the contracting public. Figures 2.1 and 2.2 illustrate two structural system configurations that initially established concerns regarding fatigue-induced fracture risk in Wisconsin. These structural systems evolve from generalized standard details. Figures 2.3 through 2.5 give standard WisDOT details for Type 9, 12 and 15 monotube signal and sign supports. The connection detail for the mast-arm to the vertical pole is of interest in the present study. It should be noted that pole-base connections may also be of concern and the present research effort includes a review and synthesis of fatigue testing for this pole-base detail as well.

WisDOT allows sign manufacturers to provide economical solutions for sign and signal supports provided materials are compatible with WisDOT specifications. The WisDOT material specifications for sign and signal support structural systems are outlined below.

Member (Component) Materials:

- ASTM A709, Grade 50 or 50W (A588) for mast arms and connecting plates
- AASHTO M 164 Type 1 or 2 High Strength Bolts (Type 3 if 50W steel used)
- Washers must conform to AASHTO M 293
- Nuts must conform to AASHTO M 291
- Zinc coating of Type 1 and 2 bolts, nuts, and their washers according to AASHTO M 298 Class 65
- All material for members and plates shall have meet Charpy V-Notch (CVN) toughness requirements specified in ASTM A709 for Zone 2:
    - Fracture-Critical Components: 25 ft-lbs at 40 deg. F for thickness less than 2 inches
    - Non-Fracture Critical Components: 15 ft-lbs at 40 deg. F for thickness less than 2 inches

***Fabrication*:**

- Sign and signal supports fabricated from ASTM A709 Grade 50 steel must be zinc coated following AASHTO M 111 after all cutting, drilling, welding, and punching.

Welding Materials

- All welding materials and procedures are required to conform to AASHTO/AWS D1.5 (Bridge Welding Code).

WisDOT requires that all sign and signal support structures be designed in accordance with the AASHTO Standard Specifications for Structural Supports for Highway Signs, Luminaires, and Traffic Signals (AASHTO 2001). The WisDOT Bridge Manual (WisDOT 2008) contains structure selection guidelines that include an outline of the process a designer can use to select a support system for signs with a variety of depths and widths of signage. When cantilevered sign structures are designed, WisDOT requires that they be considered as Category 1 structures and therefore, should consider natural wind gust loading and truck-induced gust pressure loading. Galloping-induced loading and associated deformations need not be considered in the design.

The flexibility afforded suppliers by WisDOT facilitates economic structural systems for these auxiliary structures. However, it also results in significant variety of structural systems found throughout the State. Historically speaking, there are six major suppliers of signal and sign support structures. A brief description of the usual structural configurations provided and the welding details often used in systems provided by these manufacturers is provided in the following:

Valmont

- This manufacturer traditionally has provided round or sixteen-sided tubular members. Tapered mast arms and poles are most often provided.
- Mast-arm connections have historically been socketed/fillet welded or full penetration welded. Pole-base connections have followed similar detailing.
- This manufacturer often uses the unequal fillet welded details evaluated in earlier Lehigh/Caltrans work (Fisher *et al.* 1981).

Union Metal

- This manufacturer has historically provided round, tapered mast arms and poles.
- Mast-arm and pole-base connections have historically been socketed with fillet welds.
- Equal leg fillet welds are usually provided.

Brookfield Manufacturing

- This manufacturer most often provides prismatic (non-tapered) mast arms and poles.
- The mast-arm-to-pole and pole-to-base connections are socketed fillet weld connections.
- Equal leg fillet welds are most often provided.

Ameron

- This manufacturer usually provides round cross-sections that are tapered for mast arms and poles.
- Socketed fillet weld or full penetration welded connections at the mast-arm-to-pole and pole-to-base connections are often used.
- Equal leg fillet welds are most often employed.

Millerbernd

- This manufacturer often provides round sections, but larger diameter poles will sometimes be 16-sided cross-sections. Members are most often tapered.
- Both fillet-weld socketed and full penetration welded connections have been provided.
- Equal leg fillet welds are usually utilized.

Powco

- This manufacturer has provided 8-sided tapered mast-arm and poles.
- Mast-arm-to-pole and pole-to-base connections often employ socketed fillet-weld connections.
- It is unclear if equal or unequal fillet weld legs have been used.

It is fortunate that the six manufacturers all provide similar structural systems. This is to be expected as these ancillary structures are relatively consistent in their configuration throughout the U.S. and many of the manufacturers above provide structures for many states (at least on a regional basis). The fatigue testing that has been completed to date has included many of the configurations described above and this leads the

research team to the conclusion that there is opportunity to use past research efforts conducted elsewhere in the U.S. as a basis and perform supplemental targeted testing to generate a thorough understanding of uncertainty in fatigue life of the connection details often associated with these ancillary highway structures.

There are many configurations seen in mast-arm to pole signal and sign support structures. As outlined earlier, this arises from WisDOT's acceptance of manufacturer provided systems that comply with the WisDOT material and fabrication provisions, the Bridge Manual, and the AASHTO Standard Specifications. Several incarnations of systems seen in southeastern Wisconsin are shown in Figures 2.6 through 2.8. While there is commonality among the systems shown in the figures, there are several significant differences. Therefore, it will be very important for the synthesis of fatigue testing to keep in mind these similarities and it will be equally important to identify significant differences that will make use of previous fatigue testing data questionable moving forward.

FATIGUE LIFE ESTIMATION METHODS

The goal of any fatigue testing undertaken is to gain understanding of the fatigue life of details being used in a structural system. Three fundamental approaches to characterizing and estimating the fatigue life of details and structural systems have been proposed. The most recent and complete synthesis of these method has been that provided by (Walbridge 2005). A review of these methods sheds light onto the motivations for fatigue testing and also provides insights into reviewing fatigue experiments and gleaning the experimental results for a foundation for future testing.

The first method for estimating (characterizing) fatigue life is termed a *classification method* (Walbridge 2005). The classification method begins with identifying structural details that are often found in structural systems. Taxonomy of these details is undertaken and fatigue detail categories emerge. Stress-range versus life (S-N) curves for each detail category are generated and validated. The S-N curve is often defined in log-log space and the usual form is,

$$N = \frac{A}{S_r^m} \tag{2.1}$$

where: N is the fatigue life (number of constant-amplitude stress cycles until failure); A is a fatigue detail category constant specific to each connection detail; S_r^m is the magnitude of the constant amplitude stress range; and m is an exponent often taken to be 3.

At any given stress range magnitude, it is expected that there will be a distribution of fatigue lives characterized by a cumulative distribution function (*e.g.* lognormal, normal). If a design S-N curve is to be generated, the stress-range versus life curve is usually defined for 95%, or 97.5% survival probabilities. In

other words, the value of A is defined in such a manner that 95% or 97.5% of all experimental fatigue lives are expected to see the fatigue life defined by A and at the defined stress range.

The classification method implicitly considers uncertainties regarding the precise nature of the local stresses at the eventual crack location. Nominal stresses in the global member are defined and utilized to define stress range amplitudes. Local influences (*e.g.* stress raisers caused by sudden changes in geometry) are ignored and are built into the detail categories defined. It is therefore, very important that detail categories be defined in such a manner that they can coalesce these subtle influences on fatigue life together. However, the methodology is relatively simple to implement and has a long history in structural engineering.

The classification method is not without disadvantages. First of all, the S-N curves are highly empirical. As will be seen, the variability in fatigue life for specimens with supposedly identical fabrication can be tremendous. There is also no information regarding crack size and crack growth obtained from the experiments. Experimental testing is most often terminated at the appearance of visible cracking. The S-N technique can only be implemented when there is experimental data available for the detail category being used.

A second approach to fatigue life estimation involves computation of hot spot stresses (Walbridge 2005). This technique attempts to include geometric discontinuities in the structural analysis defining the stress range. Theoretically, this should enable a more fundamental examination of stress-range versus life through utilization of S-N diagrams that can be applicable to more than one detail category. Using this approach, it is theoretically possible to use AASHTO detail category C for many more connection details. The structural analysis becomes more complicated, however, because geometric discontinuities causing stress raisers need to be considered a priori. This approach has been attempted in earlier work to help gain greater insight into uncertainty in fatigue life seen in experiments (Little and Jebe 1975).

While the hot spot stress technique appears to be a method of simplification and stream lining of fatigue life estimation, it is not without difficulty. One could make a successful argument that if the theory of the hot spot stress method were to hold true; there should only be one hot-spot stress curve. However, one should recognize that welding steel connections often results in discontinuities that are highly variable from one specimen to another (*e.g.* weld undercutting). As a result, a *size effect* has been suggested and more than one hot-spot stress S-N curve remains necessary (Walbridge 2005). This size effect is alluded to in other comprehensive discussions of the uncertainty involved in fatigue experiments (Little and Jebe 1975).

The two previous methods of fatigue-life characterization do not consider the number of stress range cycles required to initiate a crack and subsequently grow or propagate a crack to a critical crack size whereupon fracture of the cross-section initiates. Being able to characterize different stages in the life of a

structural detail subjected to repetitive loading is the goal of the linear elastic fracture mechanics method - LEFM (Walbridge 2005). The LEFM allows the engineer to predict crack size and crack growth rates at various states in the service life of the detail and therefore, structure. One highly rational aspect to the LEFM is that a crack-like defect is assumed to be present the instant the detail goes into service. There is no assumption that a crack forms or initiates. It is assumed that a crack exists and it simply grows during service to a critical size.

The LEFM can be thought of as the *holy grail* of fatigue life characterization. It affords the structural engineer much opportunity to define inspection cycles based upon in-service crack detection. It also allows the engineer to make predictions regarding the expected fatigue life following visible crack detection and the subsequent growth to critical size thereby instantiating fracture. However, characterizing uncertainty in crack initiation is difficult business. Characterizing uncertainty in crack growth rates within a detail adds another layer of complexity. Recent research efforts have begun exploring this (Walbridge 2005), but the present effort will focus on uncertainty as being defined on the basis of crack initiation.

FATIGUE TESTING OF UNREINFORCED AND UNTREATED CONNECTIONS

There have been a large number of experimental efforts attempting to characterize the fatigue life of welded connection details commonly found in mast-arm-pole sign and signal support structures conducted in the last three decades. The objective of this section is to outline what are perceived to be the most pertinent and important experimental efforts that can be used as a foundation for the present research effort. The review of these past research efforts will take place chronologically. It should be noted that this chapter of the report will contain highlights of these past efforts and an exhaustive listing of experimental specimens, testing apparatus and experimental data can be found in appendices of the report. The appendices will be liberally referenced throughout the discussions.

The following subsections of this chapter will be devoted to outlining previous research that has been conducted to evaluate the fatigue performance of welded mast-arm to plate and pole base connections. The focus will be on those connections that are unreinforced (*e.g.* un-stiffened) and have not been treated by retrofit techniques (*e.g.* ultrasonic impact treatment – UIT). Later subsections in the chapter will review retrofit techniques and their impact on fatigue performance.

(Archer and Gurney 1970)

One of the first documented efforts related to studying the fatigue life of welded connections was conducted in the United Kingdom (Archer and Gurney 1970). There were two major objectives to this effort. First of all, there was a desire to generate S-N data for round hollow shape (RHS) to plate connections as they were frequently used in practice, but their fatigue performance was relatively poorly understood. Secondly, there

was also a need to define optimum sizes of the welds within these connections so that design recommendations could be made.

The experimental effort involved two connection details categorized as Type F (flush fillet welded) and Type S (socketed-fillet welded). Schematics of these specimens are shown in Figure A.1 in Appendix A. Type S specimens have a connection configuration that will behave in a manner similar to that of a socketed mast-arm-to-plate connection with fillet welds. The Type F specimens tested could be considered to help characterize fillet welded mast-arm-to-plate butt-type connection behavior, but connections of this type are not used in sign and signal support structures.

The material used for all tubes and plates is described as being BS 15: mild steel for general structural purposes (Archer and Gurney 1970). Given the year of the research effort, 1970, it is envisioned that this steel is similar to ASTM A36. It should be noted that the yield stress, elongation at ultimate, and the ultimate stress of the material are likely not a factor in establishing the fatigue life for high-cycle, low stress fatigue testing. This is the type of testing conducted in this former research effort and it is expected that the stress range alone can be used to characterize the fatigue performance.

The importance of welding procedure on the fatigue life of the resulting connection detail was recognized and thorough description of the welding processes used for all specimens was provided. Type F series specimens included three fillet weld sizes (5/16, 7/16, and 11/16 inches). Type S specimens utilized two weld sizes (7/16 and 9/16 inches). It was mentioned that all welding was conducted in "...downhand position" (Archer and Gurney 1970). Aside from the 11/16-inch welds utilized in the Type F series specimens, all welds were made using the "... manual arc process" (Archer and Gurney 1970). It is surmised that this welding procedure is similar to submerged arc welding (SAW) used in the United State. The F-series specimens that utilized 11/16-inch welds were done using a combination of SAW and GMAW processes. In these specimens, the root pass and surface pass welds were made using SAW. Intermediate weld passes were done using Gas Metal Arc Welding (GMAW) processes. MIG welding was specifically referenced. The reason that SAW welds for the root and final surface passes were used was that it was felt to be very important to keep the weld toe conditions consistent across all specimens. MIG welding was used to reduce weld pass time for the larger dimension welds.

The testing apparatus utilized a rotating specimen and a schematic is shown in Figure A.2. The apparatus allowed a very large number of stress range cycles to be applied in relatively short periods of type as a result of the rotation. Furthermore, the apparatus was felt to be more thorough with regard to testing the fatigue life of the welded connection. The reason for this is that every point along the weld length (*i.e.* the RHS circumference) is subjected to cyclical tension. As a result, the entire weld length can be subjected to fatigue cycling with the same stress range magnitude.

The experimental data for all specimens is contained in Tables A.1 and A.2 and key to the specimen designations developed for this present study is given in Table A.3. The experimental data for Type F and Type S specimens are plotted in log-log space in Figures A.3 and A.4. The AASHTO S-N design curve for detail category E' is also provided on the graphs. It can clearly be seen that the two details tested are not well represented by the E' detail category.

Type F specimens with 5/16" and 7/16" welds failed in the weld and therefore were classified as having less than optimum weld dimensions. Type F specimens with 11/16" weld dimensions all had failures initiate at the weld toe. Type S specimens had failures initiate in both the weld material and the RHS base metal near the weld toe. One of the 11/16" weld specimens contained weld profiles that were unbalanced (*e.g.* one side of the central plate had 45-degree weld profiles and the other a much shallower 30-degree profile). Since cracking initiated at the toe of the 45-degree weld, it was felt that the 30-degree weld profile was more beneficial. This undoubtedly was the observation that instigated development of the unequal fillet weld leg profiles later studied (Fisher *et al.* 1981).

The research effort had several conclusions that can be used to generate qualitative recommendations regarding weld sizes for these types of connections. The objective of the recommendations regarding weld size was to ensure equal chance for cracks to initiate at the weld toe and in the weld itself. Optimum weld size to tube wall thicknesses was defined. This ratio was 2.16 for RHS fillet welded to the connecting plate and 1.75 for sleeved connections typical of full penetration welds.

If the fatigue failure found in the testing was crack formation in the wall of the tube, one could argue that the fatigue testing data could be used in the present research effort. However, examination of Figures 2.4 through 2.6 illustrates that the connection plates for the mast arms and the pole involve discrete bolting. Past research (Foley *et al.* 2004; Hall 2005; Hall and Connor 2008; Ocel 2006) has demonstrated that the load paths caused by discrete bolting and the flexibility of the connecting plates can have a significant effect on the state of stress at the toes of welds in these connections thereby affecting the stress ranges encountered in service. These influences are not present in this former testing and therefore, the experimental data generated through this former effort cannot be used as part of the present effort.

(Fisher et al. 1981)

The California Department of Transportation (CALTRANS) initiated a study of the fatigue performance of mast-arm-to-pole sign and signal support structures. This effort completed at Lehigh University (Fisher *et al.* 1981) was one of (if not) the first comprehensive effort devoted to understanding the fatigue performance of these structural systems. Prior to this study, design specifications (AASHTO 1975; AASHTO 1996) did not

contain fatigue design procedures for these structural system, nor did they contain fatigue life information for a mast-arm to plate connection.

The specimens used for testing included both mast arm and pole. Schematics of these specimens are shown in Figure B.1. Past observations of weld profile apparently improving fatigue strength (Archer and Gurney 1970) were evaluated in this research effort. Figure B.2 illustrates two weld profiles that were tested and Figure B.3 provides a schematic of the testing apparatus. Table M.1 contains the fatigue testing data generated in this past effort and Table M.2 provides a key to the specimen designations.

Two fabricators were utilized and two steel grades were considered. Ameron Pole Products Division fabricated six specimens (**LEH-40-A-45CA-_** series) using ASTM A283 Grade D steel poles. These specimens had equal leg fillet welds. Valmont Industries also fabricated six specimens (**LEH-40-V-34CA-_** series) using ASTM A595 Grade A steel poles. These specimens had unequal leg fillet welds and it was found that they appeared to have better fatigue performance than the LEH-40-A-45CA-_ series poles. This behavior can be seen in Figure B.5. As a result, two additional specimens with unequal-leg fillet welds were fabricated and tested (**LEH-40-A-34CA-_** series). The apparent improvement in performance for these two specimens when compared to the LEH-40-A-45CA specimens can also be seen in Figure B.5.

Positioning of the longitudinal seam weld was evaluated in this research effort. The 40-series specimens (see Table B.2) had longitudinal seam welds for the mast arms and poles were located at points of maximum stress. The 48-series specimens (see Table B.2) had random placement of longitudinal seam welds. The A283 Grade D pipe material had a yield point of 46.5 ksi and a tensile strength of 65.5 ksi. The A595 Grade A pipe had yield strength of 61.7 ksi and tensile strength of 73.3 ksi. Applied stress ranges were much less than 1/2 the yield stresses in both cases and it is expected that material strengths had little impact of the fatigue lives seen. All specimens were galvanized after fabrication and prior to testing.

The experimental testing indicated that all but three specimens (LEH-48-V-28CA-3, -5, -6) had failures reported in the mast arms. Furthermore, the experimental testing indicates that all stress ranges tend to migrate very closely to the category E' detail (see Figure B.5). The experimental results indicated that having contact angles at fillet welds less than 45 degrees provides a smoother stress transition from the mast wall through the weld to the connecting plate. Figure B.5 does appear to clearly illustrate this improvement. However, it should be emphasized that when the angle made between the exterior weld surface and the mast arm wall is reduced (*e.g.* less than 45 degrees), there will be less tendency for weld undercutting into the base metal at the toe to occur. Therefore, there will lessened tendency for the stress concentration caused by geometric discontinuity near the weld toe to occur. Thus, it is not so much the weld profile that causes improved fatigue performance, but the ability for the welding done to have less undercutting when the 28

degree and 34 degree profile is specified. It is difficult to definitively say that the alternate weld profile recommended had a definitive impact on performance when only two tests were done.

The research effort found that galvanizing can leave a coating capable of bridging fatigue cracks. As a result, it was thought that large fatigue cracks could be permitted to grow prior to their breaking through the galvanizing coating. Therefore, it may be that most of the fatigue life is exhausted prior to detection.

The mast-arm to plate connection used in this former research effort is different than the connection frequently encountered in Wisconsin as seen in Figures 2.6 through 2.8. The mast-arm plated is fillet welded around its perimeter to the pole box using 3/8-inch or 7/16-inch fillet welds. As a result, the discrete load paths created by discrete bolting are not present in these connections and the fatigue testing results should be carefully scrutinized with regard to their use in the synthesis. Most Wisconsin sign support structures are galvanized prior to going into service, or they are constructed using weathering steel materials. In this regard, the experimental results can be usable and valuable.

(South 1997)

This research effort, conducted by the Illinois Department of Transportation (IDOT) sought to develop S-N curves for socketed fillet weld tube to plate connections. The objective of the effort was to develop a statistically accurate S-N curve for these connections for later use in fatigue analysis. As a result, a large number of fatigue tests were carried out.

The testing specimens where composed of AISI 1020 DOM steel pipe (tube) with 3-inch outer diameter and 1/8-inch wall thickness. Although recent research has suggested DOM pipe material can cause questionable fatigue performance for welded Y-joints (Foley *et al.* 2006), the manner in which this former effort used the DOM material is not expected to affect the fatigue results. The connecting plate was composed of A36 steel (1-inch thick) and the ratio of weld leg to tub thickness was 2.0 in keeping with the recommendations of (Archer and Gurney 1970). Welding electrodes used were E7018. A schematic of the specimens tested and the testing apparatus utilized is shown in Appendix C (Figures C.1 and C.2). The typical weld toe cracking seen in the experiments is shown in Figure C.3.

Four testing sets were established: IDOT-1 through IDOT-4. Stress-range and fatigue life data is given in appendix Table C.1. All specimens at 11.2 ksi stress range were terminated without failure and are therefore, marked as run out tests. Four of the five tests at 8.4 ksi were also termed run outs and testing terminated without cracking being found. One exception was IDOT-4 at this stress range. The welding process was thought to be the cause for this non-run-out test as welding can cause variability in weld geometry, undercut in the base metal at the toe, inclusions of slag materials and porosity (South 1997). The S-N data for the experimental testing is shown in Figure C.4. It can be seen that all specimens tested fall well to the right of

the AASHTO E' detail category. Run out tests are indicated in the figure and it should be noted that there are many data points located beneath the circled data.

The specimens used in this research effort include a socketed fillet weld condition and a four-bolt connection plate arrangement. Thus, the specimens tested had enough similarity to WisDOT connection details to justify their potential use to help establish a foundation for characterizing uncertainty in WisDOT's mast-arm-to-pole connections. However, it should be noted that the stress ranges where run out tests were NOT present are quite high relative to stress ranges that are expected to be seen in service when considering high-cycle fatigue performance. If one were to compute the means and standard deviations for the 33.7, 22.5, 19.7, and 16.9 ksi stress ranges as done in this former effort (South 1997), one would find that the variability in fatigue life increases significantly with decrease in stress range. This phenomenon can be explained by the fact that weld geometry variability and weld undercut into the base metal can result in greater sensitivity to crack formation and variability as stress ranges decrease and it has been reported previously in the literature (Little and Jebe 1975).

The tendency for fatigue life variability to increase with decreasing stress range and its confirmation through this former experimental effort will need to be considered when establishing stress ranges for future experimental testing to quantify fatigue life variability. This issue will be revisited in later sections of this chapter when the formal synthesis of the experimental data generated through all past research efforts is undertaken.

(Deschamp 2002)

This research effort was undertaken after several mast-arm signal connection failures in the state of Wyoming. It was a final effort in a series of studies to evaluate and recommend NDE techniques to find fatigue cracking in mast-arm-to-plate connections, develop connection details with greater fatigue resistance and evaluate fatigue lives of new and existing connections found in Wyoming's signal structures.

Wyoming uses many details that are consistent with those used in Wisconsin. In fact, the details used in Wisconsin likely have been influenced and guided by this former research effort. Wyoming uses ring-stiffened, closed box, and open box mast arm to pole connections. These are shown in Figure D.1. A comparison between Figures 2.6 through 2.8 and Figure D.1 illustrates that the fatigue testing conducted in this former effort are good candidates for inclusion in the later synthesis of fatigue data and recommendations for phases 2 and 3 of the present effort. The important item of note among all these connections is that mast-arm-plate flexibility and discrete load paths forming through the four-bolts are present in these connections. These are very important and it is possible for all tests done to be used in later synthesis.

The experimental testing involved both in service (IS) and virgin (V) specimens. The virgin specimens were fabricated for the project by Ameron and Valmont Industries. Both of these manufacturers have been providers for sign and signal supports in Wisconsin. The fatigue testing results for all specimens is given in Table D.1 and a key to the specimen designations is given in Table D.2. All mast-arm specimens included in this review were of closed-box configuration with one exception: WY-IS-S-1.50-6-12.50. This connection contained an open box configuration.

It is unfortunate that only two experiments resulted in fatigue cracks defining failure and termination of the test. All but two of the experiments were classified as run outs. However, it should be noted that the experimental data from specimens WY-IS-S-1.75-4-10.00 and WY-IS-S-2.00-6-12.25 can be considered candidates for use in evaluating fatigue life variability of details similar to those in Wisconsin. The rather high stress range (24 ksi) of one of the specimens may make it this test difficult to include.

(Machietto 2002)

Valmont Industries conducted several in-house fatigue experiments and made their results public through presentations at AASHTO committee meetings (Machietto 2002). The cyclic testing conducted included both fillet welded-socketed and full penetration welded mast arm to plate connections. Unreinforced and radial stiffener reinforced specimens were tested. Schematics illustrating the connection details are given in appendix Figures E.1 and E.2 for unreinforced and reinforced connections, respectively. The rather unique rotating beam testing apparatus is shown in Figure E.3. This loading scenario is similar to that employed by (Archer and Gurney 1970) in their earlier studies. However, it is important to note that discrete bolting was utilized as shown in Figure E.3. This will make the results of the testing more amenable to use in the present effort as the discrete load paths through the mast wall to the bolts is preserved.

The specimens tested were 10-inch diameter tapered round 7 gauge (0.1793 inch) tubular shapes. Specimen fatigue test data is given in Tables E.1 and E.2 with a key to the specimen designations given in Table E.3. All stiffened specimens exhibited fatigue cracking initiating at the tip of the stiffeners and propagating down through the mast-arm wall. The failures seen in the testing for these specimens are shown in Figure E.4. The failures for unreinforced connections were similar to those found in earlier research efforts and these too are shown in Figure E.4. The stress-life data for the unreinforced and gusset-reinforced specimens are plotted in Figure E.5 and Figure E.6, respectively. The AASHSTO E' detail category S-N curve is plotted for reference on each.

Figure E.6 illustrates that reinforcing the mast-arm to plate connection with gussets does not generate improvements worthy of incurring the extra fabricating expense attaching these gussets. Several gusset plate configurations were tested and all show performance much closer to the AASHTO E' reference than the

unreinforced specimen data plotted in Figure E.5. Several FEA studies confirmed the generation of significant geometric discontinuity at the tip of the gusset and the resulting stress raising effect is the reason for the less than anticipated improvement.

The fatigue life data in Table E.2 illustrates that one-half the specimens were run outs. However, there is one socket-fillet weld connection (VAL-U-SFW-B) and two full penetration welded connections (VAL-U-FP-A and VAL-U-FP-B) that can be used in the impending synthesis of fatigue data. It should be noted that the stress range is relatively high (17.6 ksi).

(Chen et al. 2003) and (Alderson 1999)

This research effort was instigated by the Missouri Department of Transportation (MODOT) following fatigue failures seen in several mast-arm signal support structures. There were several objectives of the effort including fatigue testing evaluation of several mast-arm to plate connections fabricated by several manufacturers known to supply these structural systems to MODOT.

A schematic of the testing specimen is shown in appendix Figure F.1. It should be noted that one of the objectives was to evaluate an unequal-leg fatigue-resistant fillet weld configuration shown in Figure F.1. The specimen configuration is very similar to details used in Wisconsin (refer to Figure 2.5). The laboratory testing setup is shown in Figure F.2. Material data for the specimens was not provided in either source and the welding procedures utilized were not described in any detail. Non-Destructive Testing (NDT) using the magnetic particle procedure was used on all specimens tested to detect crack formation during experimental testing. This NDT also resulted in several flaws being detected in specimens prior to testing and this demonstrates that welding procedures are VERY important for these structural systems.

The fatigue testing data and a key to the specimen designations is given in Tables F.1 and F.2, respectively. A typical failure seen in the testing is shown in Figure F.3. Table F.1 indicates that three of the five specimens tested had flaws detected via NDT and thus, it is recommended that the data for these three specimens NOT be included in the data synthesis. The fatigue data is plotted in Figure F.4 and it can be seen that all specimens tested are near the AASHTO E' fatigue detail category S-N curve. However, the two specimens with flaws detected via NDT fall below the E' curve and this reinforces the statement welding procedures and fabrication can be critical with these structures. The present data synthesis can include two specimens (UMO-VAL-O-1 and UMO-VAL-N-1) in Table F.1. It should be noted that one involves a typical non-fatigue-resistant weld and the second used the fatigue-resistant weld profile shown in Figure F.1. The difference in the results seen in this effort are not as great as those seen in former research (Fisher *et al.* 1981). This suggests that there is variability in the benefit resulting from unequal leg fillet weld profiles.

(Koenigs et al. 2003)

This research effort is one of the most comprehensive studies of the fatigue performance of mast-arm structural systems and details and methods that can be used to retrofit connections between mast arms and plates. Two unreinforced specimen details were tested: socket fillet-welded and full-penetration welded. Schematics of these details are shown in appendix Figures G.1. Four gusset-reinforced connection configurations were also evaluated and these are shown in appendix Figure G.2. Two new collar connection details were tested as well and schematics of these are shown in Figure G.3. Significant information related to weld geometries, specimen geometry and chemical composition analysis is provided. All materials used in the specimens meet material specifications set forth by WisDOT.

Fatigue testing data for all specimens is given in Tables G.1 through G.5 and a key to specimen designations is given in Table G.6. Failures seen in the experimental testing were consistent with those seen in previous experimental efforts. Typical failures are shown in Figures G.5 through G.7. Stress-range versus life plots for all specimens are given in Figures G.8 through G.12. All specimens tested appear to be very close to, or to the right of the AASHTO E' detail category.

Most (if not all) WisDOT details involve un-stiffened mast-arm to plate connections. Experimental results of this study and those reviewed to this point indicate that stiffening does not yield appreciable benefit and therefore, only un-stiffened connections. The fatigue data for unreinforced and untreated mast-arm plate connections are given in Table G.1. The key to specimen designations provided in Table G.6 indicates that three different wall thicknesses are included in these specimens. The stress-range versus fatigue life plot given in Figure G.8 illustrate that there may be some effect on fatigue life generated by thicker mast-arm plates. Excluding run out tests, the following specimens are candidates for inclusion in the synthesis to follow: VAL-U-N series; TX-U-N series, VALN-U-N series and VALN-W-N series.

(Ocel et al. 2006) and (Ocel 2006)

This research effort was sponsored by the Minnesota Department of Transportation (MNDoT) and provided a comprehensive look at the fatigue performance of many connection details found in mast-arm-pole signal and sign support structures. The doctoral dissertation component on this effort (Ocel 2006) provides detailed examination of stress field and deformation behavior in socketed fillet-weld connections for thin-walled RHS shapes to orthogonal plates. The impact of discrete load paths caused by anchor rods with stand-off on generating significant stress raising behavior first outlined in past HML research work (Foley *et al.* 2004) was confirmed via detailed FEA.

Two connection details closely related to those seen in WisDOT structural systems are the mast-arm connection details and pole base plate connection details tested. Schematics for the unreinforced, the gusset-

stiffened and the pole base are shown in appendix Figure H.1. A second long-pole specimen was also tested and a schematic is shown in Figure H.2. Several load testing arrangements were utilized to allow in-plane, 45-degree, and out-of-plane bending on the connections. Testing system schematics are provided in Figures H.3 through H.5.

Fatigue failures seen in most of the specimens tested were typical of those seen in past research efforts. As expected, cracking was seen to initiate at the corners of multi-faceted mast-arm tubes and at the tip of gusset-plate stiffeners. Typical failures are shown in Figures H.6 through H.8.

The pole and mast-arm specimens utilized in the testing were 8-sided non-tapered tubes bent from A588 weathering sheet steel. Schematics for these poles are shown in Figure H.1(c). The long pole specimens (Figure H.2) were fabricated using ASTM A606 weathering sheet steel. All of the steel used had specified yield strength of 50 ksi. Miscellaneous plate materials (*e.g.* used for based plates, gussets, etc) were specified as ASTM A36. All tubular cross-sections were brake-pressed and automatically seam-welded using the submerged arc welding (SAW) process. Other welds on the specimens were performed manually using the gas metal arc welding (GMAW) process. All welding filler material was E70. The specimens were not galvanized.

All un-stiffened mast-arm connections tested involved full penetration welds with backing ring. The basic detail is schematically shown in Figure H.1(a). The fatigue-life data for the mast-arm connections is provided in Table H.4 and the key to specimen designations is given in Table H.6. The constant amplitude stress range data and in-plane loading condition are useful for the present synthesis. Connection plates for these mast-arm specimens are 1.25 inches and this is consistent with those seen in WisDOT structures. All specimen data in Table H.4 are candidates for the present fatigue synthesis.

The experimental fatigue life data for the un-stiffened mast-arm connections (Table H.4) is plotted in Figure H.11. All of the un-stiffened mast-arm connections meet the AASHTO E' fatigue detail category. Although a two-sided loading sequence was used for the experimental testing, the plotting of the data illustrates that this was not a factor that needs to be considered in the data synthesis.

This research effort also included thorough evaluation of socketed pole base connections that have some similarities to those connections used in Wisconsin. Schematics of the two specimen configurations tested are shown in Figure H.1(c) and H.2. As indicated, a four-rod anchor arrangement was utilized and this arrangement is different that most base connections used in Wisconsin (Figures 2.6 through 2.8). Furthermore, past research (Foley *et al.* 2004) has shown this connection configuration generates significant stress raising behavior as a result of the discrete load paths created by the anchor rods. Crack locations seen in the experimental testing are shown in Figure H.6 for the socketed pole base. As expected, cracking is

initiated near the anchor rods and in the vicinity of the "corner" on the multifaceted shape. Recent research efforts (Foley *et al.* 2004; Hall 2005; Hall and Connor 2008; Ocel 2006) demonstrate this behavior is likely.

Two base plate conditions were tested as past research (Foley *et al.* 2004; Hall 2005; Hall and Connor 2008; Ocel 2006) flexibility of the base plate can affect stress distributions and magnitudes around the base of the pole. Thin (1.25-inch) and thick (2.50-inch) base plates were tested. Fatigue life data for the specimens tested are given in Tables H.1 and H.3, respectively; and a key to the specimen designations is given in Table H.6. It should be noted that the research effort included in-plane, out-of-plane, and 45-degree loading conditions. Only the in-plane and out-of-plane testing data is included in this synthesis.

Many of the specimens in Table H.1 were run at consistent stress ranges. It appears that two of the stress range targets were approximately 5.5 ksi and 4.0 ksi with some natural variation above and below these target values. Specimens MN-P-FR1-IP and MN-P-FR2-IP at 3.8, 4.26 and 4.10-ksi stress ranges are candidates for use in the present research effort as are specimens MN-P-FR1-OP at 5.41 ksi stress range. Only non-run out tests will be considered. Thick-base plate specimens were run at very consistent stress ranges and Table H.3 indicates that all specimens in the MN-P-FR2-IP-N-CSR series at 14.9 and 15 ksi are candidates for inclusion.

Stress-life plotting for all the specimens tested is given Figures H.9 and H.10. Examination of these plots illustrates that the thin base plate connections tend to have fatigue lives well below the AASHTO E' reference line used for the review of fatigue testing in this chapter. Thick base plate connections appear to have fatigue lives that are greater than the AASHTO E' fatigue detail category.

(Rios 2007)

This research effort was conducted at the University of Texas at Austin as part of a pooled fund study sponsored by the Texas, Pennsylvania, Iowa, Wyoming, Colorado, Minnesota, North Carolina, Wisconsin, and South Dakota departments of transportation. The main objective of the study was to evaluate the fatigue performance of high-mast luminaire (HML) support base details common to these structural systems. Although the present research effort is not focused specifically on HML support bases, the detail conditions found in these structures are similar to those at the base of many signal and sign support structures in Wisconsin.

A consistent pole diameter of 24 inches was used in the research. The anchor rod diameters for the test specimens were 1.75 inches. The specimen pole diameters tapered at 0.14 inch/foot and Valmont Industries supplied all specimens for the testing. The wall thickness was 5/16 inches for all specimens. Materials for the specimens were specified to be ASTM A572 Grade 65 steel. Exhaustive material chemical composition analysis and tensile testing was conducted to validate this material was received.

Three base details were tested. Schematics of these are shown in Figure I.1. Socketed and full penetration weld connection details (with and without backing plate/ring) were tested. A reinforced stool-base connection detail was also tested and a schematic is shown in Figure I.2. The apparatus used for testing is schematically shown in Figure I.3.

Several anchor rod arrangements, base plate thicknesses, and weld configurations were tested. Tables I.1 through I.3 contain the fatigue testing results for the specimens tested. It is important to note that a consistent stress range was used for all specimens. However, it should also be noted that the base plate thickness varied in virtually all the testing done. Furthermore, the two weld configurations (socketed and full penetration) are distinct enough to be considered independently.

Failures seen in the fatigue testing are shown in Figures I.4 and I.5 for the unreinforced and stool base connections. A stress life plot of the data is shown in Figure I.6. The failures seen in testing is consistent with other tests on these systems and Figure I.6 indicates that the majority of tests perform below the AASHTO E' reference detail category used for this synthesis. In general, as the base plate thickness increases, the fatigue performance increases as well. Table I.1 indicates that this behavior is independent of the anchor rod arrangement for socketed base plates. Table I.2 illustrates that the increase is not as significant for the full penetration weld connection.

All specimens tested in this former effort can contribute to the present effort. However, it is likely that the previous testing will need to be reviewed very carefully so that consistency with WisDOT details can be maintained. The reason for the caution is that the experimental results in Tables I.1 and I.2 indicate that significant fatigue-life sensitivity to base plate thickness, anchor rod arrangement and weld detail.

FATIGUE TESTING OF REINFORCED AND TREATED CONNECTIONS

The relatively poor in-service performance of mast-arm and socketed pole-base connections has lead to application of retrofit measures and reinforcement schemes for these connections. This section of the chapter will review fatigue testing conducted to assess fatigue performance of retrofitted connections (*e.g.* hammer peening, Ultrasonic Impact Treatment) and those that include stiffening mechanisms (*e.g.* collar-type reinforcement, gusset plates). The impact of galvanizing on fatigue performance has also been evaluated and this is an important consideration for the present research effort.

There are quite a few retrofit measures that can be undertaken to improve the performance of welded connections made between hollow tubular thin-walled sections and plates. It is prudent to review the techniques that are often employed as this review will help to frame the measures that have been evaluated with the larger pool of potential measures.

The goal of most retrofit measures is to smooth out geometric discontinuities created through welding. As a result, the retrofit measures seek to physically alter the profile of welded connections and tend to focus on the toe of fillet and full-penetration welds. One common and long-standing technique is *grinding*. Grinding seeks to eliminate weld defects near the surface of the base metal (*e.g.* undercutting) and the associated stress raising behavior at these geometric discontinuities. Two common approaches are disk grinding and burr grinding. These approaches are often very aggressive and any time they are employed, there is an opportunity to over-grind and generate additional geometric discontinuity.

A second method employed can be termed *dressing*. These techniques seek to improve geometric discontinuity through additional weld material. GMAW procedures are most often utilized because their ability for welder to maintain control of the weld material being deposited. (South 1997) reports that TIG welding processes are able to address surface defects up to 6 mm below the surface of the base metal (*e.g.* a fairly severe undercut). As weld material is deposited, the heat input can alter the micro-structure of both the existing weld and base metal below the newly deposited weld material. This heat input can cause hardening and this, in turn, can cause brittle behavior and cracking. This hardening behavior tends to be more prevalent in high-carbon steels and low-carbon steels typical of those found in sign and signal supports may or may not be as susceptible to hardening and cracking caused by dressing. There is a significant level of skill needed to implement the dressing process.

The most popular and likely most effective process is peening. The peening approach seeks to smooth geometric discontinuity in the vicinity of the weld toe and introduce compressive residual stress states in the material near the surface of base metal and weld near the weld toe. There are mechanical means of peening (e.g. hammer peening, needle peening, shot (media) peening) and a relatively new approach implementing ultrasonic impact procedures. Mechanical peening methods utilize relatively common equipment, while the ultrasonic impact treatment (UIT) technique uses proprietary equipment. The equipment used for mechanical peening has significant noise and vibration associated with them and operators can suffer from fatigue. As a worker begins to tire using these mechanical peening approaches, the reliability of the technique may suffer resulting from inconsistency in peening depth and location.

A relatively new device with potential peening characteristics is currently being evaluated for removing corrosion from, and dressing, base metal surfaces prior to application of coatings (Stango and Khullar 2008). This bristle-blasting method appears to introduce peening characteristics to the surface of metals and it is conceivable that the tool can be used as a relatively economical mechanical peening device. The equipment and its potential for mechanical peening will be reviewed in greater detail in later chapters of the report. Unlike the treatment techniques discussed earlier in this section, the bristle-blaster has not had fatigue testing associated with it to the authors' knowledge.

Machietto (2002)

As discussed earlier, the focus of this research effort was mast arm connections. Welded gusset plates were considered in this effort to enhance the fatigue performance. Radial gussets with varying end termination conditions (refer to Figure E.2) were tested. Figures E.5 and E.6 illustrate how the gusset stiffened connections performed relative to the un-stiffened connections. Typical failures seen are shown in Figures E.4(a), E.4(b), and E.4(c). Specimen failures indicate that termination of the gusset plate stiffeners causes a geometric discontinuity and stress raiser behavior. Figure E.6 illustrates that all the gusset-stiffened connections migrated closer to the AASHTO E' fatigue detail category S-N curve. Therefore, the testing indicates that gusset stiffening is not as reliable as one would hope. It is not recommended for design or retrofit of mast-arm connections in the present research effort.

Koenigs (2003)

This University of Texas research effort, discussed earlier in this chapter, considered a wide variety of gusset-type stiffening configurations as well as external and internal collar reinforcement configurations. Figures G.2 and G.3 contain the gusset-type and collar-type reinforcement configurations utilized in the testing. The failures seen in the gusset stiffened specimens were similar to those seen in previous research efforts (Machietto 2002). Photographs of the typical failures seen are shown in Figures G.6 and G.7. The fatigue performance of gusset-reinforced connections is shown in Figure G.10. It is interesting to note that all tests lie very, very close to the AASHTO E' fatigue detail category. The testing data indicates that variability in fatigue performance may be reduced. This hypothesis will be discussed in later sections of this chapter that consider characterization of the uncertainty in fatigue performance.

This research effort also considered the effects of ultrasonic impact treatment (UIT) and galvanizing on fatigue performance. Figures G.8 and G.9 allow qualitative evaluation of the impact of UIT treatment and galvanizing. The data plotted in these figures are given in Tables G.2 and G.4 for unreinforced and stiffener-reinforced mast arm connections, respectively. If one compares the VAL-U-N specimens at stress ranges of approximately 12 ksi with the VAL-U-P specimen behavior at the 12 ksi stress range, it is difficult to definitively say that UIT reliably improves the fatigue performance. However, Figure G.9 illustrates that there was marked improvement in fatigue life (albeit one test) when UIT occurred post-galvanizing (VALN-U-GP versus VALN-N-U-G). Two tests with UIT treatment conducted in the unloaded state (VALN-U-P-UL) indicated significant improvement in fatigue performance at 12-ksi stress ranges as well. Therefore, the testing indicates that UIT post galvanizing and UIT performed in the unloaded state (UL specimens) may improve the fatigue life of a galvanized mast-arm-to-plate connection. It should be noted, however, that more tests need to be conducted to gain an understanding of the uncertainty associated with the UIT treatment technique. Review of past research efforts devoted exclusively to UIT (Palmatier and Frank 2005a; Palmatier

and Frank 2005b) indicates that the technique appears to be heavily dependent on operator skill and this may introduce significant variability in the fatigue-life improvement.

The gusset-reinforced specimens tested (Figures G.10 and G.12) indicate that gusset stiffening is not a reliable means with which to improve the fatigue performance of mast-arm-to-plate connections. The collar reinforced specimens also did not improve fatigue performance beyond the AASHTO E' fatigue detail category levels. Therefore, these alternate collar-type reinforcement details are not recommended in future evaluations and study.

(Ocel *et al.* 2006)

Ocel considered two general scenarios of stiffening and/or retrofit. The first was gusset plate stiffening of mast-arm-to-plate connections. The second was hammer peening of socketed fillet-weld pole base connections with and without simulation of dead loading.

Fatigue life data for the pole-base connections is given in Tables H.2, H.3, and H.5. This data is plotted along with non-retrofit connection details in Figures H.9, H.10, and H.11. The testing results in Tables H.1 and H.2 illustrate that there was an unfortunate lack of correlation between stress ranges between specimens tested with and without hammer peening. This research effort was one of, if not, the first experimental efforts devoted to studying these connections in detail and it could not directly benefit from prior testing of others. This was manifest in the use of equivalent constant amplitude stress ranges defined using Miner's Rule (MR) as indicated in Table H.2 to ensure timely testing.

One can definitely make qualitative statements regarding the benefit of hammer peening retrofit methods using the data in Tables H.1, H.2 and H.3. A direct comparison of two specimens in Table H.3 can be made. MN-P-FR2-IP-N-CSR-5-2.50-2 and MN-P-FR2-IP-HP-CSR-5-2.50-2 were both tested at 14.9 ksi stress range and were composed of the same mast arm and plate thickness in addition to being subjected to the same loading conditions (in-plane loading). There is an order of magnitude increase in fatigue life for the hammer-peened specimen (81,924 versus 978,382) indicating that hammer peening likely has a significant effect. Thus, this test comparison confirms long-standing understanding of the benefits of hammer peening in smoothing out geometric discontinuity in weld details. However, in order to fully understand the reliability associated with the peening method, additional testing at the same stress range with the same connection detail needs to be carried out.

The use of Miner's Rule to establish an equivalent constant amplitude stress range makes quantifying uncertainty difficult because there are quite a few equivalent constant amplitude stress ranges (refer to Table H.2). The potential for using these multiple Miner's Rule stress ranges in a systematic consideration of

uncertainty in fatigue life needs to be evaluated. Discussion of this will occur in a later section of this chapter.

FATIGUE-LIFE UNCERTAINTY CHARACTERIZATION

The main objective of the present study is to characterize the ***risk*** associated with fatigue-induced fracture in mast-arm signal and sign support structures. Integral to meeting this objective are outcomes associated with quantifying the uncertainty in fatigue performance of characteristic details, and the uncertainty in the performance improvement resulting from detail alterations or in-field retrofit treatments. Probability, reliability, and statistical methods have been applied in structural engineering for nearly three decades. Use of these procedures and principles, is integral to achieving the outcomes and objectives of the present research effort.

The goal of the present section in the report is to provide an overview of how uncertainty in fatigue performance can be quantified using probability theory. Much of this section is based upon two seminal works (Haldar and Mahadevan 2000; Nowak 2000). An outline discussion will be provided here and these documents contain much more details that simply cannot be addressed given the scope of the report.

Quantifying Fatigue-Life Variability

There have been a significant number of tests carried out to quantify the fatigue performance of mast-arm and pole base details similar to those used in Wisconsin for signal and sign support structures. These tests were reviewed in earlier sections of this chapter. In order to utilize these tests as the foundation for risk-assessment, there is a need to quantify the variability seen in the fatigue lives of these details. One mechanism to do this is to compare probability mass functions and cumulative distribution functions for the experimental data with those of standard probability distribution models.

Two common probability distribution models used in engineering applications are the normal and lognormal distributions. If we consider the fatigue life to be a normally distributed (or Gaussian) random variable, the probability density function (PDF) describing the fatigue life, *N*, can be written as,

$$f_N(x) = \frac{1}{\sigma_N \sqrt{2\pi}} \exp\left\{ -\frac{1}{2}\left(\frac{x-\mu_N}{\sigma_N} \right)^2 \right\} \quad -\infty < x < +\infty \tag{2.2}$$

where: μ_N is the mean (or expected) fatigue life; and σ_N is the standard deviation in fatigue life. These two quantities are often referred to as the parameters of the normal distribution. These parameters should be population parameters, but it is more likely that these parameters are defined using samples (individual experiments) taken from the population. The cumulative distribution function (CDF) that corresponds to the normal PDF is,

$$F_N(x) = \int_{-\infty}^{x} \frac{1}{\sigma_N \sqrt{2\pi}} \exp\left\{ -\frac{1}{2}\left(\frac{x-\mu_N}{\sigma_N} \right)^2 \right\} dx \tag{2.3}$$

The same parameters of the normal distribution are used.

The cumulative distribution function is a continuous function can be used to define probabilities of seeing a fatigue life equal less than a defined value. The median fatigue life, x_{med}, is defined as $F_N(x_{med}) = 0.50$. In terms of probabilities, this means that the probability of the fatigue life being less than or equal to x_{med} is 50%.

The lognormal distribution is a second very commonly used probability distribution for modeling uncertainty. The probability density function (PDF) for the lognormal random variable is,

$$f_{\ln N}(x) = \frac{1}{\sqrt{2\pi} \cdot \zeta_{\ln N} \cdot x} \cdot \exp\left\{ -\frac{1}{2}\left(\frac{\ln x - \lambda_{\ln N}}{\zeta_{\ln N}} \right)^2 \right\} \quad 0 \le x < +\infty \tag{2.4}$$

where the parameters of the lognormal distribution are,

$\lambda_{\ln N} = \ln \mu_{\ln N} - \frac{1}{2}\zeta_{\ln N}^2$, is the expected value of the lognormal random variable,

$\zeta_{\ln N}^2 = \ln\left[1 + \left(\frac{\sigma_{\ln N}}{\mu_{\ln N}} \right)^2 \right]$, is the variance of the lognormal random variable.

The term, $(\sigma_{\ln N} / \mu_{\ln N})$, is the coefficient of variation of the lognormal random variable. If this value is not large, $\zeta_{\ln N} = \sigma_{\ln N} / \mu_{\ln N}$. The cumulative distribution function (CDF) for the lognormal random variable is essentially the CDF for the standard normal random variable.

$$F_{\ln N}(x) = \Phi\left[\frac{\ln x - \lambda_{\ln N}}{\zeta_{\ln N}} \right] \tag{2.5}$$

where $\Phi[\ ]$ is the CDF for the standard normal distribution (mean zero, standard deviation of 1.0).

A *population* can be defined within the context of the present study as all mast-arm-to-plate or pole-base connections of common configuration. The review conducted earlier in this chapter defined many potential populations for connection details. A *sample* is the suite experimental tests conducted for any given connection detail at a defined stress range. Therefore, the earlier review discussed many samples taken from the potential populations and presented the data for these samples. Risk characterization demands that we have information regarding the fatigue performance of *populations*. However, we are only able to collect samples from the population. Collecting enough samples to *definitively* quantify the probability distribution and the parameters needed to define this distribution is infeasible. However, there are statistical methods

available that can be used to quantify the parameters of the distribution within confidence-level windows. These procedures, however, demand that a probability distribution be defined for the sample.

The experimental data collected and discussed in earlier sections of this chapter can be used to select the likely probability distribution for the sample. Once this probability distribution is selected, one can use the information from the sample to gain insights into the probability distribution parameters for the population from which the sample was taken.

The Kolmogorov-Smirnov (K-S) test is a *goodness of fit* test that compares the cumulative distribution frequency for a sample with the CDF of an assumed theoretical probability distribution. The K-S test allows the sample to be tested against CDF's for random variables. The goal of this testing is to select a probability distribution that is most likely to represent the population from which the sample experimental data was taken. The K-S test is used in this chapter to evaluate theoretical CDF's with regard to their applicability in representing the fatigue-life variability of connection details found in Wisconsin.

Mast-arm-to-plate connection data will be considered first. Data from the previous experimental testing was synthesized and categorized according to configuration and stress range. It should be noted that the fatigue failures seen in the connections included in this statistical synthesis occurred in the mast arm wall. There was no distinction made between socketed fillet weld connections and full penetration connections. If fatigue failure occurred in the mast-arm wall, variation in these connections was assumed to be negligible. This assumption will be proven valid after the fatigue-lives are compared.

The experimental data for un-stiffened mast-arm-to-plate connections used for the statistical synthesis and uncertainty characterization are given in Table 2.1. It should be noted that the experimental data is taken from Tables in Appendices A through I. The target stress ranges for experimental tests across research efforts are fairly close to one another in many cases. Table 2.1 contains the actual stress range reported and a rounded stress range for purposes of the present fatigue life uncertainty characterization. Three stress ranges are considered for un-stiffened mast-arm connections: 6, 12, and 15 ksi. The procedure for generating the cumulative distribution frequency for the experimental sample, $S_N(x)$, is as follows. The experimental data (*i.e.* number of cycles to failure at a given stress range) are ordered from lowest to highest. The cumulative distribution frequency for the sample is then established. Table 2.1 contains the ordered fatigue lives and the cumulative distribution frequency values. The sample mean and standard deviation for the samples at each stress range were then computed. Table 2.2 contains the mean and standard deviation for the sample. It should be noted that the natural log of each fatigue life is taken and means and standard deviations of these natural logs are used to define the parameters of the lognormal cumulative distribution function. These are also given in Table 2.2.

The K-S test consists of evaluating the difference between the cumulative distribution frequency for the sample and the cumulative distribution function for a population with the sample mean and sample standard deviation. The K-S test was applied using the experimental data, the normal CDF, and the lognormal CDF. The differences used for the K-S test are given in Table 2.1 in the column headed by $|F_E - S_n|$. F_E is the value of the lognormal CDF for the given sample test fatigue life value and S_n is the cumulative distribution frequency value for the sample test fatigue life value.

The CDF *fit* with regard to the sample experimental data can be evaluated using this maximum difference. A *significance level* for the fit can be defined (Haldar and Mahadevan 2000). The maximum difference allows the acceptability of the CDF model to be evaluated with a variety of confidence levels for various sample sizes. Tables of K-S test data are available (Haldar and Mahadevan 2000). The present analysis will assume 5% significance level. This significance level corresponds to the following statement. In 5 out of 100 fatigue tests, the defined CDF *cannot* be considered an adequate CDF model. An analogous statement is: in 95 out of 100 fatigue tests, the defined CDF can be considered an adequate CDF model. Thus, the 5% significance level can be thought of as a 95% confidence level.

The K-S test was performed for the lognormal CDF for the experimental data given in Table 2.1. The maximum difference between the cumulative distribution frequency for the sample and the lognormal CDF model is indicated in bold font in the final column in the table. The maximum differences are 0.0794, 0.1770, and 0.1783 for 6, 12, and 15 ksi stress ranges, respectively. There were 10 samples at 6 ksi stress range, 12 samples at 12 ksi stress range, and 7 samples at 15 ksi stress range. The maximum difference for 5% significance are; $D_{10}^{0.05} = 0.409$, $D_{12}^{0.05} = 0.375$, and $D_{7}^{0.05} = 0.486$; respectively (Haldar and Mahadevan 2000). As a result, a lognormal distribution can be used to model the sample data with 95% confidence. It should be noted that a normal distribution was tested as well and the lognormal model was found to be a better fit.

The quality of the representation by the CDF models can also be evaluated graphically by plotting the cumulative distribution frequency for the experimental sample and the CDF model. This graphical comparison is illustrated in Figure 2.9. The 6 ksi and 15 ksi samples follow the lognormal CDF model very well and this confirms the use of the K-S test. There is some discrepancy at the 12 ksi stress range and this suggests that it may be prudent to conduct further experimental testing at this stress range to confirm and improve the CDF modeling. One could also argue that using the data at the 6 ksi and 15 ksi stress ranges with linear interpolation between these two extremes might be a good way to model the entire range of stress ranges possible for a given connection detail. It is interesting to note that as the stress range decreases the variability in fatigue life increases. This phenomenon has been known for some time (Little and Jebe 1975) and it suggest that the stress ranges seen in service can be a critical parameter in evaluating risk of fatigue-

induced fracture. In other words, if stress ranges seen in the field are high (*e.g.* 15 ksi), there will be much less variability in fatigue life expected. However, if the stress ranges applied are very low (*e.g.* 5 ksi), then the fatigue life can vary widely. It also suggests and confirms that fatigue life at low stress ranges is highly variable and dependent upon many fabrication-related issues (Little and Jebe 1975).

A similar K-S test evaluation of CDF models was also performed for the un-stiffened pole-base connection details surveyed in the previous sections of this chapter. The data used for the K-S test are given in Tables 2.3 and 2.4. It should be noted that there are relatively few specimens tested at lower stress ranges (3 total). The final column illustrates maximum differences between cumulative distribution frequencies and lognormal CDF models of 0.1392, 0.1685, and 0.1244 for 5 ksi, 12 ksi, and 15 ksi, respectively. The maximum difference for 5% significance are; $D_3^{0.05} = n.a.$, $D_5^{0.05} = 0.563$, and $D_7^{0.05} = 0.486$; respectively (Haldar and Mahadevan 2000). Three specimens are not really enough to conduct the K-S test so the quality of the lognormal CDF to model fatigue-life variability at the 5-ksi stress range and therefore it will be done graphically. Figure 2.10 illustrates graphical comparison of lognormal CDF models for fatigue life with the cumulative distribution frequencies for the samples. As expected, the 5 ksi stress range sample is simply too small to make any statement regarding the quality of the lognormal CDF for modeling fatigue life variability. The 12-ksi and 15-ksi stress ranges are modeled quite well by a lognormal CDF. The statistical synthesis conducted for the pole-base connections suggests that more experimental data at low stress ranges is needed to more adequately characterize fatigue life variability in the pole-base connections.

There were a significant number of tests conducted at 12-ksi stress range for gusset-stiffened mast arm connections. This affords the variability in fatigue life for this connection configuration to be quantified. The failures seen in gusset-stiffened mast arm connections suggest that the geometric discontinuity present at the termination of the gusset plate is the driving factor defining the fatigue life. As a result, it was decided to include all gusset plate arrangements at the 12-ksi stress range magnitude in the statistical synthesis. The test data included in the sample of gusset-stiffened mast-arm connections are provided in Tables 2.5 and 2.6.

The K-S test conducted for the gusset-stiffened mast-arm connections included both normal and lognormal CDF's. The maximum differences between the cumulative distribution frequency for the experimental sample and the CDF models are provided in Table 2.5. Both distributions can be considered adequate at the 5% significance level using procedures employed earlier in this section (Haldar and Mahadevan 2000). The normal CDF is seen to be a slightly better model for the gusset-stiffened experimental data. Figure 2.11 illustrates a graphical comparison of the sample cumulative distribution frequency and the CDF models. The ability of the normal CDF to more accurately model the variability the gusset-stiffened mast-arm connection fatigue life can be seen in this Figure. However, one might say that the lognormal model is acceptable for engineering purposes at the 5% significance level.

The statistical review and synthesis of the experimental tests conducted on connections typically used in Wisconsin sign and signal support structures suggests that lognormal cumulative distribution functions can be used to model fatigue life variability of un-stiffened, untreated, non-galvanized mast-arm-to-plate connections. The lognormal models can be used for pole-base connections at higher stress ranges (*e.g.* 12 and 15 ksi). However, additional pole-base connections at lower stress range (*e.g.* 5 ksi) should be tested to confirm the suitability for the lognormal CDF. If gusset-stiffening is utilized, a lognormal CDF model is appropriate for a fairly wide variety of gusset arrangements. Additional fatigue testing of specimens utilizing UIT and mechanical (hammer) peening should be conducted so that CDF models can be validated.

Now that suitable CDF models have been defined for the connections, one can now proceed to evaluate the uncertainty in the distribution model parameters given the limited sample sizes used in the experimentation. This is the objective of the next section in the chapter.

Interval Estimation for Mean

One can argue that the sample experimental tests follow the lognormal distribution. However, a quantitative understanding of the parameters defining the lognormal distribution remains. In other words, it has been demonstrated that the samples are modeled by the lognormal distribution quite nicely, but one does not know the mean and standard deviation for the populations. The uncertainty and variability associated with fatigue life of connection details requires that the population mean and population variance be quantified with boundaries and confidence limits. Furthermore, there is a need to evaluate the current sample sizes and evaluate these within the context of confidence levels and boundary widths for quantifying the range(s) within which the population mean fatigue life and population fatigue life variance lie. In this manner, critical evaluation of the current sample sizes used to quantify uncertainty can take place. This is the main objective of the present section.

As with any engineering analysis, there are several assumptions that need to be made. The largest sample size for any connection detail test is 12 for un-stiffened connections and 13 for the gusset stiffened mast – arm-to-plate connections. Therefore, the standard deviation (and variance) of the samples are known and it has been recommended that if the sample size is large enough, one can assume that the sample variance is the population variance (Haldar and Mahadevan 2000). The threshold for "large enough" has been recommended as approximately 10, which is very near the largest sample size for the fatigue testing considered. Therefore, it will be assumed that the population variance *is not* known.

If one were to implement a process of taking samples from the population of connections, conducting fatigue testing, evaluating the mean fatigue life of the sample set, and collecting means for all samples; it is likely that the sample means will be normally distributed. This is, in effect, the assumption made. Therefore,

it will be assumed that the mean fatigue lives for all potential samples are normally distributed. If the mean of a sample and variance of a sample is known, but the population variance is unknown, Student's t-distribution with $(n-1)$ degrees of freedom can be used to generate interval estimations for the population mean. For a sample of size *n*, with mean, $\overline{x}_N$, and standard deviation, s_N, the $(1-\alpha)$ confidence interval for the population mean is (Haldar and Mahadevan 2000),

$$\langle \mu \rangle_{1-\alpha} = \left[\overline{x} - t_{\alpha/2,n-1} \cdot \frac{s}{\sqrt{n}} ; \overline{x} + t_{\alpha/2,n-1} \cdot \frac{s}{\sqrt{n}} \right] \tag{2.6}$$

Equation (2.6) can be used to establish 95% confidence intervals for the population means for the connection details tested and discussed earlier in this chapter.

The process of establishing mean fatigue life intervals can begin with the testing data contained in Tables 2.1 and 2.2. Table 2.7 contains the 90%, 95%, 97.5% confidence level intervals for the three tested connection configurations outlined earlier in the chapter. As expected, the width of the interval estimate increases with the level of confidence (Haldar and Mahadevan 2000). Lower stress ranges also tend to have very wide interval estimates resulting from the significant variability in the experimental results. Also, a lack of sample size tends to lead to very wide and rather inconclusive estimates for the population mean. For example, the pole base connections should definitely have additional samples tested to reduce the mean interval estimate for any given level of confidence.

It is recommended that the 90% confidence level be established as targets for the second phase of the research effort that includes fatigue testing. Sample sizes will be established using this target confidence coupled with the desire to meet practical constraints on testing time and testing equipment. Future discussion related to population variance and sample sizes will support this decision. It should be noted that the 15-ksi stress range for the un-stiffened and gusset-stiffened mast arm connections have relatively narrow mean intervals (approximately 17% of sample mean) at 90% confidence levels. As outlined earlier, the pole base connections require additional testing to help narrow the mean intervals.

Interval Estimation for Variance

The second parameter that is important for understanding the population variability is the variance. The square root of the variance is an estimate for the standard deviation. Assuming a normal distribution for the parameters describing the variability in the population (*e.g.* mean, variance), the Chi-Square distribution can be used obtain estimates for the population variance for various significant levels. The two-sided $(1-\alpha)$ confidence interval for the population variance can be estimated using (Haldar and Mahadevan 2000),

$$\langle \sigma_N^2 \rangle_{1-\alpha} = \left[\frac{(n-1)s_N^2}{c_{1-\alpha/2,n-1}} ; \frac{(n-1)s_N^2}{c_{\alpha/2,n-1}} \right] \tag{2.7}$$

where $c_{1-\alpha/2,n-1}$ and $c_{\alpha/2,n-1}$ are values of the Chi-Squared cumulative distribution function for *n* degrees of freedom. Tables of these values are available (Haldar and Mahadevan 2000).

Table 2.8 contains population variance estimates for three confidence levels: 90%, 95% and 97.5%. As in the case of the population mean; the interval estimate for variance widens as the confidence level increases. Sample size also has a significant impact on the interval width. It is recommended that the population mean be used as the target parameter for establishing sample size. Once this sample size is established, there will be direct and connected impact on the variance estimate for the population. As a result, once the experimental testing is completed using a sample size defined using a target population mean interval at 90% confidence; the interval estimate for the population variance can be used to help guide the risk assessment to be conducted in phase 3 of the research effort.

Sample Size Estimation

Perhaps the most important aspect to the present fatigue data synthesis is to help guide the number of connection tests that should be conducted moving forward. Student's *t*-distribution is also utilized to compute an estimate for the sample size required to meet a targeted population mean interval for various levels of confidence when the population variance is unknown. Assuming a target mean interval defined as $\Delta\overline{x}_N$ above and below the sample mean fatigue life, the sample standard deviation, s_N, and Student's t-distribution for the $(1-\alpha)$ confidence level can be used to estimate a sample size required to meet that interval with the target confidence. This calculation is given by (Haldar and Mahadevan 2000),

$$n = \left[\frac{s_N}{\Delta\overline{x}_N} \cdot \left(t_{\alpha/2,n-1} \right) \right]^2 \tag{2.8}$$

It should be emphasized that equation (2.8) includes the sample size, n, on both sides of the equal sign. In other words, Student's t-distribution requires a sample size to define the degrees of freedom and we are computing the sample size. Iteration is required to solve (2.8) and very few iterations are needed.

Table 2.9 contains sample sizes for target mean interval widths (above and below) the sample mean. These widths are also expressed as a percentage of the sample mean. As outlined earlier, a 90% confidence level is sought and this directly influences the sample sizes computed. The number of samples tested to date for each connection configuration is given in Table 2.9 as well. Equation (2.8) is used to establish a number of sample tests that seeks to balance connection test effort with estimated improvement in reducing the mean interval width. As an example of this process, we can consider the un-stiffened mast arm connection at 15-ksi stress range. To date, there have been seven (7) connection tests at this stress range. The mean and standard deviation of this sample is included in Table 2.9. Given this seven-test sample set, the 90% confidence interval on the population mean is 17% of the mean (refer to Table 2.7). Table 2.9 illustrates that if the

sample size is increased to 16 (9 more tests), this interval estimate can be reduced to 10% of the mean (from 17%) and the level of confidence can remain at 90%. For the gusset-stiffened mast arm connections, an additional five tests can reduce the mean interval from 18% to 15% and the confidence level will remain at 90%. This brief analysis suggests that it would be more beneficial to conduct the 9 additional tests of un-stiffened mast arm connections rather than the additional 5 gusset-stiffened connection specimens.

Lower stress ranges tend to have much greater variability and as a result, sample sizes required to meet 90% confidence levels can be quite high. The mean intervals for these confidence levels can also be quite wide as a result of this variability. Table 2.7 illustrates that the current 10-sample suite of un-stiffened mast arm connections tested at 6-ksi stress range has a mean interval estimate of 31% at 90% confidence. Table 2.9 illustrates that this mean interval can be reduced to 20% if an additional 12 tests (22 total) are performed. If these additional twelve tests are possible, it will yield a significant improvement in our understanding of the fatigue performance of un-stiffened mast arm connections.

There are very few tests conducted for pole-base connections with characteristics similar to those used in Wisconsin. As a result, Table 2.7 illustrates the mean intervals for the populations at all stress ranges are very wide (a minimum of 61% of the sample mean). Table 2.9 indicates that the largest impact on reducing these interval sizes would be to conduct additional testing at the 5-ksi and 12-ksi stress ranges. If at all possible, it is recommended that additional testing focus on the 5-ksi stress range. Furthermore, there will be an estimated 20% reduction in the mean interval at 90% confidence generated by seven additional tests at 15-ksi stress range.

SUMMARY, CONCLUSIONS AND RECOMMENDATIONS

A review of connection details commonly found in Wisconsin DOT sign and signal support structures was provided in this chapter. The material specifications used by WisDOT for steel sign and signal support structures were reviewed and the manufacturers and the typical configurations of the structural systems they historically provided to the state of Wisconsin were discussed. This information was used to frame the review and synthesis of fatigue testing completed to date. A relatively brief review of the methods often used to characterize fatigue life and variability in this life was provided.

A review of fatigue testing completed through earlier research efforts was conducted. The fatigue testing efforts reviewed included connection details that were typical of those used in the state of Wisconsin and these included unreinforced, untreated (*e.g.* no UIT, no mechanical peening), and reinforced connections. The connection configurations included those commonly found in monotube-type mast-arm structures. These were the mast-arm-to-plate connection and the connection commonly found at the pole base. I t should be noted that a research effort focusing on connections found in high-mast luminaire support structures was

included in this review as the pole-base connections commonly used for these systems are the same as those used at the pole base in mast-arm signal and sign support structures.

The fatigue testing results was synthesized using accepted and well-established statistical analysis methods. This synthesis allowed the uncertainty in fatigue life to be quantified for many of the connection configurations tested. The statistical analysis included selecting a cumulative distribution function model suitable for modeling the uncertainty in the test samples; developing bounds on population mean and population variance with various confidence levels; and recommendations for sample sizes for the fatigue testing to be conducted as part of the present study.

The synthesis of fatigue testing conducted to date affords several recommendations moving forward into the second phase of the research effort. These recommendations are based upon the knowledge of fatigue life variability gained from the testing. The Kolmogorov-Smirnov goodness of fit test indicated that the variability in all fatigue tests conducted to date can be modeled using lognormal cumulative distribution functions (CDFs). In the case of gusset-stiffened mast arm connections, a normal CDF appeared to be a better model for the sample experimental data, but a lognormal CDF was suitable.

It should be emphasized that there is a need to be sensitive to the fatigue lives that are likely to occur at low stress ranges. The experimental testing done to date follows a long-known trend with regard to variability in fatigue life: as the stress range decreases, the variability in fatigue life increases (Little and Jebe 1975). The next phase in the present research effort may not be able to include the number of tests at the low stress ranges needed to achieve targeted mean interval estimates because the testing duration may be too great (number of stress cycles required to initiate fatigue failure may be too large). This issue will require detailed evaluation as testing recommendations and protocols are finalized.

The previous testing included several protocols and specimen configurations. It is recommended that a testing arrangement similar to that used by (Koenigs *et al.* 2003) be utilized in this research effort. Rather than loading two specimens simultaneously, it is recommended that the "strong box" concept schematically shown in Figure G.4 (b) be maintained. It may be more useful to mount single specimens to a fixed mounting box. This can allow connections to be tested in multiple directions as well as "out-of-plane". Details of the testing specimen and protocol will need to be worked out with the testing contractor for the second phase of the research.

The previous statistical analysis of the fatigue testing suggests that further testing be conducted for the following connection configurations and stress ranges. It is recommended that an additional nine (9) un-stiffened mast arm connections be tested at a stress range of 15 ksi. Tables 2.7 and 2.8 indicate that any specimen in this new set of nine tests may have a fatigue life equal to 750,000 cycles (90% upper-bound mean

plus two 90% upper-bound standard deviations). Thus, an estimate for the number of test cycles at 15-ksi stress range is 6,750,000 cycles to complete the suite of tests. It is also recommended that these 15-ksi stress range tests be supplemented with an additional twelve (12) tests at 6-ksi stress range. Using the same upper-bound mean plus two upper-bound standard deviation estimation procedures, Tables 2.7 and 2.8 indicate that each test in this suite could have fatigue lives of 7,726,615 stress-range cycles. Thus, these additional tests could demand as many as 92,000,000 cycles to complete. This may or may not be feasible, and discussions with the testing contractor will need to occur. However, if the recommended tests are conducted at these two stress ranges, there will be significant enhancement in the understanding of uncertainty in the fatigue life of un-stiffened mast arm connections that will provide a very sound foundation for the risk assessment to be conducted in phase 3 of the research effort.

The expected number of stress cycles required to characterize uncertainty in the un-stiffened mast-arm connections may preclude additional testing for pole-base connections. This is felt to be an acceptable compromise as pole-base connections have not suffered from premature fatigue failures in Wisconsin. Therefore, it is expected that the present research effort will not be able to address risk of fatigue-induced fracture in pole-base connections. Future research efforts should address these connections as they are integral to characterizing fatigue performance of the entire signal or sign support structural system.

There are very few tests that have been conducted on retrofitted connections (*e.g.* hammer peening, UIT). Therefore, it is recommended that additional fatigue life testing be conducted for a single retrofit measure. It is also recommended that the rotary brush tool currently being evaluated for surface preparation (Stango and Khullar 2008) be considered as a potential retrofit measure. This will be discussed further in the final chapter of the report.

REFERENCES

AASHTO. (1975). *Standard Specifications for Structural Supports for Highway Signs, Luminaires and Traffic Signals*, American Association of State Highway Transportation Officials, Washington, D.C.

AASHTO. (1996). *Standard Specifications for Highway Bridges*, American Association of State Highway and Transportation Officials, Washington, D.C.

AASHTO. (2001). *Standard Specifications for Structural Supports for Highway Signs, Luminaires and Traffic Signals, 4th Edition with 2006 Interim Revisions*, American Association of State Highway and Transportation Officials, Washington, D.C.

Alderson, J. L. (1999). "Fatigue Study of Cantilevered Traffic Signal Mast Arms," MS Thesis, University of Missouri - Columbia.

Archer, G., and Gurney, M. (1970). "Fatigue Strength of Mild-Steel Fillet Weld Tube to Plate Joints." *Metal Construction and British Welding Journal*, 2(5), Welding Institute, Cambridge, U.K., 207-210.

Chen, G., Barker, M., Dharani, L. R., and Ramsay, C. (2003). "Signal Mast Arm Fatigue Failure Investigation." *Report RDT 03-010*, Missouri Department of Transportation, Jefferson City, MO.

Deschamp, B. (2002). "Fatigue Testing of Traffic Signal Structures," M.S. Thesis, University of Wyoming, Laramie, WY.

Fisher, J. W., Slutter, R. G., and Miki, C. (1981). "Fatigue Behavior of Steel Light Poles." *FHWA/CA/SD - 81/82*, California Department of Transportation, Sacramento, CA.

Foley, C. M., Ginal, S. J., Peronto, J. L., and Fournelle, R. A. (2004). "Structural Analysis of Sign Bridge Structures and Luminaire Supports." *WHRP 04-03*, Wisconsin Highway Research Program, Madison, WI.

Foley, C. M., Peronto, J. L., and Fournelle, R. A. (2006). "Fatigue Prediction and Variability of New and Existing Welded CHS Y-Joints." *Engineering Journal*, 43(1), American Institute of Steel Construction, 57-80.

Haldar, A., and Mahadevan, S. (2000). *Probability, Reliability, and Statistical Methods in Engineering Design*, John Wiley & Sons, Inc., New York, NY.

Hall, J. H. (2005). "The Effect of Base Plate Flexibility on the Fatigue Performance of Welded Socket Connections in Cantilevered Sign Structures," MS Thesis, Lehigh University, Bethlehem, PA.

Hall, J. H., and Connor, R. J. (2008). "Influence of Base Plate Flexibility on the Fatigue Performance of Welded Socket Connections." *Journal of Structural Engineering*, 134(6), American Society of Civil Engineers, 911-918.

Koenigs, M. T., Botros, T. A., Freytag, D., and Frank, K. H. (2003). "Fatigue Strength of Signal Mast Arm Connections." *CTR Research Report 4178-2*, Center for Transportation Research at the University of Texas at Austin, Austin, TX.

Little, R. E., and Jebe, E. H. (1975). *Statistical Design of Fatigue Experiments*, Applied Science Publishers, Ltd., London, U.K.

Machietto, C. (2002) "Valmont Fatigue Testing Presentation." *AASHTO T-12 Committee, November*, Las Vegas, NV (Electronic Presentation - Unpublished).

Nowak, A. S., Collins, Kevin R. (2000). *Reliability of Structures*, McGraw-Hill, New York, NY.

Ocel, J. M. (2006). "The Behavior of Thin Hollow Structural Section (HSS) to Plate Connections," PhD Thesis, University of Minnesota, Minneapolis, MN.

Ocel, J. M., Dexter, R. J., and Hajjar, J. F. (2006). "Fatigue-Resistant Design for Overhead Signs, Mast-Arm Signal Poles, and Lighting Standards." *Report No. MN/RC-2006-07*, Minnesota Department of Transportation, St. Paul, MN.

Palmatier, A. H., and Frank, K. H. (2005a). "Application of Ultrasonic Impact Treatment to In-Service Signal Mast Arms." *CTR Research Report 5-4178-01-2*, Center for Transportation Research at the University of Texas at Austin, Austin, TX.

Palmatier, A. H., and Frank, K. H. (2005b). "UIT Application During Fabrication." *CTR Research Report 5-4178-01-3*, Center for Transportation Research at the University of Texas at Austin, Austin, TX.

Rios, C. A. (2007). "Fatigue Performance of Multi-Sided High-Mast Lighting Towers," MS Thesis, University of Texas at Austin, Austin, TX.

South, J. (1997). "Fatigue of Tube-to-Plate Fillet Welds and Methods for Their Improvement." *Physical Research Report No. 118*, Illinois Department of Transportation, Springfield, IL.

Stango, R. J., and Khullar, P. (2008). "Introduction to the Bristle Blasting Process for Simultaneous Corrosion Removal/Anchor Profile." *Corrosion & Materials*, 33(5 - October), Australasian Corrosion Association, Victoria, Australia, 26-31.

Walbridge, S. (2005). "A Probabilistic Study of Fatigue of Post-Weld Treated Tubular Bridge Structures," D.Sc. Thesis, Ecole Polytechnique Federale de Lausanne, Lausanne, Switzerland.

WisDOT. (2008). *WisDOT Bridge Manual*, Wisconsin Department of Transportation, Bureau of Structures, Madison, WI.

Table 2.1 Kolmogorov-Smirnov (K-S) Test for Selected Experimental Un-stiffened Mast-Arm Fatigue Data and Lognormal Cumulative Distribution Function Model.

Specimen Designation	$\Delta\sigma$	$\Delta\sigma_r$	N	$S_n(e_m)$	$F_E(e_m)$	$\lvert F_E - S_n \rvert$
WY-IS-S-2.00-6-12.25	5.51	6.00	750,000	0.0909	0.0336	0.0573
LEH-40-A-45CA-5	6.40	6.00	1,208,700	0.1818	0.1572	0.0246
LEH-40-A-45CA-6	6.40	6.00	1,472,900	0.2727	0.2531	0.0196
LEH-40-A-45CA-3	6.40	6.00	1,892,400	0.3636	0.4083	0.0447
VAL-U-N-C	6.29	6.00	2,072,592	0.4545	0.4702	0.0156
TX-U-N-A	6.20	6.00	2,199,343	0.5455	0.5110	0.0344
TX-U-N-B	6.10	6.00	2,816,706	0.6364	0.6754	0.0391
LEH-40-A-34CA-2	6.40	6.00	3,573,400	0.7273	0.8067	**0.0794**
LEH-40-A-34CA-1	6.40	6.00	3,751,600	0.8182	0.8289	0.0107
LEH-48-V-28CA-5	6.40	6.00	5,186,500	0.9091	0.9344	0.0253
LEH-40-A-45CA-2	12.40	12.00	117,800	0.0769	0.1269	0.0500
LEH-40-A-45CA-4	12.40	12.00	174,200	0.1538	0.2121	0.0583
TX-U-N-D	12.00	12.00	194,694	0.2308	0.2414	0.0106
LEH-48-V-28CA-4	12.40	12.00	198,100	0.3077	0.2461	0.0616
VAL-U-N-A	11.90	12.00	249,446	0.3846	0.3138	0.0708
VALN-U-N-B	11.80	12.00	265,540	0.4615	0.3334	0.1281
LEH-48-V-28CA-2	12.40	12.00	317,500	0.5385	0.3919	0.1465
VALN-U-N-A	11.90	12.00	389,428	0.6154	0.4619	0.1535
VAL-U-N-B	11.90	12.00	453,948	0.6923	0.5153	**0.1770**
VALN-U2-N-B	11.80	12.00	1,683,127	0.7692	0.8818	0.1126
TX-U-N-C	11.80	12.00	1,775,696	0.8462	0.8908	0.0447
VALN-U2-N-A	11.90	12.00	5,144,528	0.9231	0.9847	0.0616
MN-MA-FR3-IP-N-CSR-5-1.25-1	15.37	15.00	242,060	0.1250	0.0748	0.0502
MN-MA-FR3-IP-N-CSR-5-1.25-2	15.37	15.00	267,922	0.2500	0.1540	0.0960
MN-MA-FR3-IP-N-CSR-5-1.25-2	15.37	15.00	298,023	0.3750	0.2818	0.0932
MN-MA-FR3-IP-N-CSR-5-1.25-2	15.37	15.00	372,056	0.5000	0.6345	0.1345
MN-MA-FR3-IP-N-CSR-5-1.25-2	15.37	15.00	420,662	0.6250	0.8033	**0.1783**
MN-MA-FR3-IP-N-CSR-5-1.25-1	15.37	15.00	420,785	0.7500	0.8037	0.0537
MN-MA-FR3-IP-N-CSR-5-1.25-1	15.37	15.00	434,329	0.8750	0.8380	0.0370

Table 2.2 Sample Parameters for Generation of Lognormal CDF Model for Un-stiffened Mast-Arm Fatigue Test Data.

Stress Range (ksi)	$\bar{x}$	s	$\bar{x}_{\ln N}$	$s_{\ln N}$
6	2,492,414	1,352,480	14.5876	0.5791
12	913,667	1,450,622	12.9819	1.1436
15	350,884	80,297	12.7440	0.2408

Table 2.3 Kolmogorov-Smirnov (K-S) Test for Selected Experimental Un-stiffened Pole-Base Fatigue Data and Lognormal Cumulative Distribution Model.

Specimen Designation	$\Delta\sigma$	$\Delta\sigma_r$	N	$S_n(e_m)$	$F_E(e_m)$	$\lvert F_E - S_n \rvert$
MN-P-FR1-OP-N-CSR-5-1.25	5.41	5.00	17,0606	0.2500	0.2197	0.0303
MN-P-FR1-OP-N-CSR-5-1.25	5.41	5.00	301,484	0.5000	0.3608	**0.1392**
MN-P-FR1-OP-N-CSR-5-1.25	5.41	5.00	2,293,739	0.7500	0.8706	0.1206
UTX-24-1.5-8-S	12.00	12.00	13,193	0.1667	0.0966	0.0701
UTX-24-1.5-12-S	12.00	12.00	27,977	0.3333	0.2797	0.0536
UTX-24-2.0-8-S	12.00	12.00	46,772	0.5000	0.4629	0.0371
UTX-24-2.0-12-S	12.00	12.00	143,214	0.6667	0.8352	**0.1685**
UTX-24-3.0-8-S	12.00	12.00	147,550	0.8333	0.8422	0.0088
MN-P-FR2-IP-N-CSR-5-2.50-2	14.90	15.00	81,924	0.1250	0.1653	0.0403
MN-P-FR2-IP-N-CSR-3-2.50-2	15.00	15.00	86,888	0.2500	0.1862	0.0638
MN-P-FR2-IP-N-CSR-5-2.50-2	14.90	15.00	101,916	0.3750	0.2506	**0.1244**
MN-P-FR2-IP-N-CSR-3-2.50-2	15.00	15.00	140,545	0.5000	0.4089	0.0911
MN-P-FR2-IP-N-CSR-3-2.50-1	15.00	15.00	183,638	0.6250	0.5547	0.0703
MN-P-FR2-IP-N-CSR-3-2.50-1	15.00	15.00	330,137	0.7500	0.8275	0.0775
MN-P-FR2-IP-N-CSR-5-2.50-1	14.90	15.00	566,119	0.8750	0.9541	0.0791

Table 2.4 Sample Parameters for Generation of Lognormal CDF Model for Pole-Base Fatigue Test Data

Stress Range (ksi)	$\bar{x}$	s	$\bar{x}_{\ln N}$	$s_{\ln N}$
5	921,943	1,189,811	13.1031	1.3659
12	75,741	64,695	10.8507	1.0477
15	213,024	177,928	12.0208	0.7270

Table 2.5 Kolmogorov-Smirnov (K-S) Test for Selected Experimental Gusset-Reinforced Mast-Arm Fatigue Data.

Specimen Designation	$\Delta\sigma$	$\Delta\sigma_r$	N	$S_n(e_m)$	Normal $\lvert F_E - S_n \rvert$	Lognormal $\lvert F_E - S_n \rvert$
VALN-6x3/8@45-N-B	11.98	12.00	161,843	0.0714	0.0403	0.0621
VALN-6x3/8@45-N-A	11.96	12.00	238,515	0.1429	0.0681	0.0736
VAL-3x3/8-N-A	11.70	12.00	386,253	0.2143	0.0515	**0.1301**
VAL-3x3/8N-B	11.60	12.00	410,410	0.2857	0.0256	0.1099
TX-3x1/4-N-B	11.80	12.00	416,146	0.3571	0.0346	0.0506
TX-3x3/8-N-A	11.70	12.00	473,735	0.4286	0.0148	0.0942
VAL-3x1/4-N-A	11.10	11.00	476,269	0.5000	0.0511	0.0275
TX-3x1/4-N-C-LMS	11.90	12.00	523,397	0.5714	0.0190	0.0391
TX-3x1/4-N-A	11.70	12.00	616,136	0.6429	**0.0973**	0.0981
VAL-6x3/8-N-B	11.30	11.00	653,392	0.7143	0.0879	0.0674
TX-3x3/8-N-B	11.60	12.00	657,716	0.7857	0.0231	0.0003
VAL-3x1/4-N-B	11.40	11.00	696,326	0.8571	0.0043	0.0357
TX-6x3/8-N-A	11.20	11.00	783,857	0.9286	0.0132	0.0463

Table 2.6 Sample Parameters for Generation of CDF Models for Gusset-Reinforced Mast-Arm Connections

$\bar{x}$	s	$\bar{x}_{\ln N}$	$s_{\ln N}$
499,538	181,081	13.0429	0.4460

Table 2.7 Population Mean Fatigue Life Estimates for Various Confidence Intervals for Various Connections Tested.

Connection	Stress Range	Sample Size	Mean	Std. Dev.	90% Confidence (Percentage of Mean)		95% Confidence (Percentage of Mean)		97.5% Confidence (Percentage of Mean)	
					Lower Bound	Upper Bound	Lower Bound	Upper Bound	Lower Bound	Upper Bound
Unstiffened Mast Arm	6	10	2,492,414	1,352,480	1,708,407	3,276,421	1,524,908	3,459,920	1,344,057	3,640,771
					31		39		46	
	12	12	913,667	1,450,622	161,625	1,665,709	-8,014	1,835,348	-172,213	1,999,547
					82		101		119	
	15	7	350,884	80,297	291,910	409,858	276,622	425,146	260,786	440,982
					17		21		26	
Pole-Base	5	3	921,943	1,189,811	-1,083,905	2,927,791	-2,033,711	3,877,597	-3,340,744	5,184,630
					218		321		462	
	12	5	75,741	64,695	14,061	137,421	-4,588	156,070	-25,390	176,872
					81		106		134	
	15	7	213,024	177,928	82,344	343,704	48,468	377,580	13,378	412,670
					61		77		94	
Gusset-Stiffened Mast Arm	12	13	499,538	181,081	410,026	589,050	390,112	608,964	370,966	628,110
					18		22		26	

Table 2.8 Population Standard Deviation in Fatigue Life Estimates for Various Confidence Intervals for Various Connections Tested.

Connection	Stress Range	Sample Size	Mean	Std. Dev.	90% Confidence		95% Confidence		97.5% Confidence	
					Lower Bound	Upper Bound	Lower Bound	Upper Bound	Lower Bound	Upper Bound
Unstiffened Mast Arm	6	10	2,492,414	1,352,480	986,427	2,225,097	930,283	2,469,101	884,689	2,723,426
	12	12	913,667	1,450,622	1,084,655	2,249,386	1,027,614	2,462,979	980,936	2,681,488
	15	7	350,884	80,297	55,429	153,803	51,743	176,819	48,800	201,988
Pole-Base	5	3	921,943	1,189,811	687,427	5,253,487	619,485	7,477,646	568,382	10,608,615
	12	5	75,741	64,695	42,007	153,480	38,761	185,905	36,220	223,815
	15	7	213,024	177,928	122,823	340,808	114,656	391,809	108,135	447,580
Gusset-Stiffened Mast Arm	12	13	499,538	181,081	136,799	274,396	129,851	298,917	124,147	323,821

Table 2.9 Sample Size Estimates for Various Confidence Intervals for Various Connections Tested.

Connection	Stress Range	Sample Size	Mean	Std. Dev.	Mean Interval (%)	90% Confidence		95% Confidence		97.5% Confidence	
						n_{est}	n_{comp}	n_{est}	n_{comp}	n_{est}	n_{comp}
Unstiffened Mast Arm	6	10	2,492,414	1,352,480	20	21	22	31	31	40	40
	12	12	913,667	1,450,622	60	21	21	28	29	37	38
	15	7	350,884	80,297	10	16	16	22	23	28	29
Pole-Base	5	3	921,943	1,189,811	65	12	13	17	18	22	23
	12	5	75,741	64,695	40	13	14	19	20	25	26
	15	7	213,024	177,928	40	13	14	19	19	24	25
Gusset-Stiffened Mast Arm	12	13	499,538	181,081	15	17	18	25	25	32	32

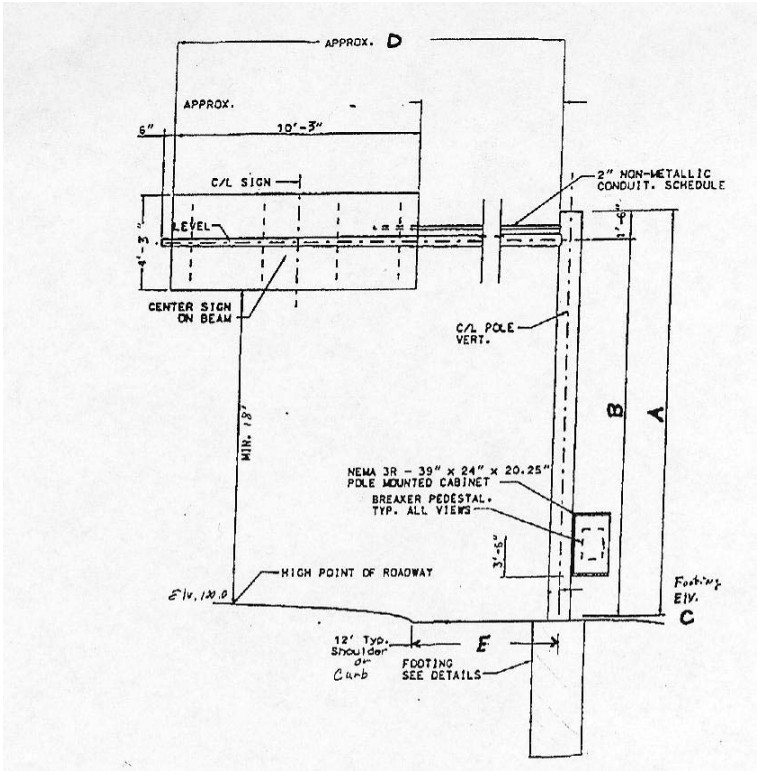

(a) Mono-Tube Cantilevered Mast-Arm-Pole VMS Sign Support Structure.

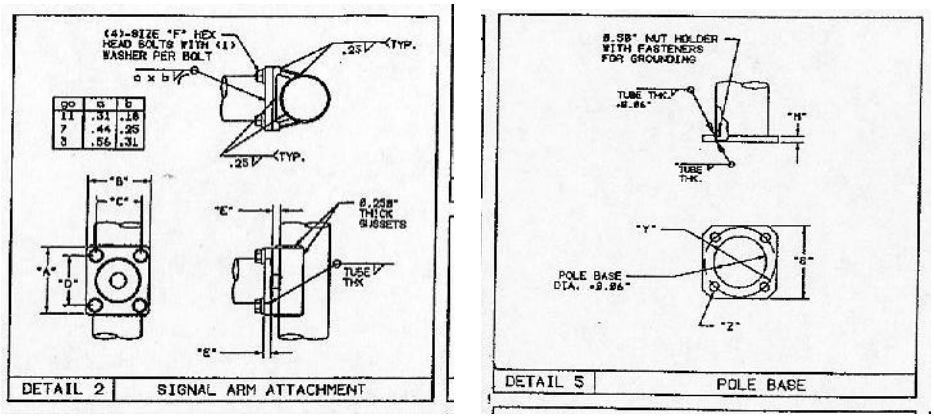

(b) Typical Mast-Arm-to-Pole and Pole-Base Connection Details.

Figure 2.1 Typical Variable Message Sign (VMS) Mono-Tube Cantilever Support Structure.

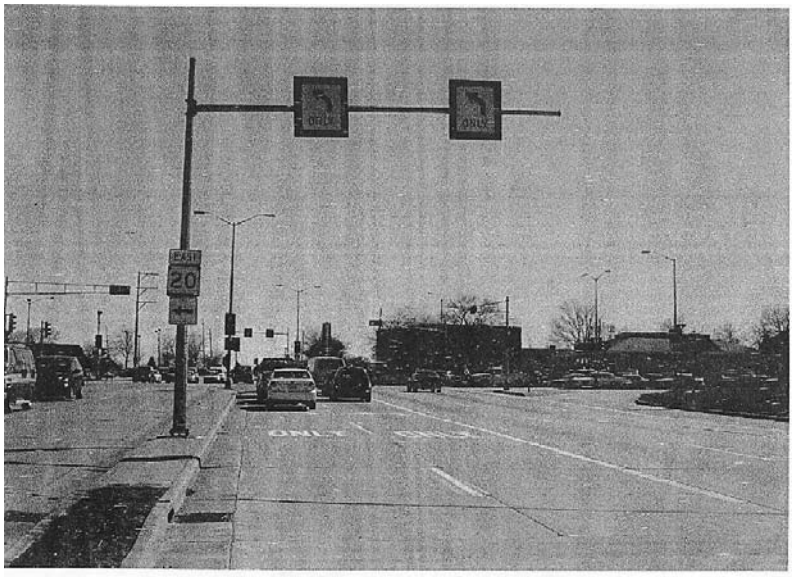

(a) In-Service Mono-Tube Sign Support Structure

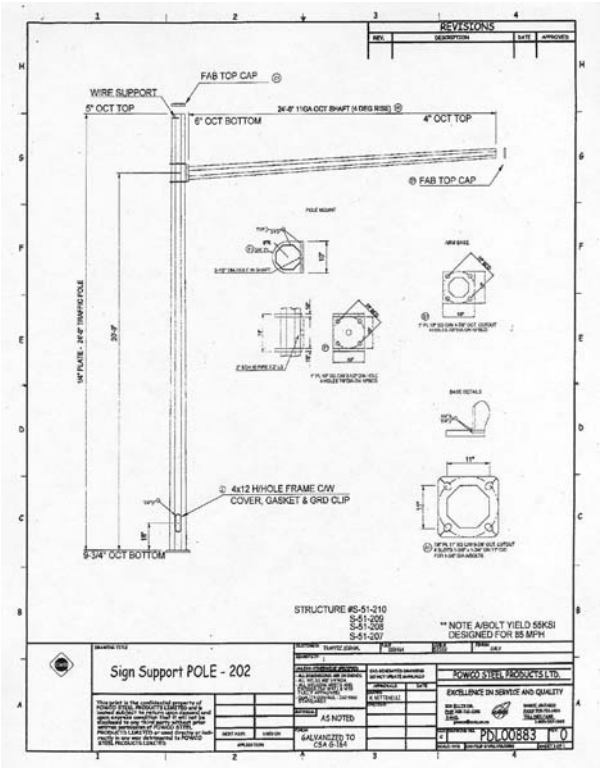

(b) Typical Shop Drawing Illustrating Connection Details.

Figure 2.2 Typical Monotube Cantilevered Sign Support Structure.

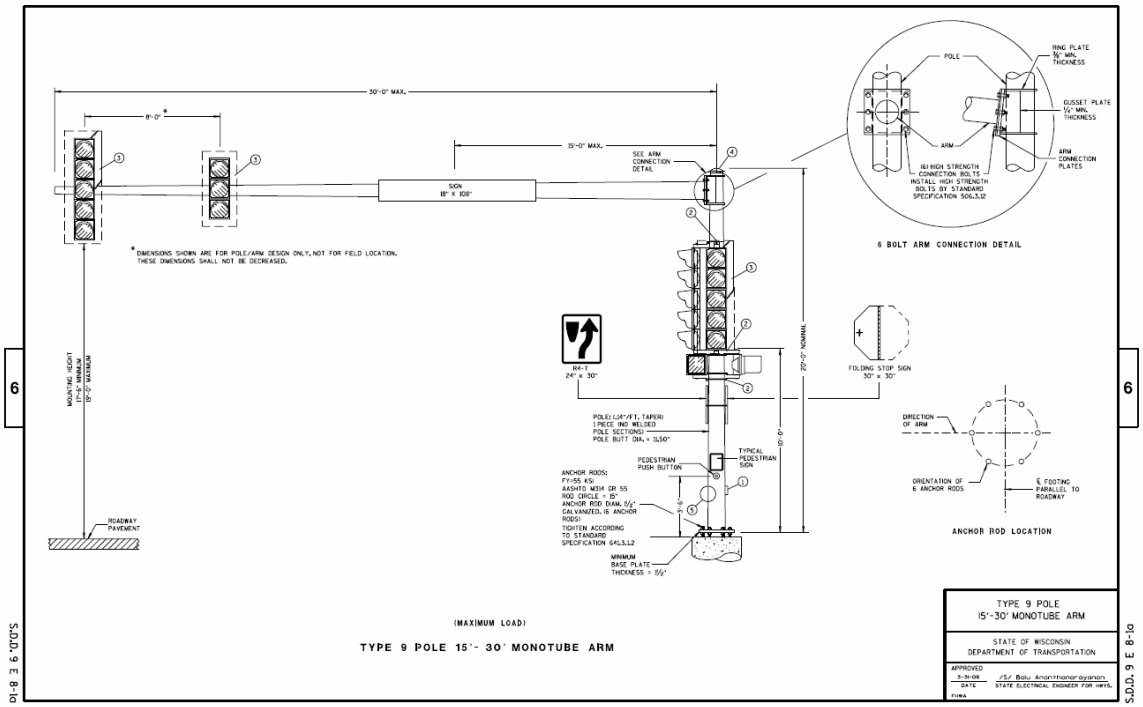

Figure 2.3 Typical WisDOT Monotube Arm Type 9 Signal Support Structure.

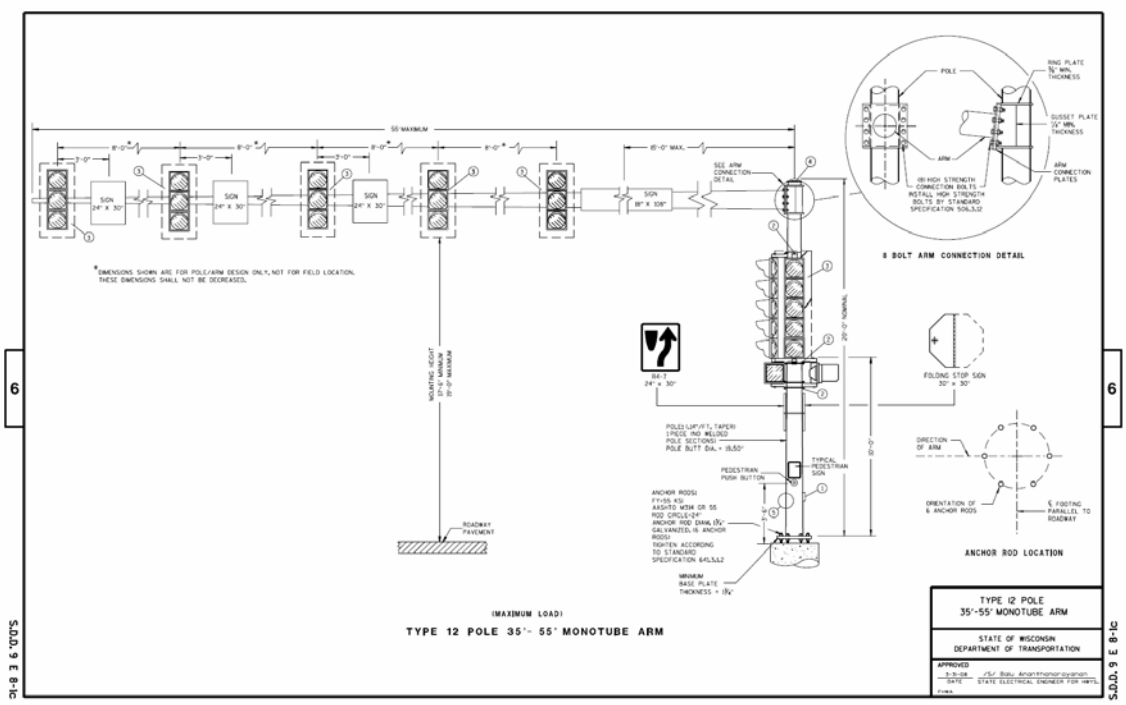

Figure 2.4 Typical WisDOT Monotube Arm Type 12 Signal Support Structure.

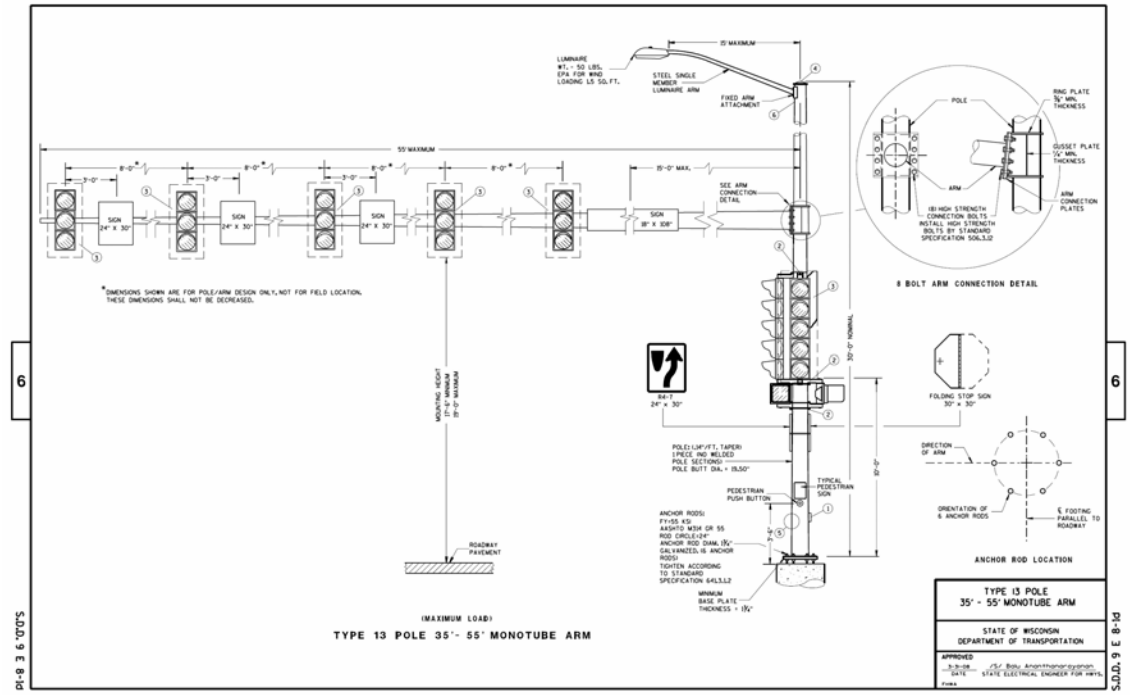

Figure 2.5 Typical WisDOT Monotube Arm Type 15 Signal Support Structure.

Figure 2.6 Double-Arm Sign Support Structure Over Wisconsin Avenue at IH-43 in Milwaukee, Wisconsin.

Figure 2.7 Monotube Cantilever Sign Support Structure Over Sixth Street in Milwaukee, Wisconsin.

Figure 2.8 Double-Arm Monotube Cantilever Sign Support Structure at IH-94 Off-Ramp at Clybourn Street in Milwaukee, Wisconsin.

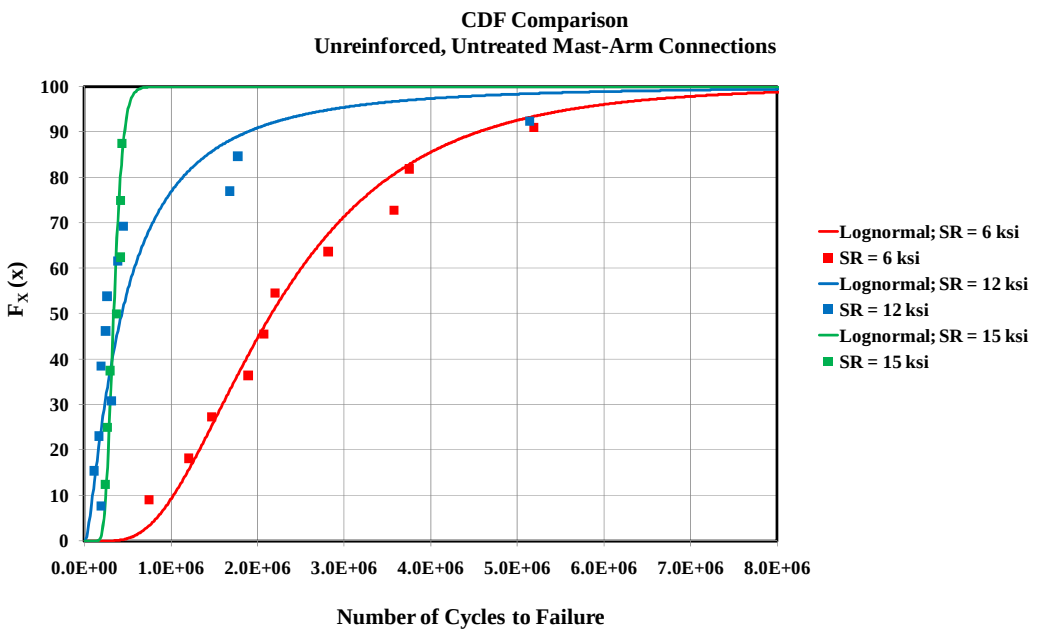

Figure 2.9 Cumulative Distribution Function Comparisons for Experimental Data and Lognormal Statistical Model.

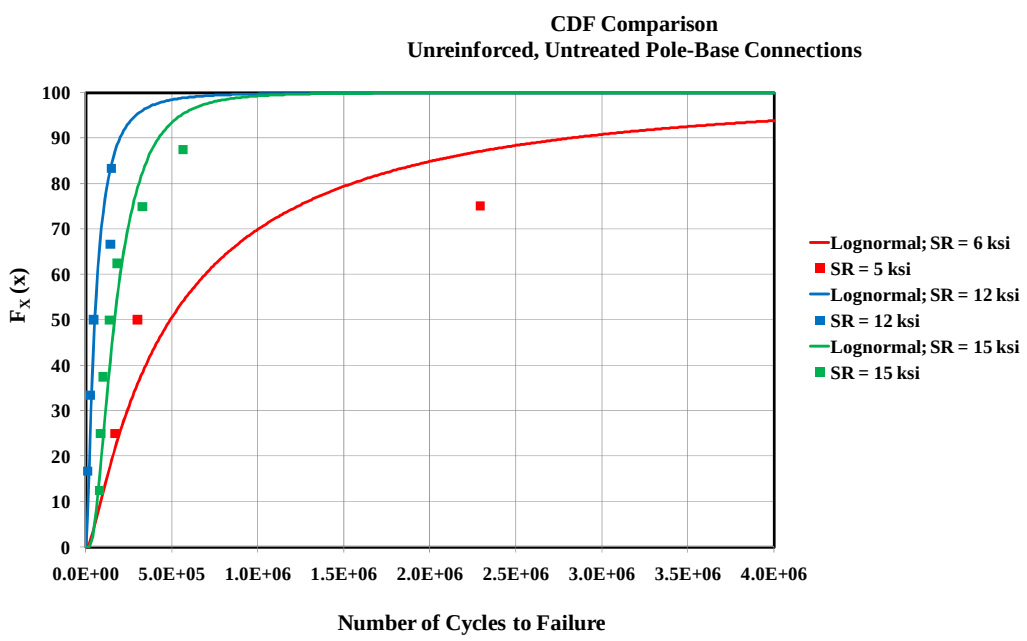

Figure 2.10 Cumulative Distribution Function Comparisons for Experimental Data and Lognormal Statistical Model.

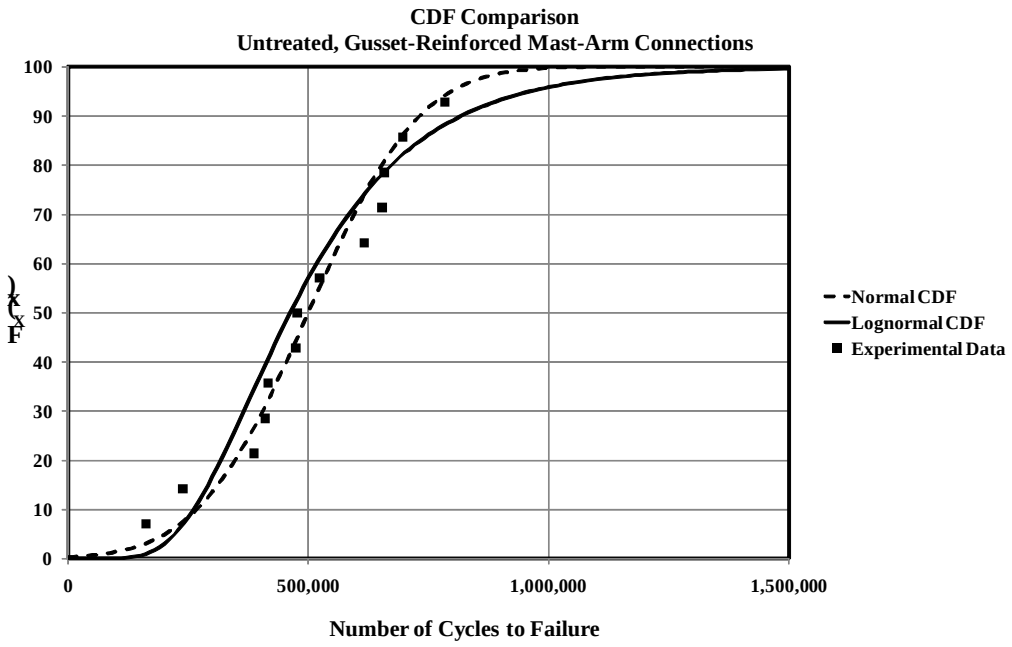

Figure 2.11 Cumulative Distribution Function Comparisons for Experimental Data and Lognormal Statistical Model for Gusset-Reinforced Mast-Arm Connections.

Chapter 3
Wind Speed Statistics

INTRODUCTION

Quantifying risk of fatigue-induced fracture in sign and signal support structures requires that both uncertainty in resistance and demand be quantified and understood. The previous chapter in the report outlined the methodology used to assess the uncertainty in the fatigue life of typical welded details found in Wisconsin signal and sign support structures. This chapter in the report seeks to present and implement a methodology for understanding the uncertainty associated with the demand (*i.e.* wind loading). The procedure implemented here is similar to that used in previous work (Foley *et al.* 2004), but additional cities around the state of Wisconsin are considered. The present chapter will describe the data collection and data synthesis process used to quantify the uncertainty in wind speed and direction for 8 cities across southern Wisconsin and will generate recommendations with regard to those cities deemed to be the most appropriate for field monitoring.

The major objective of the chapter is to provide cumulative distribution and probability density function models for naturally occurring winds throughout the portion of State where undesirable in-service performance of sign and signal support structures has been experienced. The statistical analysis of wind speed and direction throughout the state will be used to recommend areas where field instrumentation of a selected group of sign and signal support structures should occur. The statistical analysis will also provide the foundation for risk-assessment methodologies.

WIND DATA COLLECTION AND SYNTHESIS

Sign and signal supports within the State tend to be located more frequently in areas of higher population density. As a result, wind speed and direction data from the southern half of Wisconsin was collected. The cities used in the collection are shown in Figure 3.1. There is a fairly wide dispersion of data collection sites utilized. It is felt that the data collected will yield significant understanding of wind speed and direction variability throughout the areas of the state where there is a significant number of sign and signal support structures.

The National Climatic Data Center (NCDC) within the U.S. Department of Commerce maintains a weather data inventory as part of the National Oceanographic and Atmospheric Administration Satellite and Information Service. There are many U.S. controlled weather observation stations throughout the country

continually collecting weather-related data. Many of these weather collection sites are called ASOS sites. ASOS is an acronym representing Automated Surface Observation Stations. The weather observation stations are referenced by city and state as well as a Weather-Bureau-Army-Navy (WBAN) number. The city, WBAN number and weather observation station location for the 8 cities considered in this research effort are given Table 3.1. Academic and government institutions can access the data at no cost through the following web-site: http://www.ncdc.noaa.gov/oa/climate/stationlocator.html.

This phase of the research effort included collection and synthesis of hourly weather data for later use in the research. Most cities have data from 10 years synthesized. Exceptions to this are Green Bay and Appleton, Wisconsin where there are 4 years and 9 years collected, respectively. Overall, there is a significant number of data points in the sample used for statistical analysis of wind speed and direction. Appendices J through Q in the report contain the synthesized data for the eight Wisconsin cities. The process through which the information in these appendices was generated will now be described.

Hourly weather data records were acquired for all years indicated in Table 3.1. The hourly records included 2-minute average wind speeds and their associated directions. Peak gusts are also found in hourly records, but the present research effort is focused on accumulated damage resulting from fatigue loading. As a result, two minute averaged winds were felt to be more appropriate for this purpose. A two-minute averaged wind speed recorded every hour can be used in a wind speed simulation process similar to that used in previous research efforts (Foley *et al.* 2004). Figure 3.2 schematically illustrates the process. Each hourly two-minute averaged wind speed can form the basis for a simulated two-minute duration wind speed record. This simulated wind speed record includes variability above and below the average. One can assume that there are 30 of these simulations contiguously connected throughout this one-hour period, *n*, as indicated in Figure 3.2. As a result, one can construct a pseudo-continuous record of simulated two-minute averaged wind speeds for any duration desired.

A single simulation of two-minute duration can be used to assemble stress ranges within analytical models of the structural system for a one-hour period. These can then be extrapolated and accumulated over the service life. This process can be done for all two-minute averaged wind speeds defined in the simulation (*e.g.* 5 mph, 10 mph, etc.). The probability that the two-minute average wind speed will occur from a given direction can then be used to establish probabilities, or numbers of occurrence of these stress ranges in any given year. This process then becomes the foundation for stress range simulation procedures. Details of this process can be found elsewhere (Foley *et al.* 2004).

In order to execute the simulation process as described above, one needs to properly synthesize the wind speed data into a form that is suitable. As outlined earlier, the research team assembled a significant database of wind information at the eight cities. At any city the process of data collection and initial synthesis went as

follows. Hourly two-minute average wind speeds and their associated directions were collected for the time period established. There were many cases when the wind speed was very, very small such that a wind direction was not defined in the weather data (*e.g.* zero-valued direction contained in the NCDC record). Any data records with "0" entries for direction were discarded, but a zero entry for wind speed was preserved. In this way, there is a finite probability that the two-minute averaged wind speed will be zero. Therefore, if a zero entry existed in the two-minute averaged wind speed field the zero entry was preserved. However, if a zero entry existed in the direction field, the wind speed was set to zero and the direction data was discarded. There were very few of these in the database relative to the 87,000+ weather recordings synthesized.

The result of this collection process was probability mass functions (PMF's) for wind speed and direction for each of the eight cities within Wisconsin. Typical examples of the PMF's are given in Figures J.1 and J.2 in Appendix J. Other appendices have similar figures. Mean and standard deviations for the two-minute averaged wind speeds (irrespective of direction) for all eight cities are given in Table 3.2. The mean two-minute average wind speeds for the eight cities selected are fairly consistent and range from 6.75 mph to 9.00 mph. The wind roses (Figures J.2, K.2, L.2, M.2, N.2, O.2, P.2, and Q.2) indicate that only Eau Claire appears to have fairly egalitarian wind speed directions around the wind rose (*i.e.* there are nearly equal numbers of occurrences from all directions). All other cities appear to have directions that occur more frequently than others. As an example, La Crosse wind directions appear most frequently from the N-NW and S-SE directions.

It should be noted that the probability mass functions for the sample wind speed data have been binned in 5-mph intervals. Wind directions have been binned in 10-degree intervals and the wind roses given in Figure J.2 and other similar figures in other appendices reflect this 10-degree bin. The two-minute wind speed and direction were assumed to be continuous random variables. The 5-mph bins used to create discrete random variable representations of wind speed involved a +/- 2.5 mph bin. In other words, 5-mph bins included wind speeds ranging from 2.5 mph through 7.5 mph. Wind directions were discretized according to conventional directions of North, Northeast, East, Southeast, South, Southwest, West and Northwest. Discretization of wind speed into these eight cardinal directions did manipulate the data (*e.g.* compare Figures J.2 and J.3 and other similarly numbered figures in appendices J through Q). In essence, the jaggedness of the wind rose is removed when larger bins are constructed. The overall shape of the radial histogram is preserved, however.

Figure 3.3 schematically illustrates the wind speed and direction statistics for the eight cities studied. The figure gives one a sense that wind speeds are distributed in very similar ways throughout the state. Wind directions tend to be fairly well distributed throughout the eight cardinal directions with exceptions at La Crosse and Madison, which tend to exhibit leaning toward the north and south directions. Winds direction in

Appleton, Oshkosh and Green Bay also appear to distribute themselves fairly consistently with respect to one another. This might be expected given the proximity of these cities to the Fox River Valley.

WIND DATA STATISTICAL ANALYSIS

Figures J.1 and J.2 illustrate histograms that represent the probabilities of occurrence for wind speed and direction; respectively. In other words, if one would like to determine the probability that a two-minute wind speed will be 15 mph, Figure J.1 can be used. If one would like to determine what the probability that a two-minute wind will be out of a direction 100 degrees from due north, Figure J.2 can be used. If one would like to determine the probability of wind speed out of the East, Figure J.3 can be used. The data collected, however, must be able to give probabilities that wind will come from a defined direction at a defined speed. In other words, combined probabilities are needed. The process of generating these combined probabilities will now be discussed. It should be noted that further details are provided elsewhere (Foley *et al.* 2004; Ginal 2003).

(Ginal 2003) evaluated wind speeds and directions in Milwaukee, Wisconsin and determined that wind speed and direction are statistically dependent upon one another. Therefore, the intersection of a particular wind speed event, *V*, with a particular direction event, *Dir*, can be computed as,

$$P(V \cap Dir) = P(V) \cdot P(Dir \mid V) \tag{3.1}$$

In words, equation (3.1) says that the probability of the wind speed being *V* out of the direction, *Dir*, is equal to the probability that the wind speed will be *V* multiplied by the probability that the direction will be *Dir* given that the speed is *V*. Equation (3.1) and probability mass functions corresponding to the union of wind speed and direction events serve as the foundation for characterizing the variability in demand on signal and sign support structures.

The probabilities corresponding to the intersection of speed and direction events were assembled using the data collected at the eight Wisconsin cities. The eight cardinal directions (N, NE, E, SE, S, SW, W, NW) and the two-minute wind speed bins were used to establish the intersecting probabilities of speed and direction implied in equation (3.1). The wind speed data was synthesized using equation (3.1) using the procedure developed in previous research (Foley *et al.* 2004; Ginal 2003). The result is Tables J.1, K.1, L.1, M.1, N.1, O.1 and P.1 in the appendices. Each cardinal direction then has a probability mass function describing the distribution of wind speeds for that given direction. These probability mass functions are given in Figures J.4 through P.4 in the appendices.

Once the cardinal direction has been defined (*e.g.* South), it would be very useful to have continuous random variable models describing the variability in wind speed. Much of the reliability analysis for fatigue is based upon common probability density function models for both natural processes (wind speed) and

fatigue life. Assessing the risk of fatigue-induced fracture becomes mathematically very convenient if all random variables are of the same form (*e.g.* lognormal). It was therefore decided to evaluate a lognormal random variable model for the two-minute averaged wind speed for each of the eight cardinal directions.

If the two-minute average wind speed can be represented by a lognormal probability density function, it will take the following form (Haldar and Mahadevan 2000),

$$f_{\bar{V}_{2-\min}}(\bar{v}_{2-\min}) = \frac{1}{\sqrt{2\pi}\cdot\zeta_{\bar{V}_{2-\min}}\cdot\bar{v}_{2-\min}}\cdot\exp\left[-\frac{1}{2}\left(\frac{\ln\bar{v}_{2-\min}-\lambda_{\bar{V}_{2-\min}}}{\zeta_{\bar{V}_{2-\min}}}\right)\right] \text{ for } 0\le\bar{v}_{2-\min}\le\infty \tag{3.2}$$

The parameters for the lognormal model are computed using,

$\lambda_{\bar{V}_{2-\min}} = \ln\bar{v}_{2-\min} - \frac{1}{2}\zeta^2_{\bar{V}_{2-\min}}$ = is the expected value of the lognormal random variable;

$\zeta^2_{\bar{V}_{2-\min}} = \ln\left[1+\left(\frac{s_{2-\min}}{\bar{v}_{2-\min}}\right)^2\right]$ = the variance in the lognormal random variable;

with:

$s_{2-\min}$ = the standard deviation for the sample data;

$\bar{v}_{2-\min}$ = the mean for the sample data.

The suitability of the lognormal random variable model can be evaluated through comparing cumulative distribution functions for the natural process and the statistical model as done in Chapter 2 of the report with the fatigue life data. It can also be evaluated by simple comparison of natural process histograms and probability mass functions generated using the lognormal random variable model. The probability of the value of the lognormal random variable, *X*, being between two magnitudes, *a* and *b* is given by (Haldar and Mahavedan 2000),

$$P\left(a\le X\le b\right) = \Phi\left(\frac{\ln b-\lambda_X}{\zeta_X}\right) - \Phi\left(\frac{\ln a-\lambda_X}{\zeta_X}\right) \tag{3.3}$$

where: $\Phi(\,)$ is the normal cumulative distribution function for the standard normal random variable with zero mean and standard deviation of 1 and λ_X and ζ_X are the parameters of the lognormal distribution.

A comparison of lognormal model PMF's and the probability mass functions for the natural data is given in Figures J.4, K.4, L.4, M.4, N.4, O.4, and P.4. This comparison indicates that once the cardinal direction is defined, the wind speeds in that direction can be adequately represented by lognormal probability models. Table 3.3 contains the mean and standard deviations for each cardinal direction necessary to develop the lognormal probability models for wind speeds in each city. The information in this table also allows an assessment of mean wind speed and direction to be made.

The following can be surmised from the data contained in Table 3.3. Mean two-minute average winds greater than or equal to 9 mph in all the cities vary with cardinal direction and those directions with speeds exceeding 9 mph are listed in bold font. Two minute average winds of this magnitude most often come from the following directions in each of the cities:

Appleton:	NE, SW, W	Green Bay	N, NE, W, NW
La Crosse	W, NW	Eau Claire	W, NW
Madison	NE, E	Milwaukee	N, NE, E, SE, SW, W, NW
Oshkosh	N, NE, NW	Wisconsin Rapids	NW

This analysis of wind data indicates that in-field instrumentation should occur at a location where mean two-minute wind speed is likely to be the greatest and at a location where high average wind speed occurs out of as many directions as possible. Milwaukee and Green Bay are good candidate cities for field instrumentation.

SUMMARY, CONCLUSIONS AND RECOMMENDATIONS

A process by which hourly two-minute average wind speed and direction data was collected for eight cities within Wisconsin has been described. The information collected through NCDC weather observation stations was utilized to develop probability mass functions for wind speed and direction. Probability mass functions for direction were developed using 10-degree and 22.5-degree intervals (bins). The 22.5-degree PMF's for wind direction served as the basis for subsequent intersecting event probabilities for wind speed and direction. Tabulated probabilities for wind speed intersecting with direction were generated. These tabulated probabilities were utilized to evaluate lognormal probability density function models for two-minute averaged wind speeds given direction.

The statistical analysis conducted and the results in Table 3.2 indicate that two-minute wind speeds are fairly consistent throughout the eight cities in southern Wisconsin considered. It should be noted that the data in Table 3.2 does not consider direction. As indicated in previous research efforts (Foley *et al.* 2004; Ginal 2003) and the wind speed statistical analysis exhibited in Table 3.3, wind speed and direction are statistically dependent events. The data in Table 3.3 confirms this statistical dependence and indicates that Green Bay and Milwaukee are two cities that make good candidates for field instrumentation as a result of their relatively high mean two-minute average wind speeds and the frequency from which these higher speeds come from a large number of cardinal directions.

The statistical analysis of the wind speed data collected suggests that lognormal probability density and cumulative distribution functions are acceptable models for wind speed variability once a direction has been defined. As a result, there is the possibility to define a continuous random variable model for wind speed given one of eight cardinal directions. If a sign structure in the field is identified and the orientation of its

signal or signage is known, a probability model for the two-minute average wind speed distribution can be used for reliability analysis.

REFERENCES

Foley, C. M., Ginal, S. J., Peronto, J. L., and Fournelle, R. A. (2004). "Structural Analysis of Sign Bridge Structures and Luminaire Supports." *WHRP 04-03*, Wisconsin Highway Research Program, Madison, WI.

Ginal, S. J. (2003). "Fatigue Performance of Full-Span Sign Support Structures Considering Truck-Induced Gust and Natural Wind Pressures," MS Thesis, Marquette University, Milwaukee, WI.

Haldar, A., and Mahadevan, S. (2000). *Probability, Reliability, and Statistical Methods in Engineering Design*, John Wiley & Sons, Inc., New York, NY.

Table 3.1 Cities Used for Wind Speed and Direction Data Collection

City	WBAN #	Location	ASOS Site (?)	Data Collection Years
Appleton (APP)	04825	Outagamie County Airport	Yes	Dec. 2003 – Jan. 2007
Green Bay (GB)	14898	Austin Straubel International Airport	Yes	Dec. 1998 – Jan. 2007
La Crosse (LSE)	14920	La Crosse Municipal Airport	Yes	Jan. 1998 – Dec. 2007
Eau Claire (EAU)	14991	Eau Claire Regional Airport	Yes	Jan. 1998 – Dec. 2007
Madison (MSN)	14837	Dane County Regional Airport	Yes	Jan. 1998 – Dec. 2007
Milwaukee (MKE)	14839	Mitchell International Airport	Yes	Jan. 1998 – Dec. 2007
Oshkosh (OSH)	94855	Oshkosh Wittman Airport	Yes	Jan. 1998 – Dec. 2007
Wisconsin Rapids (WR)	04826	Wisconsin Rapids Alexander Field	Yes	Jan. 1998 – Dec. 2007

Table 3.2 Mean Wind Speed and Standard Deviation for Two-Minute Averaged Winds.

City	$\overline{v}_{2-\min}$ (mph)	$s_{2-\min}$ (mph)
Appleton (APP)	8.28	5.25
Green Bay (GB)	8.11	5.11
La Crosse (LSE)	7.64	4.54
Eau Claire (EAU)	6.95	4.64
Madison (MSN)	6.95	4.57
Milwaukee (MKE)	9.00	5.01
Oshkosh (OSH)	7.97	4.75
Wisconsin Rapids (WR)	6.75	4.47

Table 3.3 Statistical Parameters Needed for Lognormal Probability Models for Naturally Occurring Wind Speeds Given Direction (all wind speed information in miles per hour).

Direction	Parameter	APP	GB	LSE	EAU	MSN	MKE	OSH	WR
North	$\overline{v}_{2-\min}$ (mph)	8.79	**9.34**	8.18	7.27	8.44	**10.59**	**9.47**	8.06
	$s_{2-\min}$ (mph)	4.38	4.38	3.82	3.22	4.20	4.62	4.45	3.71
Northeast	$\overline{v}_{2-\min}$ (mph)	**9.29**	**10.88**	7.18	7.45	**9.45**	**10.21**	**10.27**	7.68
	$s_{2-\min}$ (mph)	4.38	5.09	3.19	3.66	4.41	4.38	4.48	3.38
East	$\overline{v}_{2-\min}$ (mph)	8.29	8.16	7.17	8.77	**9.09**	**9.71**	8.37	8.19
	$s_{2-\min}$ (mph)	3.86	3.71	3.24	3.99	4.44	4.89	3.68	3.78
Southeast	$\overline{v}_{2-\min}$ (mph)	8.56	8.79	6.50	8.45	8.55	**9.75**	8.16	6.44
	$s_{2-\min}$ (mph)	4.21	4.17	2.87	3.55	3.88	4.32	3.83	2.76
South	$\overline{v}_{2-\min}$ (mph)	8.70	8.03	8.97	8.60	8.79	8.31	8.51	7.45
	$s_{2-\min}$ (mph)	4.15	3.82	3.60	3.71	3.72	3.79	4.27	3.40
Southwest	$\overline{v}_{2-\min}$ (mph)	**10.02**	8.21	8.78	7.46	7.45	**10.24**	8.50	7.91
	$s_{2-\min}$ (mph)	4.82	3.87	4.17	3.62	2.90	4.76	4.08	3.55
West	$\overline{v}_{2-\min}$ (mph)	**10.08**	**9.94**	**9.88**	**9.21**	7.56	**9.56**	7.95	8.63
	$s_{2-\min}$ (mph)	5.13	4.81	4.63	4.33	3.27	4.47	3.95	3.96
Northwest	$\overline{v}_{2-\min}$ (mph)	**10.23**	**9.47**	**10.42**	**8.99**	7.91	**9.49**	**9.75**	**9.30**
	$s_{2-\min}$ (mph)	5.01	4.67	4.62	3.88	3.63	4.41	4.55	4.27

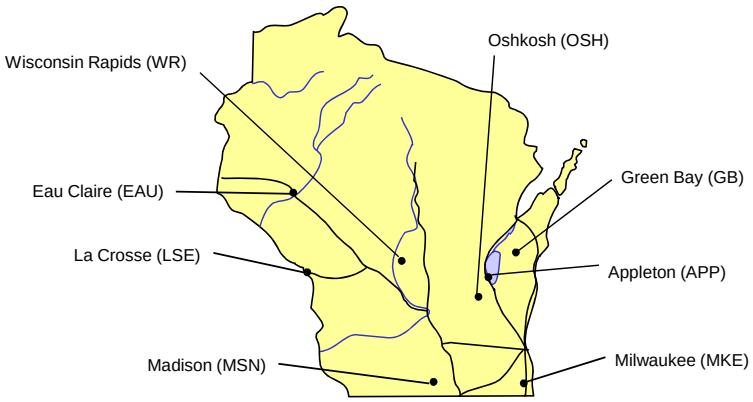

Figure 3.1 Cities Used in Wind Data Collection for Present Research Effort.

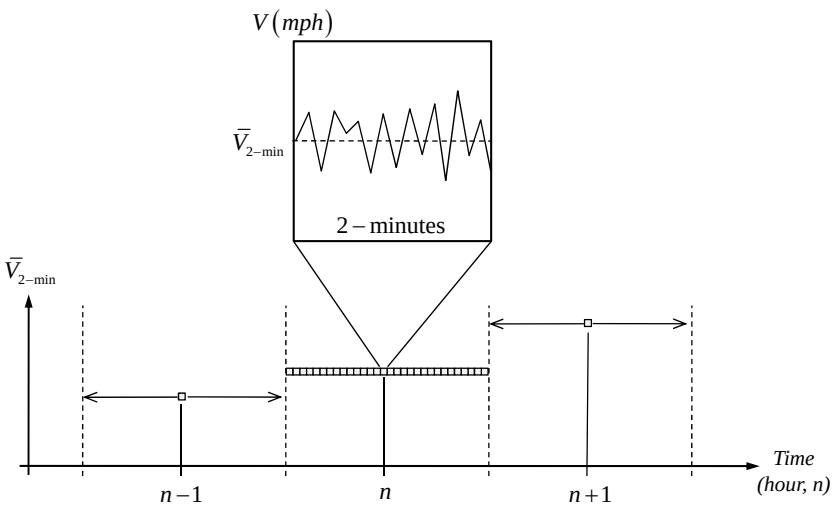

Figure 3.2 Two-Minute Wind Speed Extrapolation and Simulation.

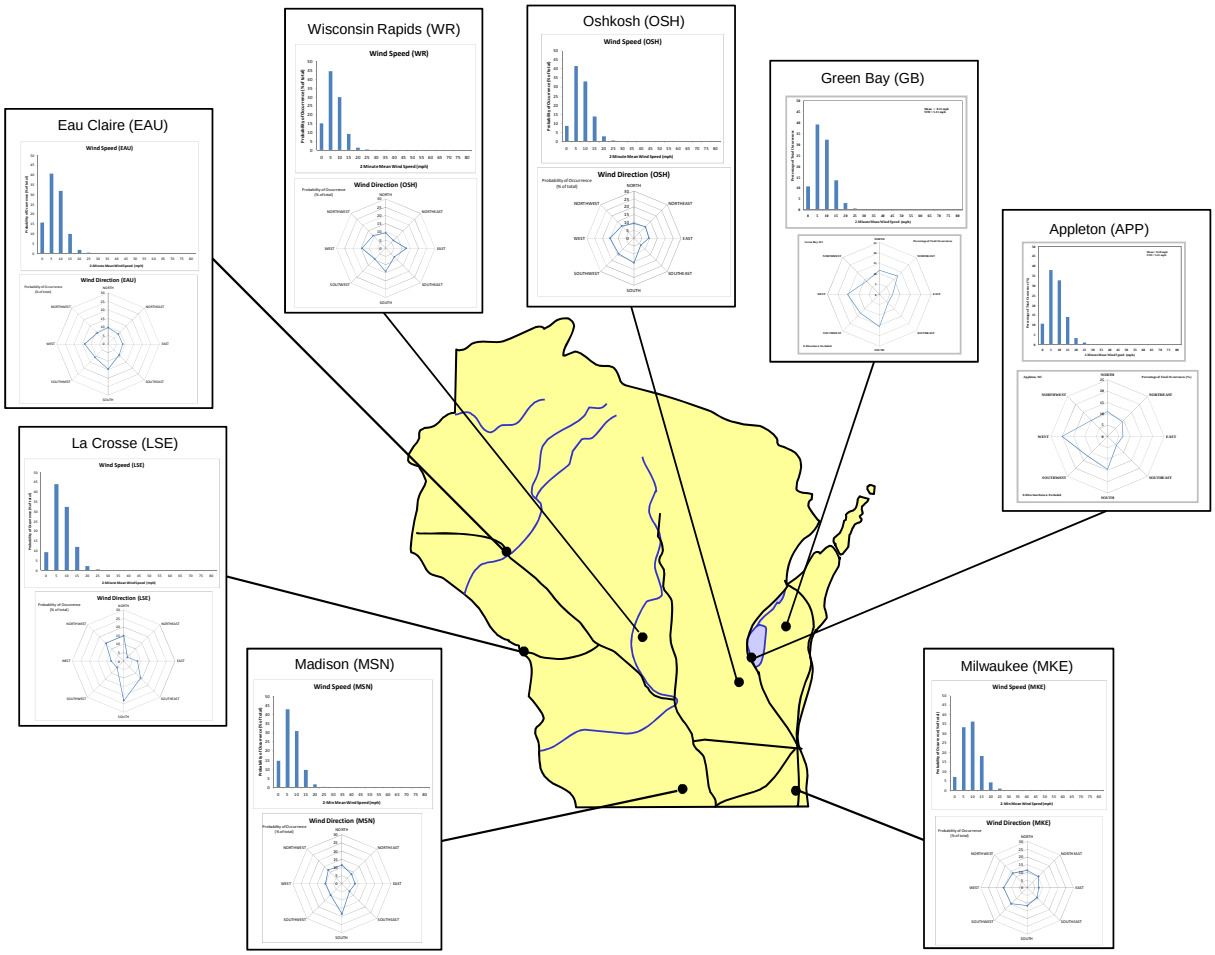

Figure 3.3. Wisconsin Two-Minute Wind Speed Probabilities and Direction Probabilities.

This page has been intentionally left blank.

Chapter 4
Finite Element Analysis

INTRODUCTION

The behavior of welded HSS-to-plate connections has been an active area of research for over two decades. The analysis conducted for evaluation of normal stress within pole and mast-arm components of signal and sign structures and the associated fatigue-based design methodology involves evaluation of:

- the sensitivity of the structural system to loading resulting from aerodynamic galloping;
- the tendency for vortex-induced shedding loads to be present during the structure's service life;
- pressures due to natural wind gusts;
- truck-induced gust pressures.

Normal stress due to bending in these structural systems is computed using the flexure formula and design specifications (AASHTO 2001) include procedures to adjust moments of inertia to account for the stress amplifying effects of multi-faceted tubular cross-sections.

The distribution of normal stress around the perimeter of hollow structural shapes (HSS) and the effects of anchor rod distribution, base plate thickness, and stiffening details have recently become the subject of several in depth studies. Early efforts examined the load path from HSS tubular cross-section to discrete anchor rod locations (Keating and Fisher 1986) and variation in base plate thickness and anchor rod arrangement in HML structural systems followed nearly two decades later (Foley *et al.* 2004). Recently, the behavior of pole-base socketed connections utilizing anchor rods with stand-off height have been studied using high-fidelity finite element analysis (Hall 2005; Hall and Connor 2008; Ocel 2006a; Ocel 2006b). These analyses confirmed the impact of anchor rod arrangement and base plate thickness along with the influence of multi-faceted tubular cross-sections on stress concentration within the HSS tube wall. High fidelity FEA has also been carried out on un-stiffened mast arm connections (Koenigs *et al.* 2003; Machietto 2002) and stiffened mast-arm connections (Azzam and Menzemer 2008; Koenigs *et al.* 2003; Machietto 2002).

Finite element analysis carried out to evaluate stress distribution within socketed fillet weld mast-arm-to-plate connections has assumed that the anchor rods have been non-pretensioned. The impact of pretensioning on the distribution of stresses within round and multi-faceted tubular mast arms was not considered. Furthermore, the studies did not include gap-contact nonlinearity among connecting plates, nor did they

include the impact of non-uniform pretensioning of bolts within the connection. The later concern was expressed by WisDOT during the project kick-off meeting as being very important. The present research effort therefore, conducted high-fidelity finite element analysis of a connection detail similar to those used in monopole mast-arm signal and sign support structures within the state of Wisconsin. The FE analysis includes gap-contact nonlinearity among component plates and bolt pretensioning. Various pretensioning arrangements were analyzed whereby bolts were left "loose" and the impact on the normal stress distribution around an octagonal mast arm shape was evaluated. The objective of this chapter is to outline and discuss the FE analysis conducted and discuss observations seen in normal stress distribution and with subsequent comparison to analysis recommendations found in design specifications (AASHTO 2001).

TARGET DETAIL AND FE MODEL TOPOLOGY

Experimental and analytical research conducted to date (including several efforts reviewed in earlier chapters of this report) indicate that gusset plate stiffeners within mast-arm connections tend to generate geometric discontinuities and stress concentrations within the connection detail. WisDOT does not currently have a significant number (if any) gusset stiffened connections in their inventory of monotube mast-arm-to-pole signal and sign support structures. The typical structure configuration and connection detail topologies used by manufacturers are shown in Figures 4.1 and 4.2.

The impact of multi-faceting on stress-raising conditions was found to be significant (Ocel 2006a; Ocel *et al.* 2006) and the present FEA focused on an octagonal tube to plate socketed connection similar to that shown in Figure 4.2. The finite element model topology is shown in Figure 4.3 and Abaqus (Simulia 2008) was used in the finite element simulations. An octagonal mast arm segment with width across the flats equal to 6 inches was utilized. The wall thickness for the mast arm was 0.12 inches. The socketed connection is shown in Figure 4.4. It should be noted that there is no connection made between the mast arm wall and the connecting plate within the socket other than the fillet weld at the top surface of the plate and seal fillet weld at the end of the octagonal tube. The fillet weld at the top surface of the mast-arm plate was modeled without the traditional fillet shape as only a cursory evaluation of stress concentration at the toe of the fillet in the mast arm was needed for this preliminary study. This modeling has little impact on the stress state in the mast-arm wall and the square shape is conservative.

A four bolt arrangement as shown in Figure 4.3 was chosen as it has a relatively small number of discrete load paths present through the connection (*i.e.* four bolts). This has been shown to cause large stress concentration in HML base connections (Foley *et al.* 2004). A back plate was used in the modeling as well and this was assumed to be connected over the central region to the vertical pole using boundary condition imposition as shown in Figure 4.5. The typical connecting detail used in an actual sign support structure could

include ring-stiffener plates as shown in Figure 4.2, but these were excluded from the present model. The present boundary conditions were felt to be adequate for the preliminary study.

A bi-directional bending moment was applied with magnitudes and directions shown in Figure 4.3. This bending moment sought to simulate the presence of self-weight moment (in-plane) and wind loading moment (out-of-plane). The bending moments were applied to the FE model using rigid body constraints defined through master-node modeling and constraint equations. The master node and constraint perimeter are shown in Figure 4.6.

The finite element modeling included gap-contact nonlinearity at the surfaces between the mast-arm-plate and the back mounting plate. The bolt models included continuous nodal connectivity between the bolt head and the adjacent plate. In other words, no gap-contact conditions were assumed at these locations. Bolt pre-strain was introduced via initial strain imposition on a surface cut through the shank of the bolt. The magnitude of the pre-strain/prestress was based upon bolt pretension conditions required by WisDOT (WisDOT 2008) and recommended elsewhere for steel buildings (AISC 2005). The bolt pretension required for 3/4" diameter A325 bolts is 28 kips and the pre-strain/prestress magnitude used for the bolts is founded upon this bolt pretension.

FINITE ELEMENT ANALYSIS

The finite element model was utilized to study variation in mast-arm stress around the perimeter of the octagonal tubular shape. Five bolt pretension conditions were considered and they are described in Table 4.1. The first involved all four bolts pretensioned to the 28-kip requirement. The remaining four pretension conditions included 1 to 3 bolts without proper pretension (essentially loose with 10 pounds of pretensioning). The variation in bolt pretension within the connection will be able to give qualitative understanding of how mast-arm wall stresses change with pretension variation within the bolts of the connection. It should be noted that bolts will be able to accept tension loading immediately upon separation of the plates in contact. As a result, it is expected that even though bolts are "loose", they will be able to accept tension loading once contacting plate separation begins.

The simulation was run in two discrete stages: (1) bolt pretension stage; and (2) bi-directional moment application. Principal and Z-direction stress contours for the bolt pretension state in pretension condition 1 are shown in Figure 4.7. Several interesting observations can be made regarding the principal stress contour. First of all, the central support boundary conditions over the back-plate can be clearly seen to influence the state of stress within the connecting plates. There are elevated principal stresses at the corners of the octagonal mast arm in this support region. The magnitude of principal stresses at these corners is on the order of 5,000 psi. The states of uniform principal tension and Z-direction stress in the bolts validate the pretension

condition. The pretensioning of the bolts can also be seen to cause principal stress gradient through the mast-arm plate in the vicinity of the bolts.

Principal and Z-directional stress contours during the follow-on stage where the bi-directional bending moment is applied are given in Figures 4.8 and 4.9. There is significant stress raising behavior occurring at the corners of the octagonal mast arm. Maximum principal stress and Z-directional stress magnitudes are given in Table 4.1 and they are on the order of 8,900 psi and 8,250 psi, respectively. There is some concentration of stress seen in the Z-directional stress contours on the inside face of the mast arm, but overall, the state of Z-direction stress is relatively uniform.

Connecting bolt stress contours at the end of the moment application stage are given in Figure 4.10. While the principal stress contours are relatively uniform through the bolt shank, the Z-directional stress contours begin to illustrate that gradient of stress is present. Therefore, the mast-arm plate is confirmed to be flexible and there is bending in the bolts generated. It should be noted that the perfect nodal continuity at the interface of the bolt head and connecting plate serves to enable this bending moment generation and the reality is not perfect continuity. However, it makes sense that bending is generated in the bolts as the plates begin to separate as the bending moments are applied.

Pretensioning condition 2 includes the top two bolts loose and the bottom two pretensioned to 28 kips. The principal stress and Z-directional stress contours during the bolt pretensioning state are given in Figure 4.11. There is a slightly elevated state of principal stress generated at the corners of the octagonal tube when compared to pretension condition 1, but the difference is slight. The loading stage that includes application of bi-direction moment appears to generate greater concentration of principal stress at the corners of the octagonal tube near the pretensioned bolts. This stress elevation is shown in Figure 4.12. The Z-directional stress contour of Figure 4.13 also illustrates the migration of stress to the load paths defined by the pretensioned bolts. One can clearly see the stress contours establishing formation of these load paths through the octagonal mast arm. This has been seen in 4-bolt HML connections as well (Foley *et al.* 2004). Table 4.1 illustrates the magnitude of this stress concentration increase for both principal as well as Z-directional stresses. Figure 4.14 illustrates similar bending behavior in the bolts as the bi-directional moment is applied.

Pretensioning condition 3 includes the upper left bolt loose and the remaining three bolts being pretensioned to 28 kips. Figure 4.15 illustrates the expected principal and Z-directional stress contours based upon comparison to previous analysis discussed. There is a slight elevation in principal stress. The principal stress contours and Z-directional stress contours shown in Figures 4.16 and 4.17 illustrate that there is a slight elevation in stress when compared to the four-bolt pretensioned condition (refer to Table 4.1). The Z-direction stress contour in Figure 4.17 illustrates that there is a fairly well-distributed state of stress around the

perimeter of the mast-arm. One can appreciate the stress concentration present when examining the inner surface of the mast arm shown in Figure 4.17. Figure 4.18 illustrates similar behavior in the bolts when compared previous analysis.

Having the upper-right bolt being loose and the remaining bolts pretensioned to 28 kips (pretension condition 4) results in similar stress contours and stress magnitudes as the previous three conditions. There is a slight reduction in principal stress when compared to prestress condition 1. The principal stress contours shown in Figure 4.20 illustrate the expected concentration at the corners of the octagonal mast arm and the formation of Z-directional stress trajectories toward the discrete load paths created by the pretensioned bolts. The stress trajectory is clearly seen in Figure 4.21. The bi-directional moment loading assumed is not conducive to generation of stress-raiser conditions for this pretensioning condition. Table 4.1 illustrates the maximum principal and Z-directional stress for this pretensioning condition are actually less than that seen in the four-bolt pretension condition. The bolt stress contours are shown in Figure 4.22 and gradient of stress through the bolt shank is present.

Pretension condition 5 is a very punishing condition given the bi-directional moment being applied. Figure 4.23 illustrates the principal stress contours and Z-directional contours for the bolt pretensioning stage. The orientation of the model obscures the stress concentrations being seen. The maximum principal stress magnitude for this condition is the greatest (on the order of 5,800 psi) for all 5 pretensioning configurations. An interesting comparison of principal stress contours can be made through examination of Figures 4.11 and 4.22. The impact of the central boundary constraints on the backing plate can be clearly seen. This boundary condition results in a relatively stiff substrate for the mast-arm plate connection and this tends to distributed principal stresses over the mast-arm plate between the bolts. In Figure 4.22, the contour of principal stresses is considerably less as the portion of backing plate is extending beyond boundary restraints. This results in a significantly different stress contour and magnitude of principal stresses.

Application of the bi-directional bending moment condition results in very interesting behavior. Figure 4.24 illustrates the principal stress contour for this loading condition. Severe demand across the mast-arm plate bottom can be see through the principal stress magnitudes in Figure 4.24 (approximately 11,180 psi). The mast arm plate is subjected to significant bending as the Y-directional bending moment component requires that a force couple be generated between the pretensioned bolts and the faying surface of the mast-arm plate in contact with the backing plate. Figure 4.25 illustrates the Z-direction stress contour that results from the applied bending moment. The mast-arm wall has a notable reduction in Z-directional stress opposite the pretensioned bolts. It is interesting to note that this condition results in the least stress demand on the mast-arm wall (see Table 4.1) of all pretensioning conditions assumed. The stress contours in the bolts shown in Figure 4.26 are similar to those seen previously in other analyses.

Five bolt pretension scenarios were evaluated using finite element analysis that included bolt pretension and gap-contact nonlinearity. A bi-directional bending moment intended to simulate the presence of self-weight bending moment and out-of-plane bending moment resulting from wind loading was applied to the mast arm. The combination of bolt pretension and applied bending moment resulted in a significant variation in stress concentration within the connection. Given the bi-directional moment assumed, the FEA illustrates that normal stresses within the mast-arm do not vary significantly with varying bolt pretension arrangements. The variation in mast-arm stresses for all five conditions evaluated is on the order of 15%.

If a requirement of four bolts pretensioned to 28-kips is maintained, then the mast arm normal stresses for the bi-directional moment assumed can be as much as 7% higher (condition 2). As a result, not having all bolts tensioned to target levels can increase the tension stress range by as much as 7%. This may not be significant for statically applied loading, but fatigue resistance may be reduced more significantly by this increase in stress range. As a result, it is recommended that all bolts in mast-arm to plate connections be pretensioned to the recommended levels and checking for loose bolts part of inspection protocols. The analysis conducted did not seek to establish lower-bound bolt pretension recommendations and this may be useful fodder for future study.

COMPARISON WITH DESIGN SPECIFICATIONS

The AASHTO design specifications (AASHTO 2001) include several useful tools for estimating the impact of shear lag through multi-faceted tubular shapes and the amplification of normal stresses due to bending. Figures 4.27 and Figure 4.28 illustrate computations that would be undertaken using traditional design methods (AASHTO 2001) to evaluate the state of stress at the corner of the octagonal mast arm (corner 8). It should be noted that traditional flexure-formula normal stress computations would be undertaken with an assumption of fixed or rigid connection at the mast-arm to connection plate. In other words, the designer would likely not include mast-arm-plate flexibility and backing plate flexibility in the analysis.

If the bi-directional moment assumed in the FEA is used in the present analysis, the state of stress at the critical corner in the mast arm can be determined. Figures 4.27 and 4.28 illustrate that normal (Z-direction) stresses due to bending using these "by-hand" analysis methods would be on the order of 3,838 psi for an octagonal mast arm and 3,365 for a round mast arm. Table 4.1 facilitates comparison of these peak tension stresses with those found via FEA with varying bolt pre-tension configurations. The results indicate that for the boundary conditions assumed, the traditional analysis methods can under-estimate the normal stresses in the mast arm by as much as 50%. This has a ***significant*** impact on the on the ability to accurately predict fatigue life in these welded connections. It is important to know that the stress concentration effects omitted in the traditional analysis are accounted for in the traditional detail category methodology. The results, therefore, are not alarming. However, it is also interesting to note that the combination of multiple facets on

the mast arm tube and mast-arm plate flexibility has a significant effect on the distribution and magnitude of normal stresses in the mast arm tube. Therefore, it is very important that the fatigue testing arrangements include this mast arm plate flexibility and, if possible, correct boundary conditions for the backing plate.

SUMMARY, CONCLUSIONS AND RECOMMENDATIONS

A series of finite element analyses were undertaken to simulate the behavior of a typical mast-arm-to-plate connection in signal and sign support structures found in WisDOT's inventory. The FE model included an octagonal mast arm tube with socketed fillet welded connection to a 1-inch thick mast-arm-plate. The FE modeling did not include all details of the mast-arm to pole connection, but it did include back-mounting plate and boundary conditions designed to simulate important restraint conditions on the mast-arm plate at this connection. Gap-contact nonlinearity was included in the finite element modeling as well as bolt pretensioning to levels established in design specifications. Five bolt-pretension arrangements were considered. Principal stresses and normal stresses in the mast-arm tube, the connecting plates, and the bolts were evaluated.

The finite element analysis conducted indicates that the normal stresses in the mast-arm wall can be affected by loose bolts. It should be noted that the analysis included a single bi-directional bending moment condition. However, given the analysis limitations, loose bolts can account for a 7% increase in normal stresses in the mast-arm wall. Furthermore, mast-arm-plate flexibility and the discrete load paths resulting from the bolted connection arrangement can conspire to create significant amplification of normal stress around the perimeter of the octagonal mast arm.

It is recommended that inspection protocols include examination of bolt pretension in mast-arm connections and that all bolts have pretension in them. While a lower-bound magnitude of pretension was not established in the present effort, the analysis clearly indicates that lack of pretension in bolts around the mast-arm connection can result in elevated states of normal stress in the mast arm. Therefore, if bolts are found loose in these connections, they should be tightened to establish contact at the faying surfaces of the connecting plates. This will help to alleviate unforeseen concentration of stress resulting from the loose connection bolt condition.

The FEA conducted also confirms the importance of plate flexibility in the fatigue testing to be conducted in phase 2 of the research effort. It is therefore recommended that any fatigue testing include a specimen configuration with this flexibility to more accurately include these effects. In other words, the fatigue tests should included a strong-box type connection and the ability for the mast-arm plate to make flush contact at a plate similar in stiffness to those welded to the vertical pole in these structures.

REFERENCES

AASHTO. (2001). *Standard Specifications for Structural Supports for Highway Signs, Luminaires and Traffic Signals, 4th Edition with 2006 Interim Revisions*, American Association of State Highway and Transportation Officials, Washington, D.C.

AISC. (2005). *Specifications for the Design and Construction of Structural Steel Buildings*, American Insititute of Steel Construction, Chicago, IL.

Azzam, D. M., and Menzemer, C. C. (2008). "Numerical Study of Stiffened Socket Connections for Highway Signs, Traffic Signals and Luminaire Structures." *Journal of Structural Engineering*, 134(2), American Society of Civil Engineers, 173-180.

Foley, C. M., Ginal, S. J., Peronto, J. L., and Fournelle, R. A. (2004). "Structural Analysis of Sign Bridge Structures and Luminaire Supports." *WHRP 04-03*, Wisconsin Highway Research Program, Madison, WI.

Hall, J. H. (2005). "The Effect of Base Plate Flexibility on the Fatigue Performance of Welded Socket Connections in Cantilevered Sign Structures," MS Thesis, Lehigh University, Bethlehem, PA.

Hall, J. H., and Connor, R. J. (2008). "Influence of Base Plate Flexibility on the Fatigue Performance of Welded Socket Connections." *Journal of Structural Engineering*, 134(6), American Society of Civil Engineers, 911-918.

Keating, P. B., and Fisher, J. W. (1986). "Fatigue Resistance Design of Cantilevered Signal, Sign and Light Supports." *(NCHRP Report 286)*, ATLSS Engineering Research Center, Bethlehem, PA.

Koenigs, M. T., Botros, T. A., Freytag, D., and Frank, K. H. (2003). "Fatigue Strength of Signal Mast Arm Connections." *CTR Research Report 4178-2*, Center for Transportation Research at the University of Texas at Austin, Austin, TX.

Machietto, C. (2002) "Valmont Fatigue Testing Presentation." *AASHTO T-12 Committee, November*, Las Vegas, NV (Electronic Presentation - Unpublished).

Ocel, J. M. (2006a). "The Behavior of Thin Hollow Structural Section (HSS) to Plate Connections," PhD Thesis, University of Minnesota, Minneapolis, MN.

Ocel, J. M. (2006b) "Fatigue Resistance of Minnesota's Traffic Signal Structures." *2006 TRB Annual Meeting*, (CD-ROM).

Ocel, J. M., Dexter, R. J., and Hajjar, J. F. (2006). "Fatigue-Resistant Design for Overhead Signs, Mast-Arm Signal Poles, and Lighting Standards." *Report No. MN/RC-2006-07*, Minnesota Department of Transportation, St. Paul, MN.

Simulia. (2008). "Abaqus Standard, Version 6.8-1." Simulia, Dassault Systemes, Providence, RI.

WisDOT. (2008). *Wisconsin Construction Specifications*, Wisconsin Department of Transportation, Bureau of Structures, Madison, WI.

Table 4.1 Mast-Arm Wall Stress Comparisons for Finite Element Solution, Hand Computations for Octagonal Mast Arm (AASHTO 2001) and Hand Computations for Round Mast Arm (AASHTO 2001).

Bolt Pretension Condition	Pretension Pattern Description	S_{max} (psi)	σ_z (psi)	Octagon (psi)	Round (psi)
1	All four bolts pretensioned to 28 kips.	8,959	8,254	3,838	3,365
2	Top two bolts loose (1) and bottom two bolts pretensioned to 28 kips.	9,399	8,856		
3	Upper-left bolt loose (1) and remaining three bolts pretensioned to 28 kips.	9,202	8,492		
4	Upper-right bolt loose (1) and remaining three bolts pretensioned to 28 kips.	8,878	8,194		
5	Left vertical stack of bolts pretensioned to 28 kips and right vertical stack of bolts loose (1).	11,180	7,723		

Notes:

(1) Loose indicates that small pretension was provided to these bolts (10 lbs. force). This small pretension was required to ensure numerical convergence with finite element software.

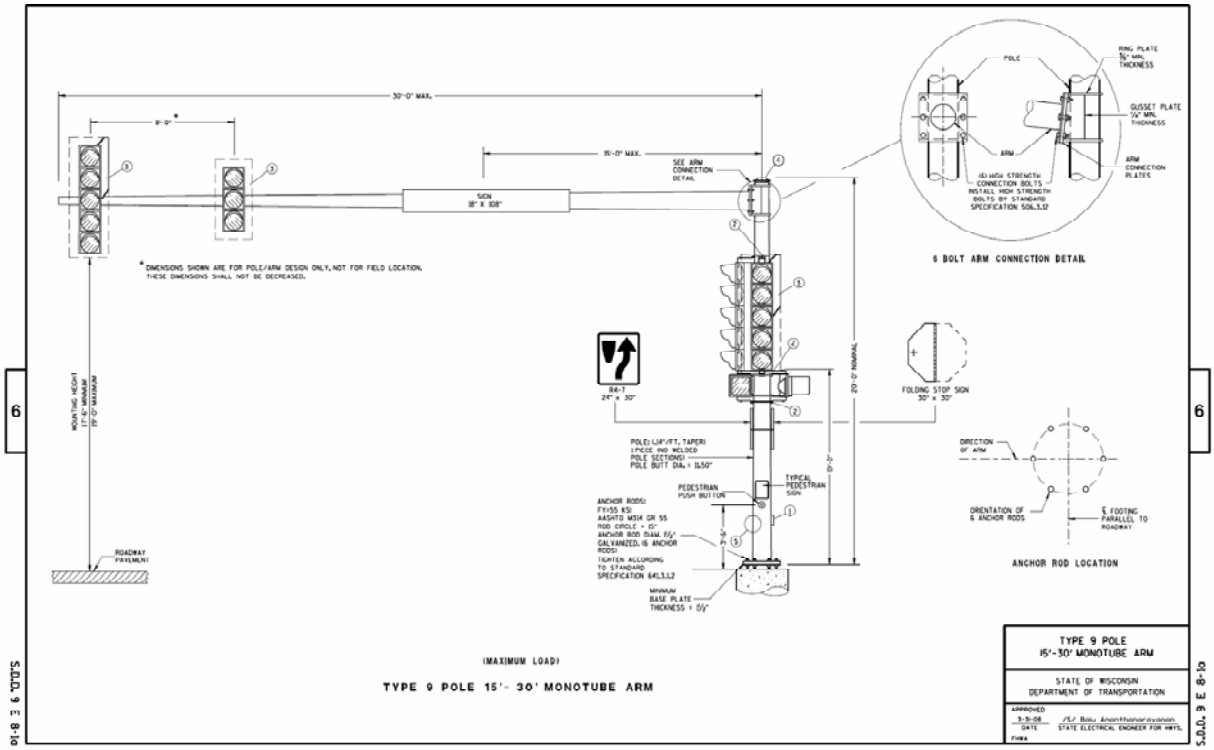

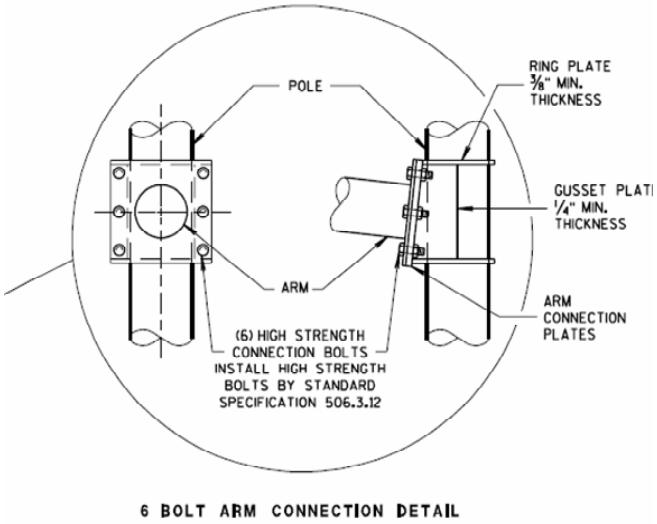

Figure 4.1 WisDOT Type 9 Pole with 15'-30' Monotube Arm Standard Detail.

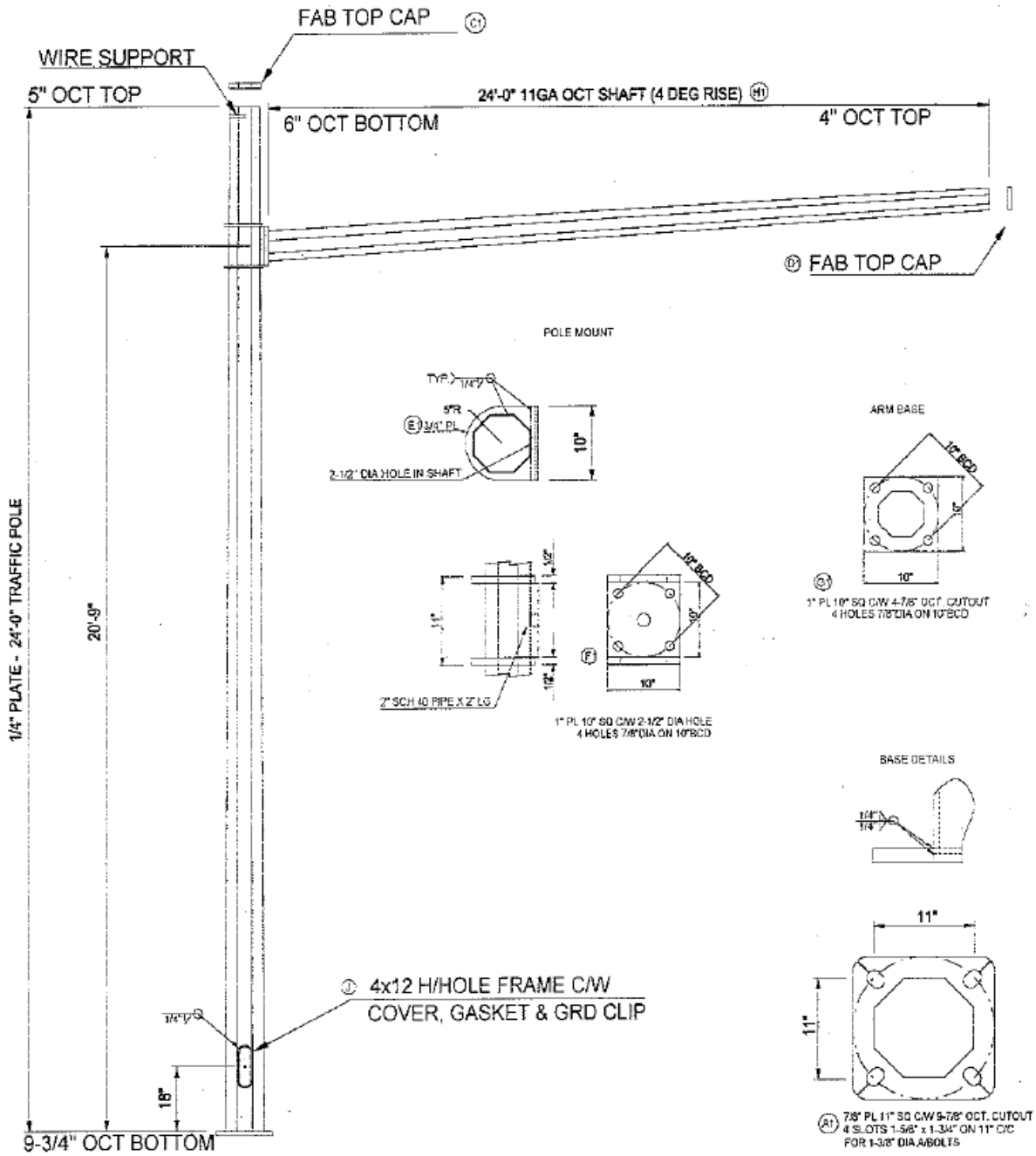

Figure 4.2 Mast-Arm and Pole Connection Detail Used as the Basis for Finite Element Analysis Undertaken.

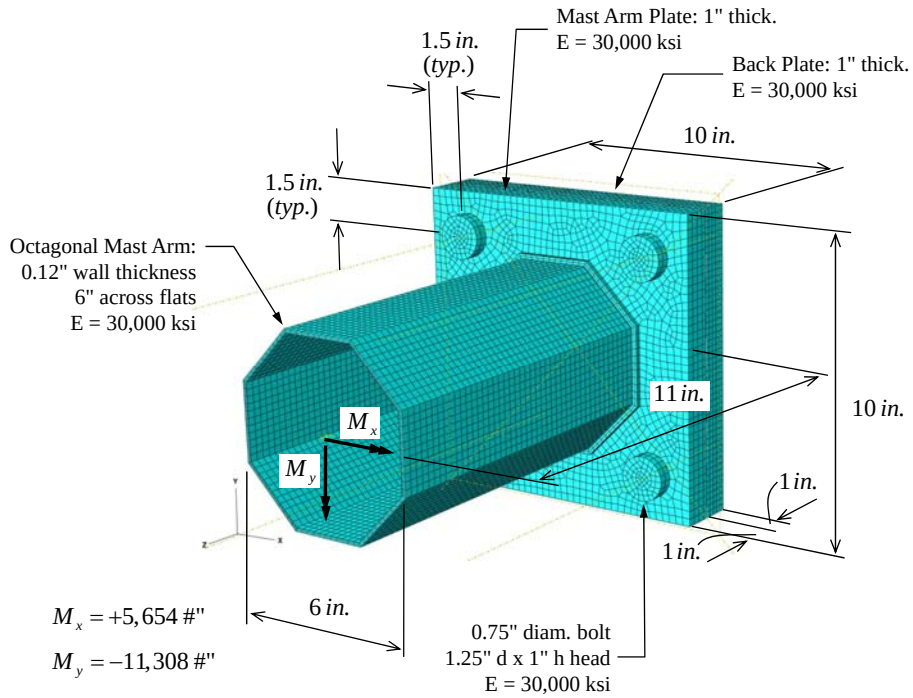

Figure 4.3 Finite Element Model Topology and Loading.

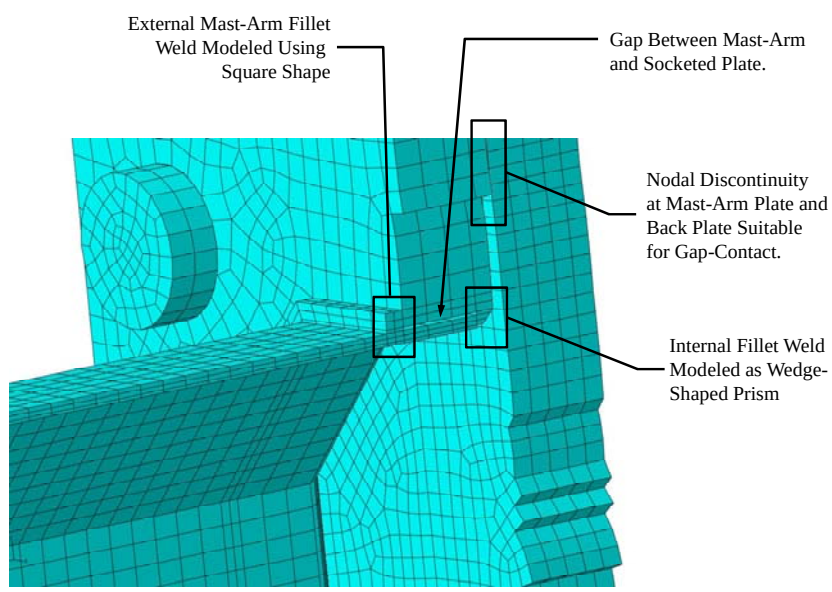

Figure 4.4 Mast-Arm Connection Cut-Away Illustrating Weld and Socket Modeling.

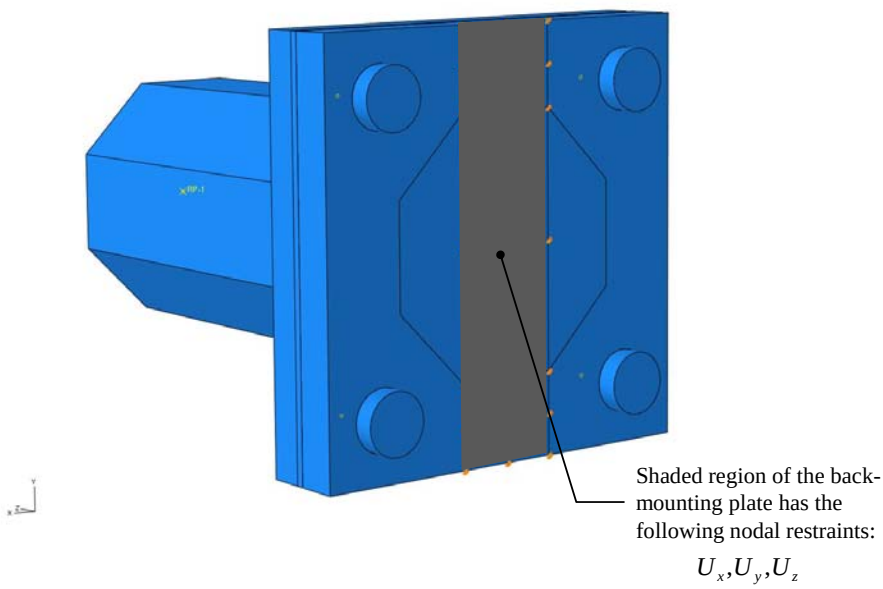

Figure 4.5 Rigid Body Constraint on Back-Mounting Plate.

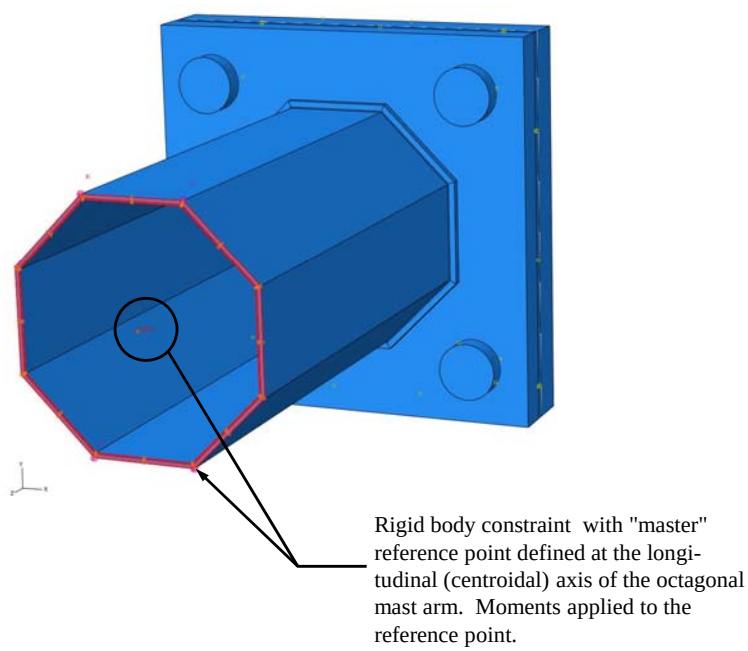

Figure 4.6 Rigid-Body Constraint to Facilitate Application of Bending Moment.

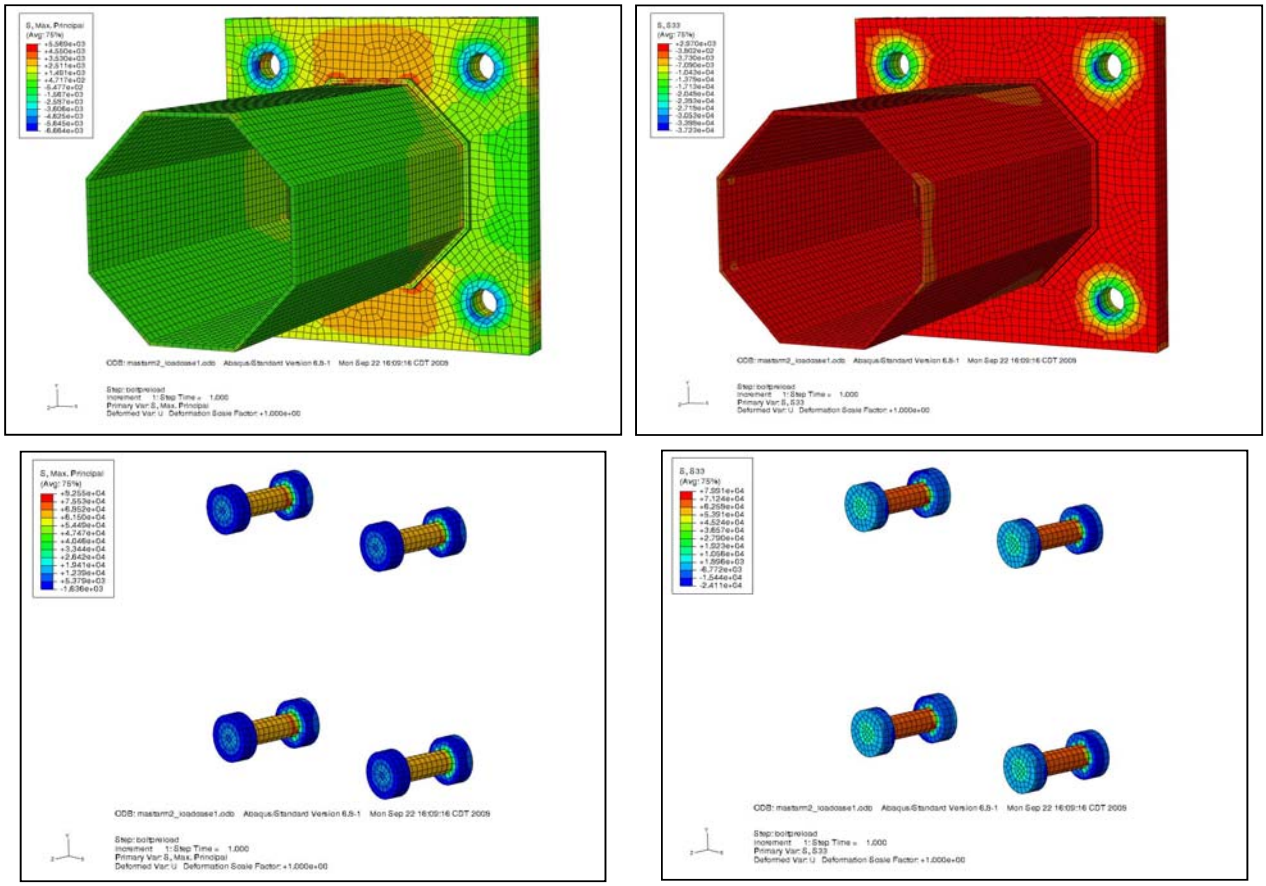

Figure 4.7 Stress Contours for Pretension Load Case 1: Left Column – Maximum Principal Stress; Right Column – Z-direction Stress.

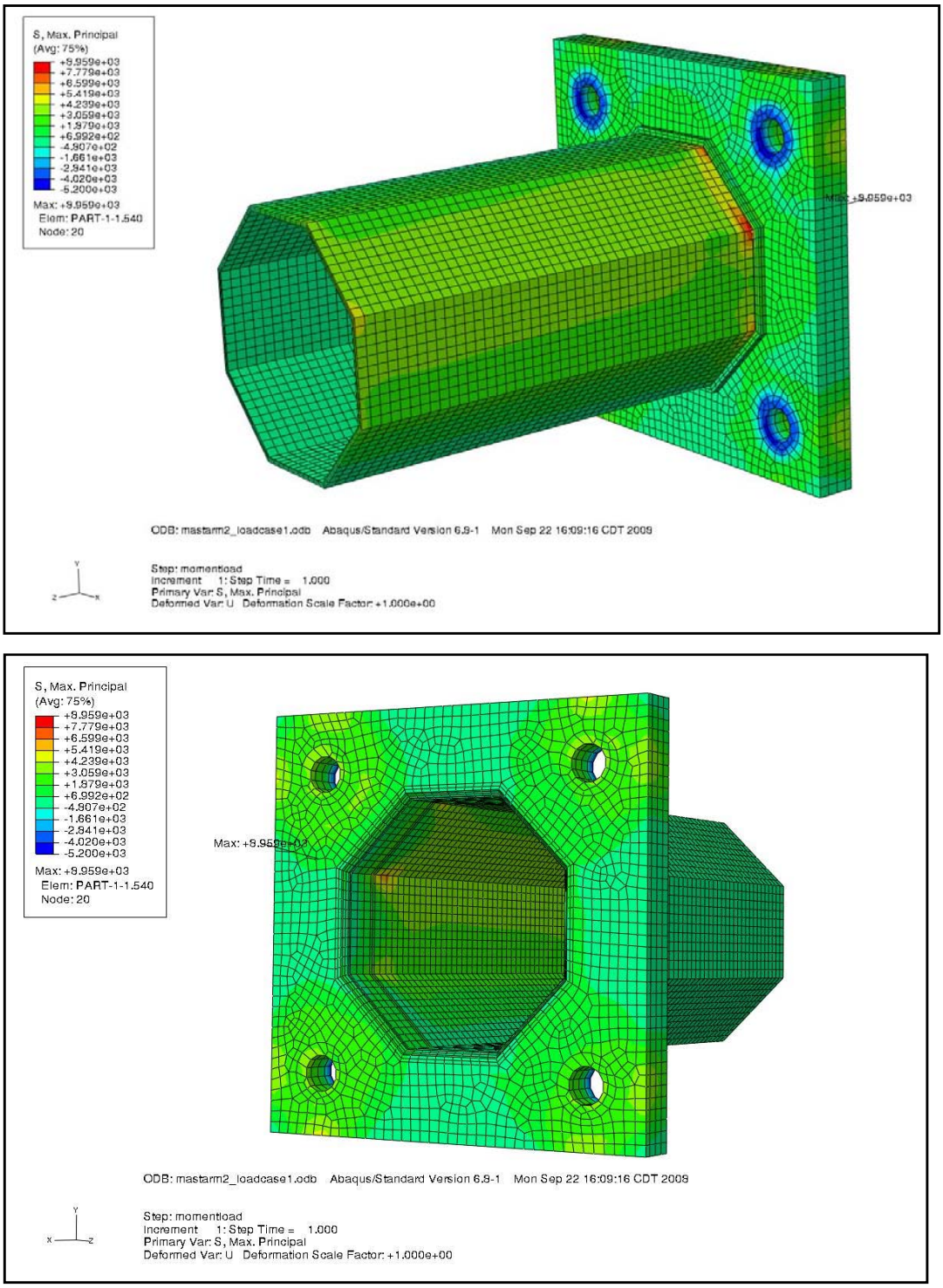

Figure 4.8 Maximum Principal Stress Contours for Bending Moments Applied with Bolt Pretension Condition 1.

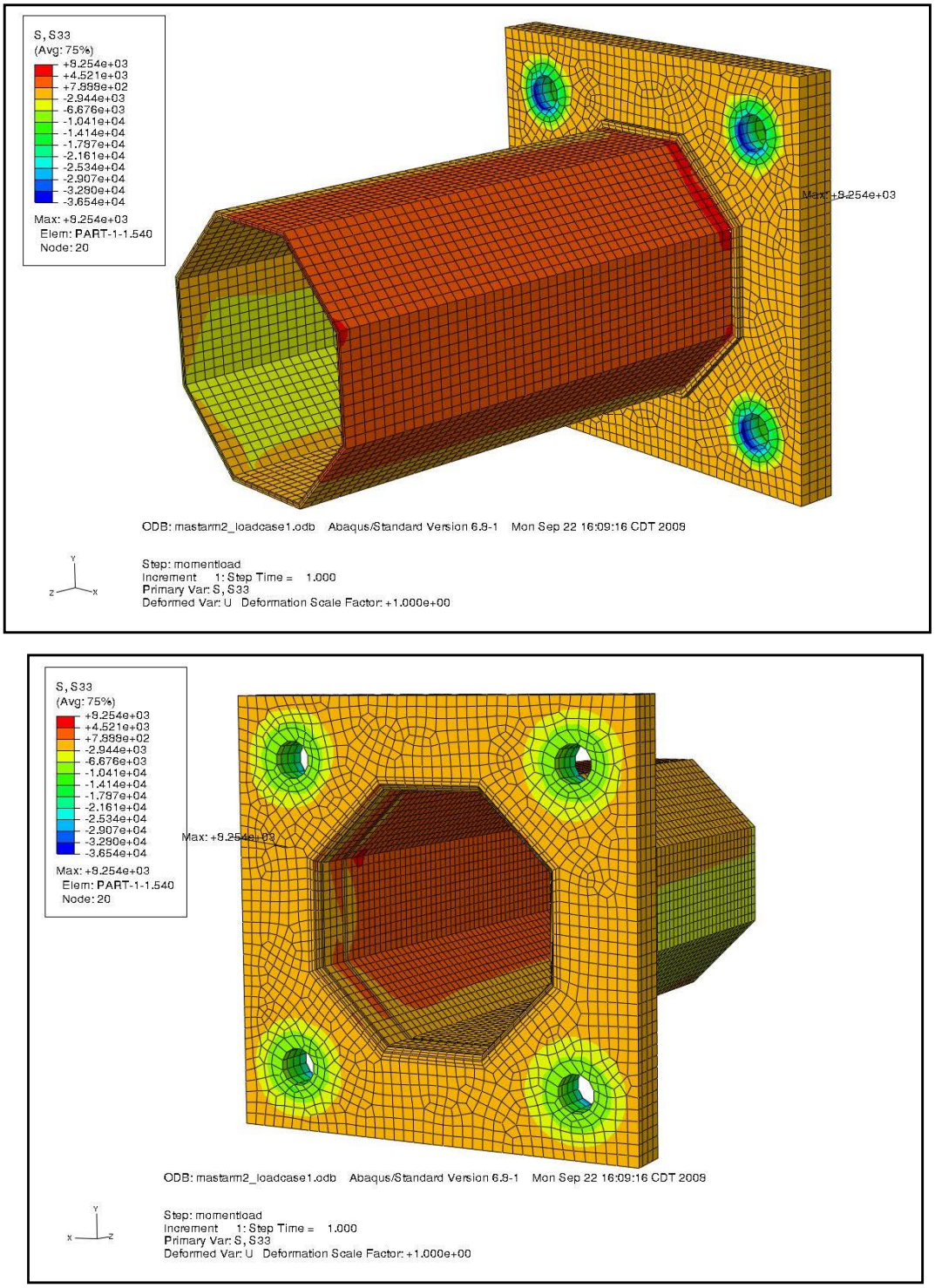

Figure 4.9 Z-Direction Stress Contours for Bending Moments Applied with Bolt Pretension Condition 1.

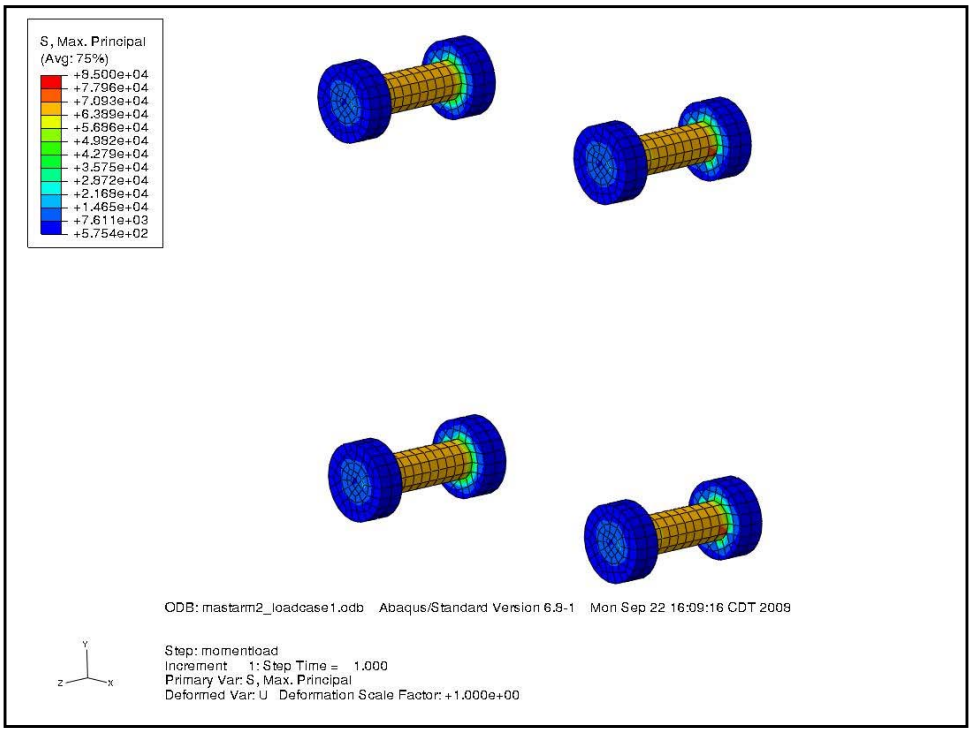

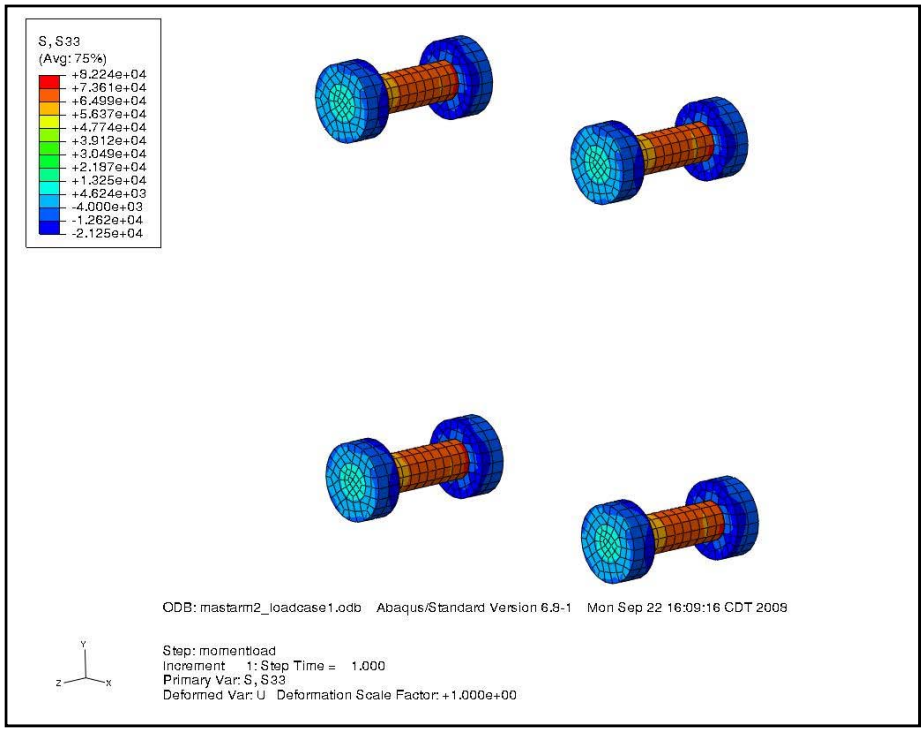

Figure 4.10 Bolt Stress Contours for Bolt Pretension Load Case 1: Top – Maximum Principal Stress Contour; Bottom – Z-direction Stress Contour.

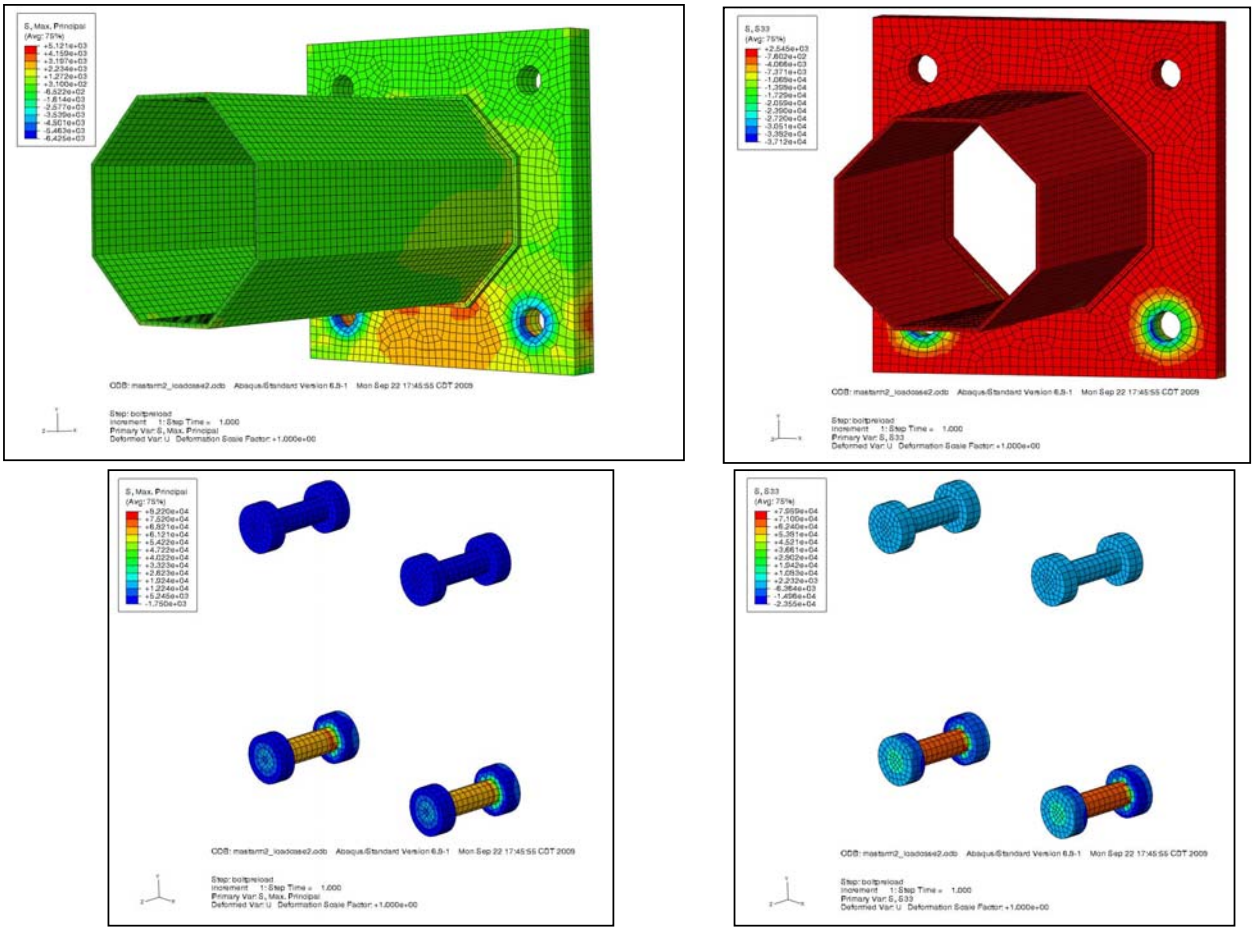

Figure 4.11 Stress Contours for Pretension Load Case 2: Left Column – Maximum Principal Stress; Right Column – Z-direction Stress.

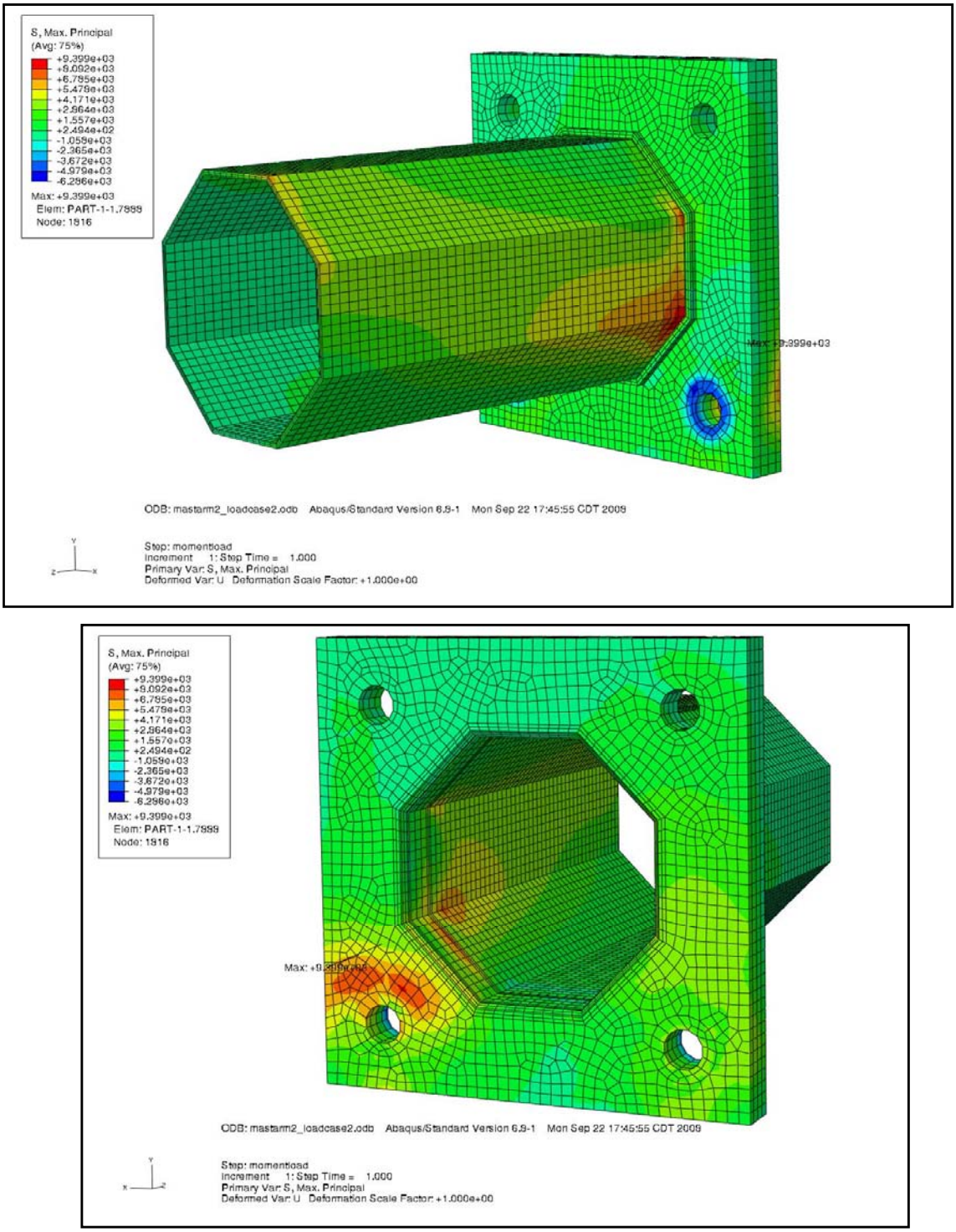

Figure 4.12 Maximum Principal Stress Contours for Bending Moments Applied with Bolt Pretension Condition 2.

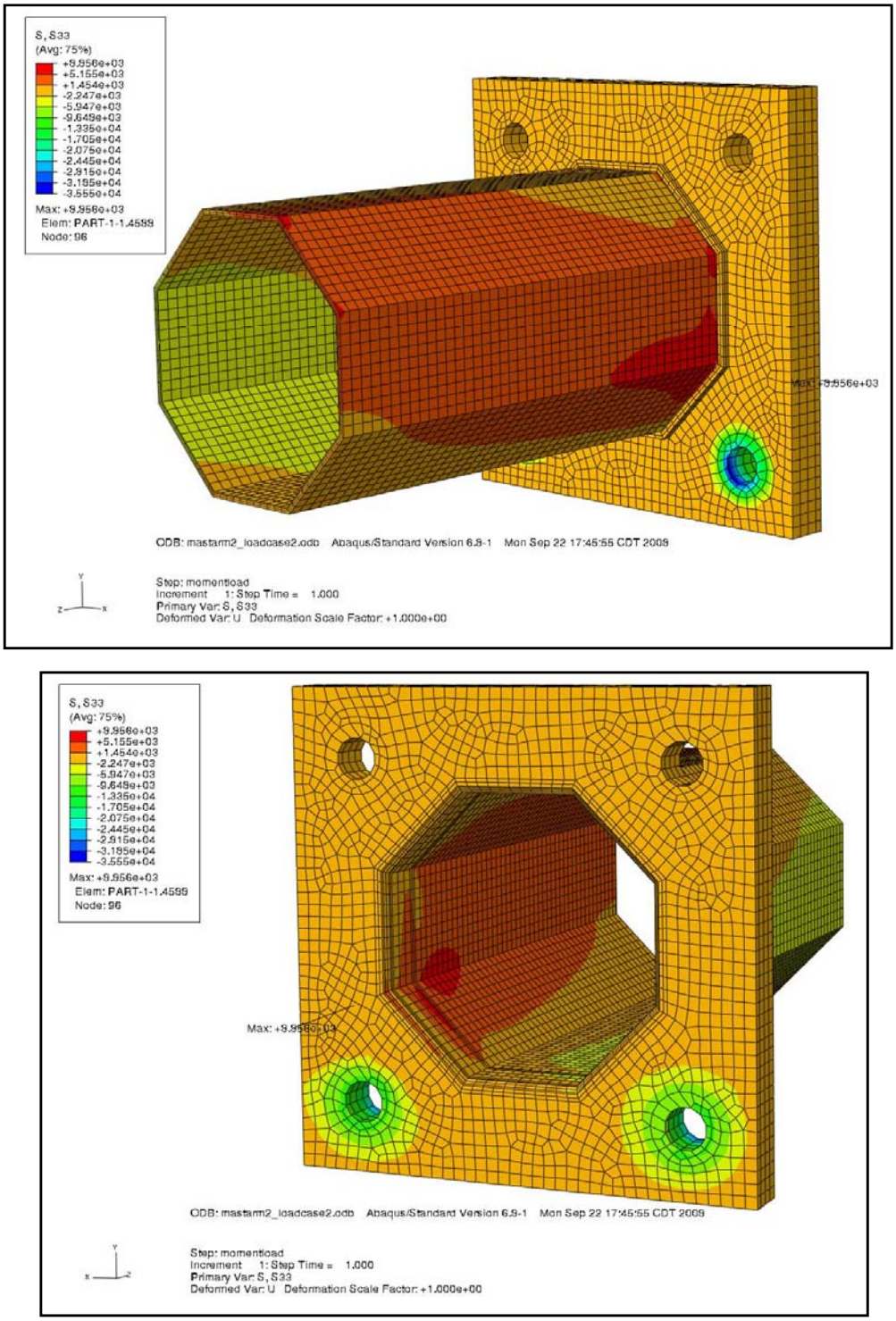

Figure 4.13 Z-Direction Stress Contours for Bending Moments Applied with Bolt Pretension Condition 2.

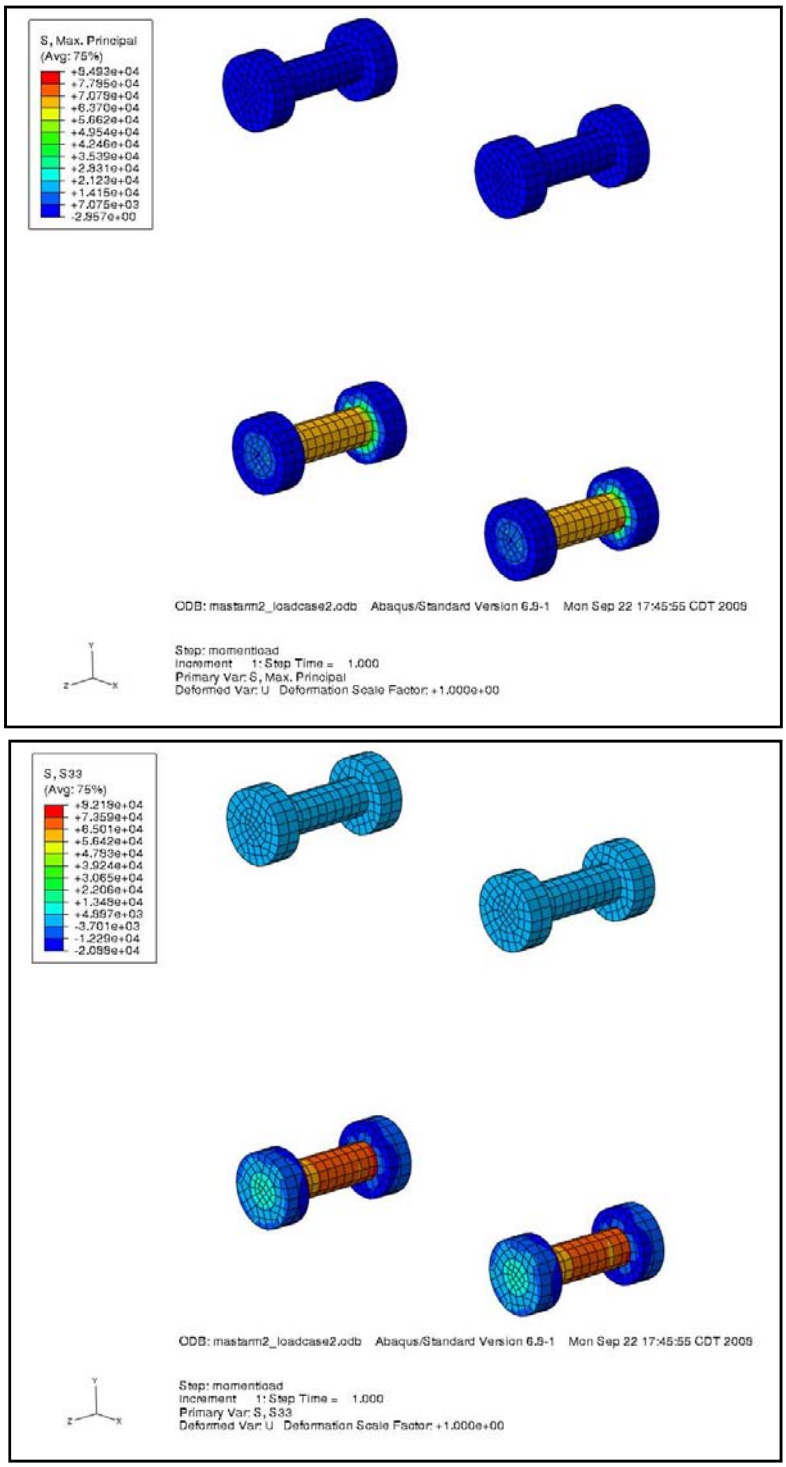

Figure 4.14 Bolt Stress Contours for Bolt Pretension Load Case 2: Top – Maximum Principal Stress Contour; Bottom – Z-direction Stress Contour.

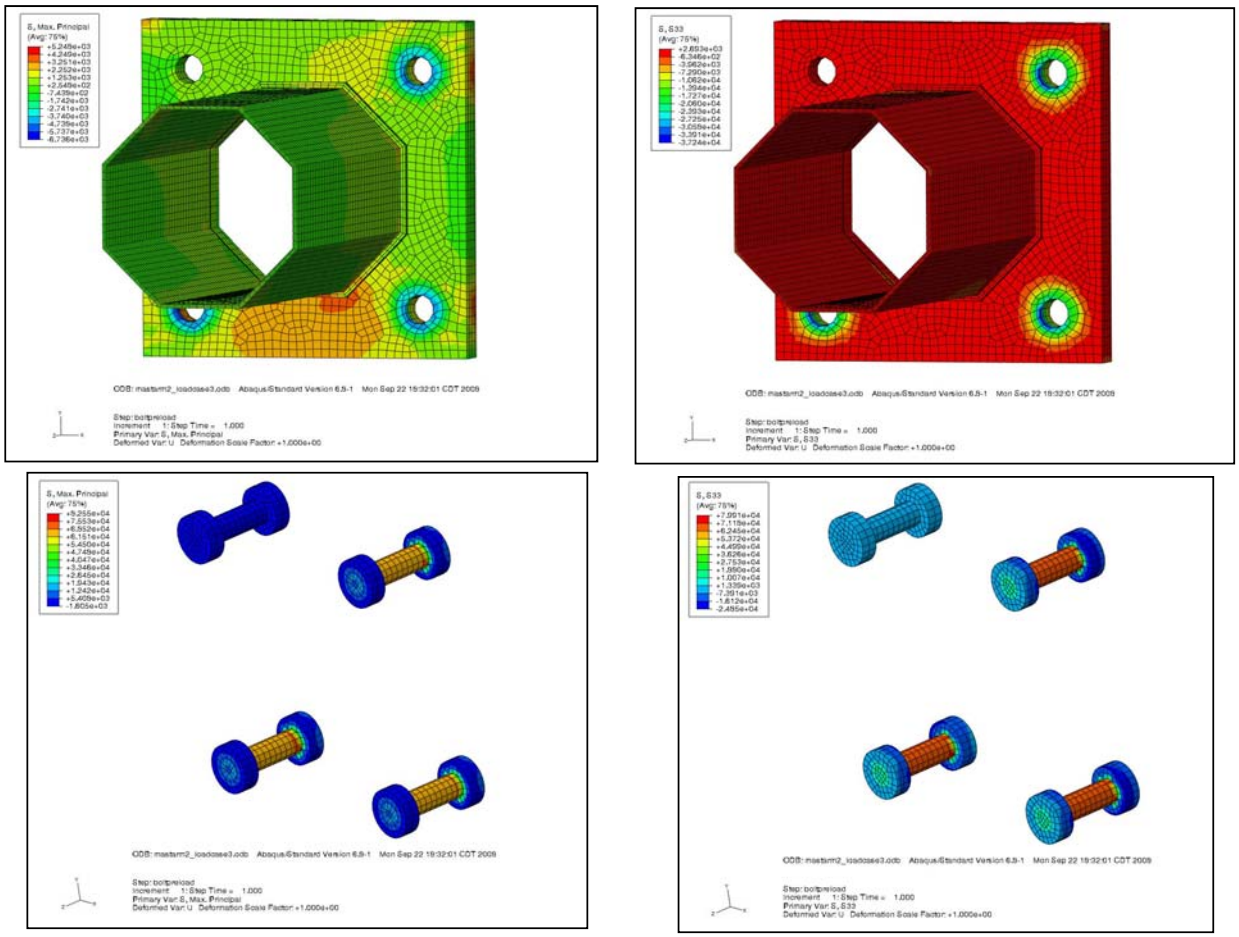

Figure 4.15 Stress Contours for Pretension Load Case 3: Left Column – Maximum Principal Stress; Right Column – Z-direction Stress.

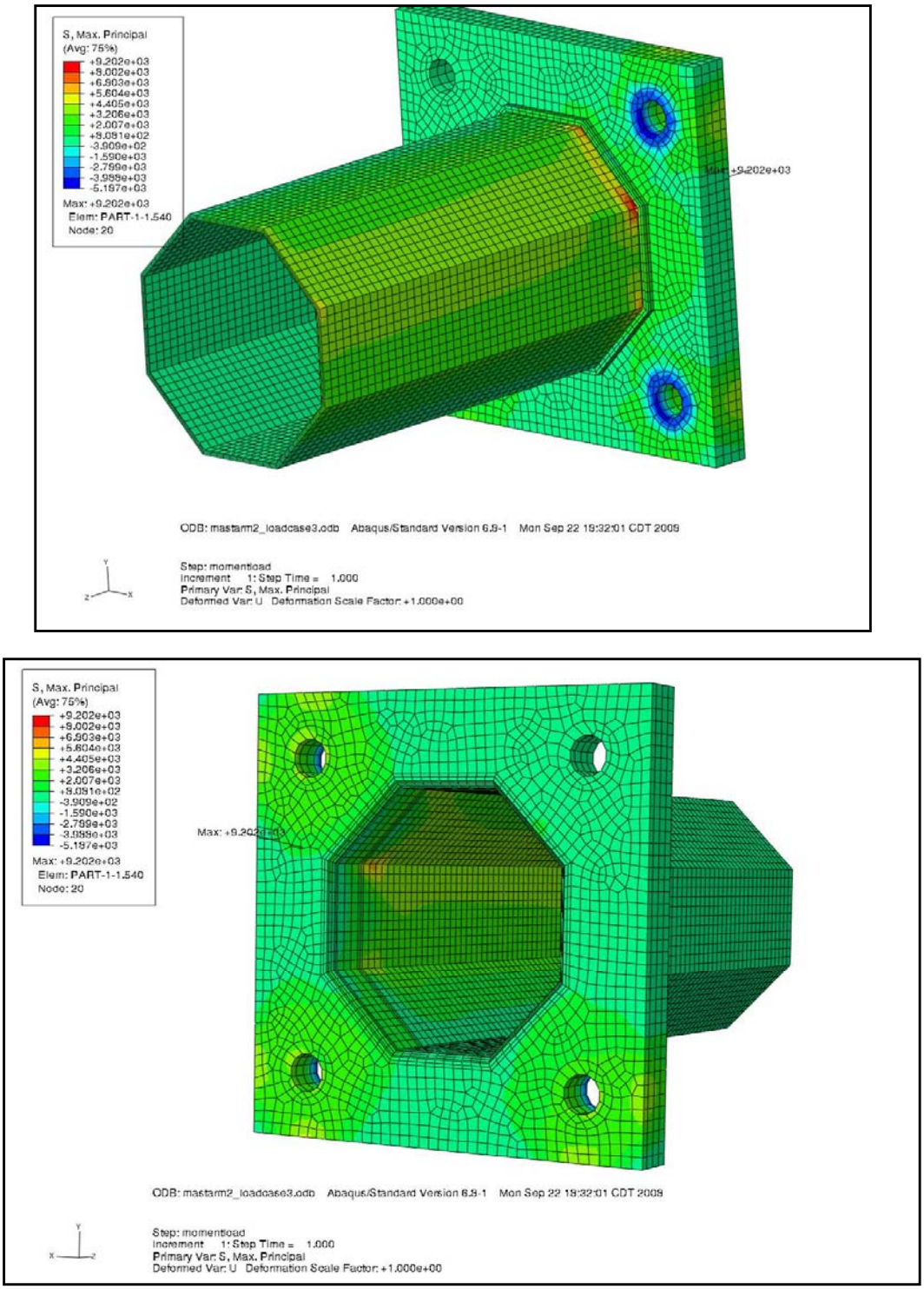

Figure 4.16 Maximum Principal Stress Contours for Bending Moments Applied with Bolt Pretension Condition 3.

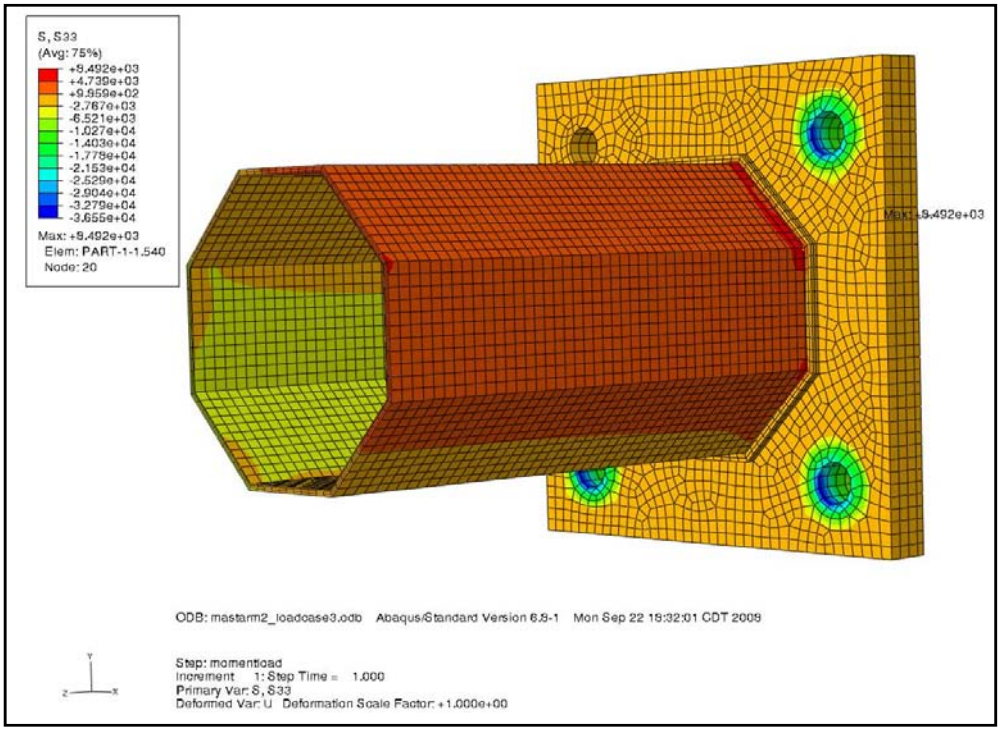

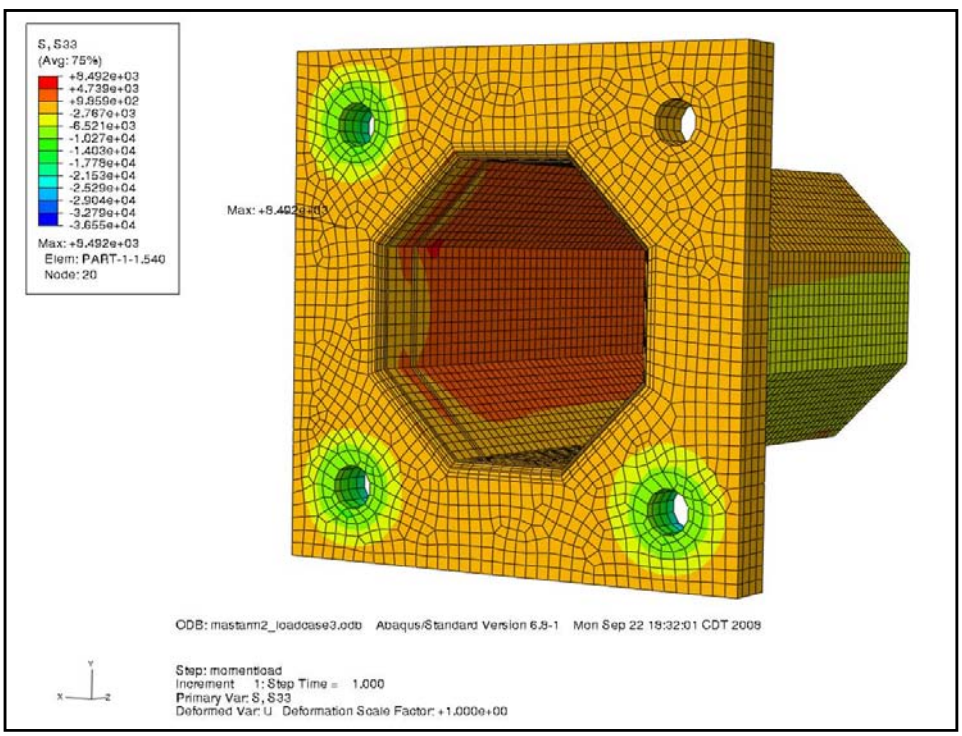

Figure 4.17 Z-Direction Stress Contours for Bending Moments Applied with Bolt Pretension Condition 3.

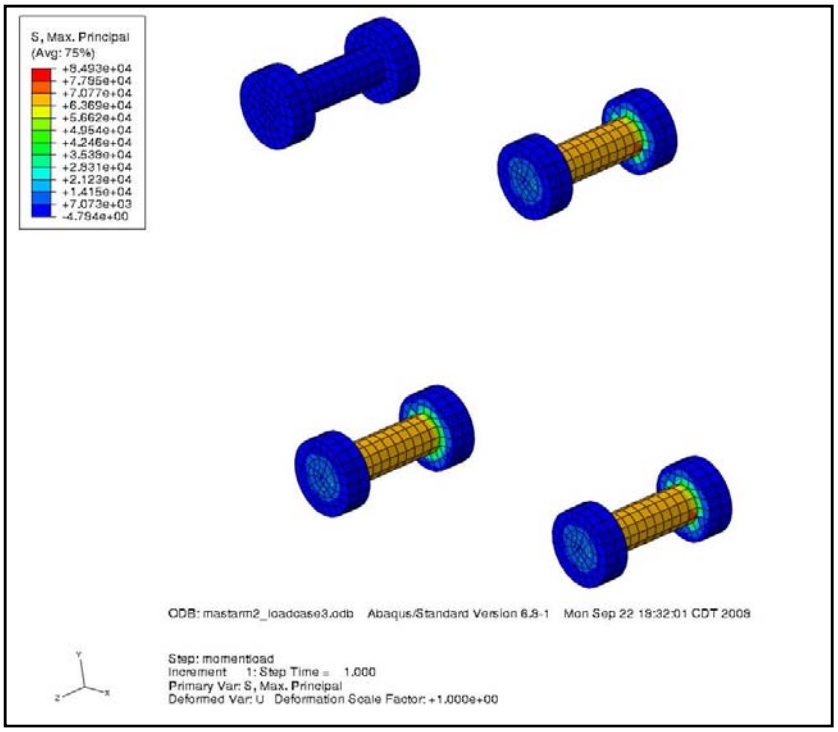

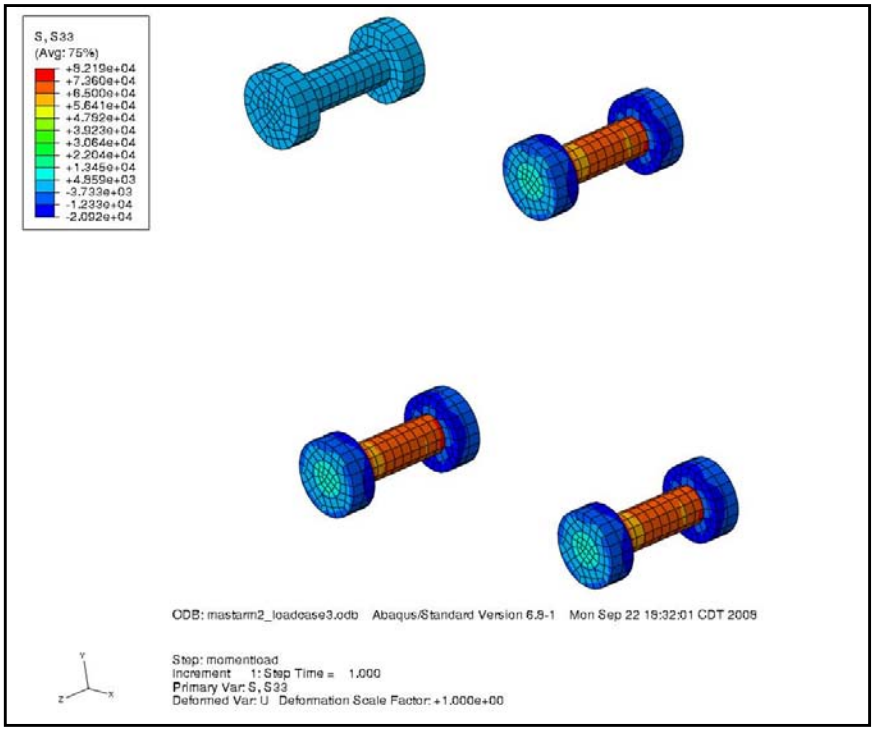

Figure 4.18 Bolt Stress Contours for Bolt Pretension Load Case 3: Top – Maximum Principal Stress Contour; Bottom – Z-direction Stress Contour.

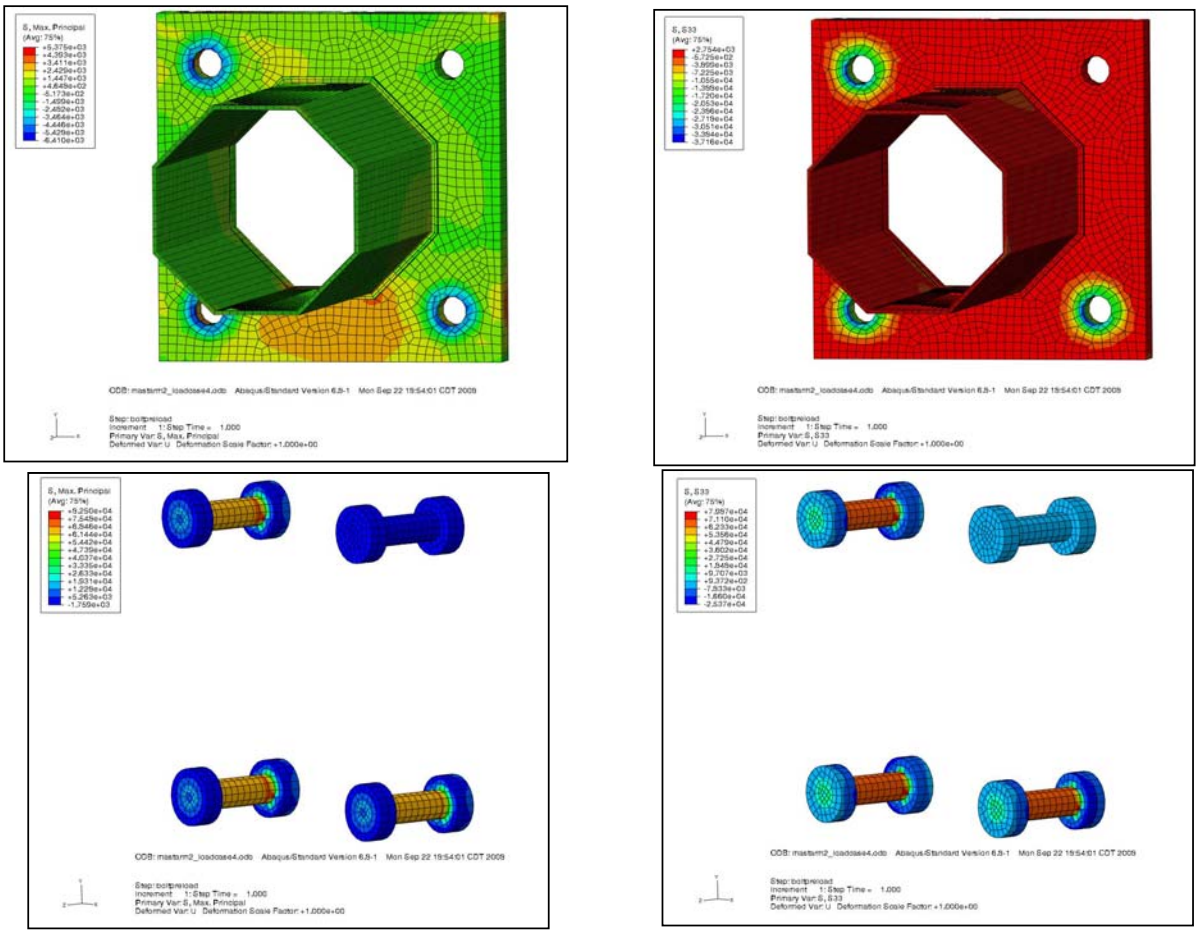

Figure 4.19 Stress Contours for Pretension Load Case 4: Left Column – Maximum Principal Stress; Right Column – Z-direction Stress.

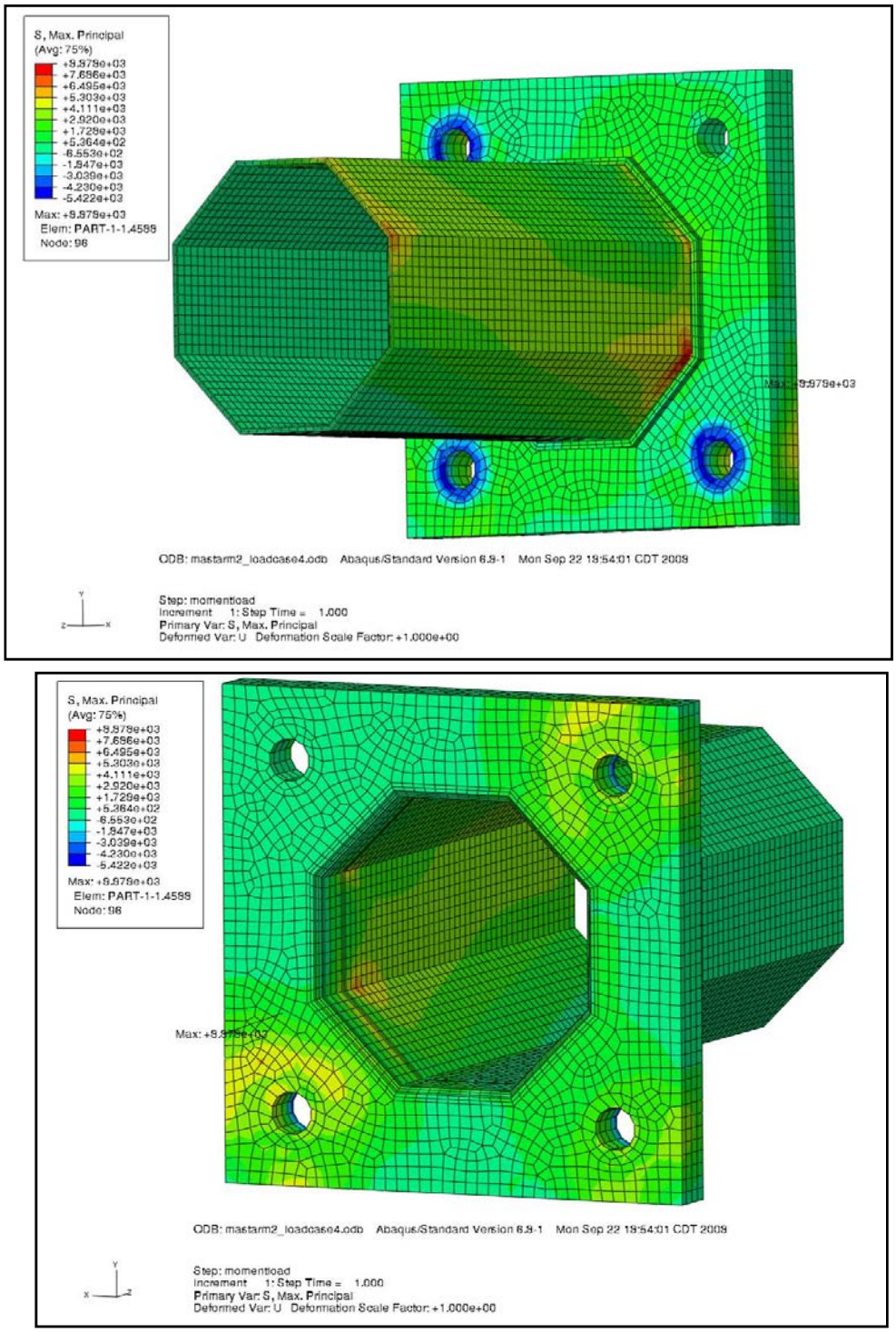

Figure 4.20 Maximum Principal Stress Contours for Bending Moments Applied with Bolt Pretension Condition 4.

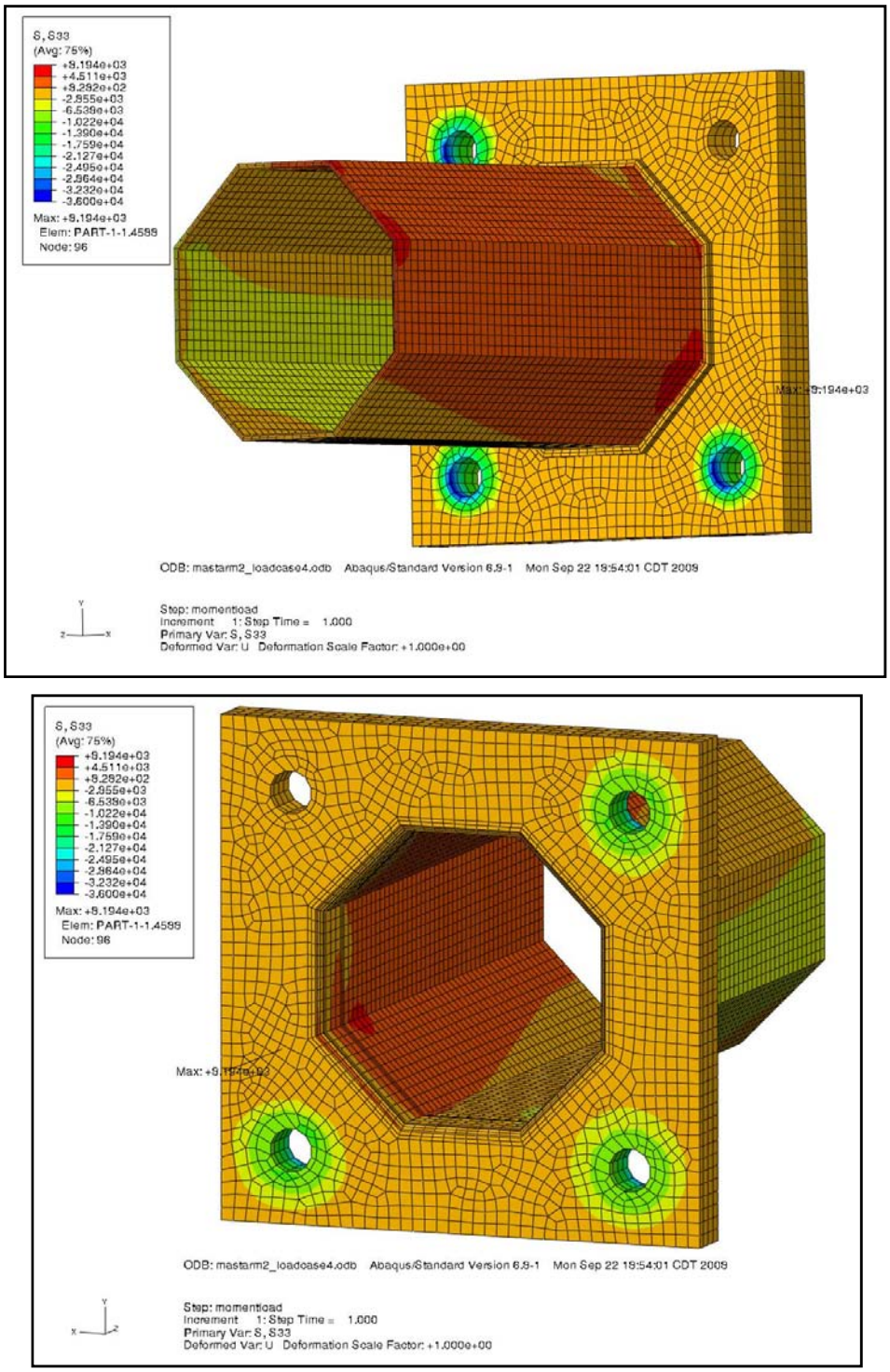

Figure 4.21 Z-Direction Stress Contours for Bending Moments Applied with Bolt Pretension Condition 4.

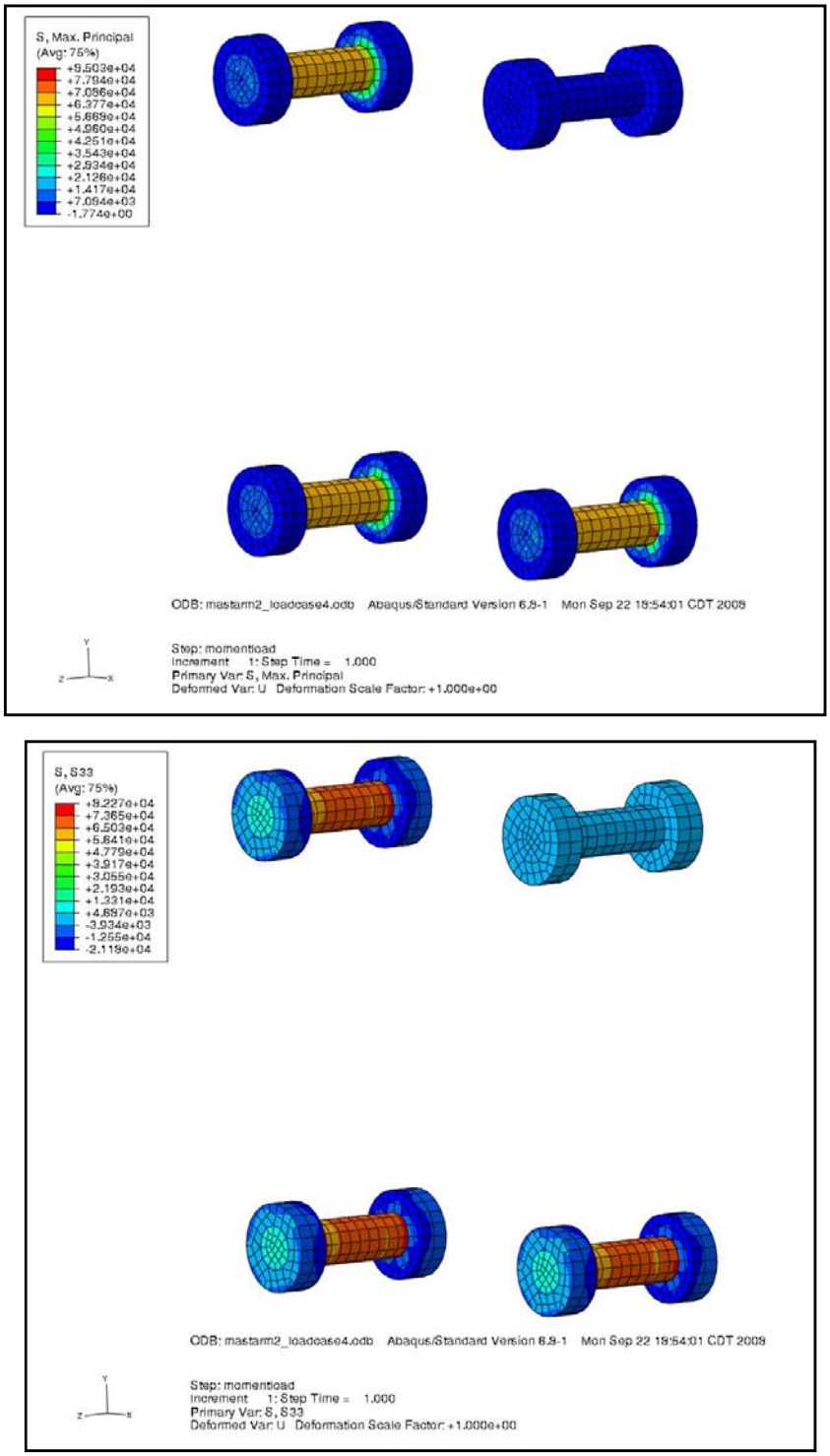

Figure 4.22 Bolt Stress Contours for Bolt Pretension Load Case 4: Top – Maximum Principal Stress Contour; Bottom – Z-direction Stress Contour.

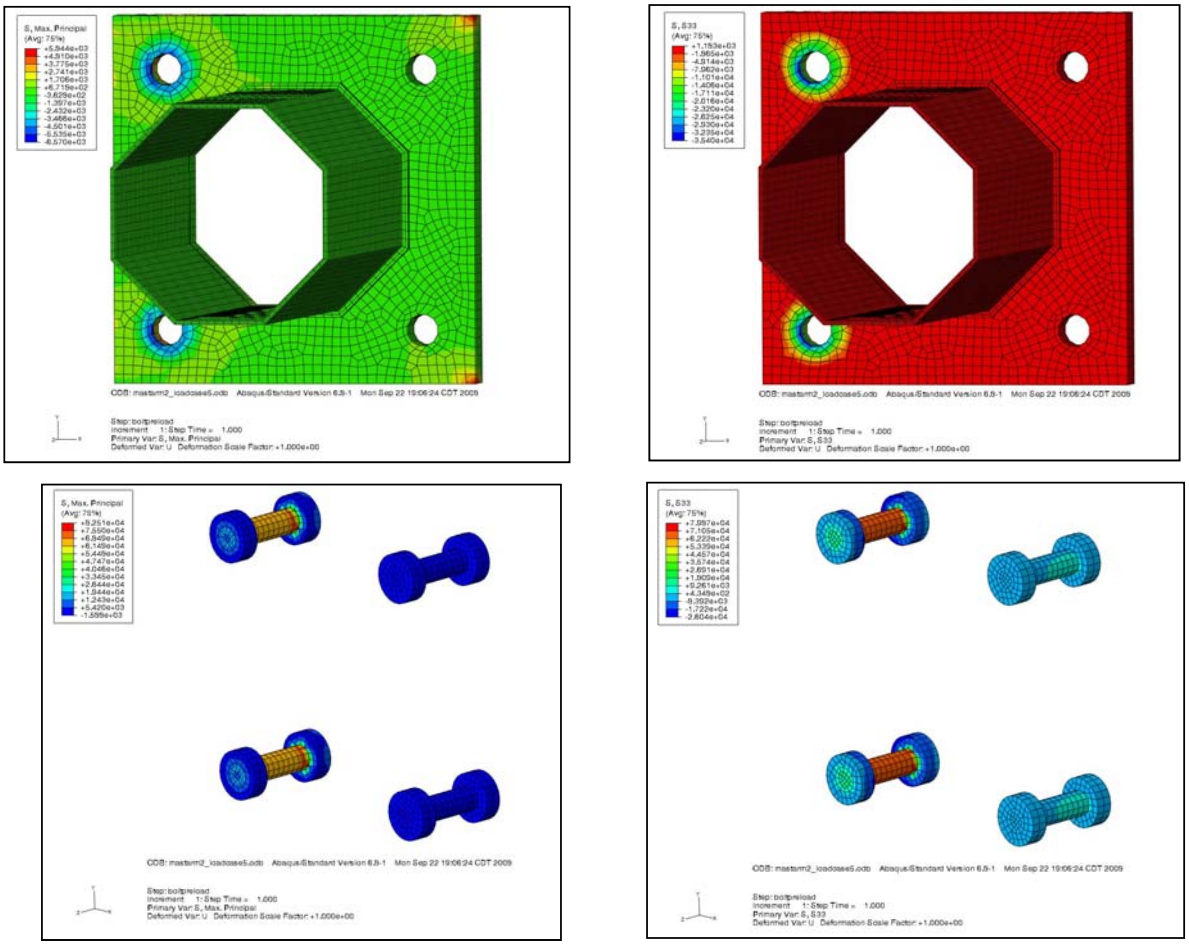

Figure 4.23 Stress Contours for Pretension Load Case 5: Left Column – Maximum Principal Stress; Right Column – Z-direction Stress.

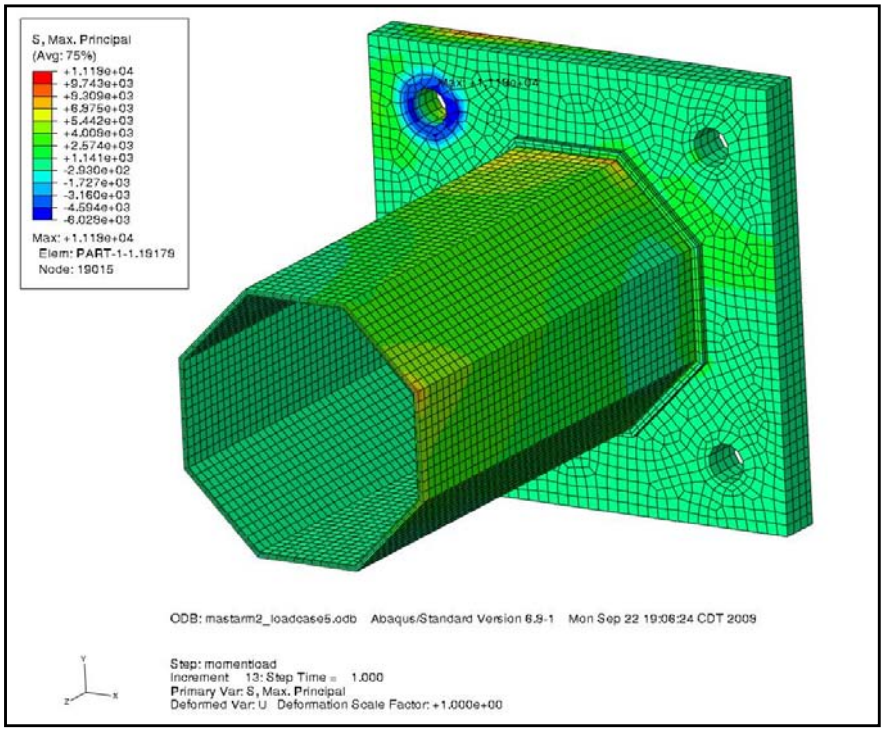

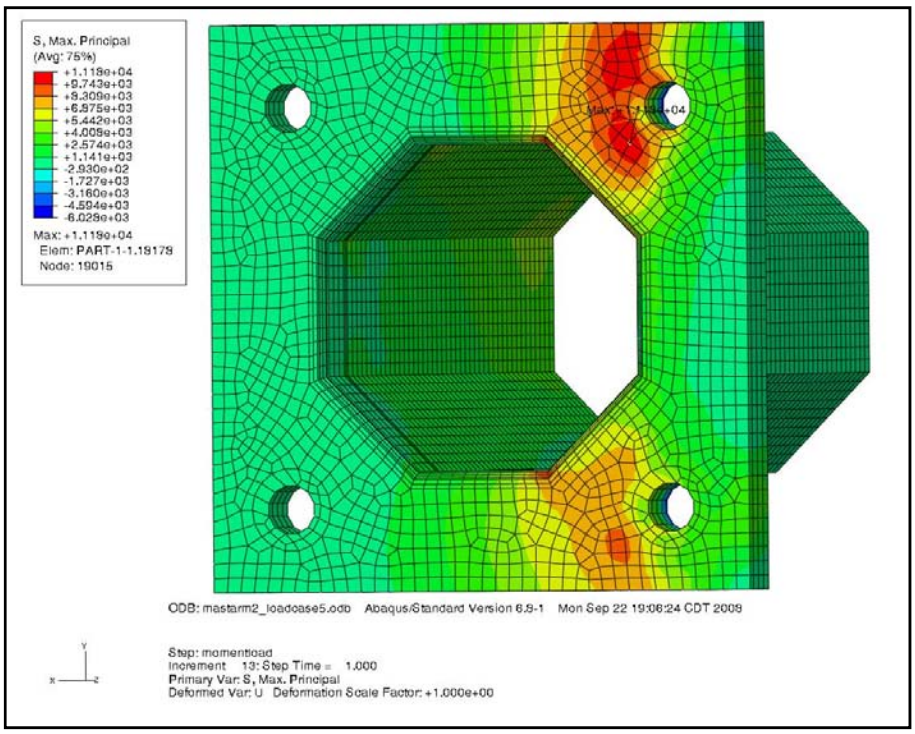

Figure 4.24 Maximum Principal Stress Contours for Bending Moments Applied with Bolt Pretension Condition 5.

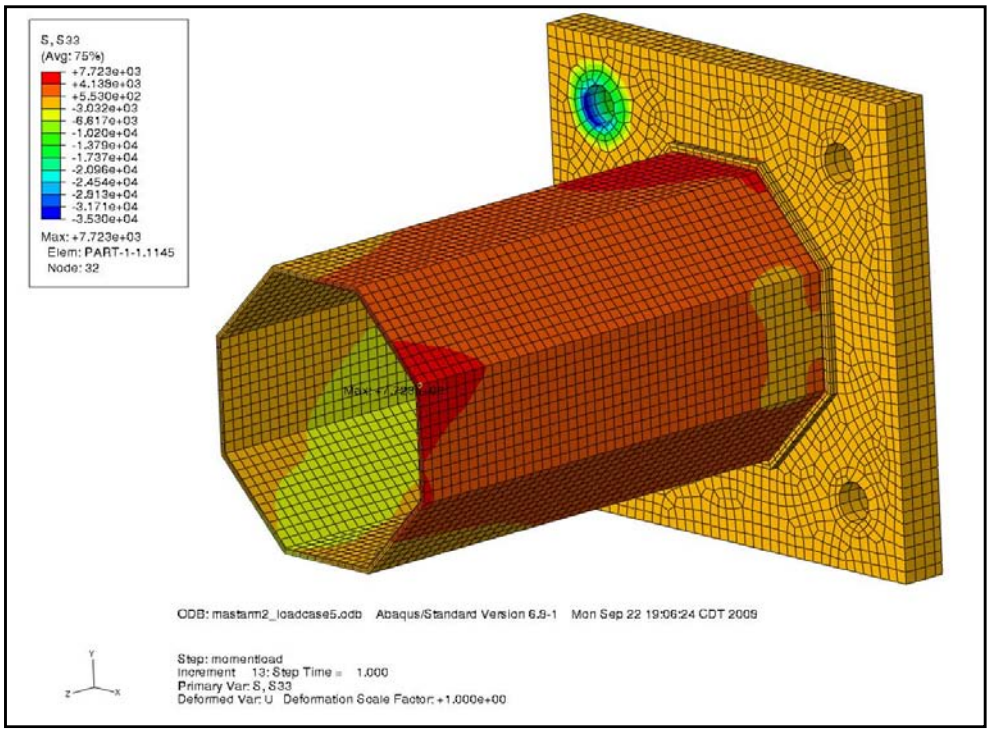

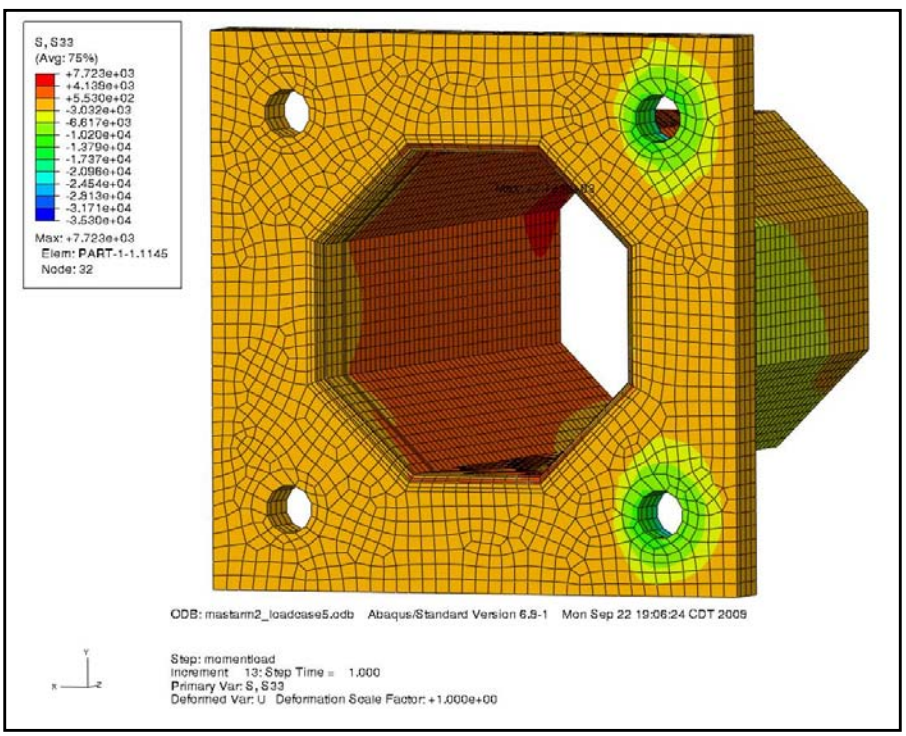

Figure 4.25 Z-Direction Stress Contours for Bending Moments Applied with Bolt Pretension Condition 5.

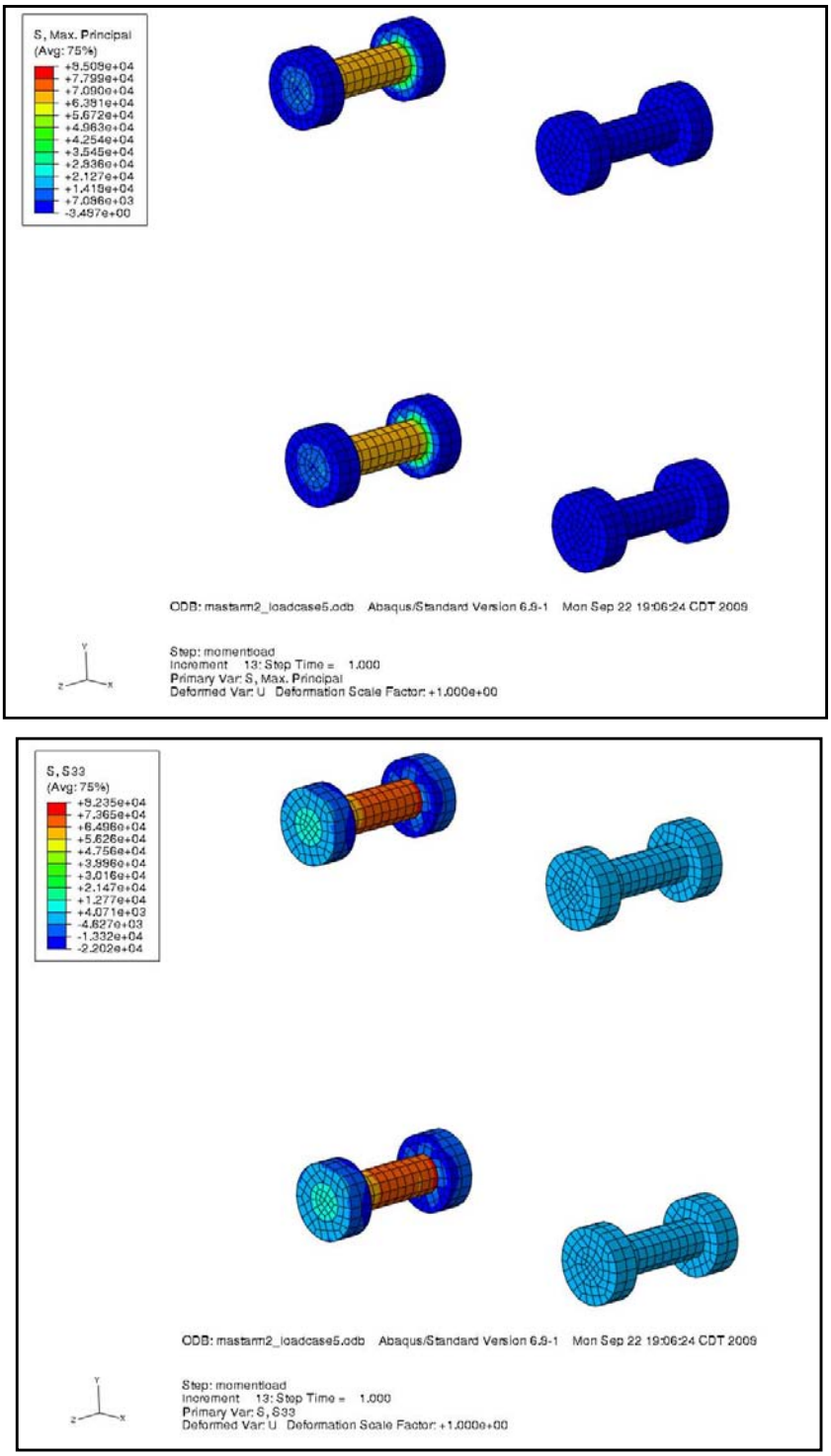

Figure 4.26 Bolt Stress Contours for Bolt Pretension Load Case 5: Top – Maximum Principal Stress Contour; Bottom – Z-direction Stress Contour.

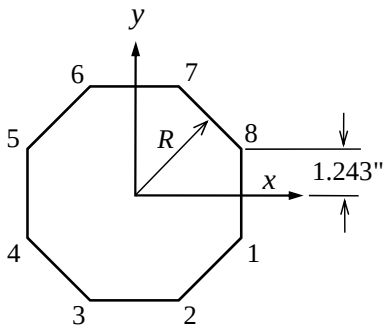

$$R = 3'' - \frac{0.12''}{2} = 2.94'' \quad (\textit{to wall centerline})$$

$$\approx 3'' \ (\textit{thin wall})$$

$$I = I_x = I_y = 3.50 R^3 t = 3.50\left(2.94''\right)^3\left(0.12''\right)$$

$$= 10.67\ in^4$$

$$M_x = +5,654\ \#'' \qquad M_y = -11,308\ \#''$$

$$f_x^8 = \frac{(5,654\ \#'')(1.243'')}{(10.67\ in^4)} = 658\ psi$$

$$f_y^8 = \frac{(11,308\ \#'')(3'')}{(10.67\ in^4)} = 3,179\ psi$$

$$\boxed{f^8 = 658 + 3,179 = 3,838\ psi}$$

$$f_x^7 = \frac{(5,654\ \#'')(3'')}{(10.67\ in^4)} = 1,590\ psi$$

$$f_y^7 = \frac{(11,308\ \#'')(1.243'')}{(10.67\ in^4)} = 1,317\ psi$$

$$f^8 = 1,590 + 1,317 = 2,907\ psi$$

Figure 4.27 Stress Computations for Octagonal Mast-Arm.

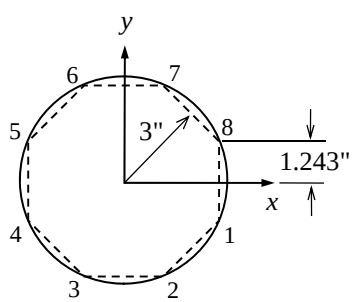

$$R = \sqrt{(3'')^2 + (1.243'')^2} - \frac{0.12''}{2}$$

$$= 3.187''$$

$$I = 3.14 R^3 t = 3.14(3.187'')^3(0.12'')$$

$$= 12.2\ in^4$$

$$M_x = +5,654\ \#'' \qquad M_y = -11,308\ \#''$$

$$M_R = \sqrt{(5,564)^2 + (11,308)^2} = 12,643\ \#''$$

$$\boxed{f_{\max} = \frac{(12,643\ \#'')(3.247'')}{12.20\ in^4} = 3,365\ psi}$$

Figure 4.28 Stress Computations for Round Mast-Arm.

Chapter 5
Summary, Conclusions, Recommendations

SUMMARY

A review of connection details commonly found in Wisconsin DOT sign and signal support structures was provided. The material specifications used by WisDOT for steel sign and signal support structures were reviewed and the manufacturers and typical configurations of the structural systems they historically provided to the state of Wisconsin were discussed. This information was used to frame the review and synthesis of fatigue testing completed to date.

A complete review of fatigue testing completed through earlier research efforts was conducted. The fatigue testing efforts reviewed included specimen configurations similar to typical details used in the state of Wisconsin, including unreinforced, untreated (*e.g.* no UIT, no mechanical peening), and reinforced connections. The connection configurations included those commonly found in monotube-type mast-arm structures.

The fatigue testing results were synthesized using accepted and well-established statistical analysis methods. This synthesis allowed the uncertainty in fatigue life to be quantified for many of the connection configurations tested. The statistical analysis included selecting a cumulative distribution function model suitable for modeling the uncertainty in the test samples; developing bounds on population mean and population variance with various confidence levels; and recommendations for sample sizes for the fatigue testing to be conducted as part of the present study.

A process by which hourly two-minute average wind speed and direction data was collected for eight cities within Wisconsin has been described. The information collected through NCDC weather observation stations was utilized to develop probability mass functions for wind speed and direction. Probability mass functions (PMF's) for direction were developed using 10-degree and 22.5-degree intervals (bins). The 22.5-degree PMF's for wind direction served as the basis for subsequent intersecting event probabilities for wind speed and direction. Tabulated probabilities for wind speed intersecting with direction were generated. These tabulated probabilities were utilized to evaluate lognormal probability density function models for two-minute averaged wind speeds given one of eight cardinal directions.

A series of finite element analyses were undertaken to simulate the behavior of a typical mast-arm-to-plate connection in signal and sign support structures found in WisDOT's inventory. The FE model included

an octagonal mast arm tube with socketed fillet welded connection to a 1-inch thick mast-arm-plate. The FE modeling did not include all details of the mast-arm to pole connection, but it did include back-mounting plate and boundary conditions designed to simulate important restraint conditions on the mast-arm plate at this connection. Gap-contact nonlinearity was included in the finite element modeling as well as bolt pretensioning to levels established in design specifications. Five bolt-pretension arrangements were considered. Principal stresses and normal stresses in the mast-arm tube, the connecting plates, and the bolts were evaluated.

CONCLUSIONS

The synthesis of fatigue testing conducted to date affords several recommendations moving forward into the second phase of the research effort. These recommendations are based upon the knowledge of fatigue life variability gained from the testing. The Kolmogorov-Smirnov goodness of fit test indicated that the variability in all fatigue tests conducted to date can be modeled using lognormal cumulative distribution functions (CDFs) and the corresponding probability density function. In the case of gusset-stiffened mast arm connections, a normal CDF appeared to be a better model for the sample experimental data, but a lognormal CDF was suitable.

It should be emphasized that there is a need to be sensitive to the fatigue lives that are likely to occur at low stress ranges. The experimental testing done to date follows a long-known trend with regard to variability in fatigue life: as the stress range is reduced, the variability in fatigue life increases (Little and Jebe 1975). The next phase in the present research effort may not be able to include the number of tests at the low stress ranges needed to achieve targeted mean interval estimates because the testing duration may be too great (number of stress cycles required to initiate fatigue failure may be too large). This issue will require detailed evaluation as testing recommendations and protocols are finalized.

The statistical analysis conducted indicates that two-minute wind speeds are fairly consistent throughout the eight cities in southern Wisconsin considered. The present research effort confirmed the previous research effort (Foley *et al.* 2004; Ginal 2003) finding that wind speed and direction are statistically dependent events.

The statistical analysis of the wind speed data collected suggests that lognormal probability density and cumulative distribution functions are acceptable models for wind speed variability once a direction has been defined. As a result, there is the possibility to define a continuous random variable model for wind speed given each of the eight cardinal directions considered. If a sign structure in the field is identified and the orientation of its signal or signage is known, a probability model for the two-minute average wind speed distribution can be used for reliability analysis.

The finite element analysis conducted indicates that the normal stresses in the mast-arm wall can be affected by loose bolts. It should be noted that the analysis included a single bi-directional bending moment condition. However, given the analysis limitations, loose bolts can account for a 7% increase in normal stresses in the mast-arm wall. Furthermore, mast-arm-plate flexibility and the discrete load paths resulting from the bolted connection arrangement can conspire to create significant amplification of normal stress around the perimeter of the octagonal mast arm.

RECOMMENDATIONS

The previous testing included several protocols and specimen configurations. It is recommended that a testing arrangement similar to that used by (Koenigs *et al.* 2003) be utilized in this research effort. Rather than loading two specimens simultaneously, it is recommended that the "strong box" concept schematically shown in Figure G.4 (b) be maintained. It may be more useful to mount single specimens to a fixed mounting box. This can allow connections to be tested in multiple directions as well as "out-of-plane". Details of the testing specimen and protocol will need to be worked out with the testing contractor for the second phase of the research. However, it is felt that simulating the flexibility of the pole mounting plate in the experiments is important and should be included if at all possible.

The previous statistical analysis of the fatigue testing suggests that further testing be conducted for the following connection configurations and stress ranges. It is recommended that an additional nine (9) un-stiffened mast arm connections be tested at a stress range of 15 ksi. Analysis of the previous fatigue testing indicates that any specimen in this new set of nine tests may have a fatigue life equal to 750,000 cycles . Thus, an estimate for the number of test cycles at 15-ksi stress range is 6,750,000 cycles to complete the suite of tests. It is also recommended that these 15-ksi stress range tests be supplemented with an additional twelve (12) tests at 6-ksi stress range. A similar analysis of previous fatigue data indicates that each test in this suite could have fatigue lives of 7,726,615 stress-range cycles. Thus, these additional tests could demand as many as 92,000,000 cycles to complete. This may or may not be feasible, and discussions with the testing contractor will need to occur. However, if the recommended tests are conducted at these two stress ranges, there will be significant enhancement in the understanding of uncertainty in the fatigue life of un-stiffened mast arm connections that will provide a very sound foundation for the risk assessment to be conducted in phase 3 of the research effort.

The expected number of stress cycles required to characterize uncertainty in the un-stiffened mast-arm connections may preclude additional testing for pole-base connections. This is felt to be an acceptable compromise as pole-base connections have not suffered from premature fatigue failures in Wisconsin. Therefore, it is expected that the present research effort will not be able to address risk of fatigue-induced

fracture in pole-base connections. Future research efforts should address these connections as they are integral to characterizing fatigue performance of the entire signal or sign support structural system.

There are very few tests that have been conducted on retrofitted connections (*e.g.* hammer peening, UIT). Therefore, it is recommended that additional fatigue life testing be conducted for a single retrofit measure. In addition, there is a relatively new tool used for surface preparation (corrosion product removal) that may serve beneficial as a result of its ability to mildly peen the surface of steel. The tool is the MBX® Bristle Blaster (Monti 2008). The research team became aware of this tool through conversation with colleagues at Marquette University in the mechanical engineering department (Stango and Khullar 2008). A brief description of this tool will be provided in this chapter as it will support its possible consideration as a retrofit tool in relation to the present research effort.

The Bristle Blaster tool is shown in Figure 5.1. The tool utilizes a high-speed rotating spindle and reinforced belt mounted bristles. Each bristle has four functional components termed: the tip, the shank, the knee and the bristle. The rotating bristles are able to penetrate the base material and leave micro-indentations as shown in Figure 5.2. Although the tool was originally intended to serve as surface preparation tool for painted and epoxy coatings, the fact that the tool is able to mildly mechanically peen the surface may make it useful for weld toe treatment as a means to smooth geometric discontinuity resulting from the welding.

The general appearance of the surface after treating is shown in Figure 5.3. Scanning electron micrographs indicate that the surface is indeed mechanically peened by the tool. The amount of material removed through the treatment process has been evaluated (Stango and Khullar 2008) and Figure 5.4 illustrates that duration of contact and age of the bristles affect material removal amounts. Overall, the MBX® Bristle Blaster tool appears to be a portable means with which to mechanically peen the surface of base metal in the vicinity of weld toes with potential to smooth the geometric discontinuities normally present at these locations within welded components. Therefore, it is recommended that this tool be considered as a potential retrofit measure in the present research effort.

The statistical analysis of wind speed and direction indicates that Green Bay and Milwaukee are two cities that make good candidates for field instrumentation as a result of their relatively high mean two-minute average wind speeds and the frequency from which these higher speeds come from a large number of cardinal directions.

The finite element analysis conducted suggests that inspection protocols include examination of bolt pretension in mast-arm connections and that all bolts have pretension in them. While a lower-bound magnitude of pretension was not established in the present effort, the analysis clearly indicates that lack of pretension in bolts around the mast-arm connection can result in elevated states of normal stress in the mast

arm. Therefore, if bolts are found loose in these connections, they should be tightened to establish contact at the faying surfaces of the connecting plates. This will help to alleviate unforeseen concentration of stress resulting from the loose condition.

The FEA conducted also confirms the importance of plate flexibility in the fatigue testing to be conducted in phase 2 of the research effort. It is therefore recommended that any fatigue testing include a specimen configuration with this flexibility to more accurately include these effects.

REFERENCES

Foley, C. M., Ginal, S. J., Peronto, J. L., and Fournelle, R. A. (2004). "Structural Analysis of Sign Bridge Structures and Luminaire Supports." *WHRP 04-03*, Wisconsin Highway Research Program, Madison, WI.

Ginal, S. J. (2003). "Fatigue Performance of Full-Span Sign Support Structures Considering Truck-Induced Gust and Natural Wind Pressures," MS Thesis, Marquette University, Milwaukee, WI.

Koenigs, M. T., Botros, T. A., Freytag, D., and Frank, K. H. (2003). "Fatigue Strength of Signal Mast Arm Connections." *CTR Research Report 4178-2*, Center for Transportation Research at the University of Texas at Austin, Austin, TX.

Little, R. E., and Jebe, E. H. (1975). *Statistical Design of Fatigue Experiments*, Applied Science Publishers, Ltd., London, U.K.

Monti. (2008). "MBX Bristle Blaster." MONTI Werkeuge GmbH, http://monti.de, Bonn, Germany.

Stango, R. J., and Khullar, P. (2008). "Introduction to the Bristle Blasting Process for Simultaneous Corrosion Removal/Anchor Profile." *Corrosion & Materials*, 33(5 - October), Australasian Corrosion Association, Victoria, Australia, 26-31.

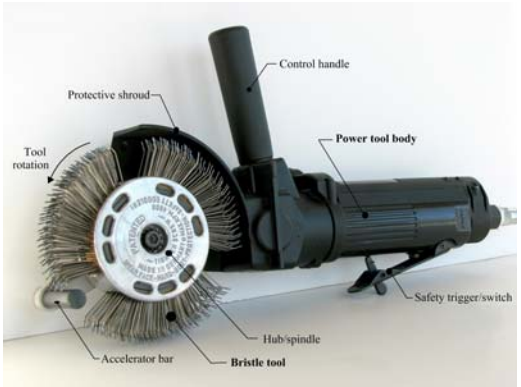

(a) MBX Bristle Blaster Surface Preparation Tool

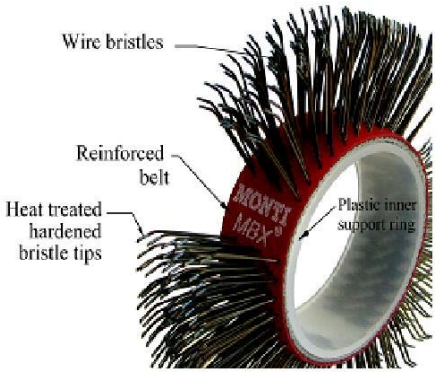

(b) Belt Mounted Bristles

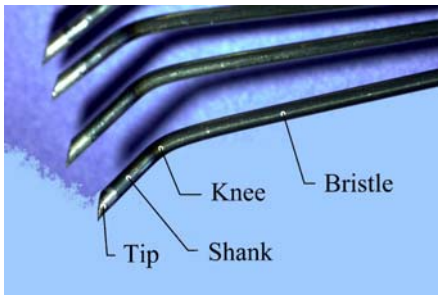

(c) Bristle Terminology

Figure 5.1 MBX Bristle Blaster Surface Preparation Tool (Monti 2008; Stango and Khullar 2008).

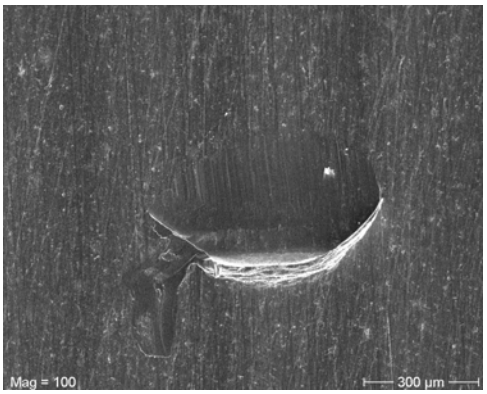

Figure 5.2 Micro-Indentation Caused by Bristle Tip Impact (Stango and Khullar 2008).

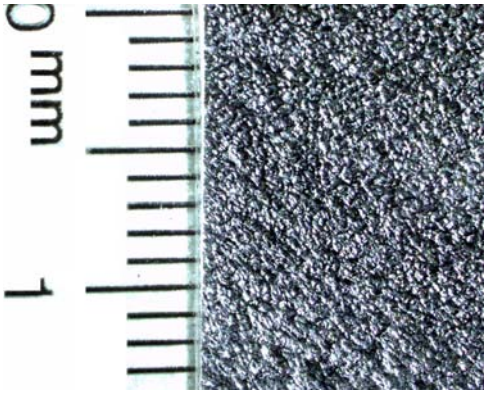

(a) General Appearance of Treated Surface

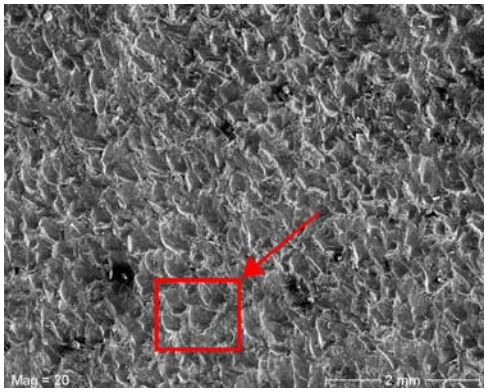

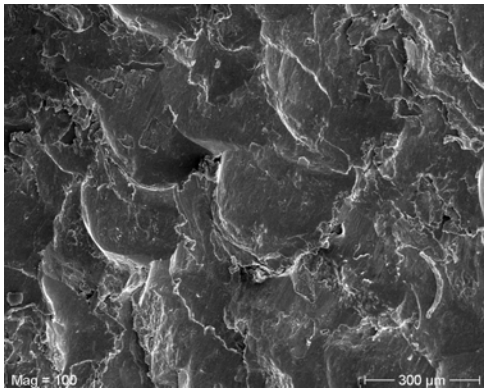

(b) 20x Scanning Electron Micrograph (c) 100x Scanning Electron Micrograph

Figure 5.3 Treated Surface Topology (Stango and Khullar 2008).

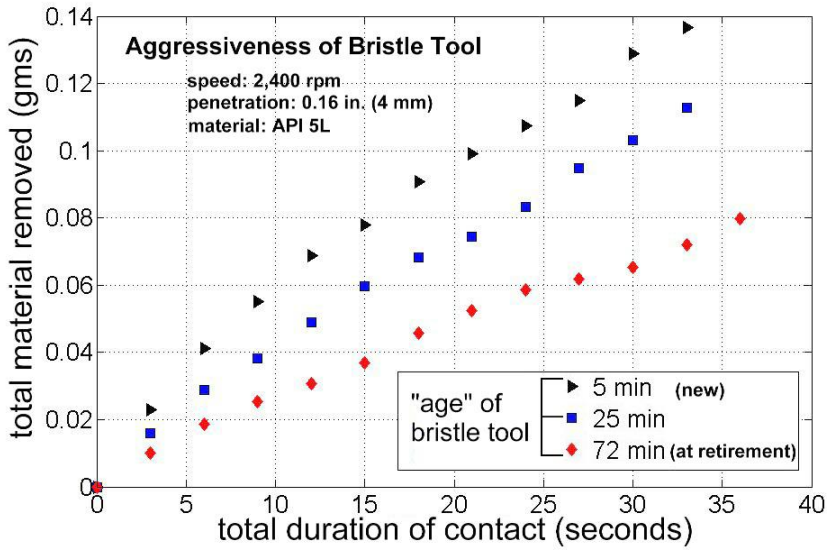

Figure 5.4 Material Removal Rate for Flat Specimen with Service Duration Variation (Stango and Khullar 2008).

Appendices

Appendices A through K include synthesis information for fatigue testing that has been conducted from 1970 to the present for connection details that are similar to those considered in the present research effort.

Appendices J through Q contain data stemming from a wind speed statistical analysis for eight cities within the state of Wisconsin.

This page has intentionally been left blank.

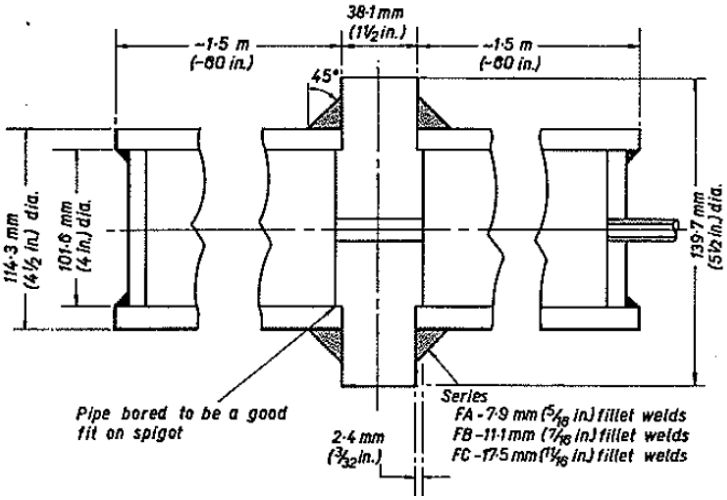

(a) Flush Fillet-Weld Connection (Type F Specimens)

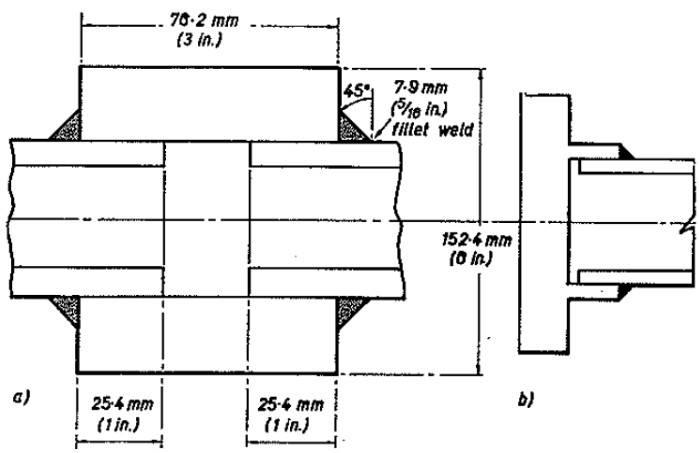

(b) Socketed Fillet-Weld Connection (Type S Specimens)

Figure A.1 Round Hollow Shape (RHS) Connection Details (Archer and Gurney 1970).

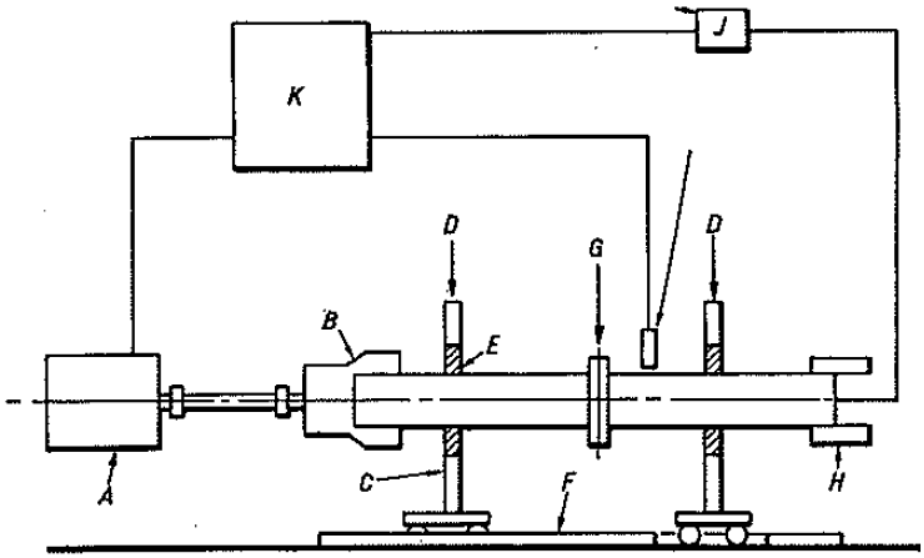

Figure A.2 Testing Apparatus for Cyclic Fatigue Testing (Archer and Gurney 1970).

Table A.1 Fatigue Testing Results for Type F Specimens (Archer and Gurney 1970).

Specimen Designation	No. of Cycles at Cracking	Stress Range (ksi)
AG-F-5/16-W-A	28,000	12.60
-B	130,000	10.60
-C	230,000	9.20
-D	420,000	8.00
-E	600,000	6.90
-F	850,000	5.60
-G	2,700,000	4.60
AG-F-7/16-W-A	360,000	8.20
-B	430,000	7.60
-C	750,000	5.30
-D	1,250,000	4.50
AG-F-5/16-RHS-A	28,000	11.00
-B	120,000	9.00
-C	240,000	8.00
-D	430,000	7.00
-E	550,000	6.00
-F	850,000	5.00
-G	2,700,000	4.00
AG-F-7/16-RHS-A	550,000	9.00
-B	1,400,000	6.00
-C	3,400,000	4.00
AG-F-11/16-RHS-A	800,000	11.00
-B	850,000	10.00
-C	1,200,000	8.00
-D	1,300,000	9.00
-E	1,900,000	7.00
-F	2,000,000	7.00

Table A.2 Fatigue Testing Results for Type S Specimens (Archer and Gurney 1970).

Specimen Designation	No. of Cycles at Cracking	Stress Range (ksi)
AG-S-7/16-W-A	550,000	7.50
-B	1,400,000	4.90
-C	3,300,000	5.30
AG-S-9/16-W-A	310,000	7.00
-B	600,000	5.10
-C	2,400,000	5.70
AG-S-7/16-RHS-A	310,000	11.00
-B	440,000	7.00
-C	600,000	8.00
-D	2,500,000	6.00
AG-S-9/16-RHS-A	380,000	10.0
-B	430,000	8.00
-C	800,000	6.50
-D	1,300,000	5.50

Table A.3 Key to Testing Specimens

AG – A – B – C – D		
Connection Detail Configuration		
A	S	sleeved connection similar to fillet-welded socket connection
	F	flush fillet welds
Weld Configuration and Size		
B	Weld Size	
	5/16	5/16-in fillet weld
	7/16	7/16-in fillet weld
	9/16	9/16-in fillet weld
	11/16	11/16-in fillet weld
Failure Location		
C	W	failure in fillet weld
	RHS	failure in round hollow shape wall
Specimen Designation for Series		
D		specimen designation: A, B, C, etc....

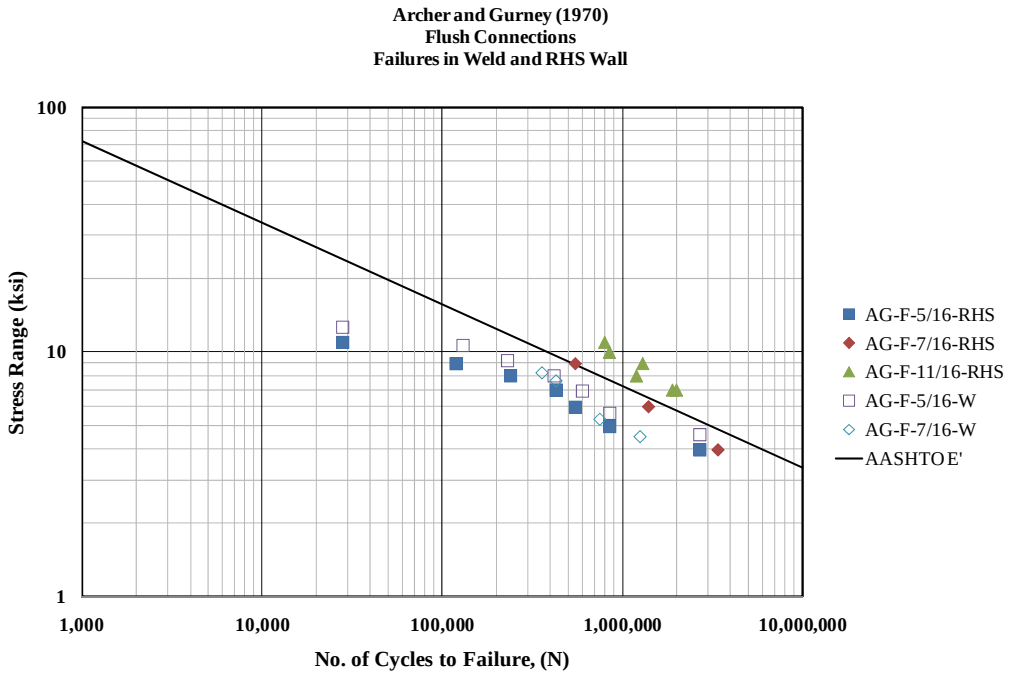

Figure A.3 Fatigue Lives for Flush Type (F) Fillet Welded Connections (Archer and Gurney 1970).

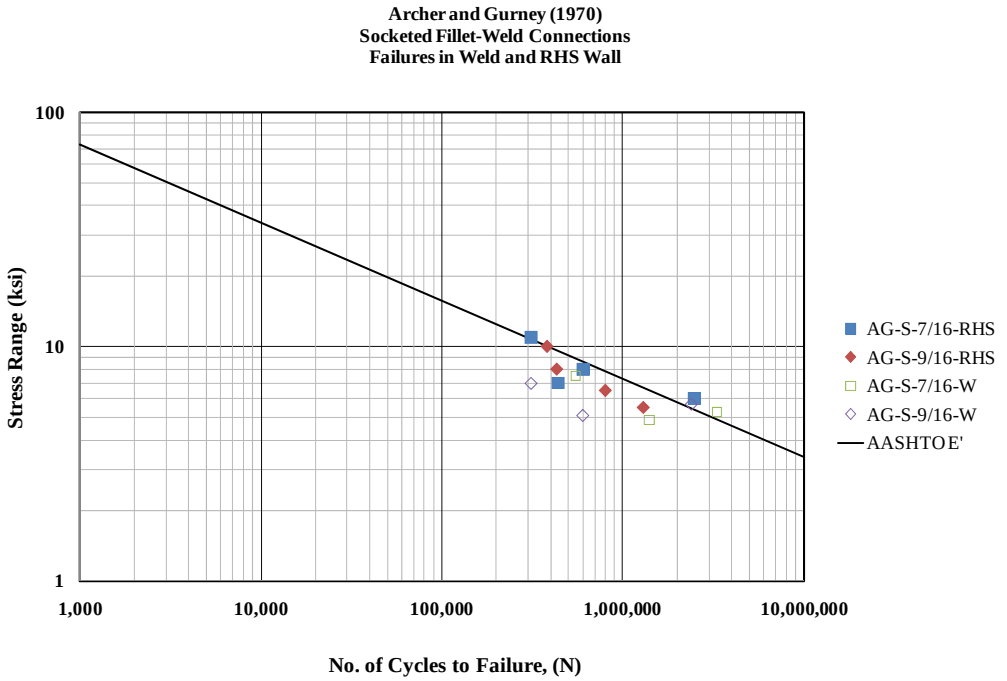

Figure A.4 Fatigue Lives for Socketed Type (S) Fillet Welded Connections (Archer and Gurney 1970).

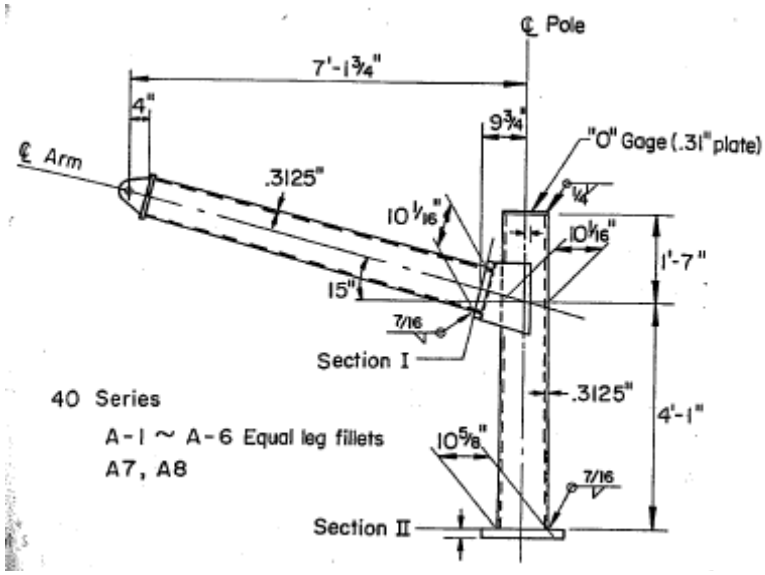

(a) Lehigh 40-series Specimens (LEH-40-A-45CA and LEH-40-A-34CA series).

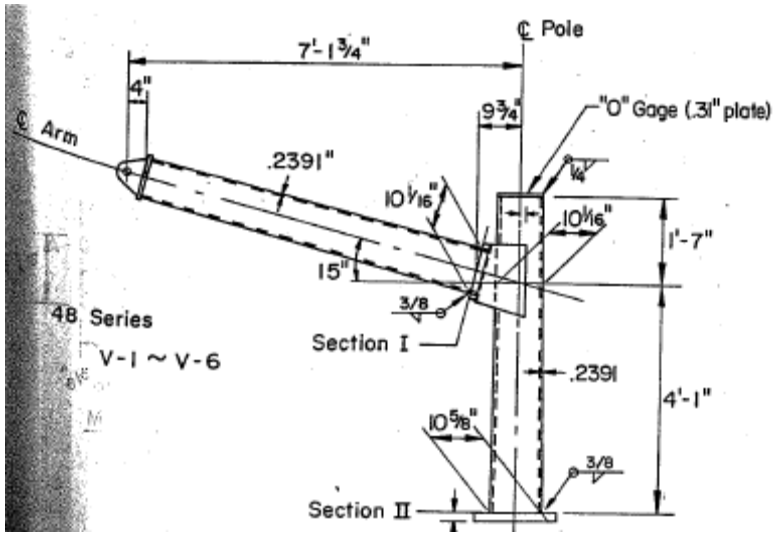

(b) Lehigh 48-series Specimens (LEH-48-V-28CA series).

Figure B.1 Lehigh Series Specimen Geometries (Fisher *et al* 1981).

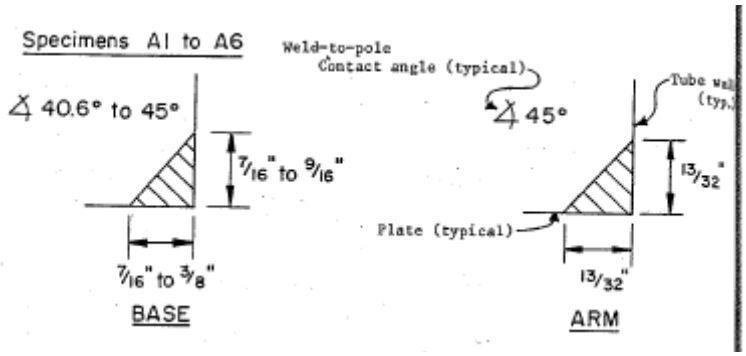

(a) LEH-40-A-45CA Specimen Series Measured Fillet Weld Profiles

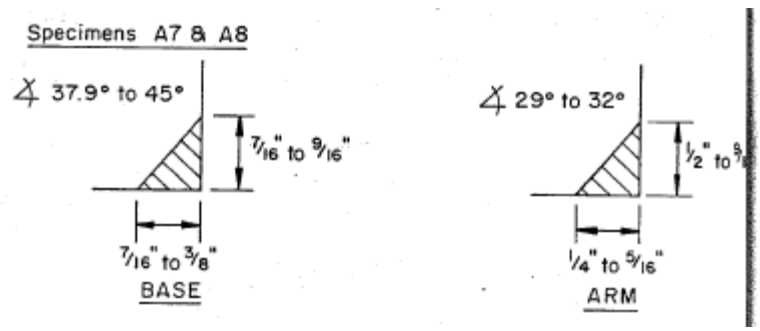

(b) LEH-40-A-34CA Specimen Series Measured Fillet Weld Profiles

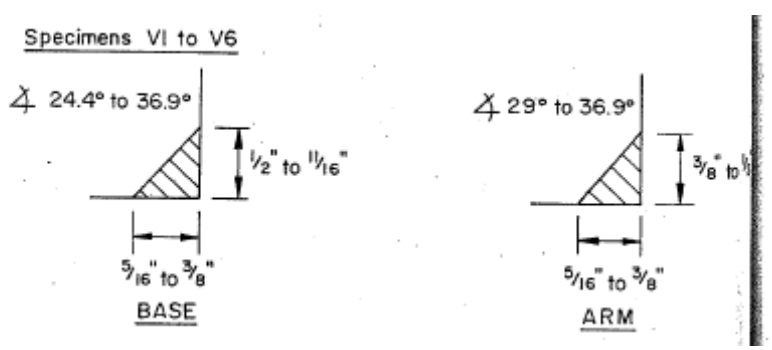

(c) LEH-48-V-28CA Specimen Series Measured Fillet Weld Profiles

Figure B.2 Fillet Weld Profiles (Fisher *et al* 1981).

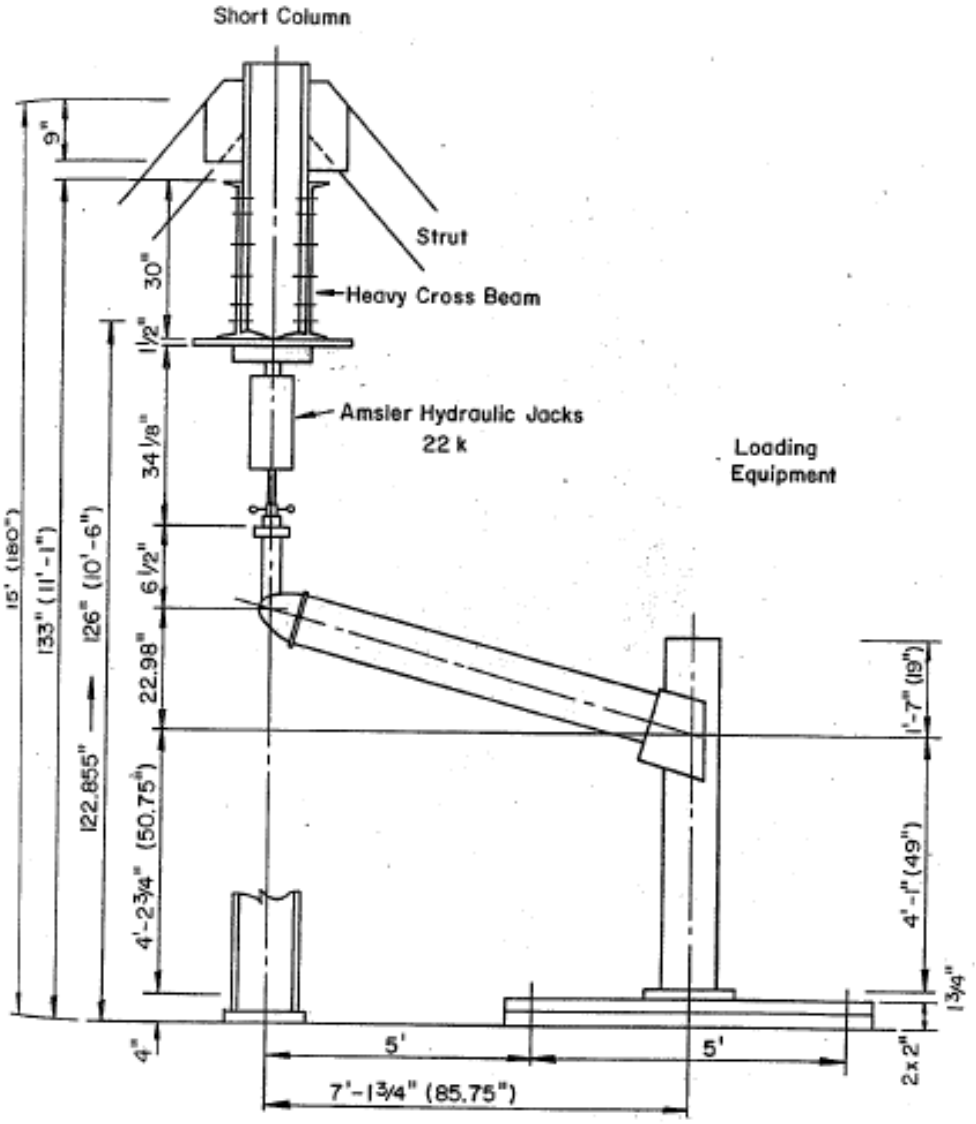

Figure B.3 Testing Apparatus Schematic (Fisher *et al* 1981).

Table B.1 Fatigue Testing Results (Fisher *et al* 1981).

Specimen Designation	No. of Cycles at Cracking	Stress Range (ksi)
LEH-40-A-45CA-1	36,100	18.8
LEH-40-A-45CA-2	117,800	12.4
LEH-40-A-45CA-3	1,892,400	6.4
LEH-40-A-45CA-4	174,200	12.4
LEH-40-A-45CA-5	1,208,700	6.4
LEH-40-A-45CA-6	1,472,900	6.4
LEH-40-A-34CA-1	3,751,600	6.4
LEH-40-A-34CA-2	3,573,400	6.4
LEH-48-V-28CA-1	87,000	18.9
LEH-48-V-28CA-2	317,500	12.4
LEH-48-V-28CA-3 (1)	5,244,000	6.5
LEH-48-V-28CA-4	198,100	12.4
LEH-48-V-28CA-5 (2)	5,186,500	6.4
LEH-48-V-28CA-6 (3)	8,832,300	6.4

Notes:
(1) – Large crack reported in mast-arm, but failure reported in pole at base connection.
(2) – Failure in pole at base, but failure seen in mast-arm.
(3) – Small crack reported in mast-arm, but no failure in pole.

Table B.2 Key to Testing Specimens

LEH – A – B – C – D		
Mast Arm and Vertical Pole Seam Weld Location		
A	40	mast arm and vertical column seam welds located at points of maximum tension or compression stress
	48	mast arm and vertical column seam welds located randomly
Mast Arm and Vertical Pole Material Type		
B	A	ASTM A283 Grade D Steel , galvanized after fabrication
	V	ASTM A595 Grade A Steel, galvanized after fabrication
Fillet Weld Configuration – Contact Angle		
C	45CA	45-degree contact angle
	34CA	34-degree contact angle
	28CA	28-degree contact angle
Specimen Designation for Series		
D		specimen designation: 1, 2, 3, etc....

Figure B.4 Typical Fillet Weld Failure (Fisher *et al* 1981).

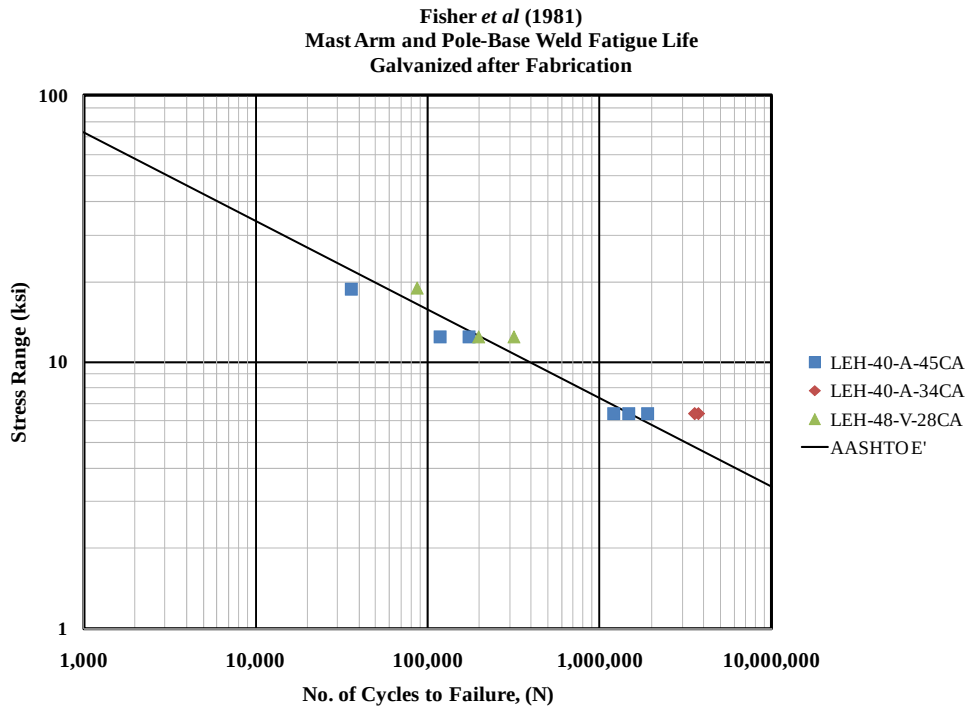

Figure B.5 Fatigue Lives for Mast-Arm and Pole Base Fillet Welded Connections (Fisher *et al* 1981).

This Page Intentionally Left Blank

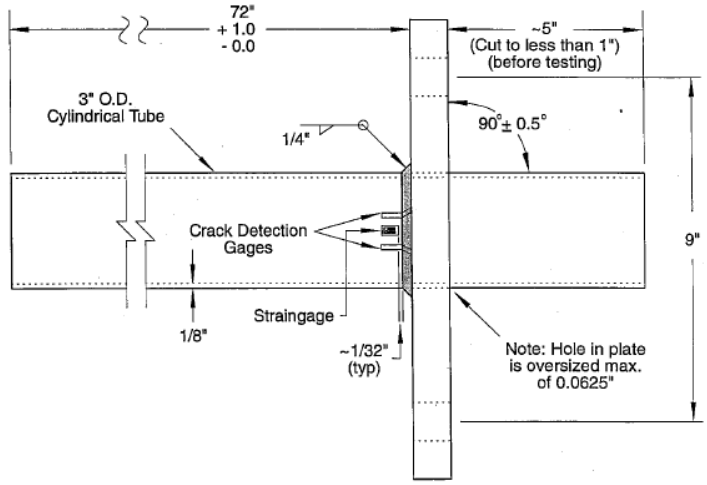

Figure C.1 Mast-Arm Specimen Detail (South 1997).

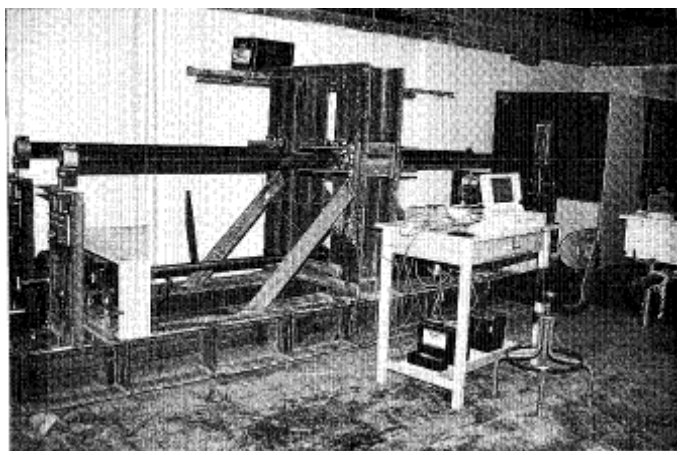

Figure C.2. Experimental Test Setup (South 1997).

Table C.1. Fatigue Testing Results (South 1997).

Specimen Designation	Nominal Stress Range (ksi)					
	33.7	**22.5**	**19.7**	**16.9**	**11.2**	**8.4**
IDOT-1	62,565	216,372	581,212	299,657	15,000,000 (ro)	10,416,673 (ro)
IDOT-2	157,804	213,422	570,601	2,568,000	15,000,000 (ro)	10,416,673 (ro)
IDOT-3	35,629	291,300	199,694	1,322,214	15,000,000 (ro)	10,416,673 (ro)
IDOT-4	40,819	182,166	581,206	1,181,967	15,000,000 (ro)	6,243,700

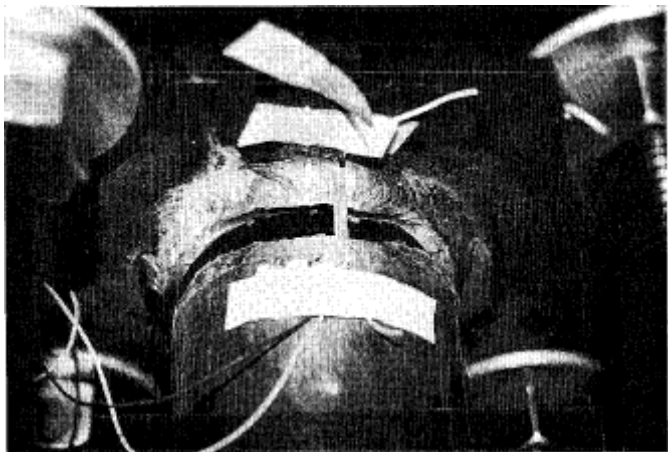

Figure C.3. Typical Specimen Failure (South (1997).

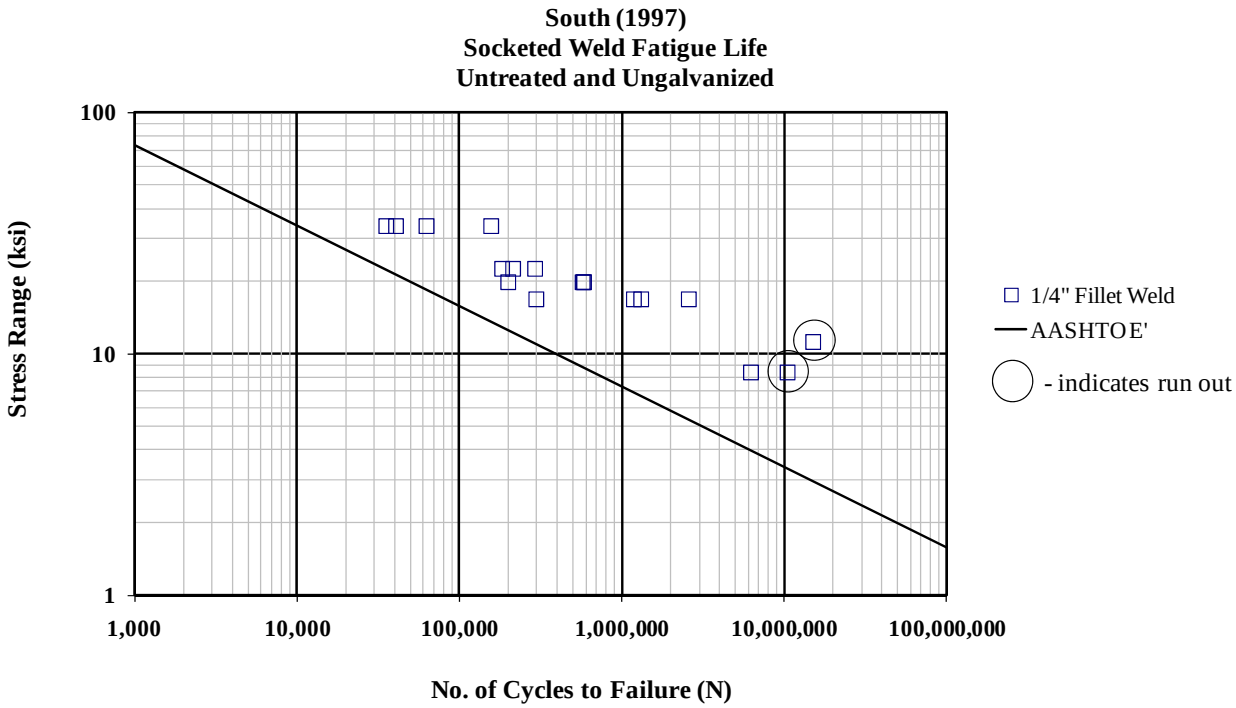

Figure C.4. Fatigue Lives for Socketed Mast-Arm to Plate Connections with Single Fillet Weld (South 1997).

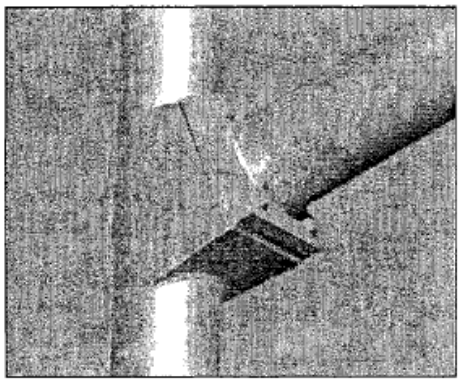

Closed Box Connection

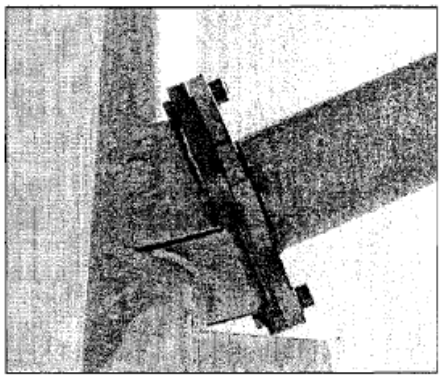

Open Box Connection

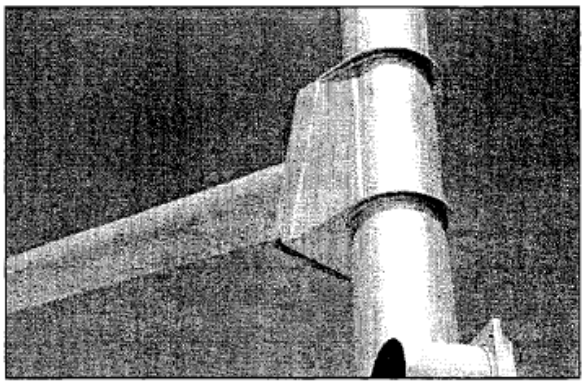

Ring-Stiffened Closed Box Connection

(a) Typical Signal Mast-Arm Connection Types used in Wyoming (Deschamp 2002).

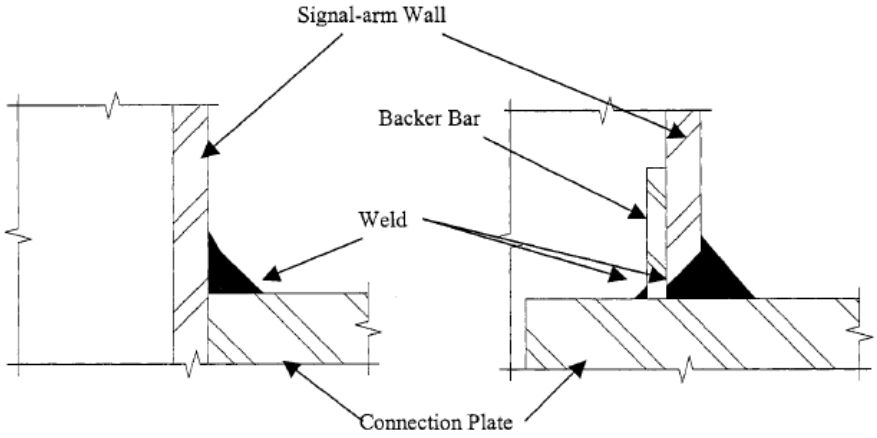

(b) Socketed and Full-Penetration Weld Connections

Figure D.1 Unreinforced Signal Mast-Arm Connection Details (Deschamp 2002).

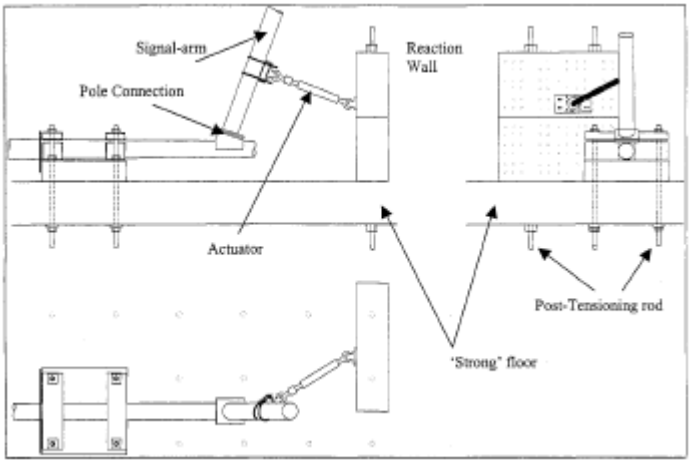

(a) Laboratory Testing Schematic (note the capability of 45-degree out-of-plane loading)

(b) Specimen in Fixture

Figure D.2 Laboratory Testing Apparatus for Fatigue Testing (Deschamp 2002).

Table D.1 Fatigue Testing Results for Mast-Arm Connections (Deschamp 2002).

Specimen Designation	Stress Range (ksi) or ECASR (1)	Cycles to Cracking
WY–IS–S–1.75–4–10.00	24.02	500,000
WY–IS–S–2.00–6–12.25	5.51	750,000
WY–IS–FP–2.00–5–11.50	8.47 (1)	6,250,000 (2)
WY–IS–S–1.50–6–12.50 (5)	5.17	2,750,000 (2)
WY–V–FP–2.00–4–10.00 (3)	19.58	3,712,687 (2)
WY–V–FP–2.00–4–10.00 (3)	10.00	3,750,000 (2)
WY–V–FP–2.00–4–10.50 (3)	17.00	3,250,000 (2)
WY–V–FP–2.00–4–10.50 (3)	16.98	3,000,000 (2)
WY–V–FP–2.00–4–11.25 (4)	8.36	19,500,000 (2)
WY–V–FP–2.00–4–12.75 (4)	6.39	2,250,000 (2)

Notes:

(1) ECASR represents an Equivalent Constant Amplitude Stress Range generated using Miner's cumulative fatigue damage rule.
(2) Indicates specimen was considered as a run-out (no cracking found when testing terminated)
(3) Mast-Arm Wall Thickness Rounded Up to 4/16-in (actually 0.239 inches)
(4) Mast-Arm Wall Thickness Rounded Down to 4/16-in (actually 0.267 inches)
(5) Indicates an open-box connection configuration (only one in test matrix).

Table D.2 Key to Specimen Designations

WY – A – B – C – D – E		
Specimen Designation		
A	IS	In-Service Specimen
	V	Virgin (Manufactured) Specimen
Mast-Arm Connection Configuration		
B	S	Socketed with Fillet Weld (see Figure D.1)
	FP	Full-Penetration Weld (see Figure D.1)
Mast Arm Connection Plate Thickness		
C	#	Connection Plate Thickness Value (inches)
Mast-Arm Wall Thickness		
D	#	Mast-Arm Wall Thickness (number of sixteenths of an inch)
Mast-Arm Diameter		
E	#	Mast-Arm Diameter Value (inches)

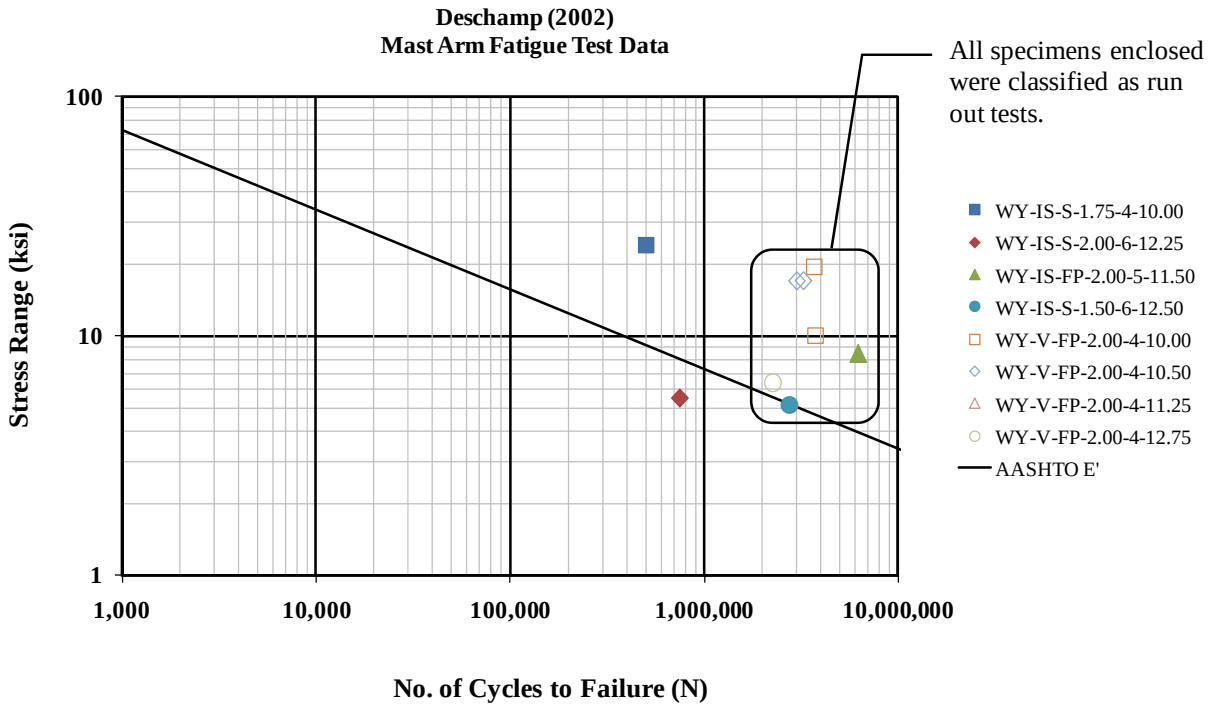

Figure D.3 Fatigue Life Comparison for Wyoming Specimens Tested (Deschamp 2002).

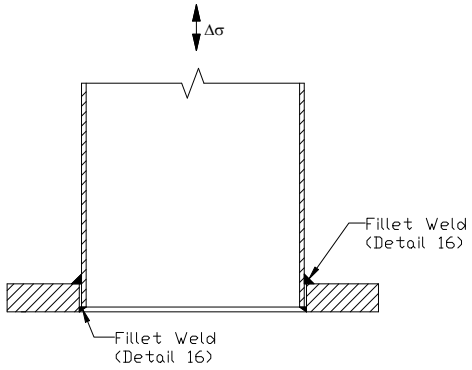

(a) Fillet Welded Socketed Connection (VAL-U-SFW Specimens)

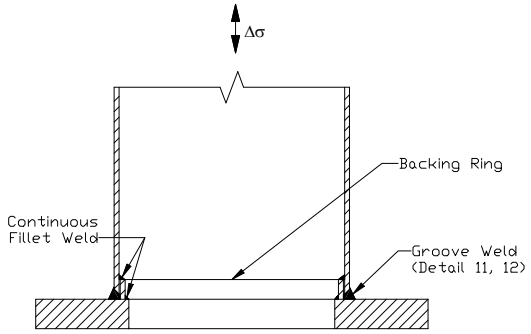

(b) Full-Penetration Welded Connection (VAL-U-FP Specimens)

Figure E.1 Unreinforced Mast-Arm to Plate Connection Details (Macchietto 2002).

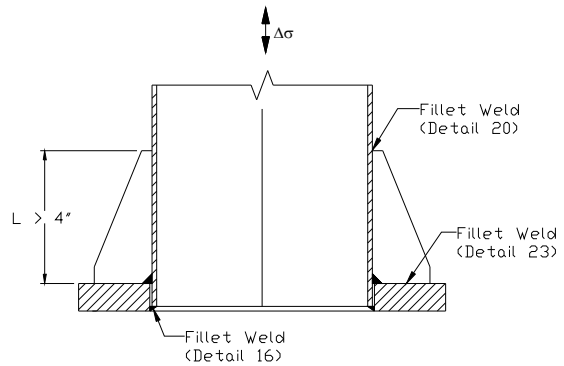

a) Fillet-Welded Gusset Connection (VAL-R-xxFW Specimens)

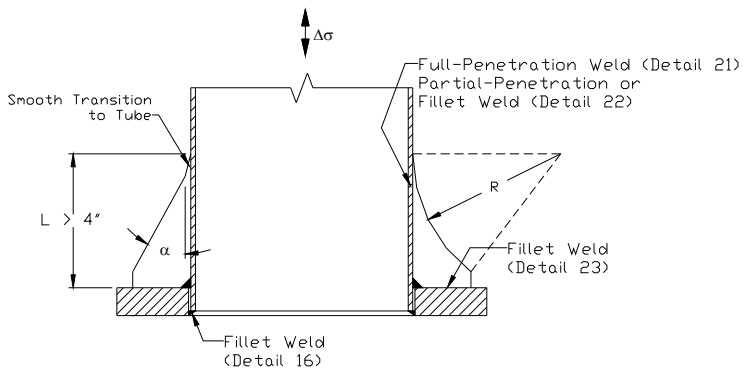

(b) Full-Penetration Tangent Contour Gusset Connection (VAL-R-xxFP and VAL-R-RFWS Specimens)

Figure E.2 Reinforced Mast-Arm to Plate Connection Details (Macchietto 2002).

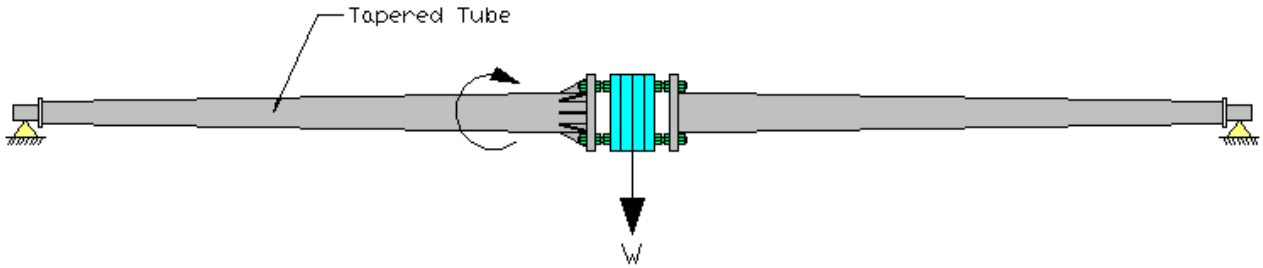

(a) Rotating Beam Testing Apparatus Schematic

(b) Rotating Beam Apparatus Photograph.

Figure E.3 Rotating Beam Fatigue Testing Apparatus Schematic and Photograph (Macchietto 2002).

Table E.1 Fatigue Testing Results for Reinforced Mast-Arm to Plate Connections (Macchietto 2002).

Specimen Designation	No. of Cycles at Cracking	Stress Range (ksi)
VAL-R-45FW-A	802,620 (575,000)	13.4
VAL-R-45FW-B	376,740	13.4
VAL-R-15FP-A	950,040	13.4
VAL-R-TCFP-A	657,540	17.6
VAL-R-RFWS-A	514,085	17.6
VAL-R-RFWS-B	673,989	17.6

Notes:
(xxx,xxx) – indicates the number of cycles where cracking was thought to initiate

Table E.2 Fatigue Testing Results for Un-Reinforced Mast-Arm to Plate Connections (Macchietto 2002).

Specimen Designation	No. of Cycles at Cracking	Stress Range (ksi)
VAL-U-SFW-A	4,808,700 (ro)	13.4
VAL-U-SFW-B	1,240,000	17.6
VAL-U-SFW-C	5,231,160 (ro)	17.6
VAL-U-SFW-D	1,982,743 (ro)	17.6
VAL-U-FP-A	498,960	17.6
VAL-U-FP-B	4,504,500	17.6

Notes:
(ro) – indicates test termination as a result of run out.

Table E.3 Key to Specimen Designations (adapted from Macchietto 2002).

VAL – A – B – C		
Reinforcement Configuration		
A	U	unreinforced specimen
	R	reinforced specimen
Connection Detail Configuration		
B	If U-type Specimen	
	SFW	socketed connection, unequal-leg fillet welds (long leg on mast-arm)
	FP	full penetration welds, backing ring attached with continuous fillet welds, 1-in tall backing ring
	If R-type Specimen	
	45FW	45-degree gussets, fillet welded, 3.25-in long
	15FP	15-degree contour gussets, full-penetration welds, 6-in long, weld ground smooth at transition
	TCFP	Tangent-contour gussets, full-penetration welds, 5.83-in long, weld ground smooth at transition
	RFWS	Radial gusset, fillet welds terminated 1/2-in short of gusset ends, 5.44-in long
Specimen Designation for Series		
C		specimen designation: A, B, C, etc....

(a) VAL-R-45FW Specimens

(b) VAL-R-15FP Specimens

(c) VAL-R-TCFP Specimens

(d) VAL-U-SFW Specimens

(e) VAL-U-FP Specimens

Figure E.4 Typical Specimen Fatigue Failures Seen in Testing (Macchietto 2002).

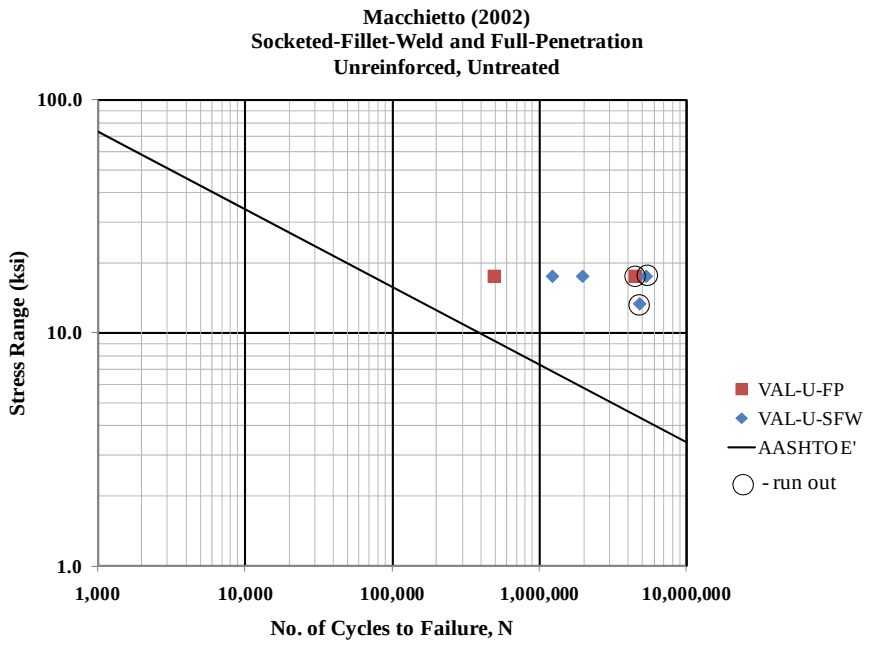

Figure E.5 Fatigue Testing Results for Socket Fillet-Weld and Full-Penetration Unreinforced Mast-Arm to Plate Connections (Macchietto 2002).

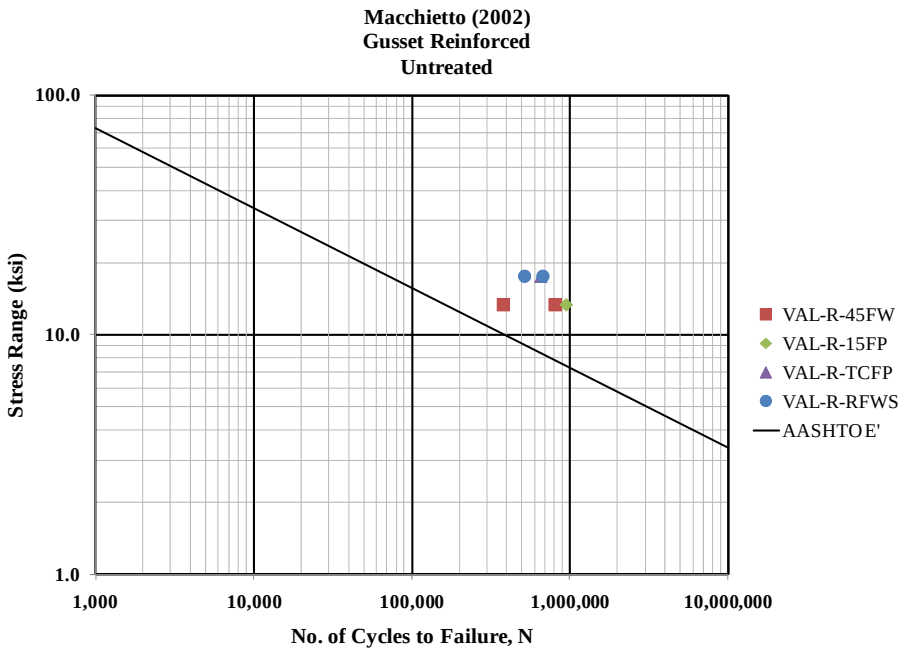

Figure E.6. Fatigue Testing Results for Gusset-Plate Reinforced Mast-Arm to Plate Connections (Macchietto 2002).

This Page Intentionally Left Blank

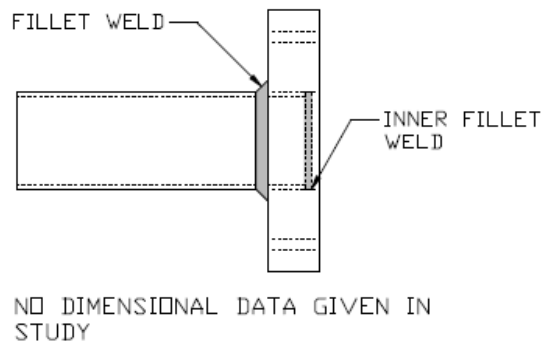

(a) Fatigue Specimen Schematic

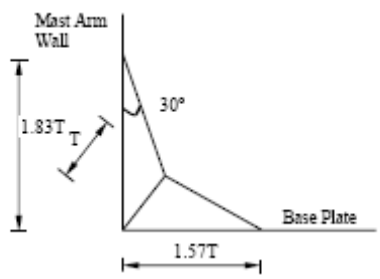

(b) Fatigue-Resistant Weld Profile (UMO-xxx-N series specimens)

Figure F.1 Fatigue Testing Specimen Schematic and Fatigue-Resistant Weld Profile (Chen *et al* 2003; Alderson 1999).

Figure F.2 Laboratory Testing Apparatus (Alderson 1999).

Table F.1 Fatigue Testing Results (Chen *et al* 2003; Alderson 1999).

Specimen Designation	No. of Cycles at Cracking	Stress Range (ksi)
UMO-VAL-O-1	1,800,000	8.0
UMO-VAL-N-1	2,100,000	8.0
UMO-VAL-N-2	400,000 (1)	8.0
UMO-UM-O-1	500,000 (3)	8.0
UMO-JEM-O-1	n.a. (2)	n.a.

Notes:
(1) – Lack of fusion noted as potential cause for low cycle count.
(2) – NDT inspection resulted in weld flaw being detected and no testing conducted.
(3) – NDT using magnetic particle testing indicated a flaw was present in weld.

Table F.2 Key to Testing Specimens

UMO– A – B – C		
Fabricator		
A	VAL	Valmont
	JEM	Acronym Unknown
	UM	Union Metals
Fillet Weld Configuration		
B	O	Standard (equal-leg) fillet weld
	N	New (fatigue-resistant, unequal leg) fillet weld
Fillet Weld Configuration – Contact Angle		
Specimen Designation for Series		
C		specimen designation: 1, 2, 3, etc....

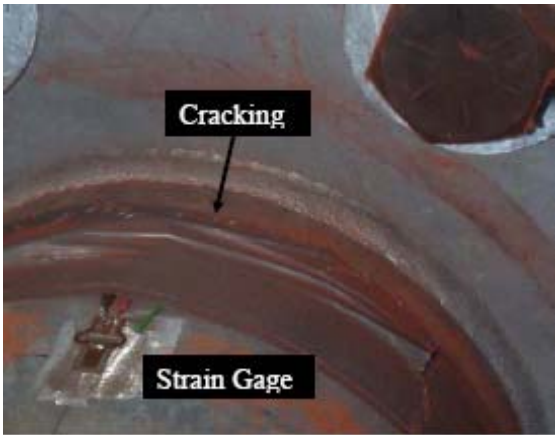

Figure F.3 Typical Fatigue Failure (Alderson 1999, Chen *et al* 2003).

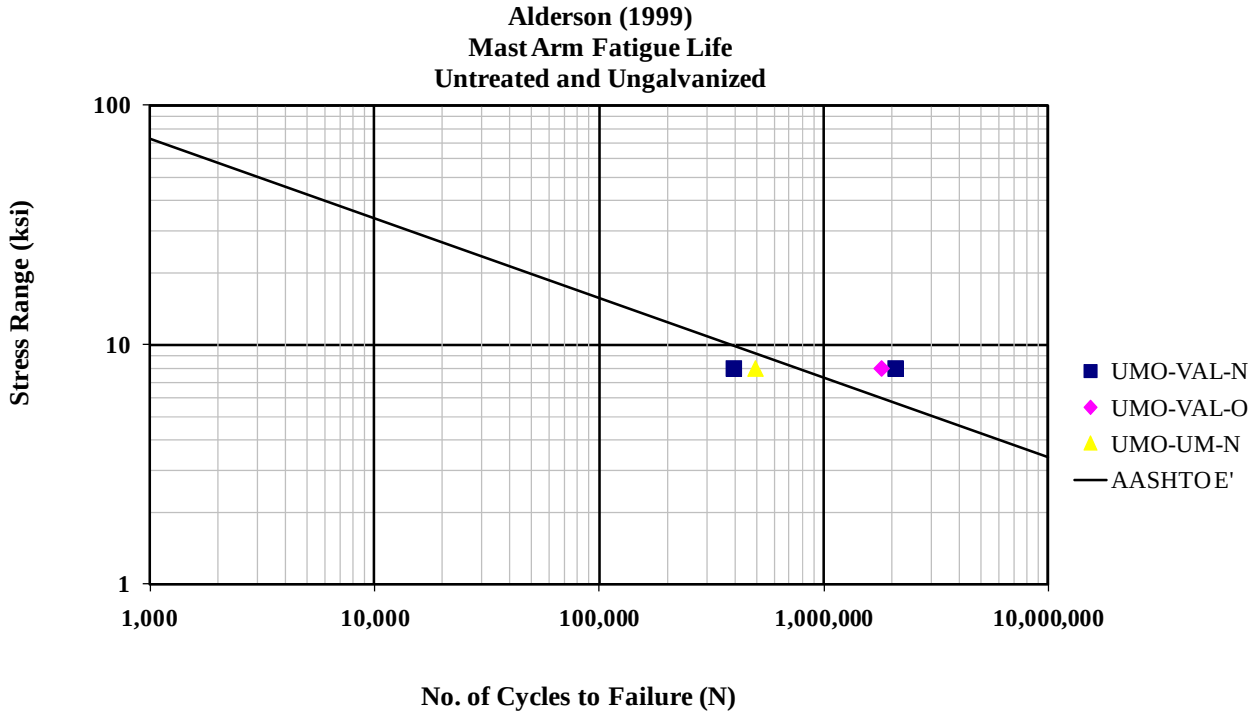

Figure F.4 Fatigue Lives for Mast-Arm Welded Connections (Alderson 1999).

This Page Intentionally Left Blank

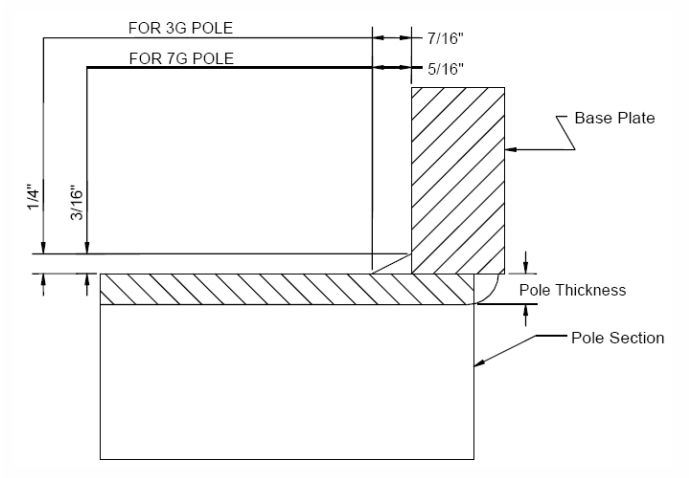

(a) Socketed Fillet-Weld ("U" Series Specimens)

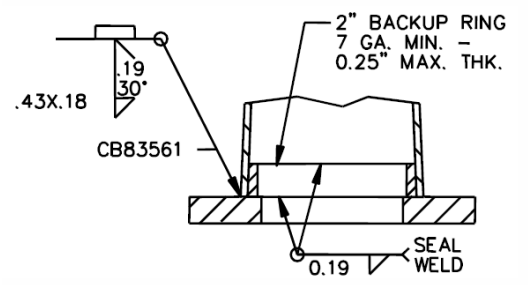

(b) Full-Penetration Weld with Backing Ring ("W" Series)

Figure G.1 Unreinforced Mast-Arm to Plate Connection Details (Koenigs *et al* 2003).

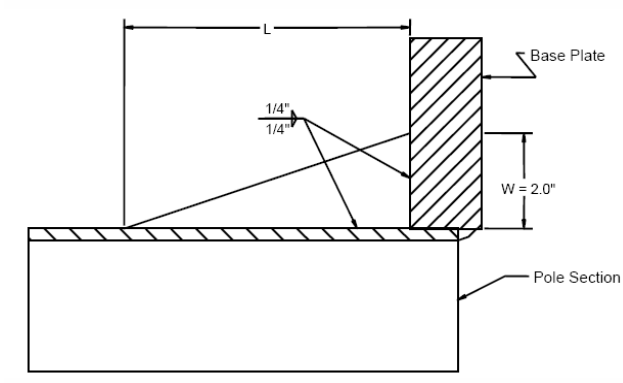

(a) Stiffener Reinforcement Schematic

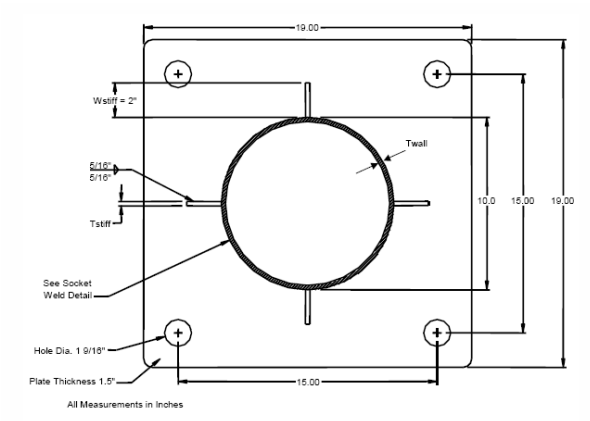

(b) Basic Orientation ($L \times t_s$ Series)

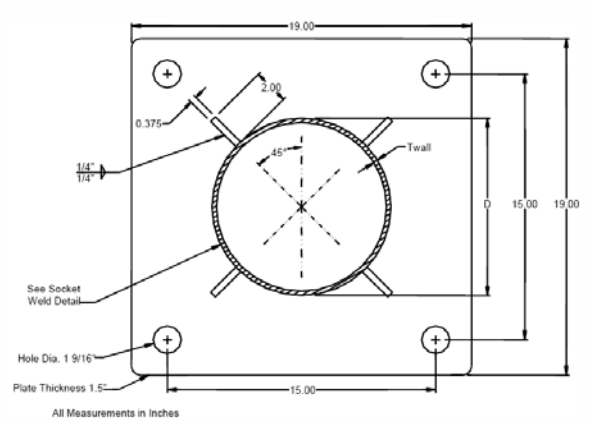

(c) 45-Degree Orientation ($L \times t_s$ @ 45 Series)

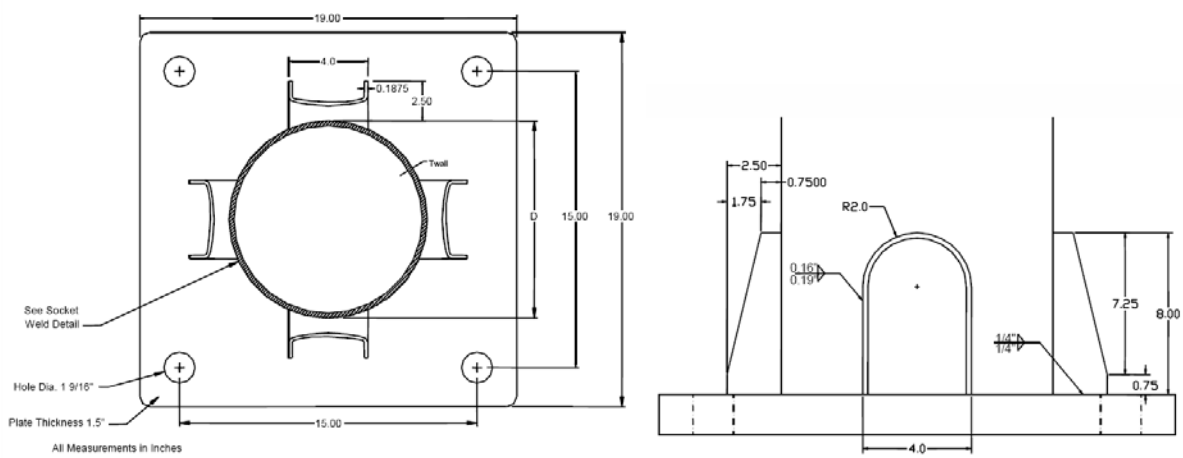

(d) U-Rib Configuration (UR Series)

Figure G.2 Stiffener Reinforced Connection Details (Koenigs *et al* 2003).

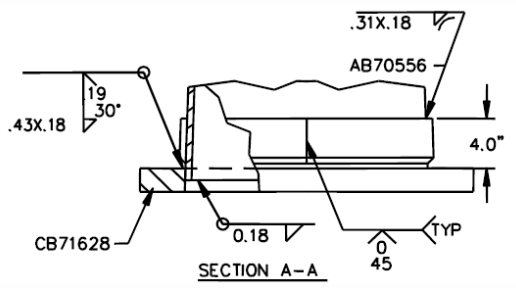

(a) External Collar Connection Detail ("EC" Series Specimens)

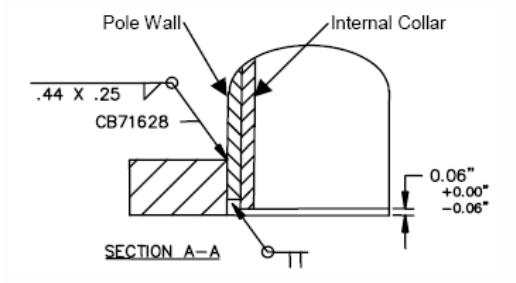

(b) Internal Collar Connection Detail ("IC" Series Specimens)

Figure G.3 Non-Stiffener Reinforced Connection Details (Koenigs *et al* 2003).

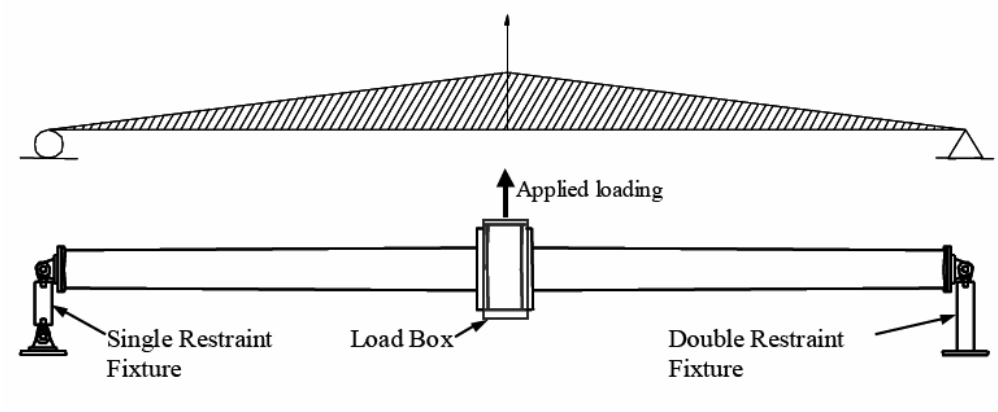

(a) Testing Schematic

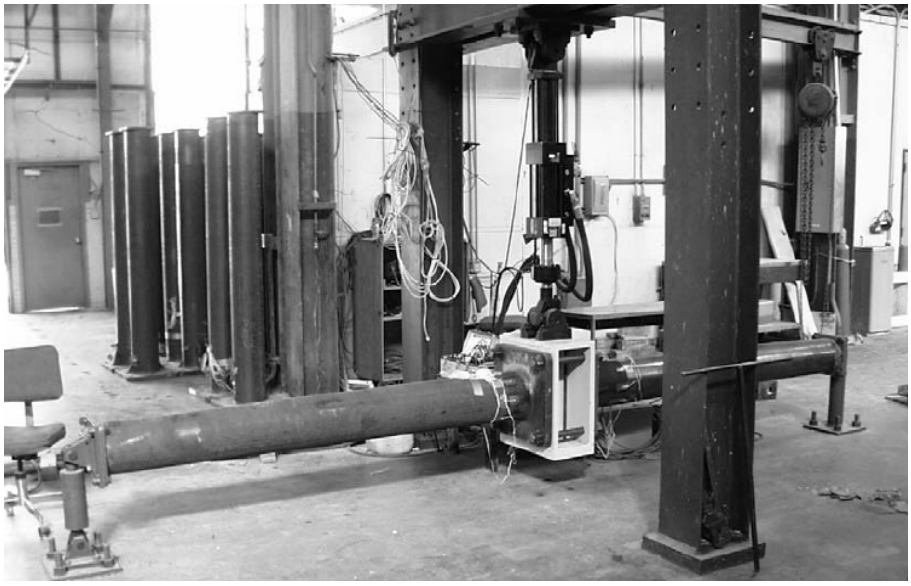

(b) Laboratory Implementation

Figure G.4 Fatigue Testing Setup Schematics and Implementation (Koenigs *et al* 2003).

Table G.1. Fatigue Testing Results for Unreinforced and Untreated Mast-Arm to Plate Connection Details (Koenigs *et al* 2003).

Specimen Designation	No. of Cycles at Failure	Stress Range (ksi)
VAL-U-N-A	249,446	11.90
VAL-U-N-B	453,948	11.90
VAL-U-N-C	2,072,592	6.29
VAL-U-N-D	6,856,881(ro)	6.20
TX-U-N-A	2,199,343	6.00
TX-U-N-B	2,816,706	6.10
TX-U-N-C	177,596	11.80
TX-U-N-D	194,694	12.00
VALN-U-N-A	389,428	11.90
VALN-U-N-B	265,540	11.80
VALN-U2-N-A	5,144,528	11.90
VALN-U2-N-B	1,683,127	11.80
VALN-W-N-A	422,400	17.71
VALN-W-N-B	422,400	17.56

Notes:
ro – indicates run out.

Table G.2. Fatigue Testing Results for Unreinforced, UI Treated, and Galvanized Mast-Arm to Plate Connection Details (Koenigs *et al* 2003).

Specimen Designation	No. of Cycles at Failure	Stress Range (ksi)
VALN-U-P-A	4,557,126 (ro)	11.60
VALN-U-P-B	4,557,126 (ro)	11.50
VALN-U-P-C	1,301,077	19.95
VAL-U-P-E	393,767	11.40
VAL-U-P-F	353,103	11.50
VALN-U-G-A	183,132	11.60
VALN-U-G-B	151,679	11.50
VALN-U-GP-A	4,545,952	11.60
VALN-U-GP-B	224,240	19.91
VALN-U-PG-A	277,634	11.60
VALN-U-PG-B	313,727	11.50
VALN-U-P-A-UL	5,004,729	11.60
VALN-U-P-B-UL	5,440,165	11.50

Notes:
ro – indicates run out.

Table G.3. Fatigue Testing Results for Non-Stiffener Reinforced, Non-UI Treated, Mast-Arm to Plate Connection Details (Koenigs *et al* 2003).

Specimen Designation	No. of Cycles at Failure	Stress Range (ksi)
VALN-EC-N-A	4,245,460	5.49
VALN-EC-N-B	2,363,152	5.79
VALN-IC-N-A	227,030	10.75
VALN-IC-N-B	227,030	10.68

Table G.4. Fatigue Testing Results for Stiffener Reinforced, UI Treated, Mast-Arm to Plate Connection Details (Koenigs *et al* 2003).

Specimen Designation	No. of Cycles at Failure	Stress Range (ksi)
VAL-$3\times3/8$-P-C	393,767	11.50
VAL-$3\times3/8$-P-C2	353,103	11.50
VAL-$3\times3/8$-P-C-LMS	1,707,128	12.10

Table G.5. Fatigue Testing Results for Stiffener Reinforced, Non-UI Treated, Mast-Arm to Plate Connection Details (Koenigs *et al* 2003).

Specimen Designation	No. of Cycles at Failure	Stress Range (ksi)
VAL-3×1/4-N-A	476,269	11.10
VAL-3×1/4-N-B	696,326	11.40
VAL-3×1/4-N-C	3,592,372	6.10
TX-3×1/4-N-A	616,136	11.70
TX-3×1/4-N-B	416,146	11.80
TX-3×1/4-N-C-LMS	523,397	11.90
VAL-3×3/8-N-A	386,253	11.70
VAL-3×3/8-N-B	410,410	11.60
TX-3×3/8-N-A	473,735	11.70
TX-3×3/8-N-B	657,716	11.60
VAL-6×3/8-N-A	242,728 (1)	11.20
VAL-6×3/8-N-B	653,392	11.30
VAL-6×3/8-N-C	3,592,372	5.90
TX-6×3/8-N-A	783,857	11.20
TX-6×3/8-N-B	783,857	11.30
TX-6×3/8-N-C	7,503,037	5.76
VALN-6×3/8@45-N-A	238,515	11.96
VALN-6×3/8@45-N-B	161,843	11.98
VALN-6×3/8@45-N-C	6,066,817	4.30
VALN-6×3/8@45-N-D	6,066,817	4.30
VALN-UR-N-A	1,776,724	7.62
VALN-UR-N-B	950,670	7.60
VALN-UR-N-B2	339,152	12.57

Notes:
(1) – lack of fusion defect detected post-testing

Table G.6 Key to Specimen Designations (adapted from Koenigs *et al* 2003)

A – B – C – D – E		
Mast-Arm Wall Thickness and Manufacturing Entity		
A	VAL	0.179-in. thick, Brenham, TX
	TX	0.239-in. thick, Brenham, TX
	VALN	0.179-in. thick, Valley, NE
Connection Detail Configuration		
B	U	unreinforced, fillet weld, socketed
	U2	unreinforced, fillet weld, socketed, 2-inch plate
	W	unreinforced, full-penetration weld with backing ring
	EC	reinforced, external collar
	IC	reinforced, internal collar
	UR	reinforced, U-rib stiffener
	$L \times t_s$	reinforced, triangular stiffener L - length (in.) t_s - thickness (in.)
	$L \times t_s @ 45$	reinforced, triangular stiffener at 45-degree orientation
Retrofit Treatment or Specialized Coating		
C	N	no retrofit treatment or galvanizing
	P	ultra-sonic impact treatment (UIT)
	G	galvanized
	PG	UI treated then galvanized
	GP	galvanized then UI treated
Specimen Designation for Series		
D		specimen designation: A, B, C, etc.
Special Notes (no entry indicates no special testing or treatment scenario)		
E	LMS	fatigue testing done at low mean stress
	UL	UIT performed in unloaded state

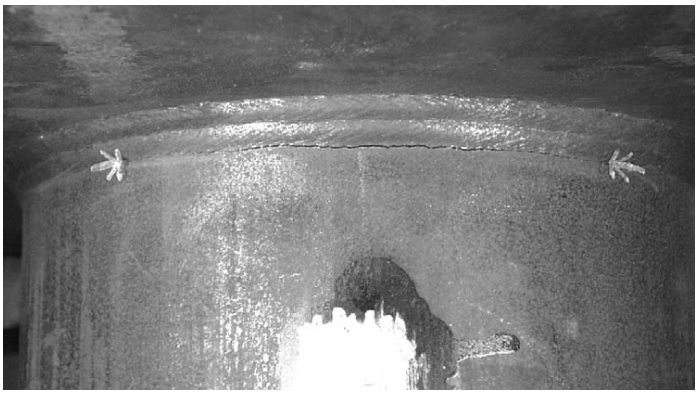

Figure G.5. Typical Fatigue Failure of Fillet-Welded Socketed Connections (Koenigs *et al* 2003).

Figure G.6. Typical Fatigue Failure of 45-Degree Wedge-Type Stiffener Reinforced Connection (Koenigs *et al* 2003).

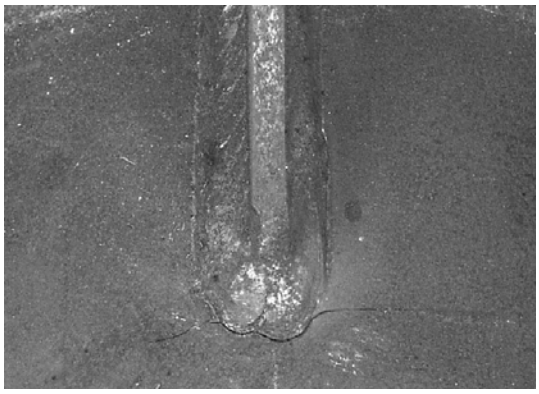

(a) VAL-$3\times1/4$ and VAL-$6\times3/8$ Specimens at Stiffener Toe

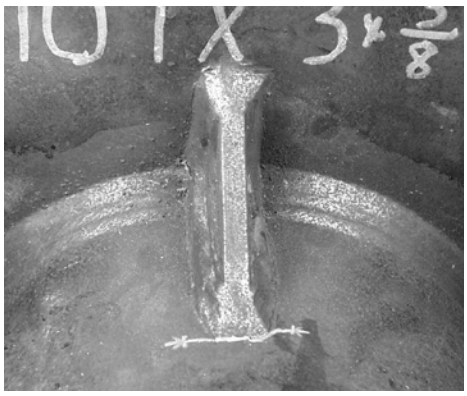

(b) VAL-$3\times3/8$ Specimen

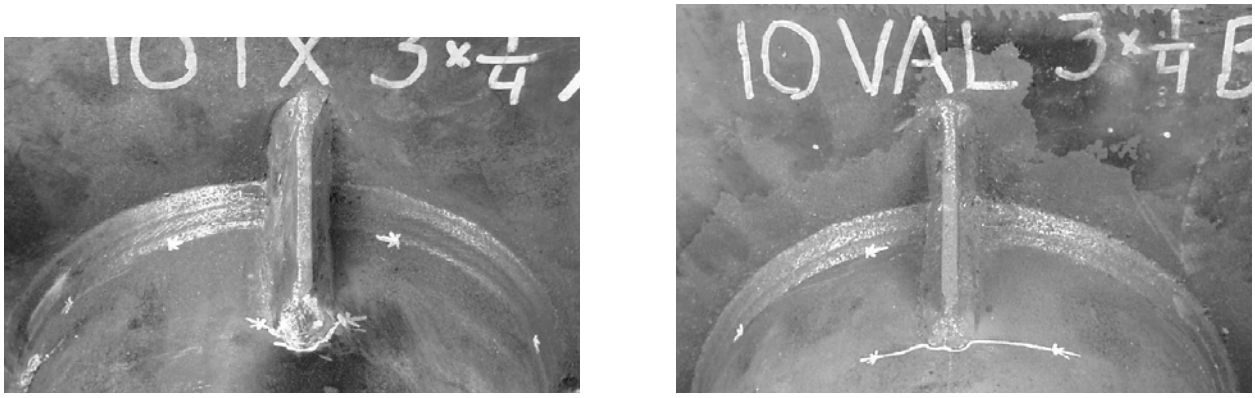

(c) TX-$3\times1/4$ and VAL-$3\times1/4$ Specimens at Stiffener Toe and Socketed Fillet-Weld Toe

Figure G.7 Typical Fatigue Failures for Wedge-Type Stiffener Connections (Koenigs *et al* 2003).

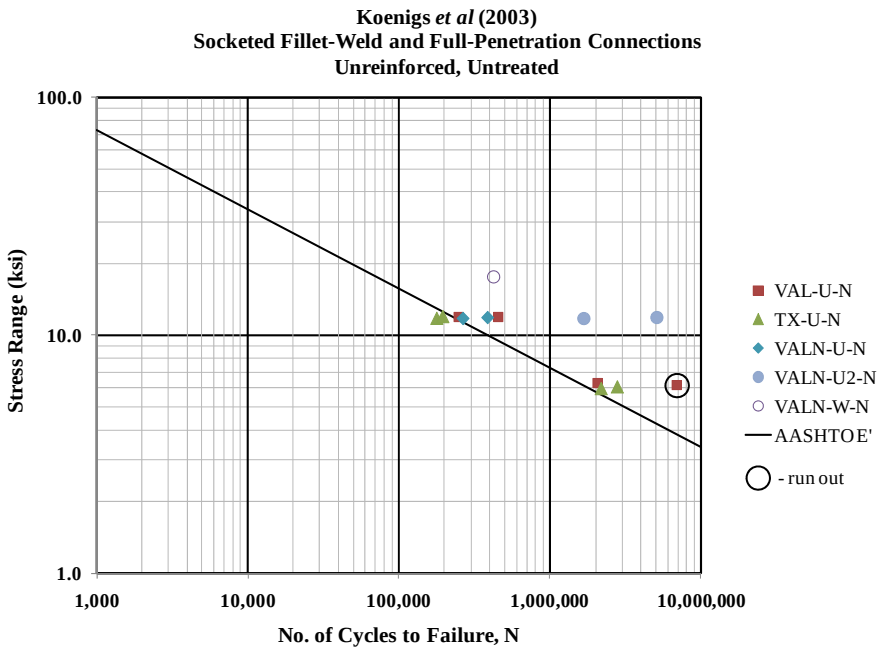

Figure G.8 Fatigue Testing Results for Unreinforced and Untreated Mast-Arm to Plate Connection Details (Koenigs *et al* 2003).

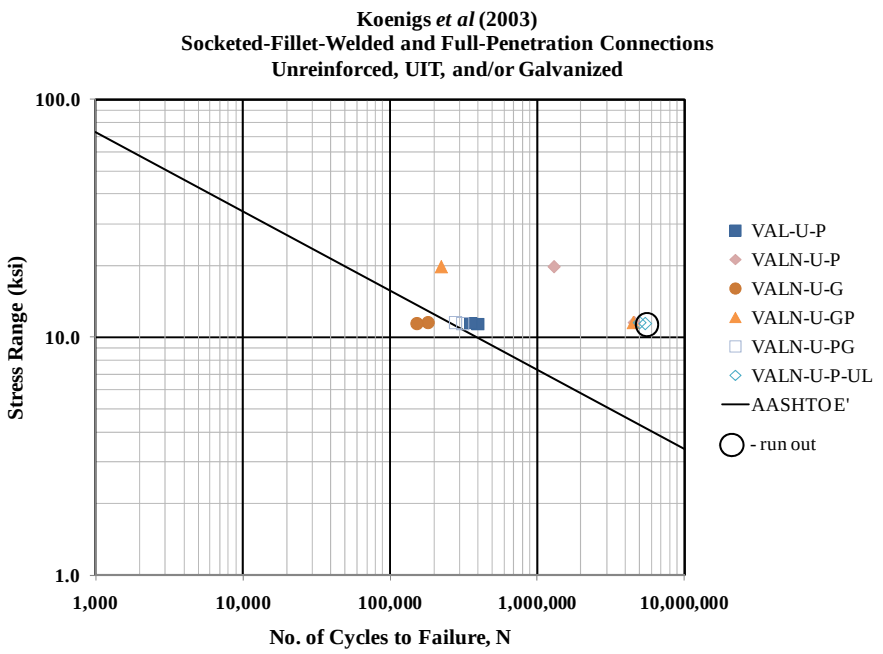

Figure G.9 Fatigue Testing Results for Unreinforced, UIT and/or Galvanized Mast-Arm to Plate Connection Details (Koenigs *et al* 2003).

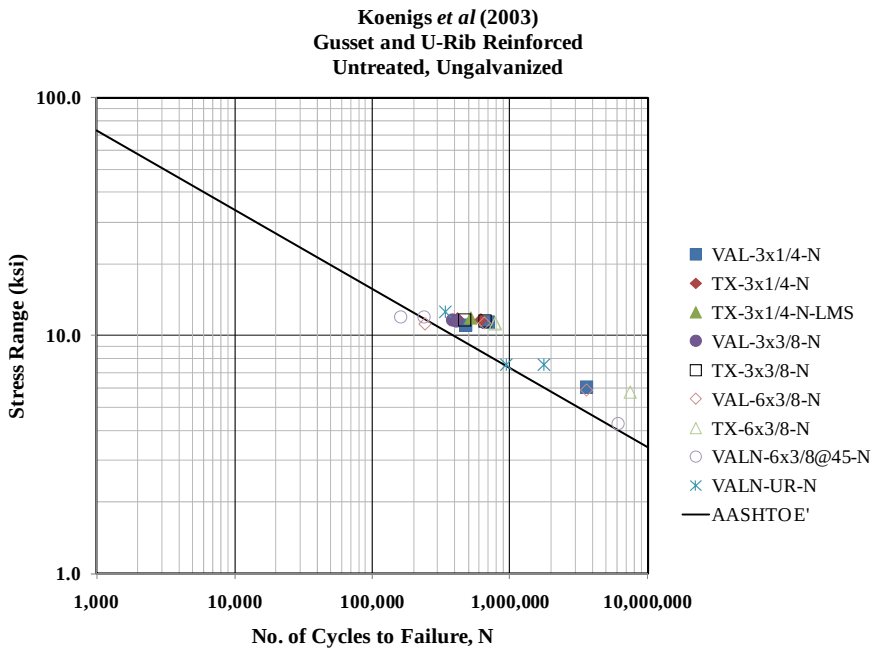

Figure G.10 Fatigue Testing Results for Gusset and U-Rib Reinforced, Untreated, Non-galvanized Mast-Arm to Plate Connection Details (Koenigs *et al* 2003).

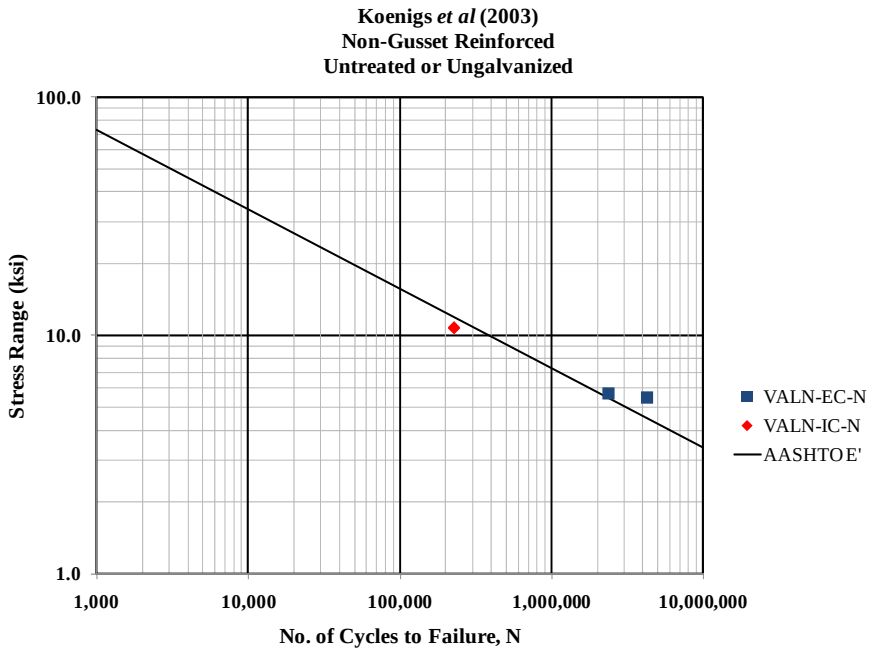

Figure G.11. Fatigue Testing Results for Non-Gusset Reinforced, Non-UI Treated, Non-Galvanized Mast-Arm to Plate Connections (Koenigs *et al* 2003).

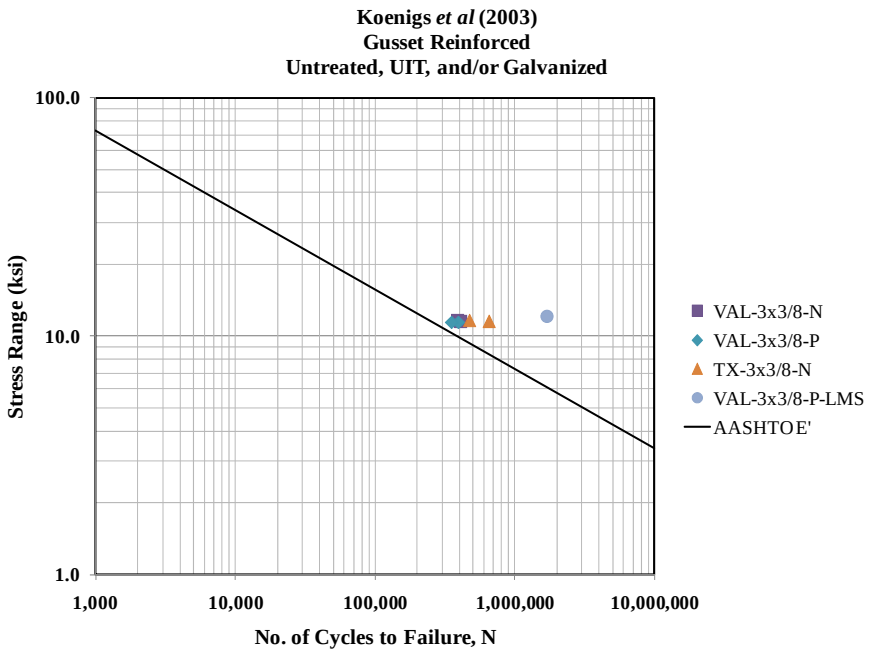

Figure G.12. Fatigue Testing Results for Gusset Reinforced, UI Treated and/or Galvanized Mast-Arm to Plate Connections (Koenigs *et al* 2003).

This Page Intentionally Left Blank

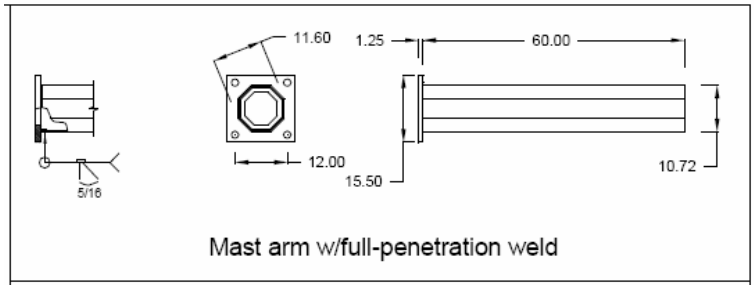

(a) Un-Stiffened Mast-Arm Plate Connection Specimens

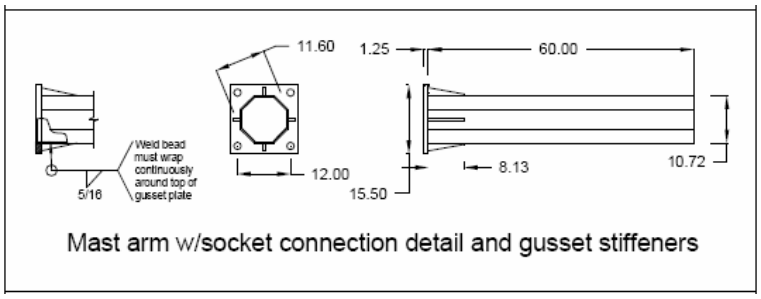

(b) Gusset Stiffened Mast-Arm Plate Connection Specimens

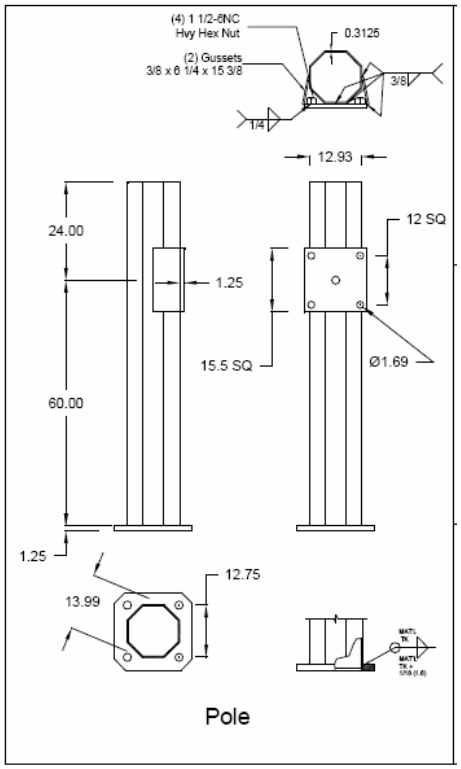

(c) Socketed Pole Base Plate Connections

Figure H.1 Mast-Arm and Pole Connection Specimens (Ocel *et al* 2006).

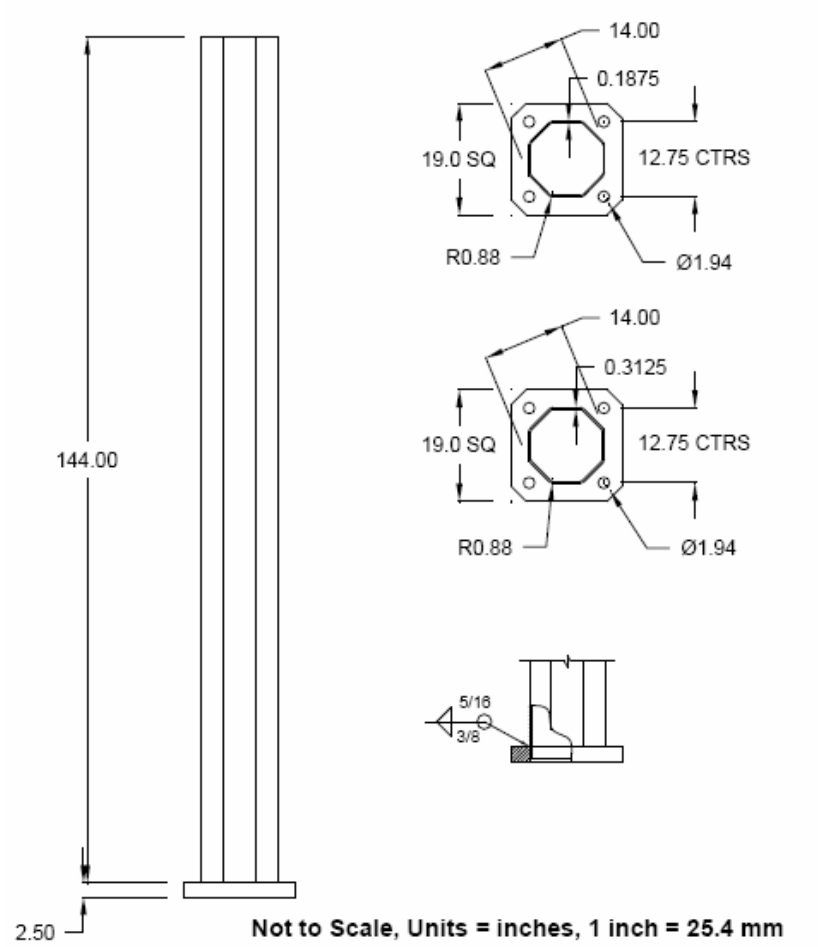

Figure H.2 Long Pole Connection Specimens (Ocel *et al* 2006)

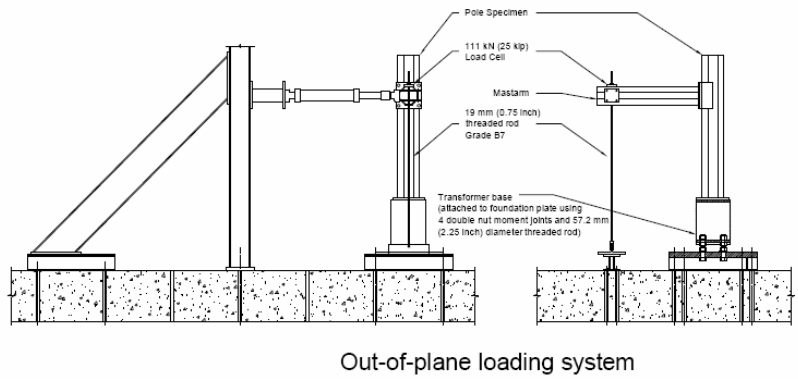

(a) Out-of-Plane Load Testing Configuration

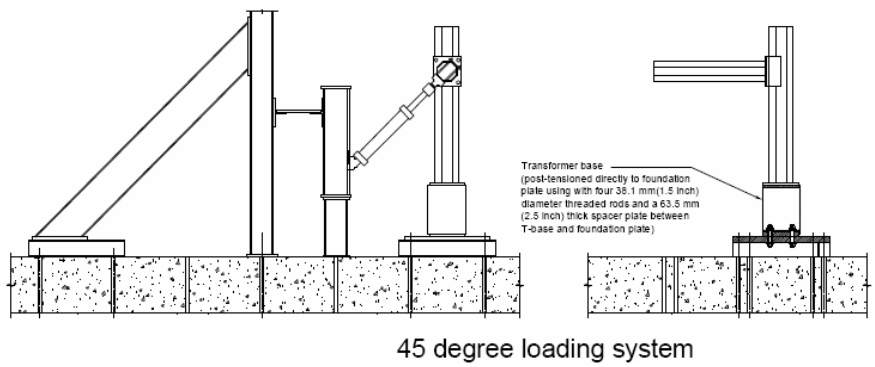

(b) 45-degree Load Testing Configuration

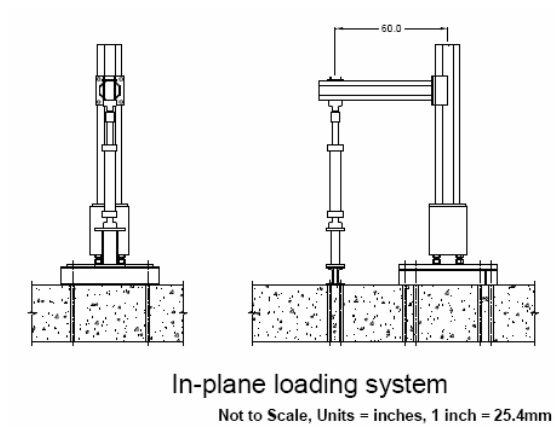

(c) In-Plane Load Testing Configuration

Figure H.3 Frame 1 Load Testing System Schematics (Ocel *et al* 2006).

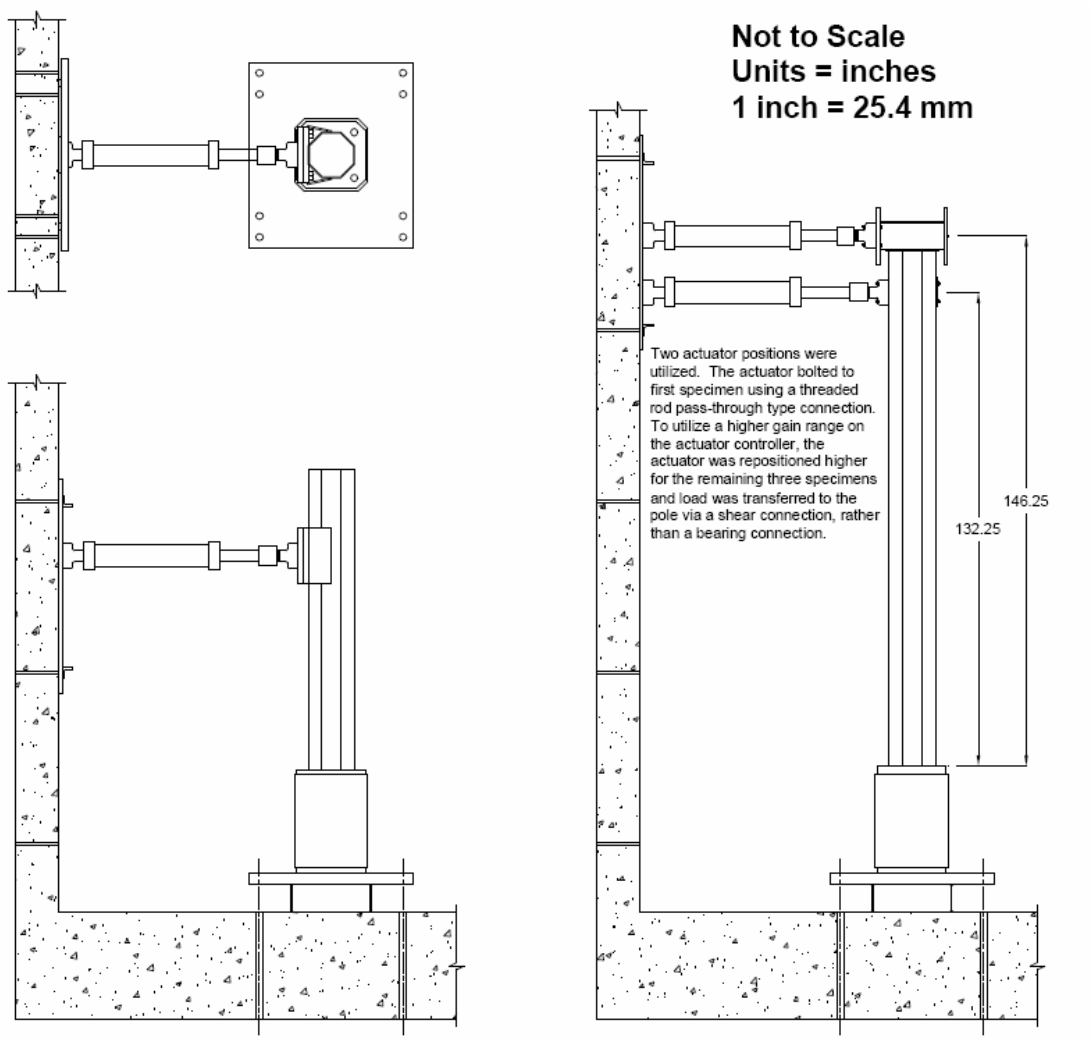

Figure H.4 Frame 2 Load Testing System Schematic (Ocel *et al* 2006).

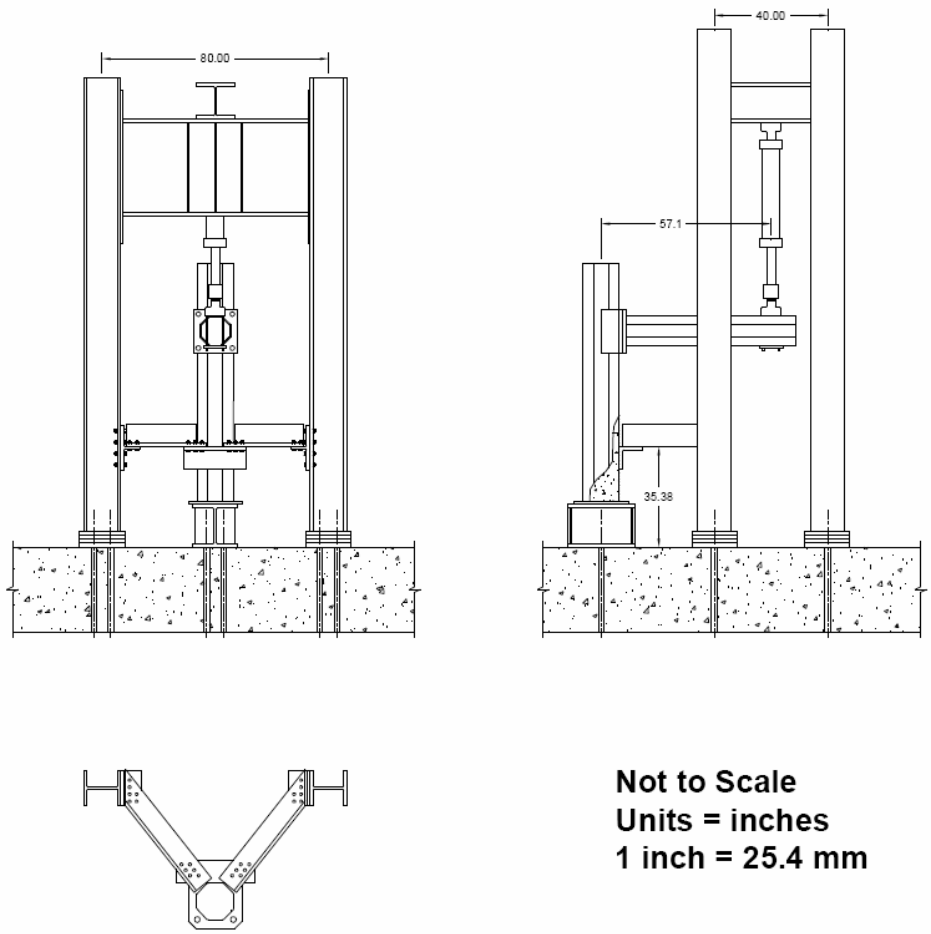

Figure H.5 Frame 3 Load Testing System Schematic (Ocel *et al* 2006).

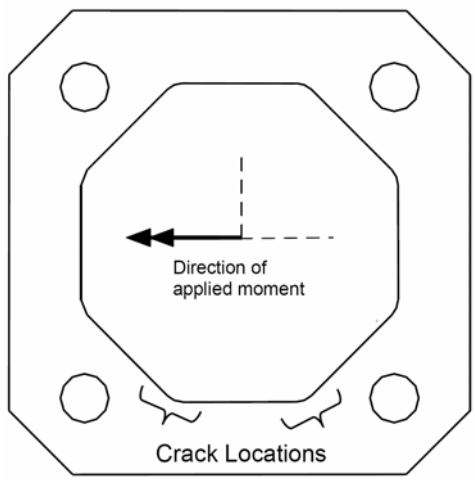

(a) Crack Location Schematic

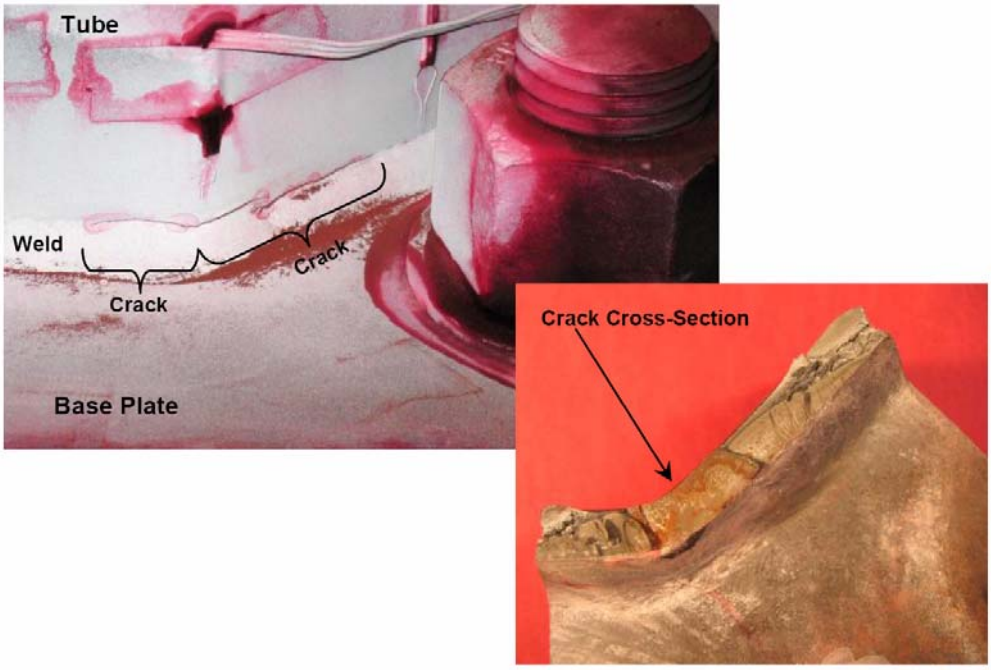

(b) Typical Crack Location and Size Seen in Experimental Testing.

Figure H.6 Crack Locations and Weld Toe Crack Photographs Typical of Socketed Pole Base Connections (Ocel *et al* 2006).

Figure H.7 Typical Crack Formation and Configuration Seen in Testing of Un-Stiffened Full-Penetration Mast-Arm to Plate Connection Details (Ocel *et al* 2006).

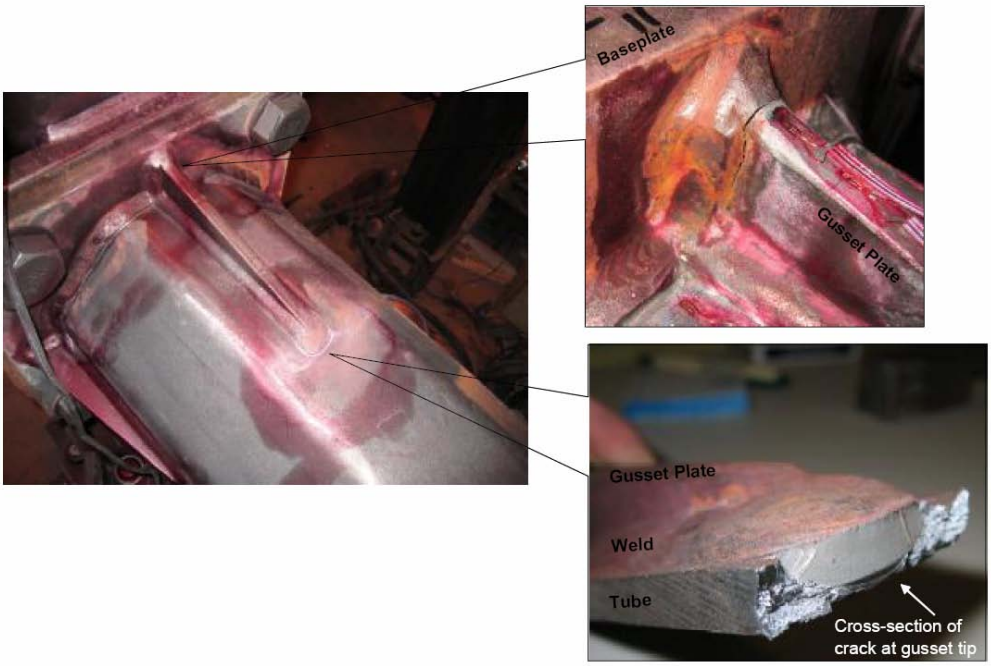

Figure H.8 Typical Crack Formation and Configuration Seen in Testing of Gusset Plate Stiffened Mast-Arm to Plate Connection Details (Ocel *et al* 2006).

Table H.1 Fatigue Life Data for Socketed Pole Thin-Base-Plate Connections with No Retrofit Treatment (Ocel *et al* 2006).

Specimen Designation	No. of Cycles at Failure	Stress Range (ksi)
MN-P-FR1-IP-N-CSR-5-1.25	83,806	8.25
MN-P-FR1-IP-N-CSR-5-1.25	981,490	3.43
MN-P-FR1-IP-N-CSR-5-1.25	610,124	3.80
MN-P-FR1-OP-N-CSR-5-1.25	5,038,549 (ro)	4.09
MN-P-FR1-OP-N-CSR-5-1.25	170,606	5.41
MN-P-FR1-OP-N-CSR-5-1.25	1,292,565 (ro)	5.41
MN-P-FR1-OP-N-CSR-5-1.25	301,484	5.41
MN-P-FR1-OP-N-CSR-5-1.25	2,293,739	5.41
MN-P-FR2-IP-N-CSR-5-1.25	591,696	4.26
MN-P-FR2-IP-N-CSR-5-1.25	868,266	3.65
MN-P-FR2-IP-N-CSR-5-1.25	1,658,906	4.10

Notes:
ro – indicates run out test (no cracks detected at termination of test).

Table H.2 Fatigue Life Data for Socketed Pole Thin-Base-Plate Connections with Hammer Peening Retrofit Measures (Ocel *et al* 2006).

Specimen Designation	No. of Cycles at Failure	Stress Range (ksi)
MN-P-FR1-IP-HPR-MR-5-1.25	4,126,888	4.55
MN-P-FR2-IP-HPR-CSR-5-1.25	1,106,830	6.99
MN-P-FR2-IP-HP-MR-5-1.25	8,501,877	5.82
MN-P-FR2-IP-HP-MR-5-1.25	2,558,528	7.10
MN-P-FR2-IP-HP-MR-5-1.25	124,147	10.00
MN-P-FR2-IP-HP-MR-5-1.25	5,571,296	6.00
MN-P-FR2-IP-HPR-MR-5-1.25	1,131,798	7.91
MN-P-FR2-IP-HP-MR-5-1.25	5,366,869	7.91

Table H.3 Fatigue Life Data for Socketed Pole Thick-Base-Plate Connections with and without Retrofit Techniques (Ocel *et al* 2006).

Specimen Designation	No. of Cycles at Failure	Stress Range (ksi)
MN-P-FR2-IP-N-MR-5-2.50-1	4,222,993	11.17
MN-P-FR2-IP-N-CSR-5-2.50-2	81,924	14.90
MN-P-FR2-IP-HP-CSR-5-2.50-2	978,382	14.90
MN-P-FR2-IP-N-CSR-5-2.50-1	566,119	14.90
MN-P-FR2-IP-N-CSR-5-2.50-2	101,916	14.90
MN-P-FR2-IP-N-CSR-3-2.50-1	330,137	15.00
MN-P-FR2-IP-N-CSR-3-2.50-2	140,545	15.00
MN-P-FR2-IP-N-CSR-3-2.50-1	183,638	15.00
MN-P-FR2-IP-N-CSR-3-2.50-2	86,888	15.00

Table H.4 Fatigue Life Data for Un-Stiffened Mast-Arm Plate Connections without Retrofit Measures (Ocel *et al* 2006).

Specimen Designation	No. of Cycles at Failure	Stress Range (ksi)
MN-MA-FR3-IP-N-CSR-5-1.25-1	6,997,582	8.54
MN-MA-FR3-IP-N-CSR-5-1.25-1	420,785	15.37
MN-MA-FR3-IP-N-CSR-5-1.25-1	434,329	15.37
MN-MA-FR3-IP-N-CSR-5-1.25-1	242,060	15.37
MN-MA-FR3-IP-N-CSR-5-1.25-2	420,662	15.37
MN-MA-FR3-IP-N-CSR-5-1.25-2	372,056	15.37
MN-MA-FR3-IP-N-CSR-5-1.25-2	298,023	15.37
MN-MA-FR3-IP-N-CSR-5-1.25-2	267,922	15.37

Table H.5 Fatigue Life Data for Stiffened Mast-Arm Plate Connections without Retrofit Measures (Ocel *et al* 2006).

Specimen Designation	No. of Cycles at Failure	Stress Range (ksi)
MN-MAG-FR3-IP-N-MR-5-1.25-1	1,642,305	4.15
MN-MAG-FR3-IP-N-MR-5-1.25-1	1,300,949	11.30
MN-MAG-FR3-IP-N-CSR-5-1.25-1	171,695	10.38
MN-MAG-FR3-IP-N-CSR-5-1.25-1	186,036	10.33
MN-MAG-FR3-IP-N-CSR-5-1.25-2	223,987	10.38
MN-MAG-FR3-IP-N-CSR-5-1.25-2	157,123	10.33

Table H.6 Key to Specimen Designation for Socketed Pole Connections

MN – A – B – C – D – E – F –G – H		
Specimen Designation		
A	P	Pole Base Plate Connection
	MA	Unstiffened Mast-Arm Connection
	MAG	Gusset Stiffened Mast-Arm Connection
Test Frame Configuration		
B	FR1	Test Frame Configuration 1 (see Figure Q.3)
	FR2	Test Frame Configuration 2 (see Figure Q.4)
	FR3	Test Frame Configuration 3 (see Figure Q.5)
Loading Direction		
C	IP	In-Plane Loading
	OP	Out-of-Plane Loading
Retrofit Treatment Implemented		
D	N	None
	HP	Hammer Peening
	HPR	Hammer Peening with Simulated Dead Load and Crack Present
Stress Range Methodology		
E	CSR	Constant Amplitude Stress Range
	MR	Miner's Cumulative Fatigue Damage Rule used to Define Equivalent Constant Amplitude Stress Range
Pole or Mast-Arm Tube Wall Thickness		
F	#	Number of Sixteenths of an Inch (*e.g.* 5 – indicates 5/16 inch)
Connection Plate Thickness		
G	#	Plate Thickness (*e.g.* 1.25 in. or 2.50 in.)
Test Direction		
H	1	Indicates First Side Testing
	2	Indicates Second Side Testing after Moment Reversal

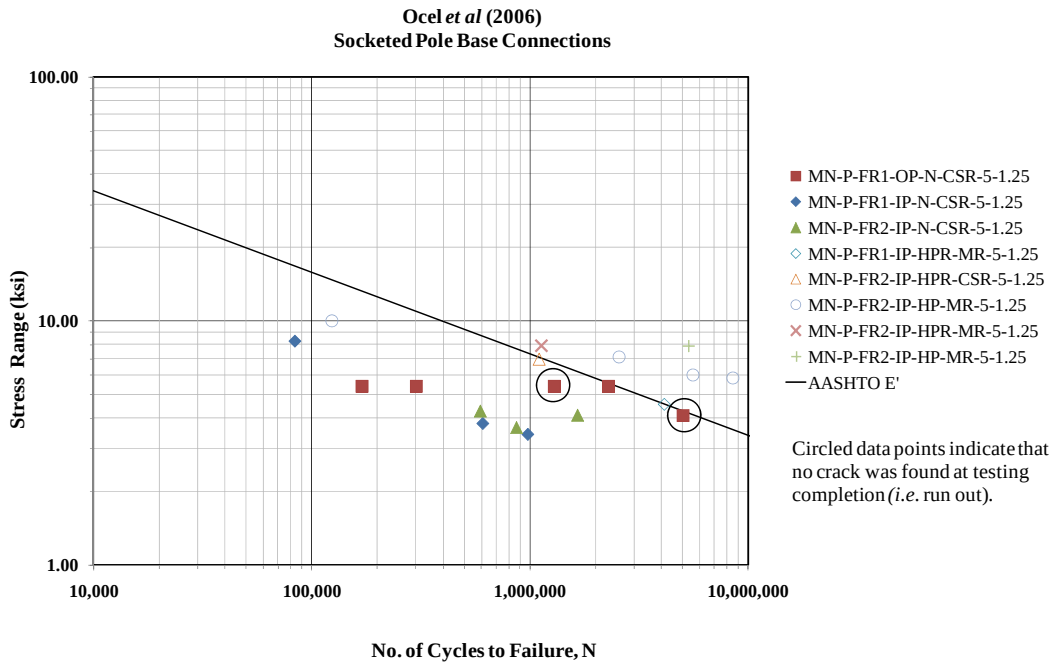

Figure H.9 Fatigue Lives Seen in Experimental Testing of Socketed Pole Thin-Base-Plate Connections (Ocel *et al* 2006).

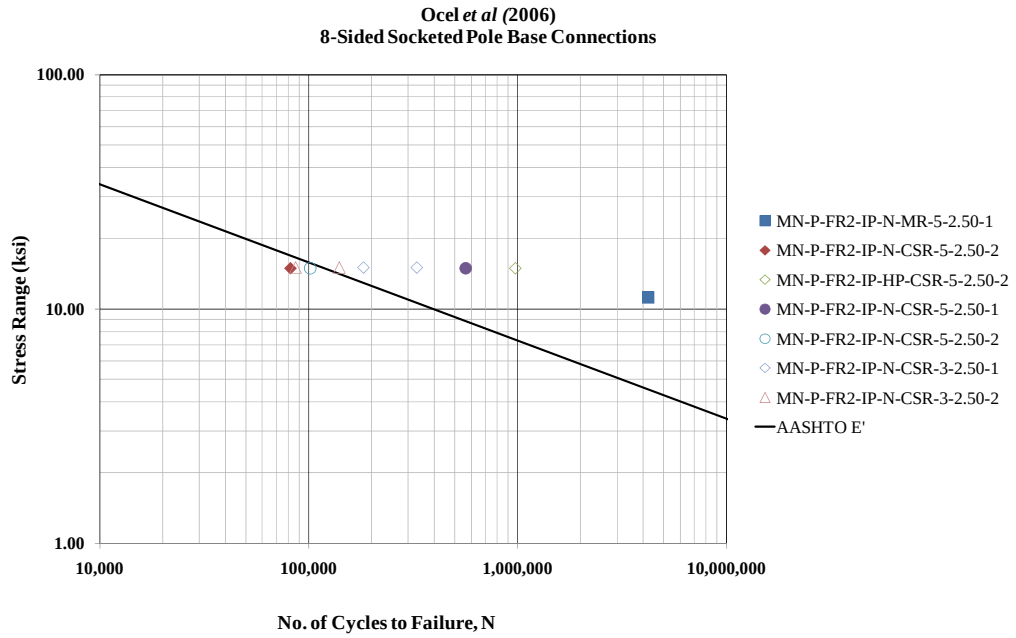

Figure H.10 Fatigue Lives Seen in Experimental Testing of Socketed Pole Thick-Base-Plate Connections (Ocel *et al* 2006).

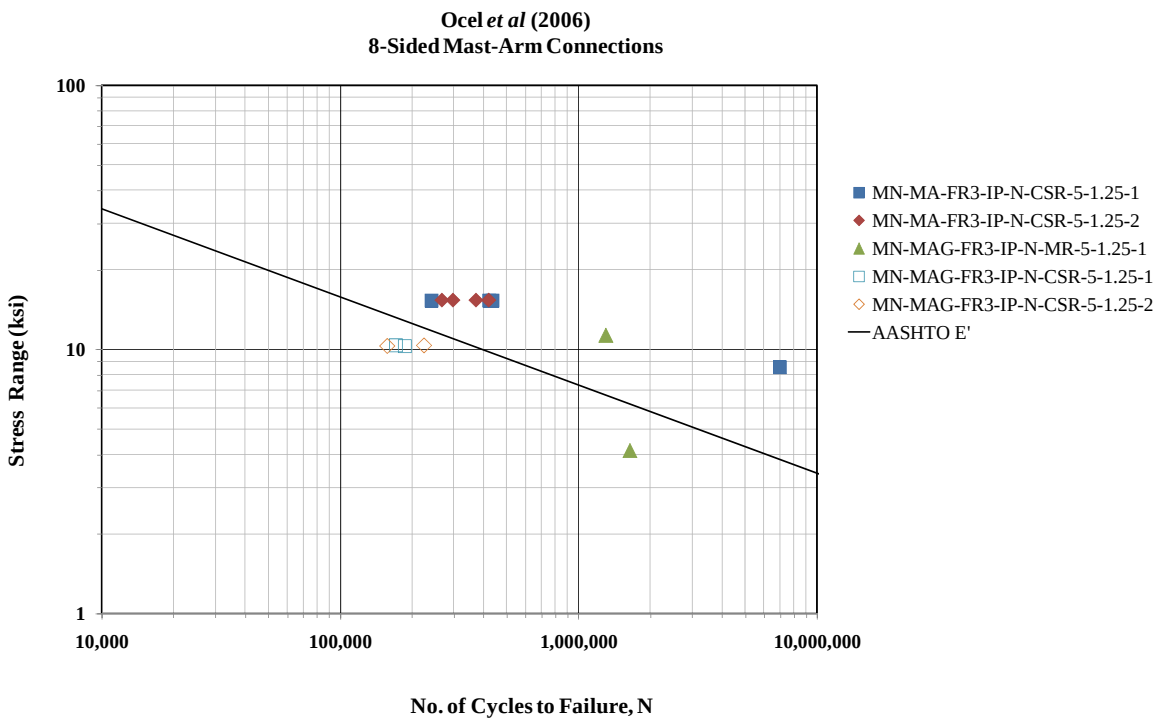

Figure H.11 Fatigue Lives Seen in Experimental Testing of Un-Stiffened and Stiffened Mast-Arm-Plate Connections (Ocel *et al* 2006).

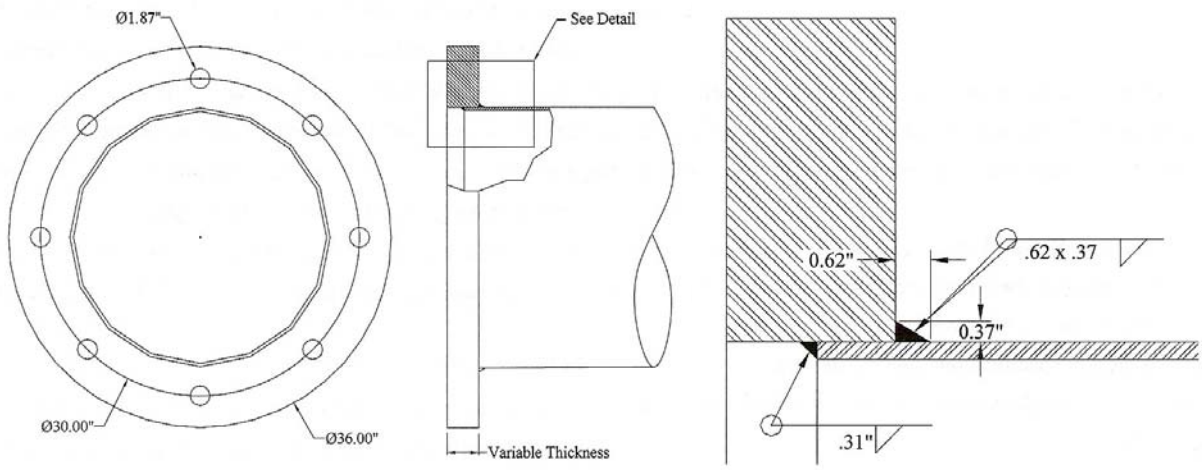

(a) Socketed Fillet Weld Connection – Unequal-Leg Fillet with Seal Weld

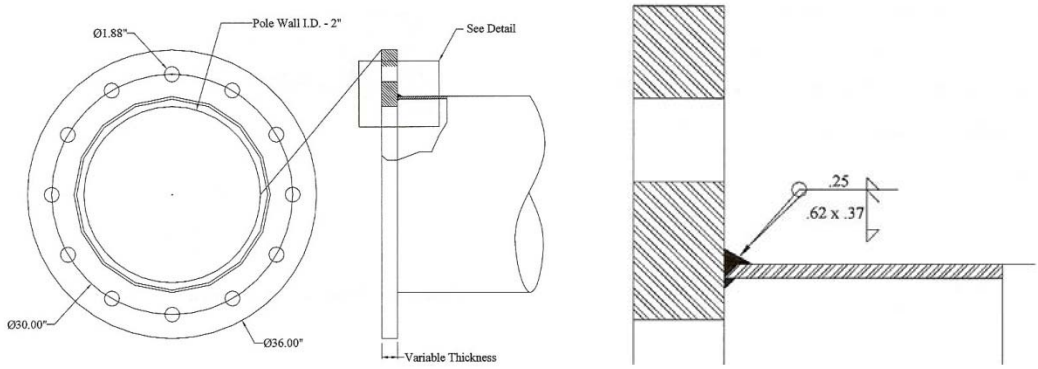

(b) Texas Detail – Full Pentration without Backing Ring

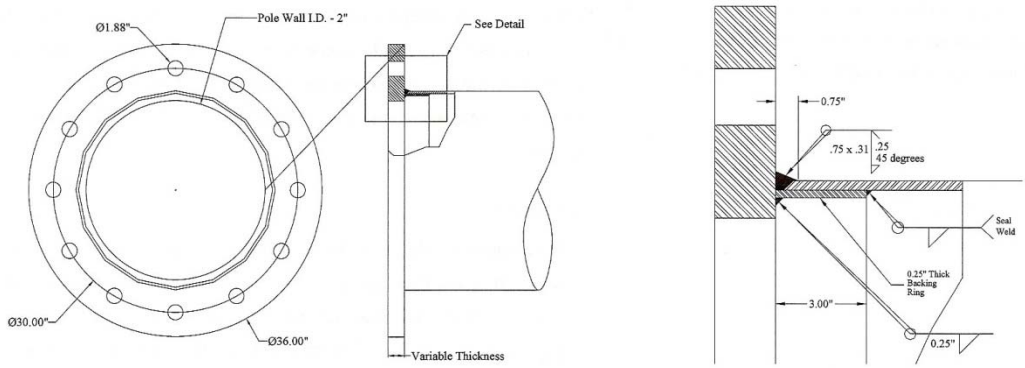

(c) Wyoming Detail – Full Penetration with Backing Ring

Figure I.1 Unreinforced High-Mast Luminiare Support Base Details (Rios 2007)

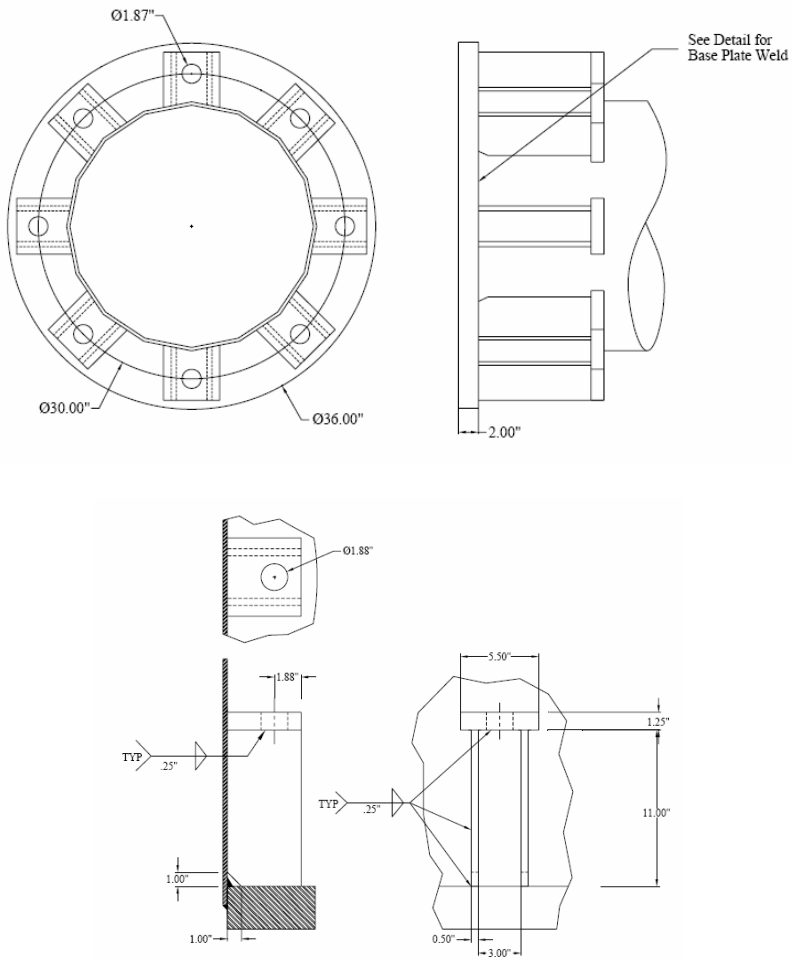

Figure I.2 Reinforced (Stool Base) High-Mast Luminaire Support Base Details (Rios 2007).

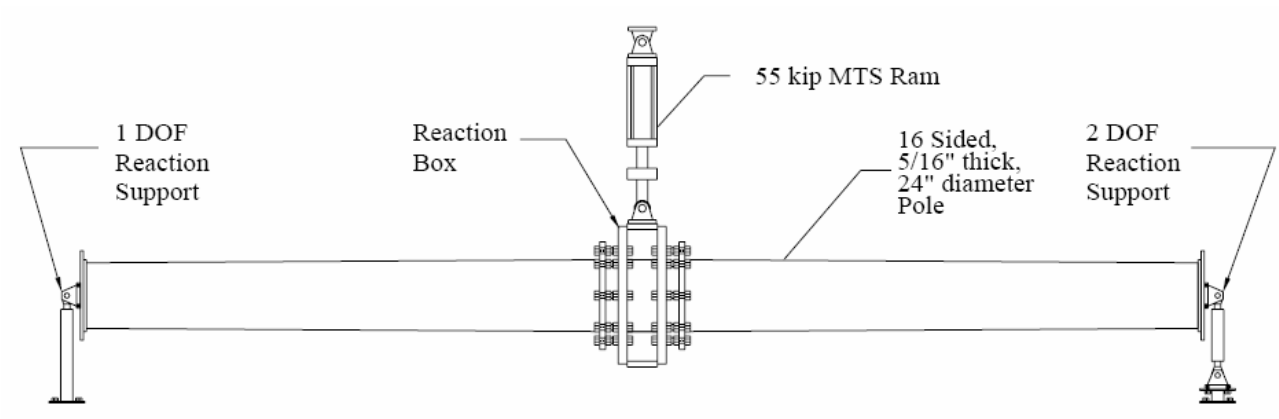

Figure I.3 Testing Apparatus for Cyclic Fatigue Testing (Rios 2007).

Table I.1. Fatigue Testing Results for Socketed Fillet Welded Connection Specimens (Rios 2007).

Specimen Designation	No. of Bolts	Base Plate Thickness (in.)	No. of Cycles at Failure	Stress Range (ksi)
UTX-24-1.5-8-S	8	1.50	13,193	12.0
UTX-24-2.0-8-S	8	2.00	46,772	12.0
UTX-24-3.0-8-S	8	3.00	147,550	12.0
UTX-24-1.5-12-S	12	1.50	27,977	12.0
UTX-24-2.0-12-S	12	2.00	143,214	12.0

Table I.2. Fatigue Testing Results for Full Penetration Weld Connection Specimens with and without Backing Ring (Rios 2007).

Specimen Designation	No. of Bolts	Base Plate Thickness (in.)	No. of Cycles at Failure	Stress Range (ksi)
UTX-24-2.0-8-WY	8	2.00	133,819	12.0
UTX-24-3.0-12-TX-A	12	3.00	236,154	12.0
UTX-24-3.0-12-TX-B	12	3.00	327,487	12.0

Table I.3 Fatigue Testing Results for Stool Base Connection Specimens (Rios 2007).

Specimen Designation	No. of Bolts	Base Plate Thickness (in.)	No. of Cycles at Failure	Stress Range (ksi)
UTX-24-2.0-8-SB-A	8	2.00	785,058	12.0
UTX-24-2.0-8-SB-B	8	2.00	483,314	12.0

Specimen Designations:

UTX-AA-B.B-C-DD-E

AA – Number of sides on faceted cross-section
B.B – Base Plate Thickness
C – Number of Bolts in Connection Arrangement
DD – Configuration: S = socketed fillet weld; WY = Wyoming standard; TX = Texas standard, SB = stool base
E – Specimen designation

Figure 5.1: Typical failure of fillet welded socket connection

(a) Fillet Welded Socket Connection (S – connection)

Figure 5.3: Typical failure of Wyoming full penetration weld connection

(b) Full-Penetration Welded Connection with Backing Ring (WY – connection)

Figure 5.4: Typical Failure of Texas full penetration weld connection

(c) Full-Penetration Welded Connection without Backing Ring (TX – connection)

Figure I.4 Unreinforced Specimen Fatigue Failures Seen in Testing (Rios 2007).

Figure I.5 Stool Base Specimen Fatigue Failures Seen in Testing (Rios 2007).

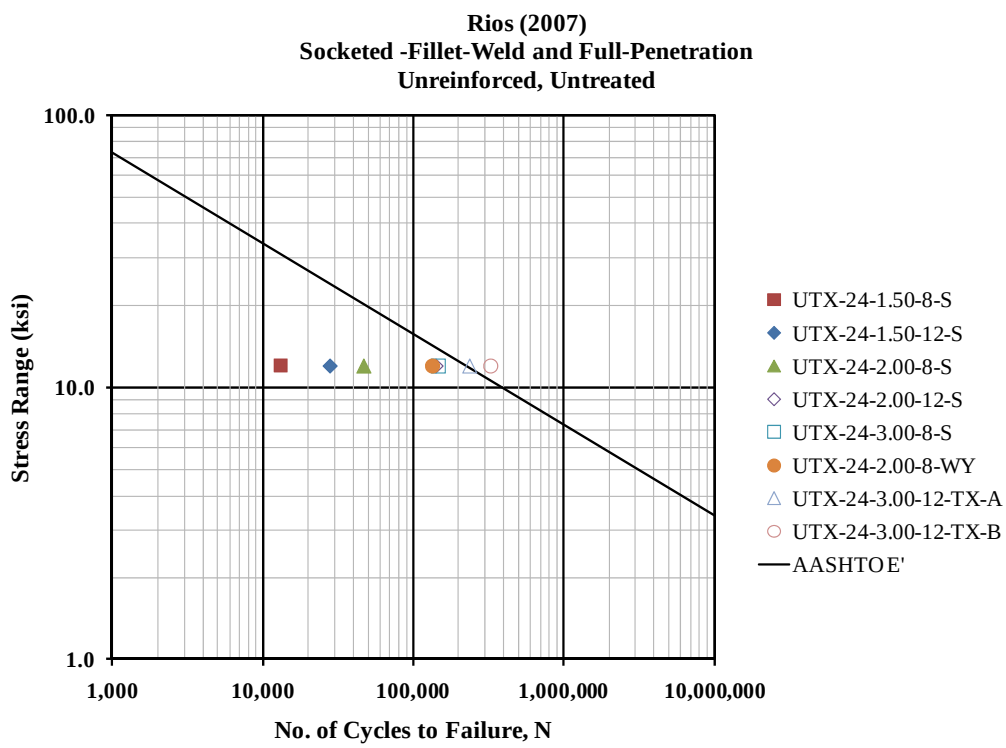

Figure I.6 Fatigue Lives for Unreinforced Socketed and Full-Penetration High-Mast Luminaire Support Base Connections (Rios 2007).

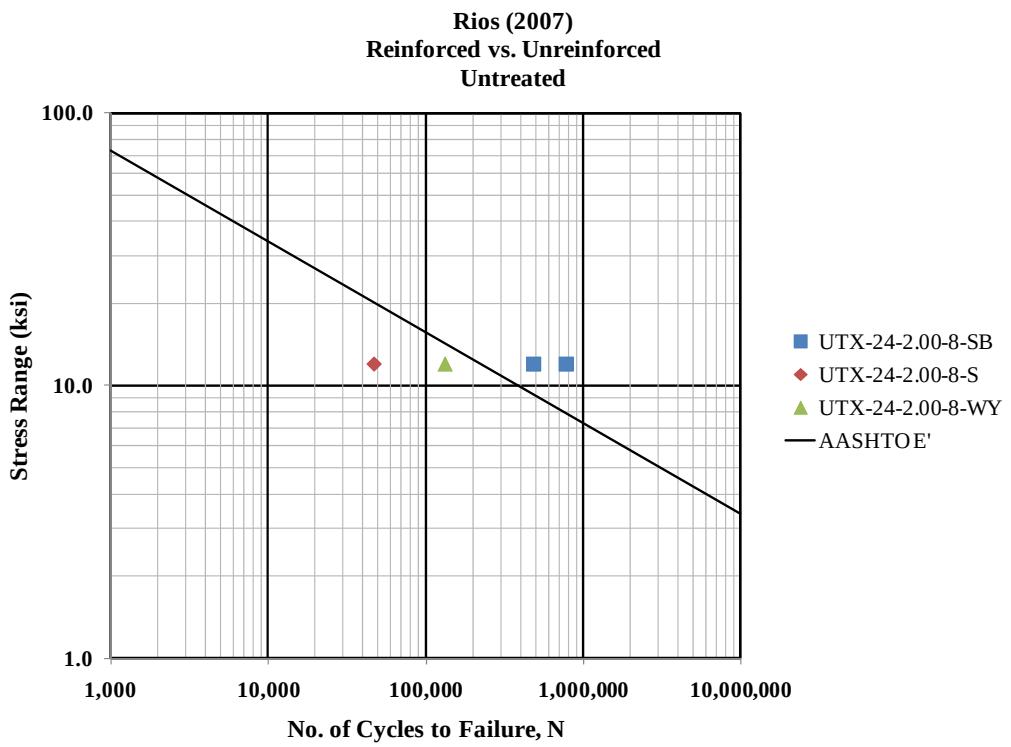

Figure I.7 Fatigue Life Comparison of Unreinforced and Reinforced High-Mast Luminiare Support Base Connections (Rios 2007).

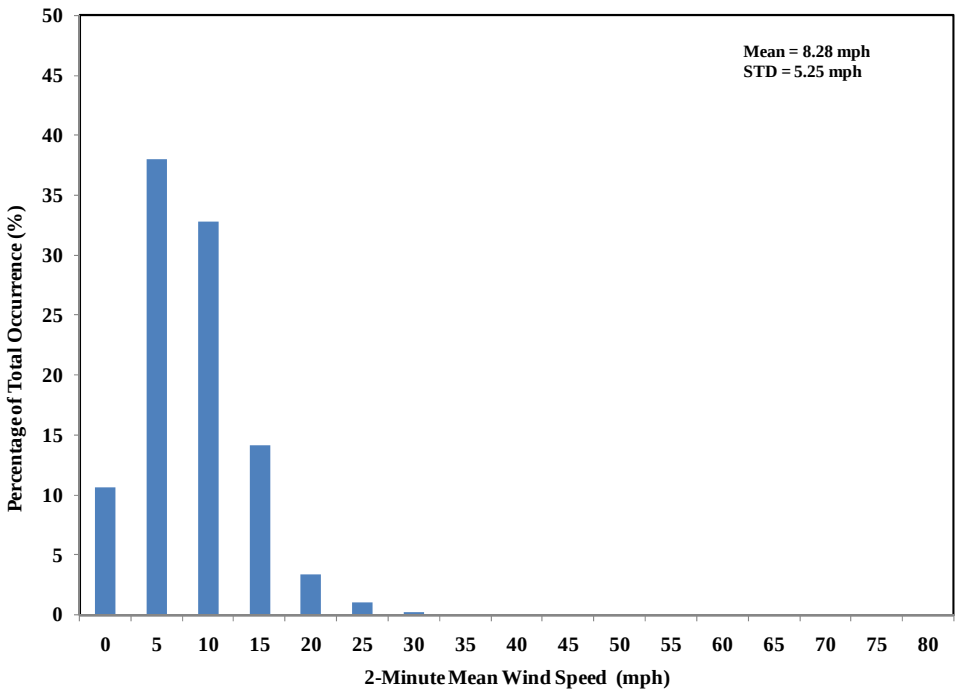

Figure J.1. Probability Mass Function for Wind Speed Irrespective of Direction for Appleton, WI for Period December 2003 through January 2007.

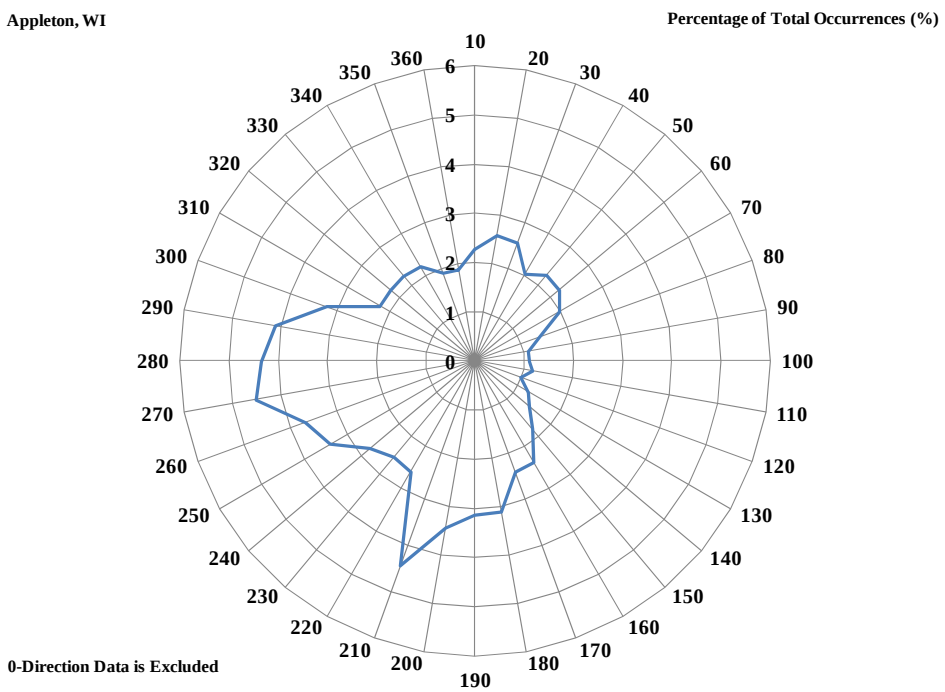

Figure J.2. Probability Mass Function for Wind Direction Irrespective of Speed for Appleton, WI for Period December 2003 through January 2007.

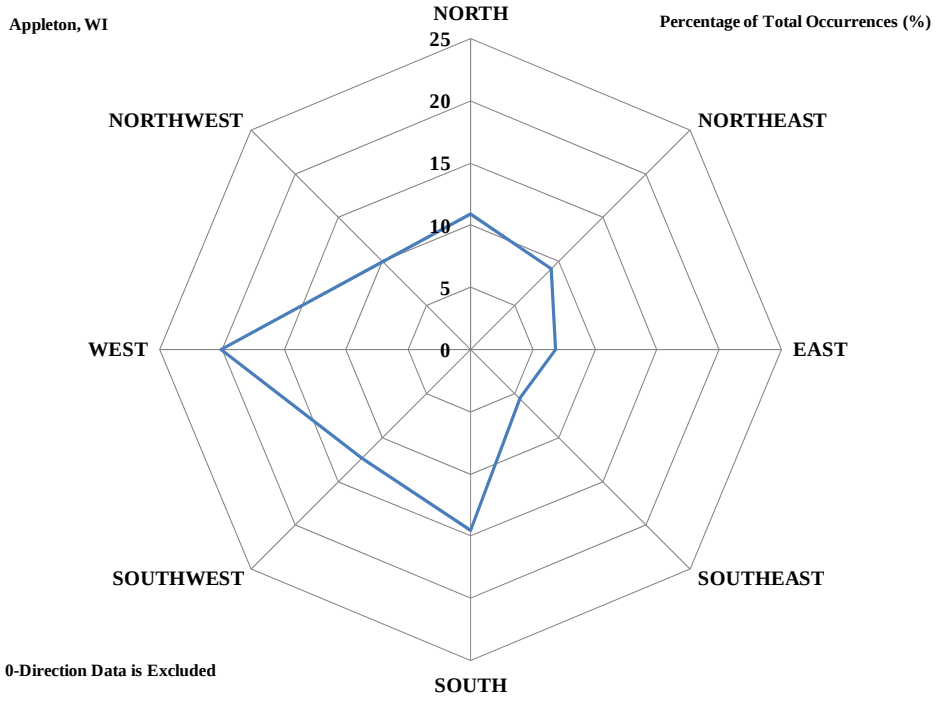

Figure J.3. Probability Mass Function for Wind Direction Irrespective of Speed for Appleton, WI for Period December 2003 through January 2007.

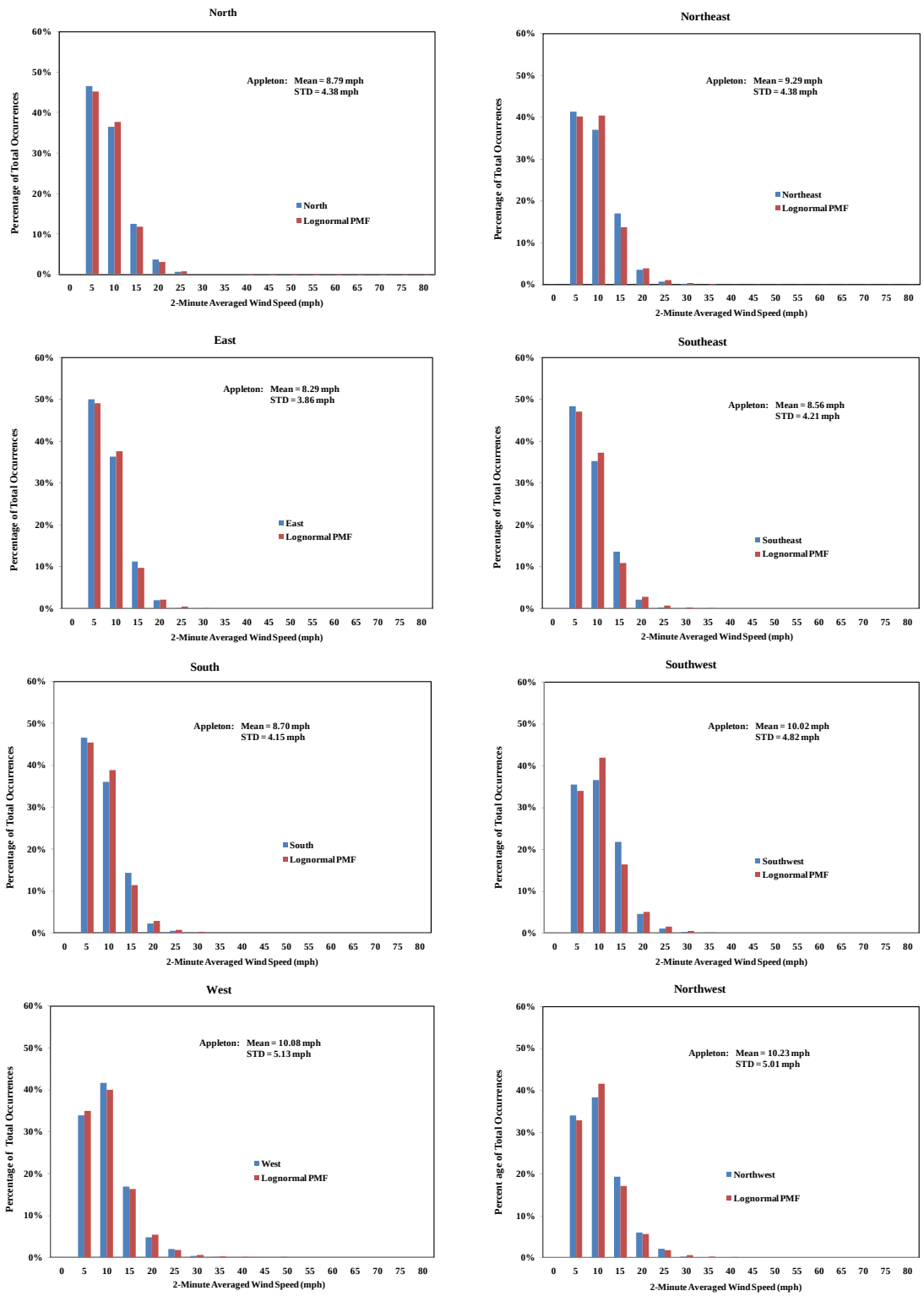

Figure J.4. Probability Mass Functions (Histograms) for Measured Direction-Dependent Wind Speeds and Lognormal PDF Models for Appleton, Wisconsin (December 2003 to January 2007).

Table J.1. Combined Probabilities, $P\left[Speed \cap Direction\right]$, for Appleton, Wisconsin (December 2003 to January 2007).

2-Minute Averaged Wind Speed (mph)	Wind Direction									
	N/A	**North**	**Northeast**	**East**	**Southeast**	**South**	**Southwest**	**West**	**Northwest**	**SUM**
0	0.15782	0.00003	0.00003	0.00004	0.00005	0.00006	0.00000	0.00000	0.00000	0.15803
5	0.00086	0.04488	0.03461	0.04258	0.04388	0.06874	0.03894	0.04671	0.03084	0.35205
10	0.00077	0.03519	0.03094	0.03091	0.03202	0.05317	0.04007	0.05727	0.03477	0.31512
15	0.00000	0.01202	0.01420	0.00960	0.01238	0.02113	0.02383	0.02327	0.01750	0.13394
20	0.00000	0.00349	0.00298	0.00176	0.00194	0.00329	0.00508	0.00656	0.00542	0.03051
25	0.00000	0.00066	0.00066	0.00016	0.00031	0.00079	0.00113	0.00278	0.00191	0.00840
30	0.00000	0.00011	0.00014	0.00000	0.00005	0.00006	0.00030	0.00049	0.00026	0.00142
35	0.00000	0.00000	0.00000	0.00000	0.00000	0.00000	0.00011	0.00011	0.00000	0.00022
40	0.00000	0.00003	0.00000	0.00000	0.00000	0.00000	0.00003	0.00002	0.00000	0.00008
45	0.00000	0.00000	0.00000	0.00000	0.00000	0.00000	0.00000	0.00000	0.00000	0.00000
50	0.00000	0.00000	0.00000	0.00000	0.00000	0.00000	0.00000	0.00019	0.00000	0.00019
55	0.00000	0.00000	0.00000	0.00000	0.00005	0.00000	0.00000	0.00000	0.00000	0.00005
60	0.00000	0.00000	0.00000	0.00000	0.00000	0.00000	0.00000	0.00000	0.00000	0.00000
65	0.00000	0.00000	0.00000	0.00000	0.00000	0.00000	0.00000	0.00000	0.00000	0.00000
70	0.00000	0.00000	0.00000	0.00000	0.00000	0.00000	0.00000	0.00000	0.00000	0.00000
75	0.00000	0.00000	0.00000	0.00000	0.00000	0.00000	0.00000	0.00000	0.00000	0.00000
80	0.00000	0.00000	0.00000	0.00000	0.00000	0.00000	0.00000	0.00000	0.00000	0.00000
SUM	0.15946	0.09641	0.08356	0.08505	0.09068	0.14725	0.10951	0.13740	0.09069	1.00000

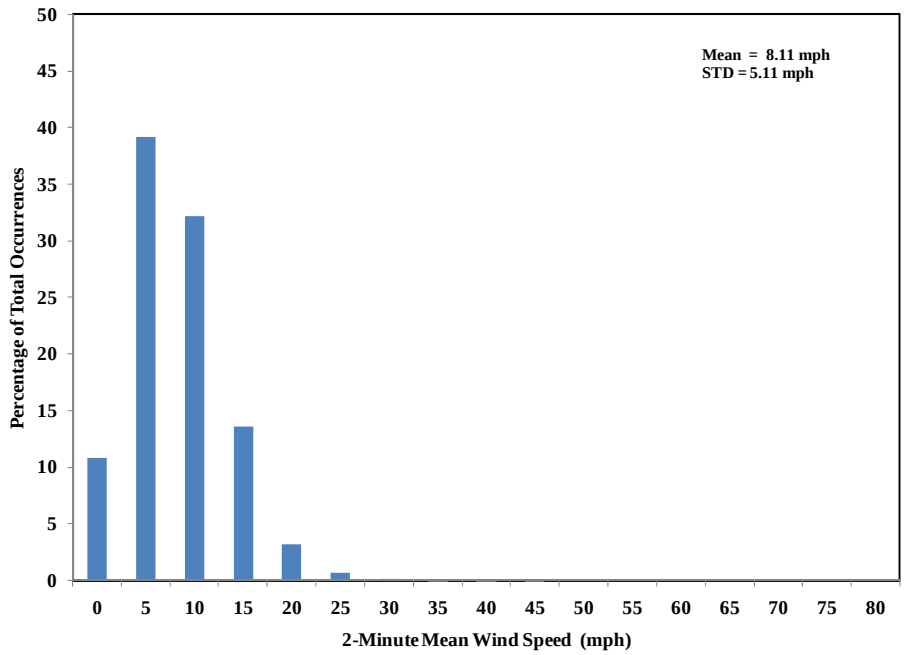

Figure K.1. Probability Mass Function for Wind Speed Irrespective of Direction for Green Bay, WI for Period December 2008 through January 2007.

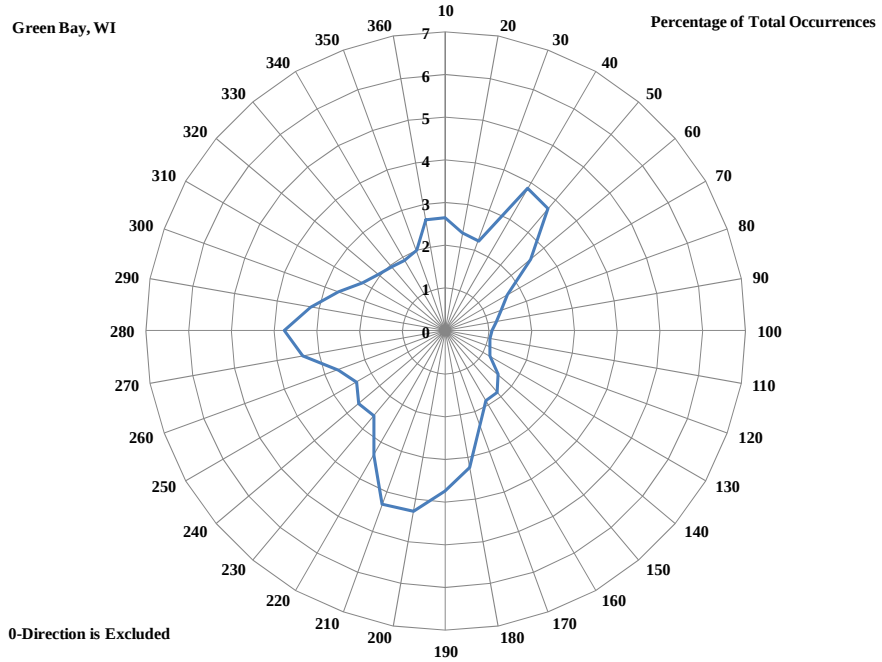

Figure K.2. Probability Mass Function for Wind Direction Irrespective of Speed for Green Bay, WI for Period December 1998 through January 2007.

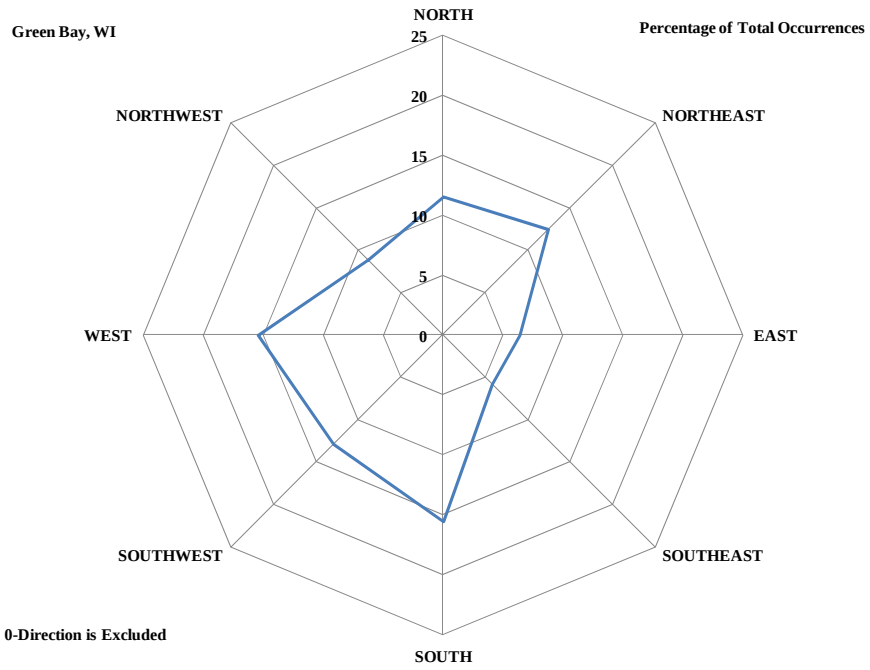

Figure K3. Probability Mass Function for Wind Direction Irrespective of Speed for Green Bay, WI for Period December 1998 through January 2007.

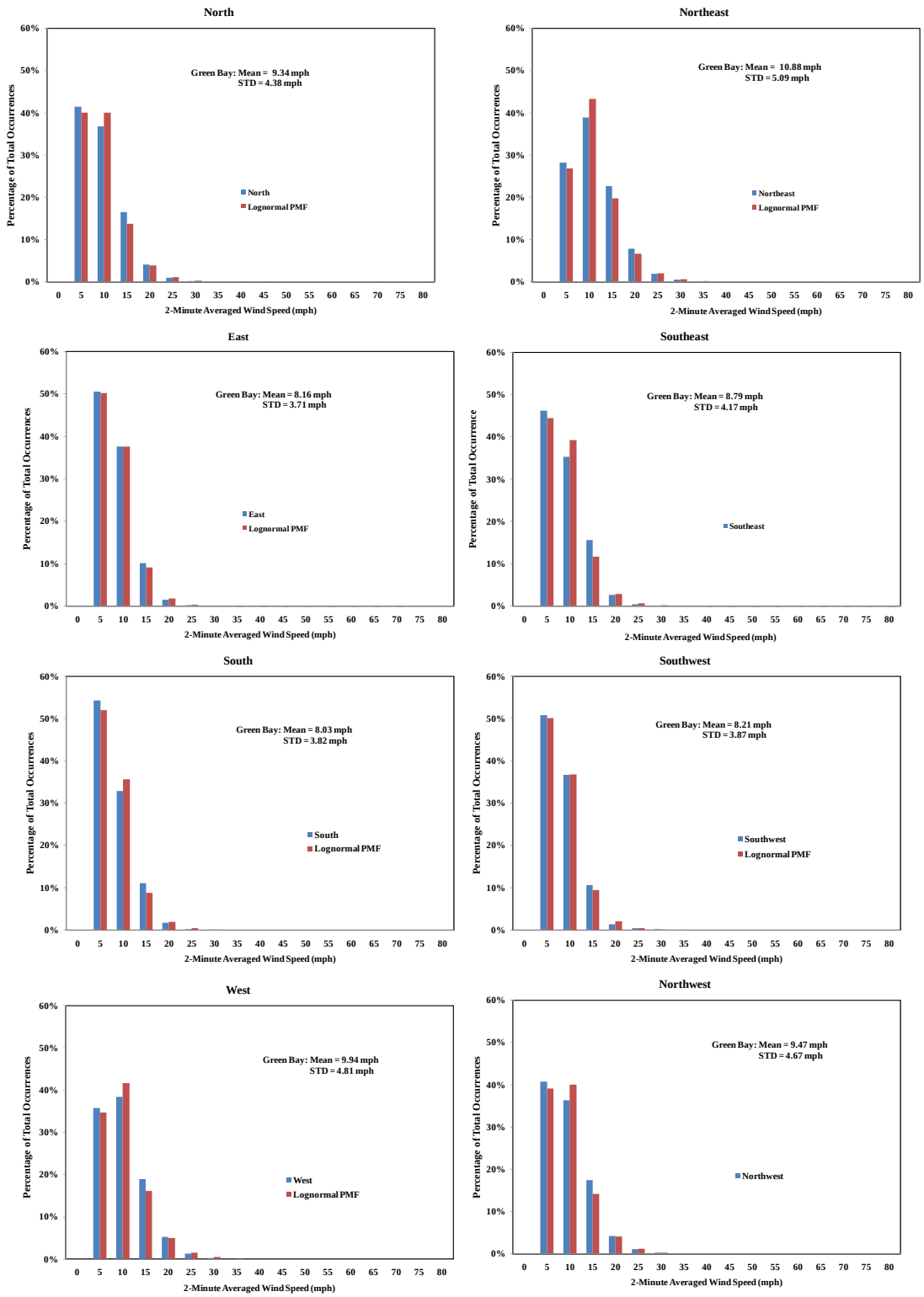

Figure K.4. Probability Mass Functions (Histograms) for Measured Direction-Dependent Wind Speeds and Lognormal PDF Models for Green Bay, Wisconsin (December 1998 to January 2007).

Table K.1. Combined Probabilities, $P\left[Speed \cap Direction\right]$, for Green Bay, Wisconsin (December 1998 to January 2007).

		Wind Direction									
		N/A	**North**	**Northeast**	**East**	**Southeast**	**South**	**Southwest**	**West**	**Northwest**	**SUM**
2-Minute Averaged Wind Speed (mph)	0	0.15946	0.00000	0.00000	0.00000	0.00000	0.00000	0.00000	0.00000	0.00000	0.15946
	5	0.00000	0.03997	0.02360	0.04296	0.04184	0.07990	0.05570	0.04912	0.03691	0.37001
	10	0.00000	0.03550	0.03252	0.03201	0.03203	0.04838	0.04017	0.05282	0.03294	0.30637
	15	0.00000	0.01591	0.01896	0.00861	0.01415	0.01627	0.01159	0.02605	0.01584	0.12737
	20	0.00000	0.00398	0.00654	0.00132	0.00230	0.00241	0.00147	0.00719	0.00383	0.02904
	25	0.00000	0.00090	0.00154	0.00015	0.00033	0.00025	0.00042	0.00182	0.00096	0.00638
	30	0.00000	0.00015	0.00039	0.00000	0.00001	0.00004	0.00014	0.00035	0.00018	0.00127
	35	0.00000	0.00001	0.00002	0.00000	0.00000	0.00000	0.00002	0.00003	0.00000	0.00007
	40	0.00000	0.00000	0.00000	0.00000	0.00000	0.00000	0.00000	0.00001	0.00002	0.00003
	45	0.00000	0.00000	0.00000	0.00000	0.00000	0.00000	0.00000	0.00001	0.00000	0.00001
	50	0.00000	0.00000	0.00000	0.00000	0.00000	0.00000	0.00000	0.00000	0.00000	0.00000
	55	0.00000	0.00000	0.00000	0.00000	0.00000	0.00000	0.00000	0.00000	0.00000	0.00000
	60	0.00000	0.00000	0.00000	0.00000	0.00000	0.00000	0.00000	0.00000	0.00000	0.00000
	65	0.00000	0.00000	0.00000	0.00000	0.00000	0.00000	0.00000	0.00000	0.00000	0.00000
	70	0.00000	0.00000	0.00000	0.00000	0.00000	0.00000	0.00000	0.00000	0.00000	0.00000
	75	0.00000	0.00000	0.00000	0.00000	0.00000	0.00000	0.00000	0.00000	0.00000	0.00000
	80	0.00000	0.00000	0.00000	0.00000	0.00000	0.00000	0.00000	0.00000	0.00000	0.00000
	SUM	0.15946	0.09641	0.08356	0.08505	0.09068	0.14725	0.10951	0.13740	0.09069	1.00000

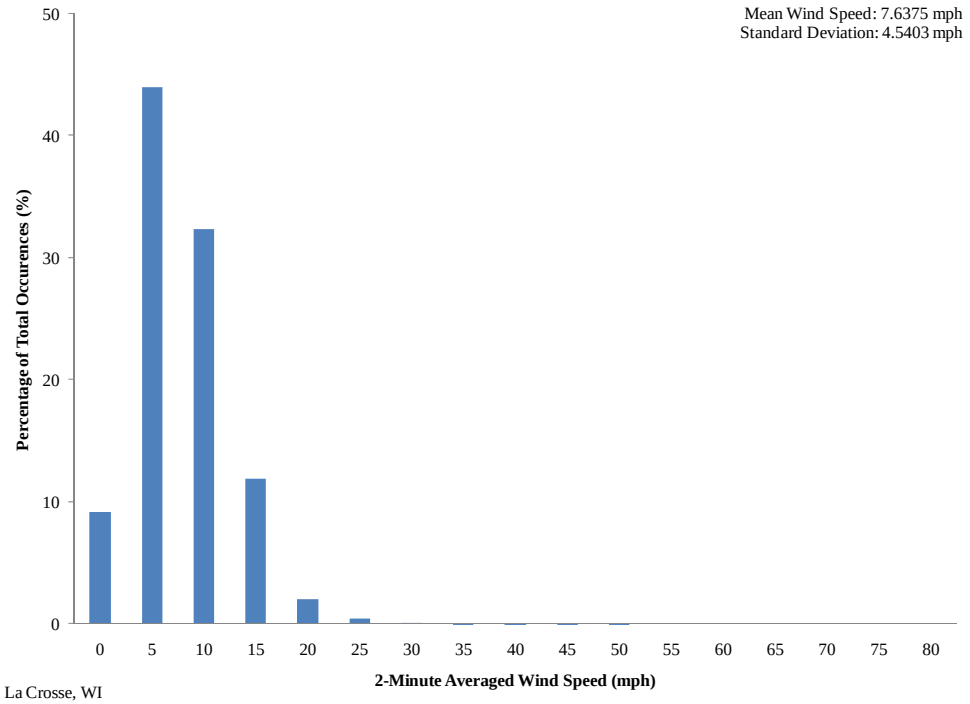

Figure L.1. Probability Mass Function for Wind Speed Irrespective of Direction for La Crosse, WI for Period Jan. 1998 through Dec. 2007.

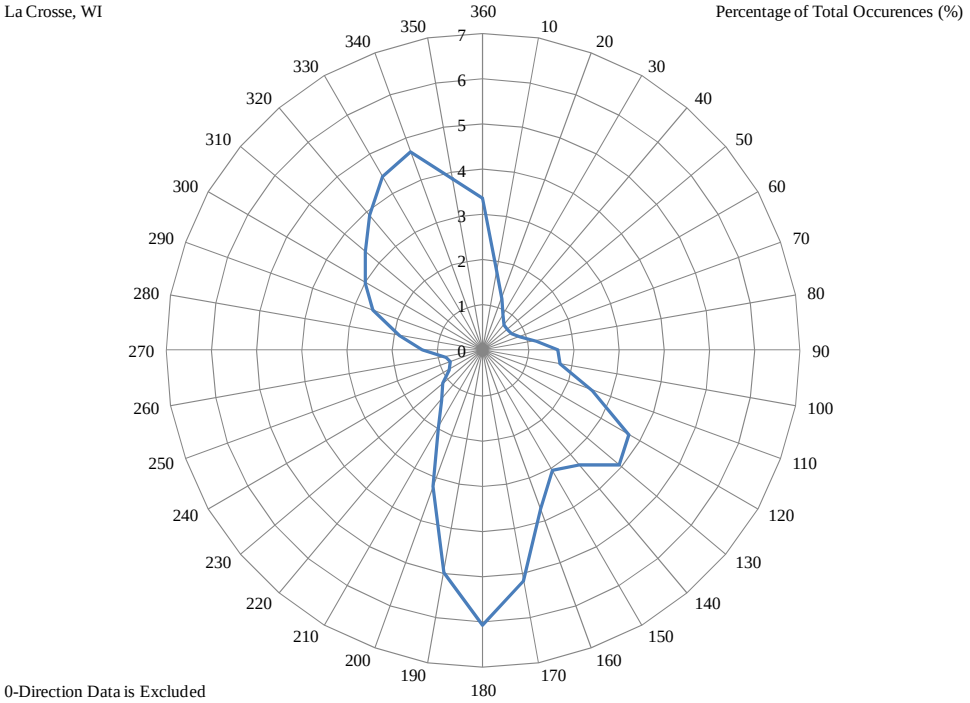

Figure L.2. Probability Mass Functions for Wind Direction Irrespective of Speed for La Crosse, WI for Period Jan. 1998 through Dec. 2007.

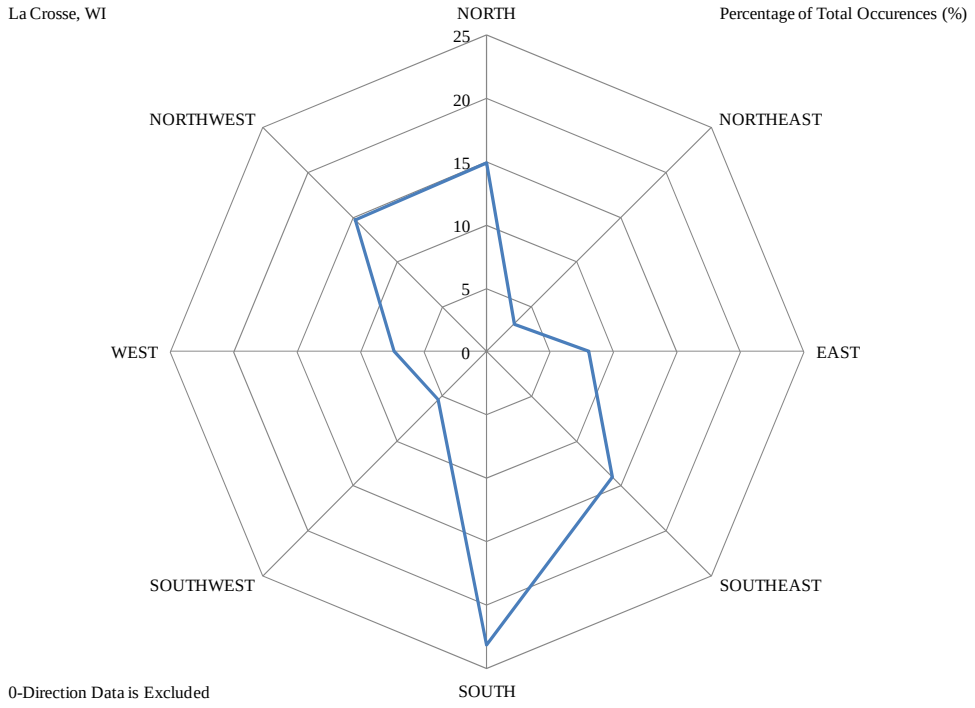

Figure L.3. Probability Mass Functions for Wind Direction Irrespective of Speed for La Crosse, WI for Period Jan. 1998 through Dec. 2007.

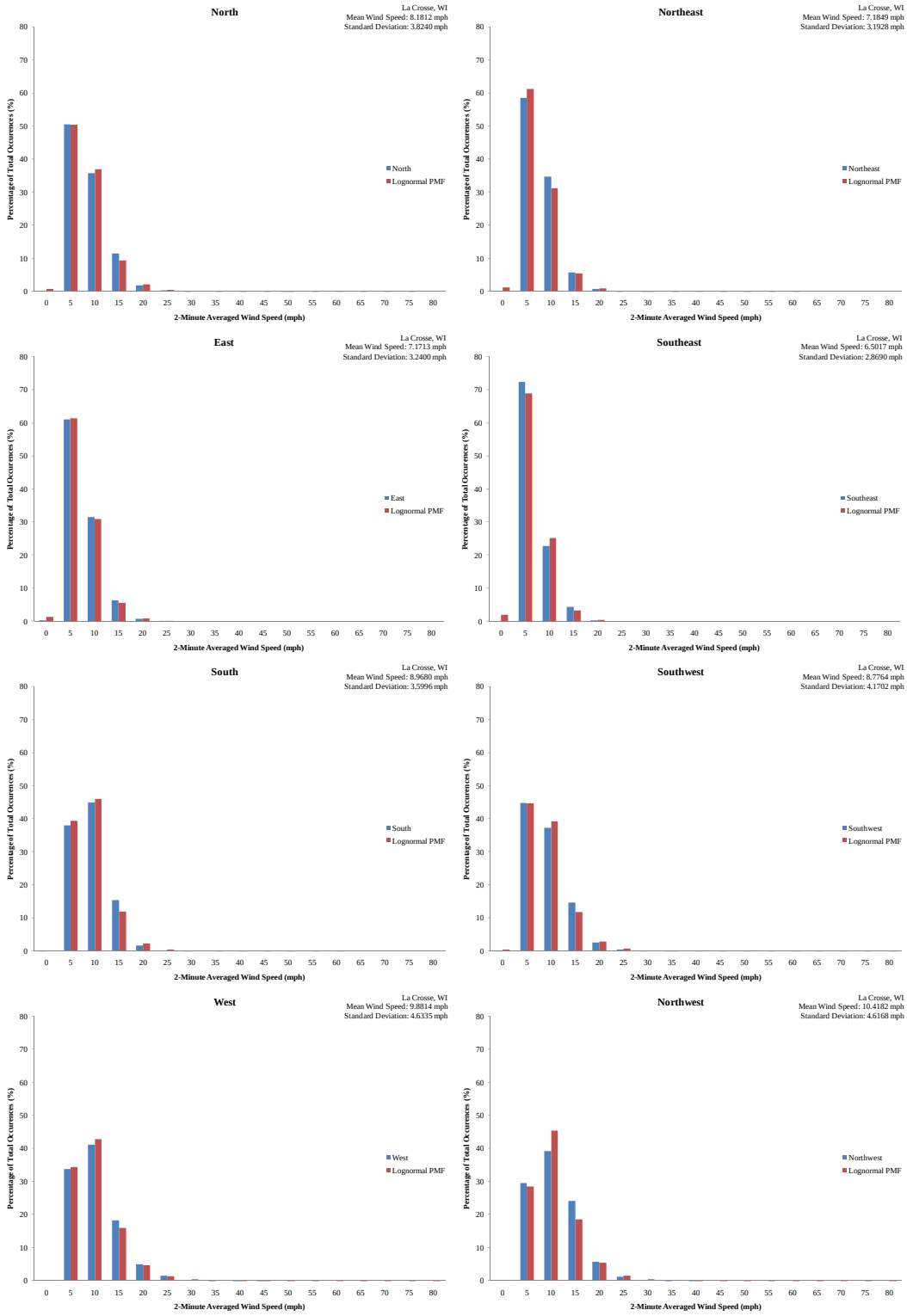

Figure L.4. Probability Mass Functions for Wind Speeds for Specific Directions for *La Crosse, WI* for Period *Jan. 1998* through *Dec. 2007*.

Table L.1. Combined Probabilities, *P[Speed ∩ Direction]*, for *La Crosse, WI* for Period *Jan. 1998* through *Dec. 2007*.

		Wind Direction									
		N/A	**North**	**Northeast**	**East**	**Southeast**	**South**	**Southwest**	**West**	**Northwest**	**SUM**
2-Minute Averaged Wind Speed (mph)	0	0.09338	0.00015	0.00007	0.00020	0.00016	0.00008	0.00004	0.00013	0.00017	0.09439
	5	0.00000	0.07503	0.01802	0.04914	0.10130	0.08783	0.02420	0.02485	0.04340	0.42376
	10	0.00000	0.05320	0.01071	0.02536	0.03201	0.10394	0.02009	0.03021	0.05753	0.33306
	15	0.00000	0.01709	0.00179	0.00518	0.00618	0.03555	0.00793	0.01341	0.03547	0.12258
	20	0.00000	0.00279	0.00024	0.00063	0.00047	0.00379	0.00139	0.00366	0.00836	0.02132
	25	0.00000	0.00051	0.00001	0.00009	0.00008	0.00034	0.00030	0.00108	0.00186	0.00428
	30	0.00000	0.00001	0.00001	0.00002	0.00000	0.00004	0.00006	0.00011	0.00024	0.00050
	35	0.00000	0.00000	0.00000	0.00000	0.00000	0.00000	0.00003	0.00002	0.00001	0.00006
	40	0.00000	0.00000	0.00000	0.00000	0.00000	0.00000	0.00000	0.00002	0.00001	0.00003
	45	0.00000	0.00000	0.00000	0.00000	0.00000	0.00000	0.00000	0.00001	0.00000	0.00001
	50	0.00000	0.00001	0.00000	0.00000	0.00000	0.00000	0.00000	0.00000	0.00000	0.00001
	55	0.00000	0.00000	0.00000	0.00000	0.00000	0.00000	0.00000	0.00000	0.00000	0.00000
	60	0.00000	0.00000	0.00000	0.00000	0.00000	0.00000	0.00000	0.00000	0.00000	0.00000
	65	0.00000	0.00000	0.00000	0.00000	0.00000	0.00000	0.00000	0.00000	0.00000	0.00000
	70	0.00000	0.00000	0.00000	0.00000	0.00000	0.00000	0.00000	0.00000	0.00000	0.00000
	75	0.00000	0.00000	0.00000	0.00000	0.00000	0.00000	0.00000	0.00000	0.00000	0.00000
	80	0.00000	0.00000	0.00000	0.00000	0.00000	0.00000	0.00000	0.00000	0.00000	0.00000
	SUM	0.09338	0.14879	0.03085	0.08061	0.14020	0.23158	0.05403	0.07351	0.14705	1.00000

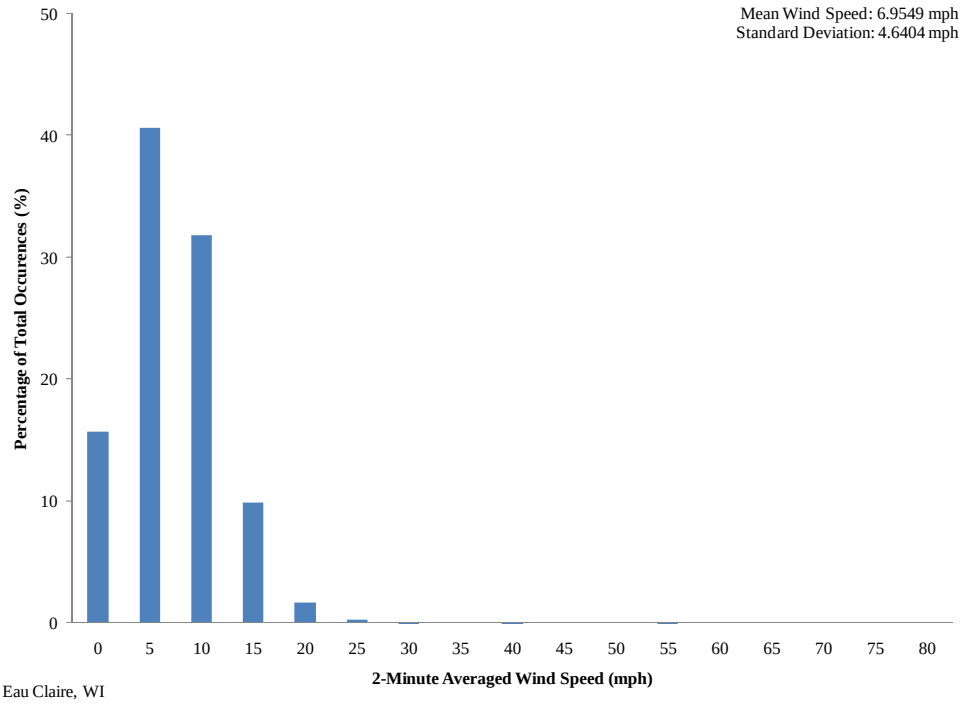

Figure M.1. Probability Mass Function for Wind Speed Irrespective of Direction for Eau Claire, WI for Period January 1998 through December 2007.

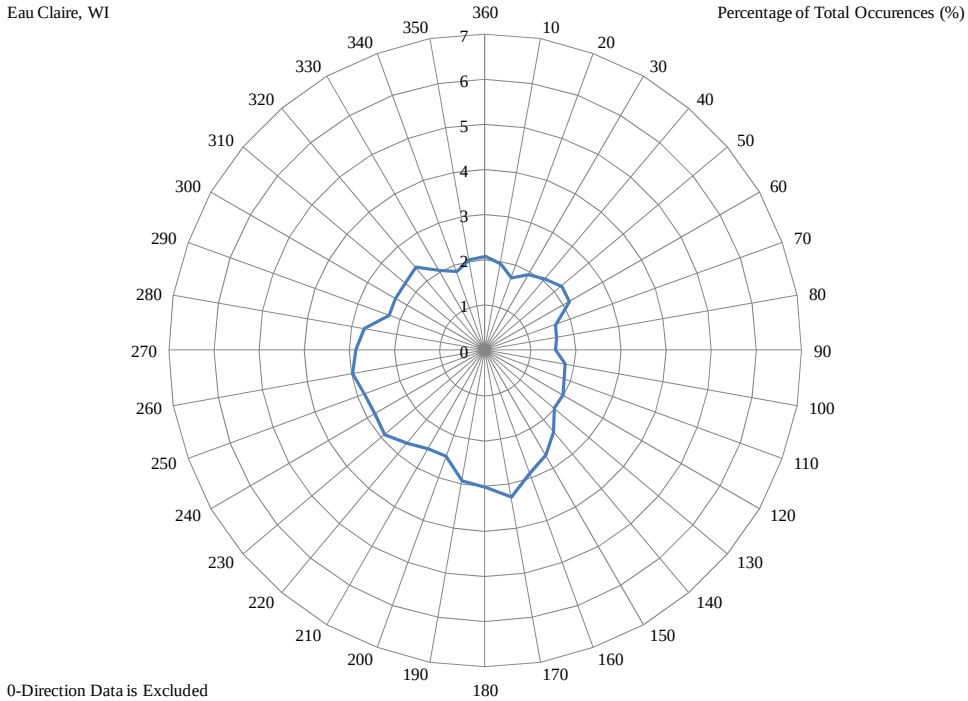

Figure M.2. Probability Mass Functions for Wind Direction Irrespective of Speed for Eau Claire, WI for Period January 1998 through December 2007.

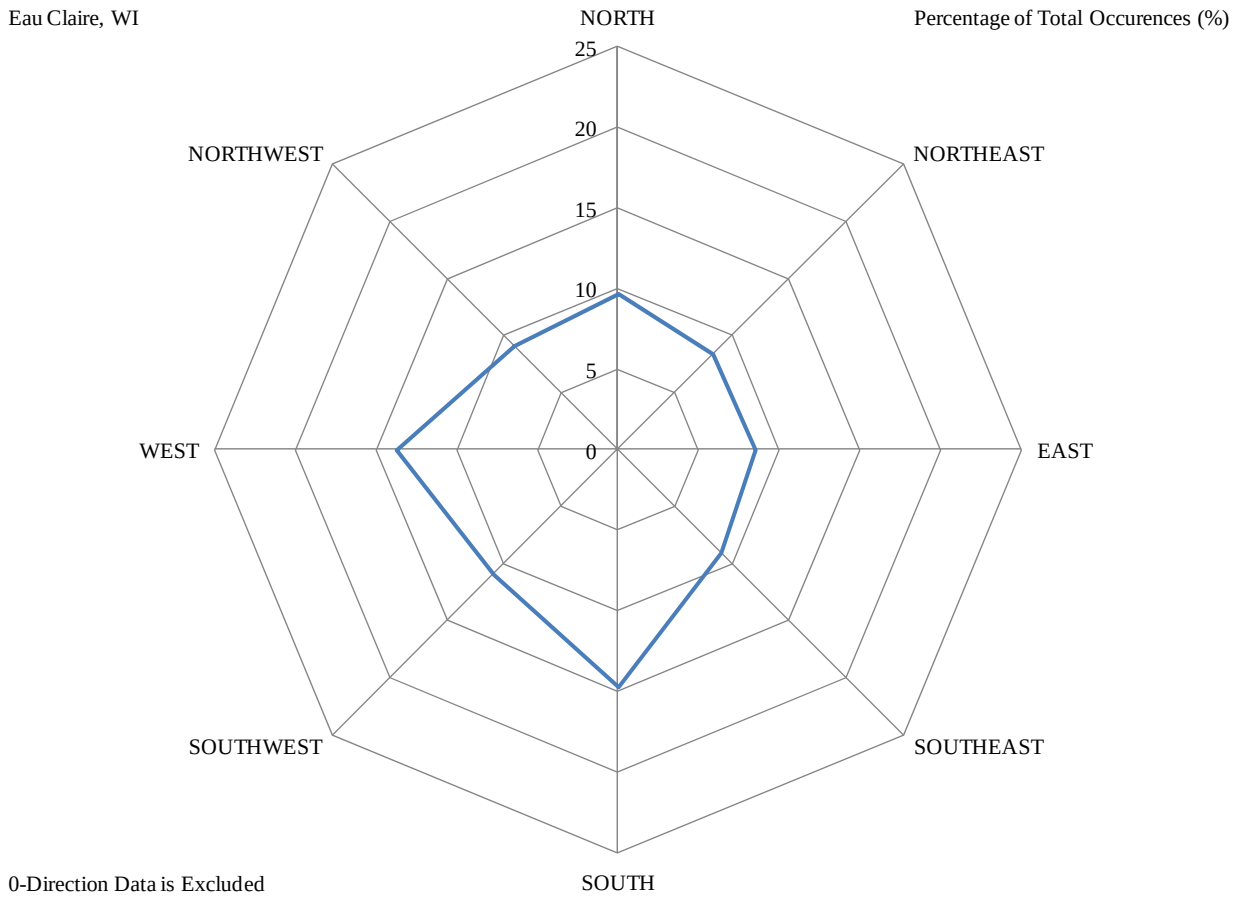

Figure M.3. Probability Mass Functions for Wind Direction Irrespective of Speed for Eau Claire, WI for Period Jan. 1998 through Dec. 2007.

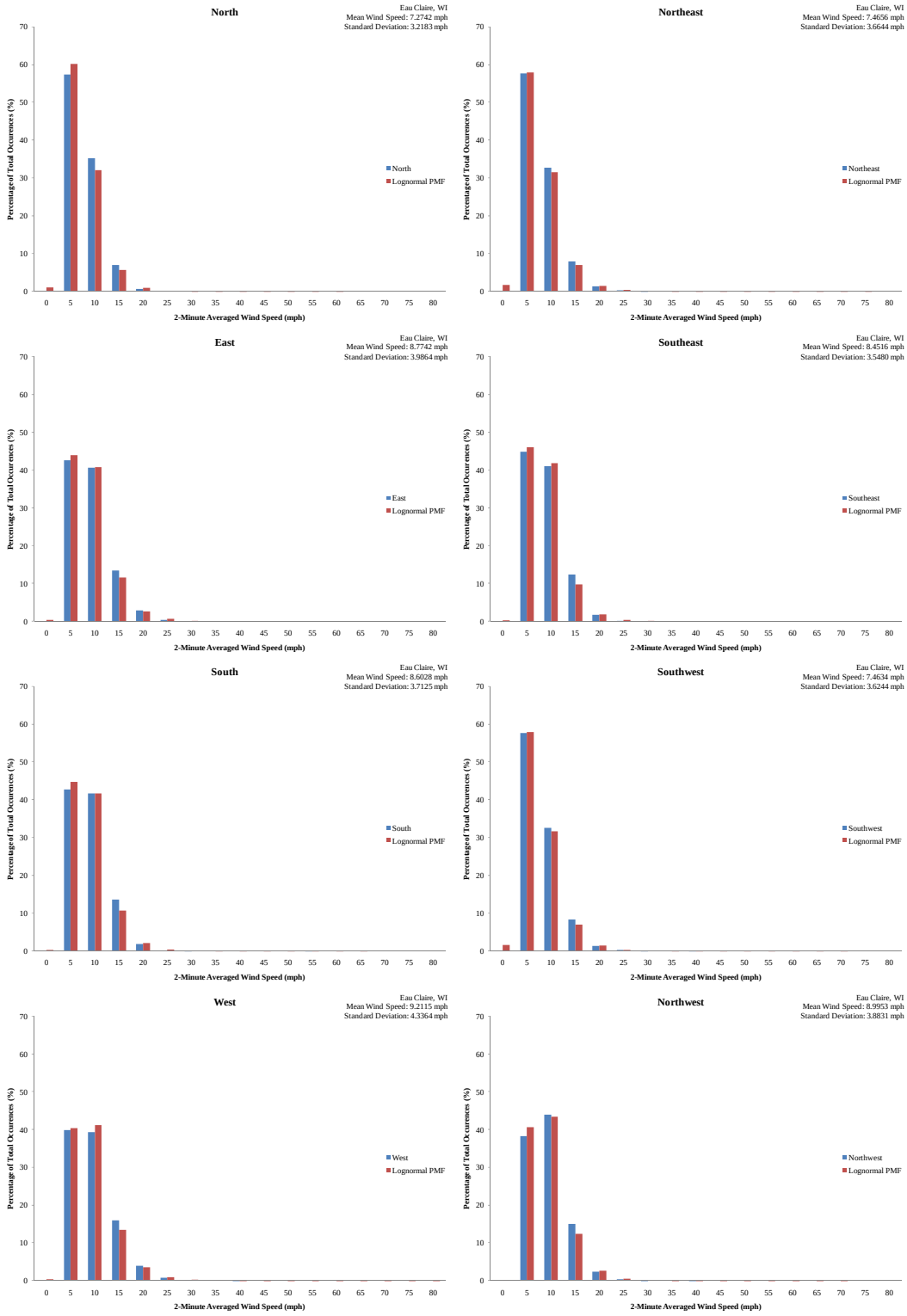

Figure M.4. Probability Mass Functions for Wind Speeds for Specific Directions for Eau Claire, WI for Period January 1998 through December 2007.

Table M.1. Combined Probabilities, $P\left[Speed \cap Direction\right]$, for Eau Claire, WI for Period January 1998 through December 2007.

		Wind Direction									
		N/A	**North**	**Northeast**	**East**	**Southeast**	**South**	**Southwest**	**West**	**Northwest**	**SUM**
2-Minute Averaged Wind Speed (mph)	0	0.15946	0.00000	0.00000	0.00000	0.00001	0.00000	0.00000	0.00000	0.00000	0.15947
	5	0.00000	0.05529	0.04813	0.03617	0.04062	0.06288	0.06306	0.05464	0.03471	0.39551
	10	0.00000	0.03392	0.02736	0.03451	0.03718	0.06136	0.03564	0.05407	0.03985	0.32389
	15	0.00000	0.00662	0.00665	0.01146	0.01125	0.02000	0.00914	0.02201	0.01358	0.10071
	20	0.00000	0.00052	0.00118	0.00249	0.00153	0.00271	0.00139	0.00546	0.00214	0.01742
	25	0.00000	0.00007	0.00021	0.00038	0.00009	0.00023	0.00024	0.00105	0.00035	0.00261
	30	0.00000	0.00000	0.00003	0.00003	0.00000	0.00006	0.00003	0.00015	0.00004	0.00034
	35	0.00000	0.00000	0.00000	0.00000	0.00000	0.00000	0.00000	0.00000	0.00000	0.00000
	40	0.00000	0.00000	0.00000	0.00000	0.00000	0.00000	0.00001	0.00002	0.00001	0.00004
	45	0.00000	0.00000	0.00000	0.00000	0.00000	0.00000	0.00000	0.00000	0.00000	0.00000
	50	0.00000	0.00000	0.00000	0.00000	0.00000	0.00000	0.00000	0.00000	0.00000	0.00000
	55	0.00000	0.00000	0.00000	0.00000	0.00000	0.00001	0.00000	0.00000	0.00000	0.00001
	60	0.00000	0.00000	0.00000	0.00000	0.00000	0.00000	0.00000	0.00000	0.00000	0.00000
	65	0.00000	0.00000	0.00000	0.00000	0.00000	0.00000	0.00000	0.00000	0.00000	0.00000
	70	0.00000	0.00000	0.00000	0.00000	0.00000	0.00000	0.00000	0.00000	0.00000	0.00000
	75	0.00000	0.00000	0.00000	0.00000	0.00000	0.00000	0.00000	0.00000	0.00000	0.00000
	80	0.00000	0.00000	0.00000	0.00000	0.00000	0.00000	0.00000	0.00000	0.00000	0.00000
	SUM	0.15946	0.09641	0.08356	0.08505	0.09068	0.14725	0.10951	0.13740	0.09069	1.00000

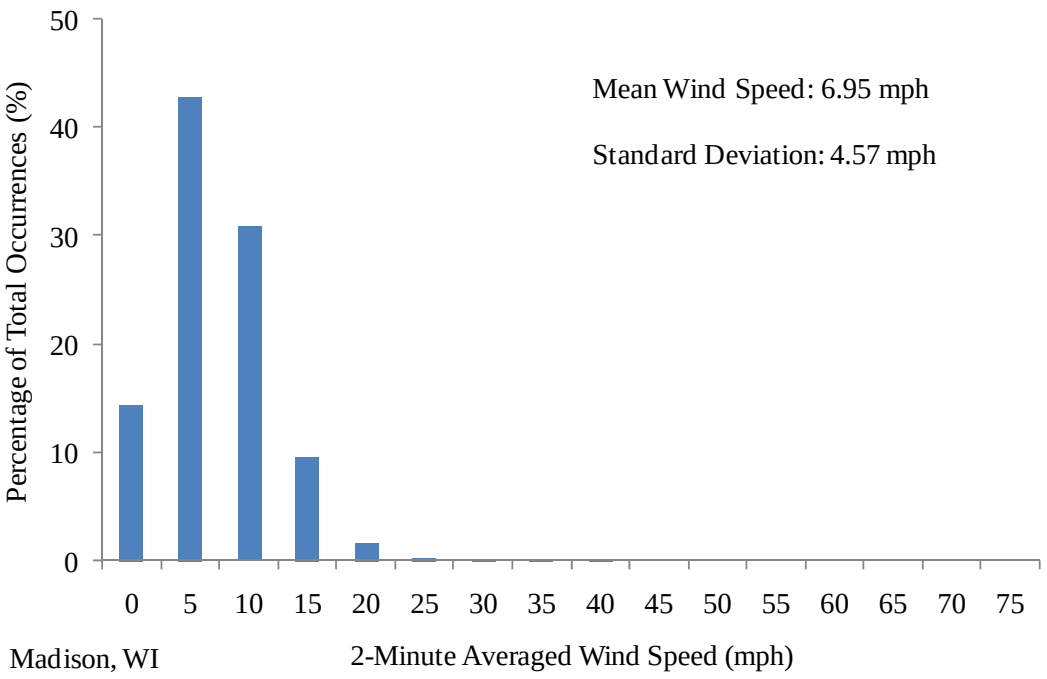

Figure N.1. Probability Mass Function for Wind Speed Irrespective of Direction for Madison, Wisconsin for Period January 1998 through December 2007.

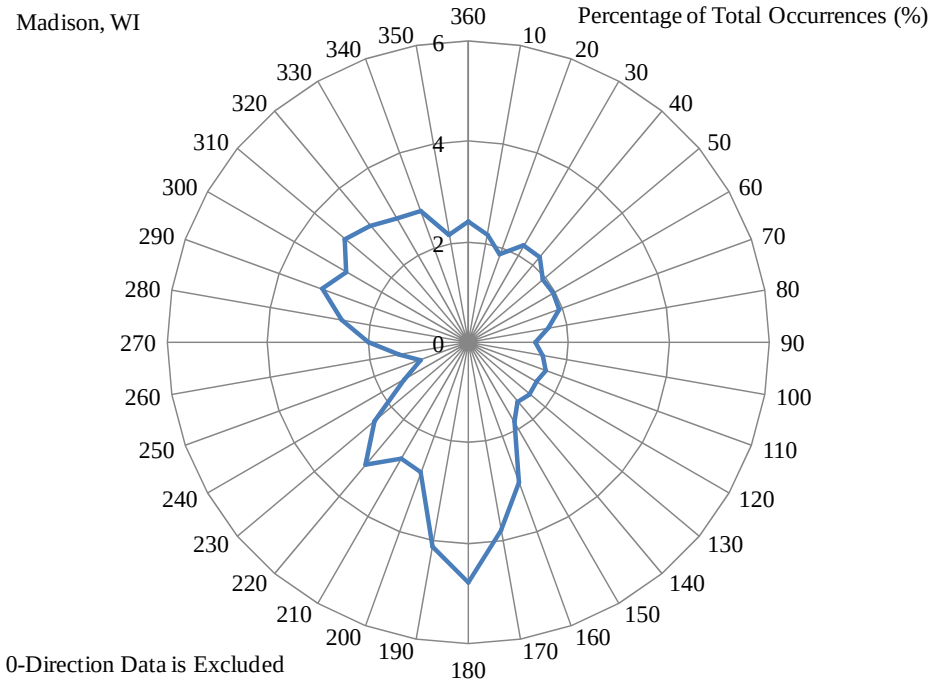

Figure N.2. Probability Mass Function for Wind Direction Irrespective of Speed for Madison, Wisconsin for Period January 1998 through December 2007.

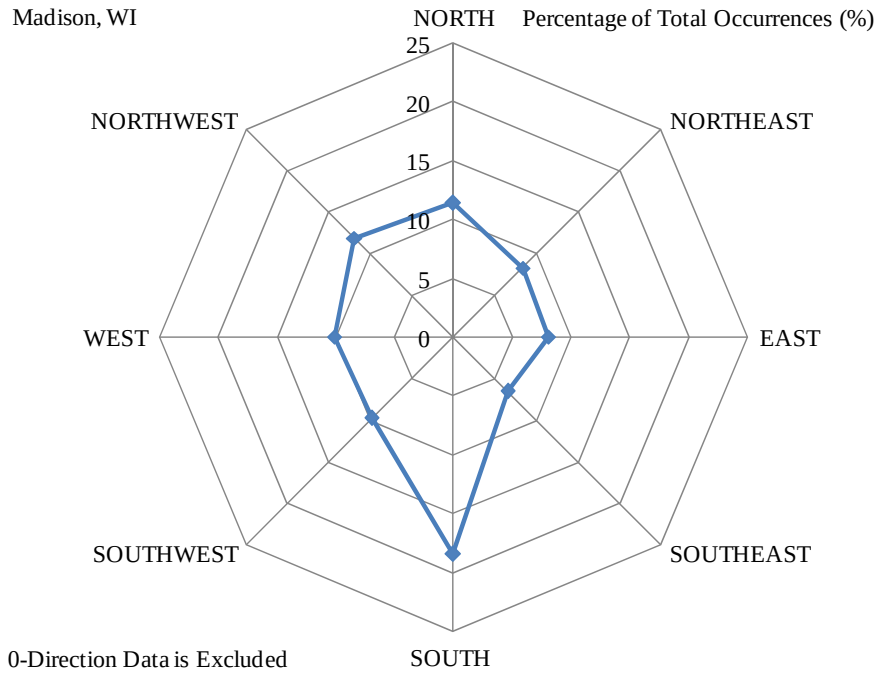

Figure N.3. Probability Mass Function for Wind Direction Irrespective of Speed for Madison, Wisconsin for Period January 1998 through December 2007.

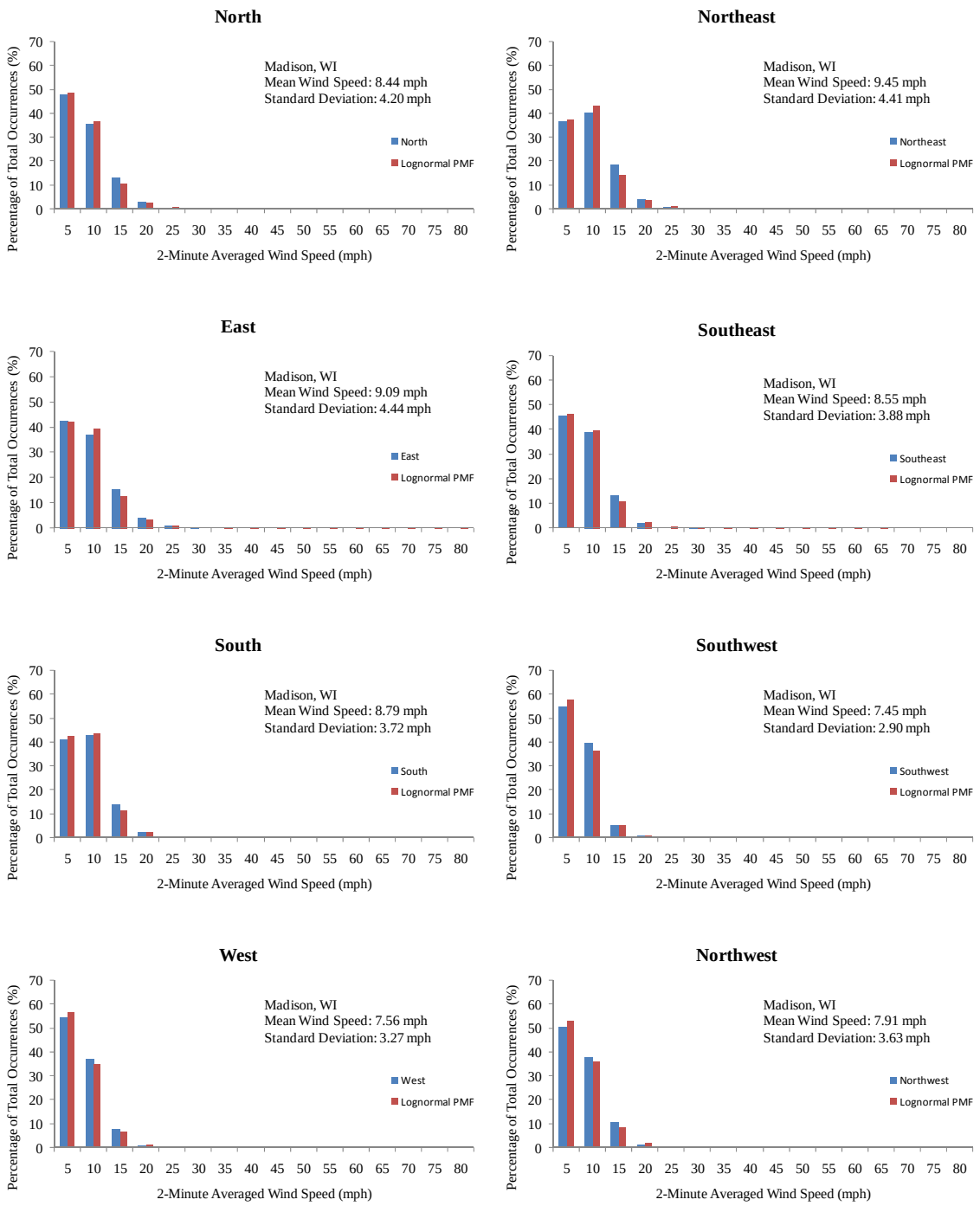

Figure N.4. Probability Mass Functions for Wind Speeds for Specific Directions for Madison, Wisconsin for Period January 1998 through December 2007.

Table N.1. Combined Probabilities, $P[Speed \cap Direction]$, for Madison, Wisconsin for Period January 1998 through December 2007.

2-Minute Averaged Wind Speed (mph)	Wind Direction									
	0	North	Northeast	East	Southeast	South	Southwest	West	Northwest	SUM
0 mph	0.15402	0.00000	0.00000	0.00000	0.00000	0.00000	0.00000	0.00000	0.00000	0.15402
5 mph	0.00000	0.05465	0.03054	0.03430	0.02971	0.07540	0.05361	0.05516	0.05993	0.39329
10 mph	0.00000	0.04033	0.03340	0.02972	0.02555	0.07921	0.03859	0.03741	0.04477	0.32898
15 mph	0.00000	0.01508	0.01538	0.01238	0.00848	0.02588	0.00485	0.00768	0.01271	0.10244
20 mph	0.00000	0.00347	0.00341	0.00319	0.00146	0.00377	0.00060	0.00075	0.00142	0.01806
25 mph	0.00000	0.00052	0.00046	0.00087	0.00025	0.00050	0.00009	0.00008	0.00012	0.00289
30 mph	0.00000	0.00004	0.00004	0.00008	0.00001	0.00004	0.00000	0.00002	0.00004	0.00027
35 mph	0.00000	0.00001	0.00001	0.00000	0.00000	0.00000	0.00000	0.00000	0.00002	0.00004
40 mph	0.00000	0.00000	0.00000	0.00000	0.00000	0.00000	0.00000	0.00000	0.00001	0.00001
45 mph	0.00000	0.00000	0.00000	0.00000	0.00000	0.00000	0.00000	0.00000	0.00000	0.00000
50 mph	0.00000	0.00000	0.00000	0.00000	0.00000	0.00000	0.00000	0.00000	0.00000	0.00000
55 mph	0.00000	0.00000	0.00000	0.00000	0.00000	0.00000	0.00000	0.00000	0.00000	0.00000
60 mph	0.00000	0.00000	0.00000	0.00000	0.00000	0.00000	0.00000	0.00000	0.00000	0.00000
65 mph	0.00000	0.00000	0.00000	0.00000	0.00000	0.00000	0.00000	0.00000	0.00000	0.00000
70 mph	0.00000	0.00000	0.00000	0.00000	0.00000	0.00000	0.00000	0.00000	0.00000	0.00000
75 mph	0.00000	0.00000	0.00000	0.00000	0.00000	0.00000	0.00000	0.00000	0.00000	0.00000
80 mph	0.00000	0.00000	0.00000	0.00000	0.00000	0.00000	0.00000	0.00000	0.00000	0.00000
SUM	0.15402	0.11409	0.08324	0.08055	0.06546	0.18480	0.09773	0.10109	0.11903	1.00000

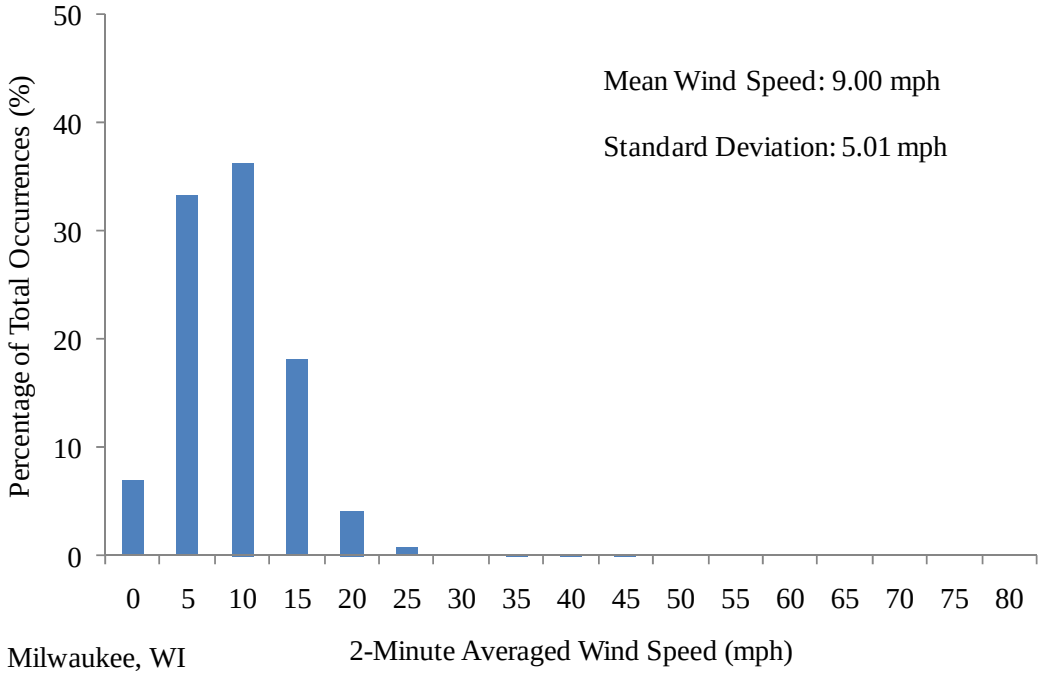

Figure O.1. Probability Mass Function for Wind Speed Irrespective of Direction for Milwaukee, Wisconsin for Period January 1998 through December 2007.

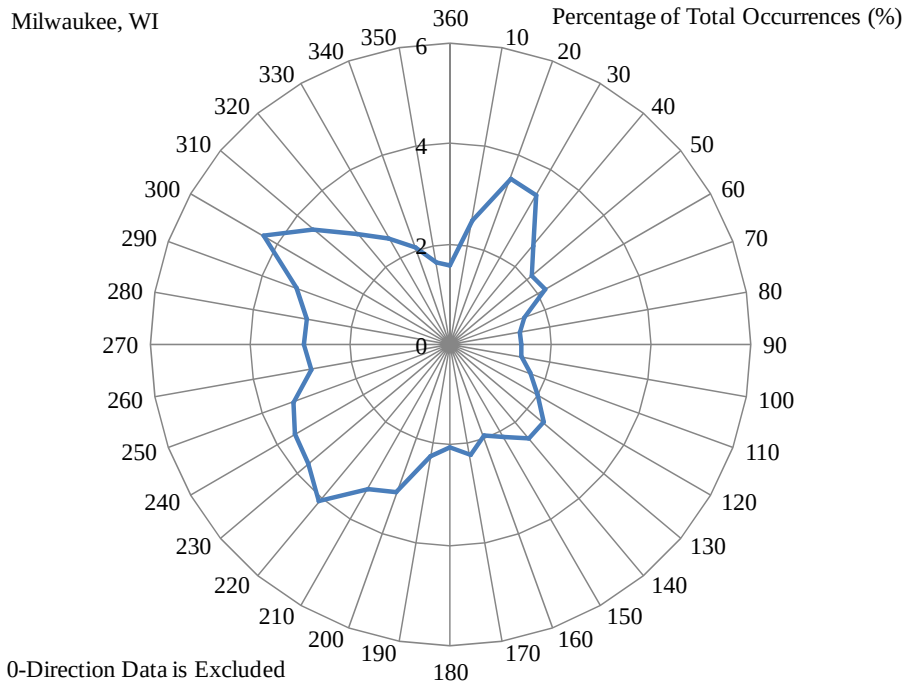

Figure O.2. Probability Mass Functions for Wind Direction Irrespective of Speed for Milwaukee, Wisconsin for Period January 1998 through December 2007.

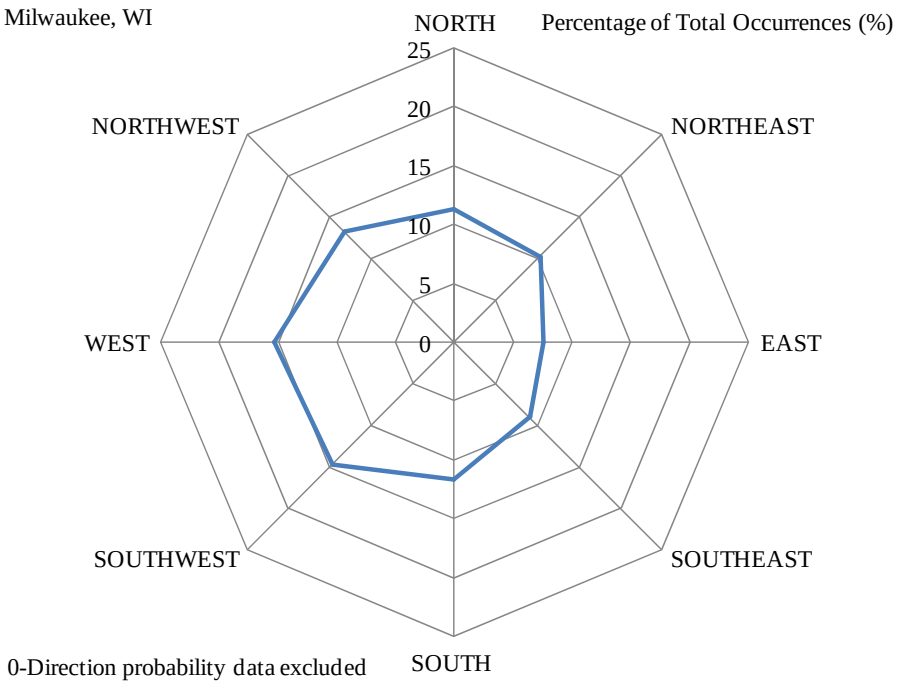

Figure O.3. Probability Mass Functions for Wind Direction Irrespective of Speed for Milwaukee, Wisconsin for Period January 1998 through December 2007.

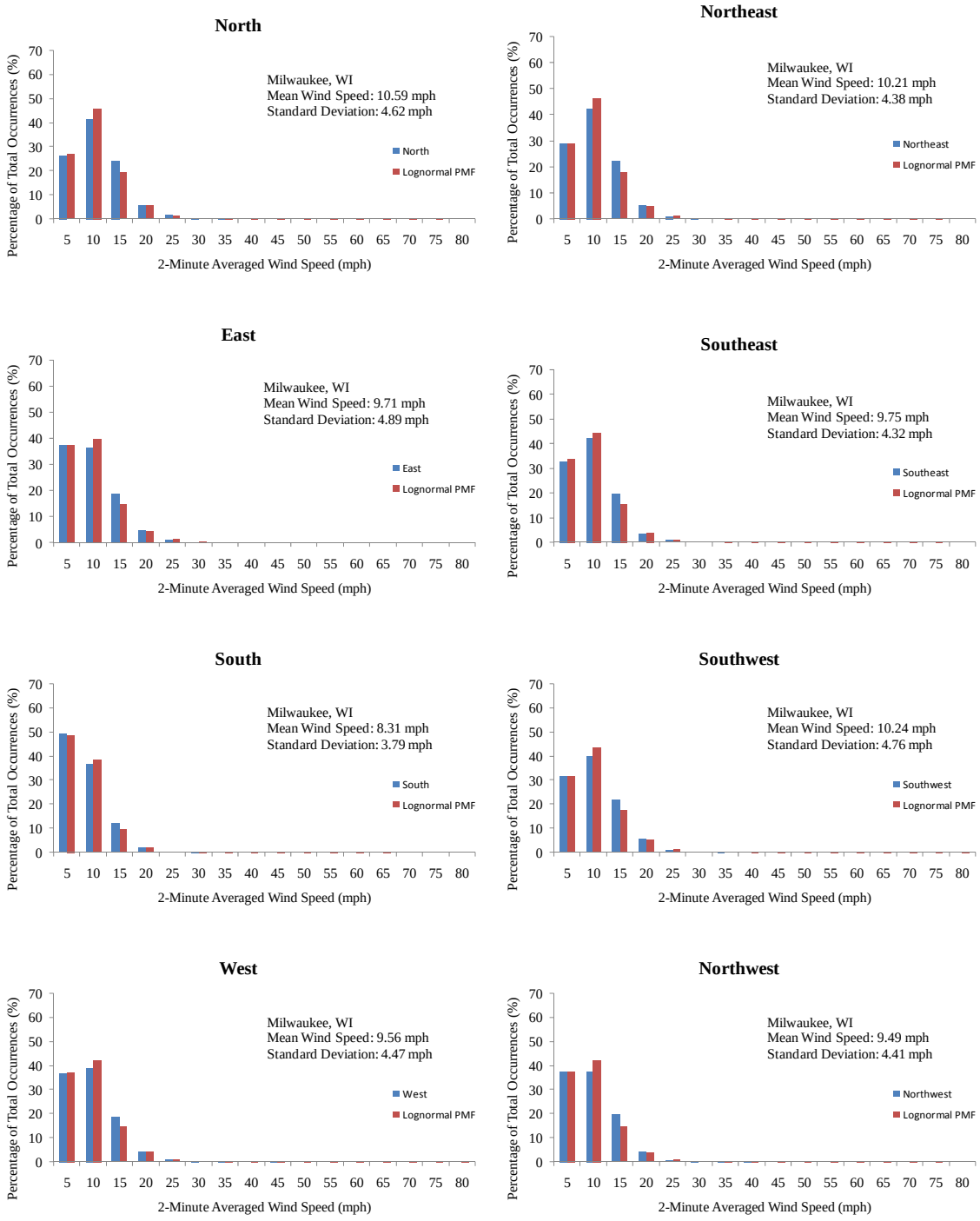

Figure O.4. Probability Mass Functions for Wind Speeds for Specific Directions for Milwaukee, Wisconsin for Period January 1998 through December 2007.

Table O.1. Combined Probabilities, $P[Speed \cap Direction]$, for Milwaukee, Wisconsin for Period January 1998 through December 2007.

		Wind Direction									
		0	North	Northeast	East	Southeast	South	Southwest	West	Northwest	SUM
2-Minute Averaged Wind Speed (mph)	0 mph	0.07077	0.00000	0.00000	0.00000	0.00000	0.00000	0.00000	0.00000	0.00000	0.07077
	5 mph	0.00000	0.02984	0.03008	0.02825	0.02971	0.05679	0.04610	0.05640	0.04995	0.32711
	10 mph	0.00000	0.04698	0.04363	0.02738	0.03821	0.04256	0.05817	0.05981	0.04996	0.36670
	15 mph	0.00000	0.02758	0.02299	0.01424	0.01791	0.01421	0.03177	0.02816	0.02600	0.18285
	20 mph	0.00000	0.00650	0.00538	0.00378	0.00328	0.00232	0.00844	0.00659	0.00549	0.04179
	25 mph	0.00000	0.00180	0.00103	0.00093	0.00078	0.00032	0.00168	0.00150	0.00085	0.00890
	30 mph	0.00000	0.00013	0.00007	0.00034	0.00015	0.00006	0.00052	0.00021	0.00015	0.00162
	35 mph	0.00000	0.00001	0.00000	0.00009	0.00000	0.00000	0.00012	0.00002	0.00001	0.00024
	40 mph	0.00000	0.00000	0.00000	0.00001	0.00000	0.00000	0.00000	0.00000	0.00001	0.00002
	45 mph	0.00000	0.00000	0.00000	0.00000	0.00000	0.00000	0.00000	0.00001	0.00000	0.00001
	50 mph	0.00000	0.00000	0.00000	0.00000	0.00000	0.00000	0.00000	0.00000	0.00000	0.00000
	55 mph	0.00000	0.00000	0.00000	0.00000	0.00000	0.00000	0.00000	0.00000	0.00000	0.00000
	60 mph	0.00000	0.00000	0.00000	0.00000	0.00000	0.00000	0.00000	0.00000	0.00000	0.00000
	65 mph	0.00000	0.00000	0.00000	0.00000	0.00000	0.00000	0.00000	0.00000	0.00000	0.00000
	70 mph	0.00000	0.00000	0.00000	0.00000	0.00000	0.00000	0.00000	0.00000	0.00000	0.00000
	75 mph	0.00000	0.00000	0.00000	0.00000	0.00000	0.00000	0.00000	0.00000	0.00000	0.00000
	80 mph	0.00000	0.00000	0.00000	0.00000	0.00000	0.00000	0.00000	0.00000	0.00000	0.00000
	SUM	0.07077	0.11284	0.10317	0.07501	0.09003	0.11627	0.14680	0.15270	0.13241	1.00000

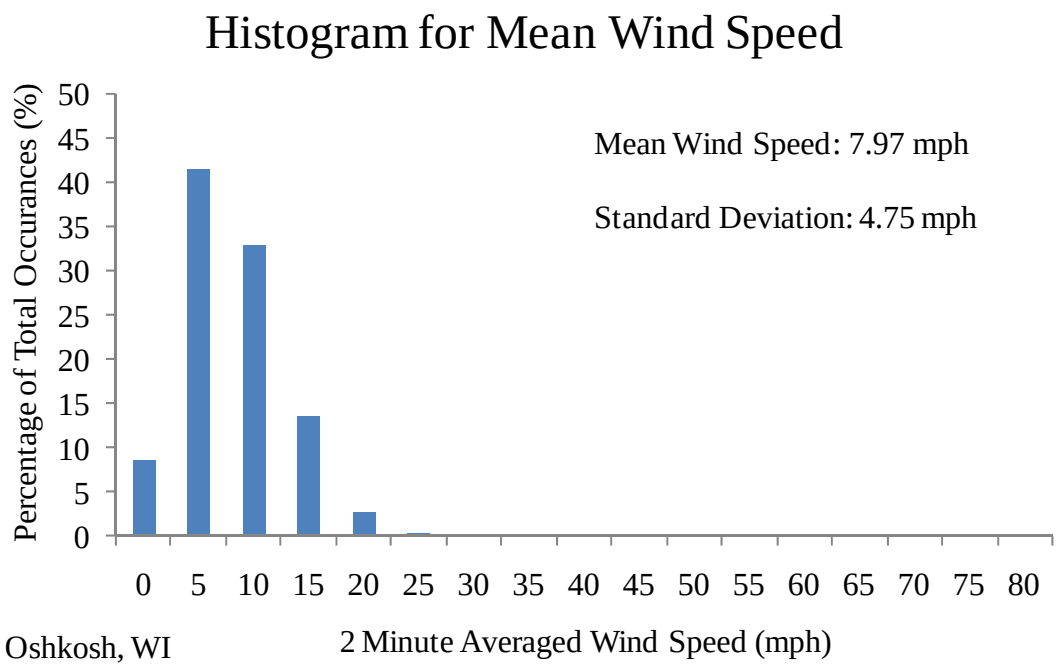

Figure P.1. Probability Mass Function for Wind Speed Irrespective of Direction for Oshkosh, Wisconsin for Period January 1998 through December 2007.

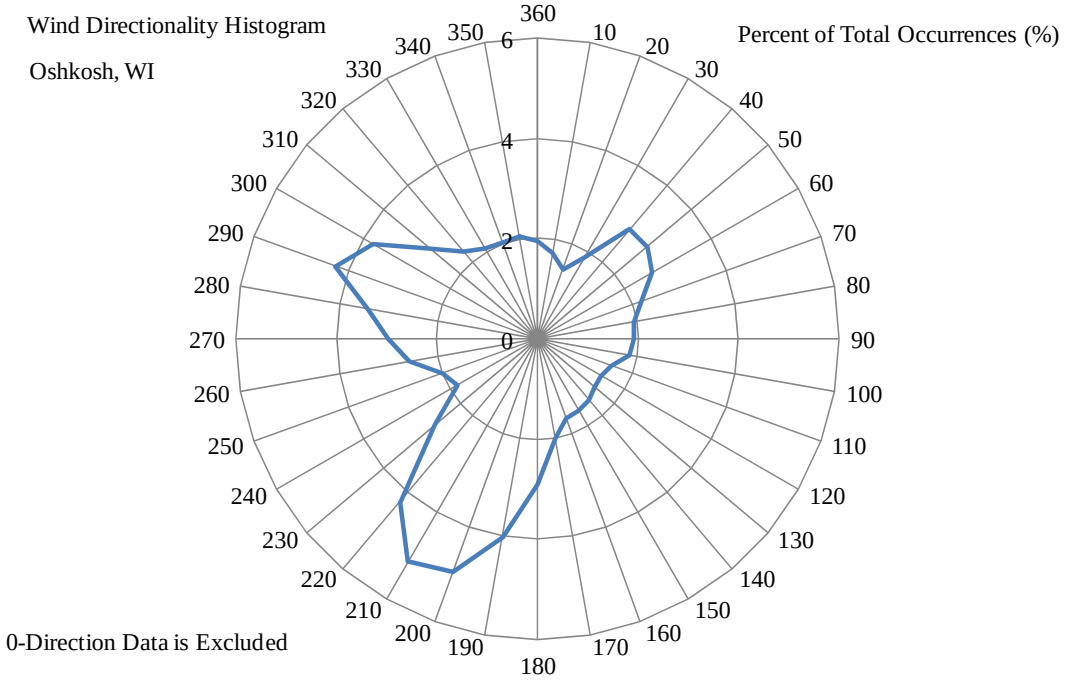

Figure P.2. Probability Mass Functions for Wind Direction Irrespective of Speed for Oshkosh, Wisconsin for January 1998 through December 2007.

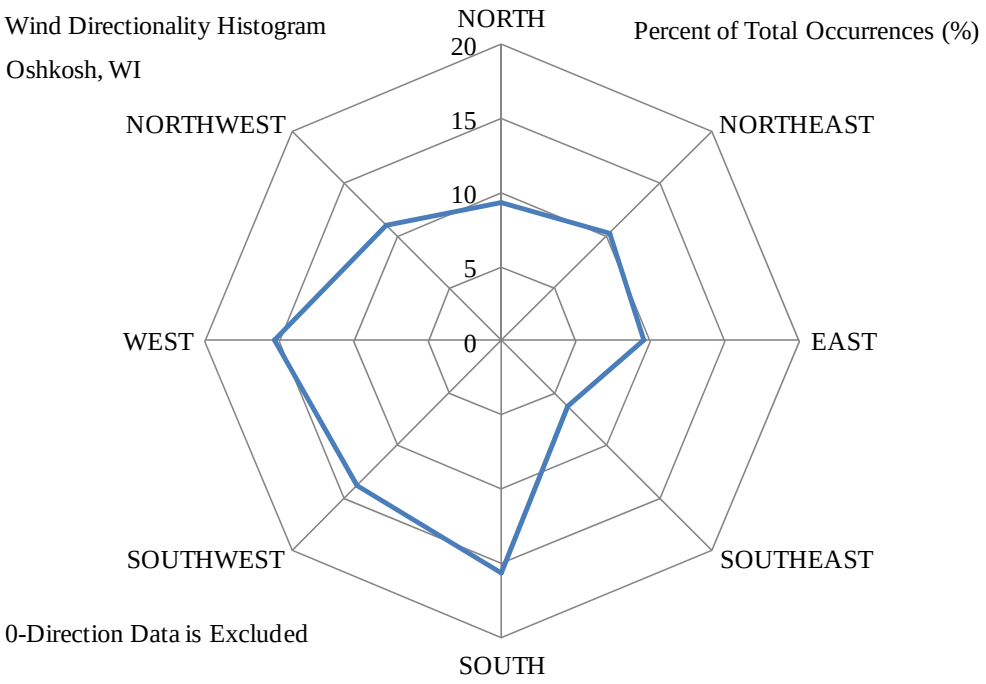

Figure P.3. Probability Mass Functions for Wind Direction Irrespective of Speed for Oshkosh, Wisconsin for January 1998 through December 2007.

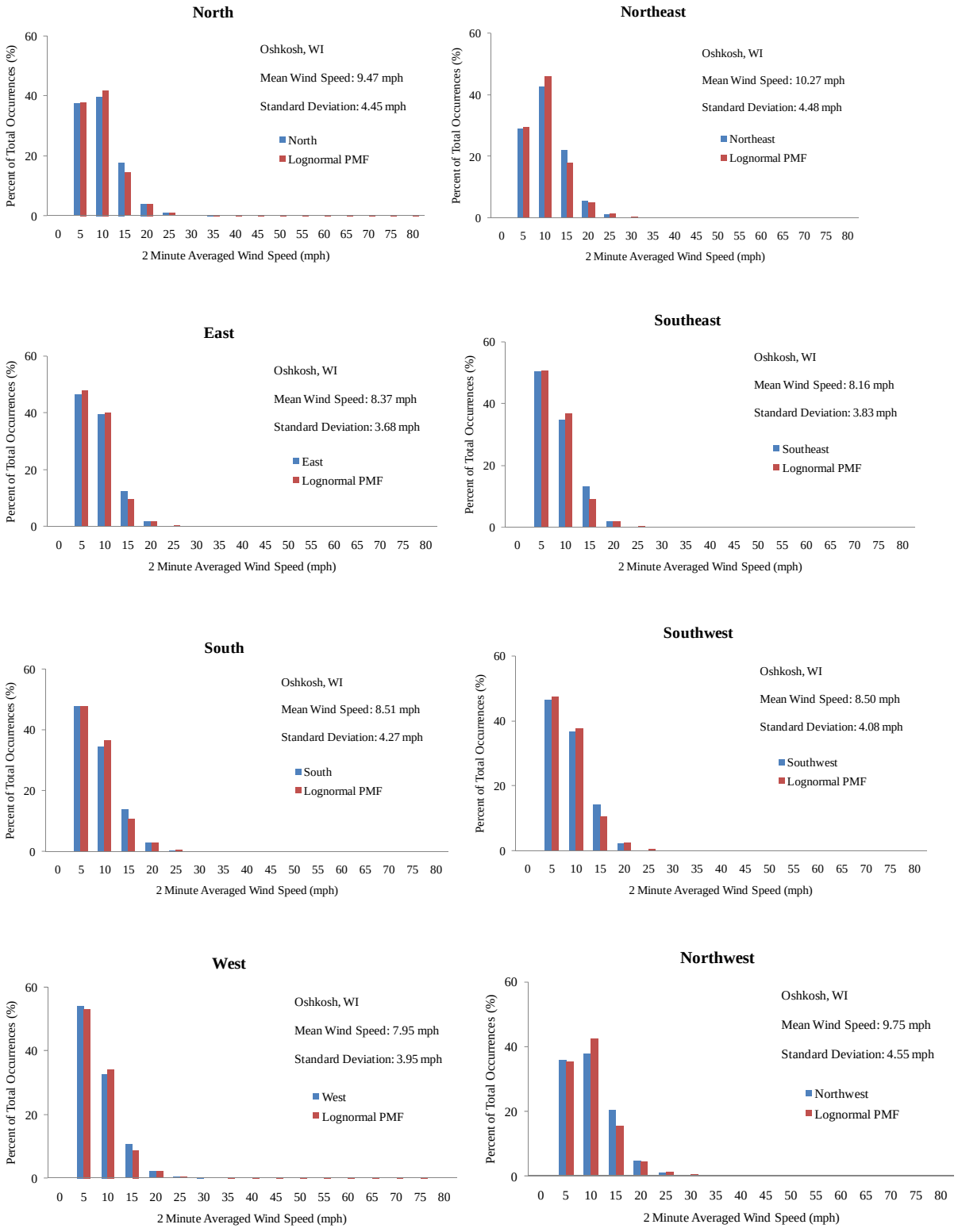

Figure P.4. Probability Mass Functions for Wind Speeds for Specific Directions for Oshkosh, Wisconsin for January 1998 through December 2007.

Table P.1. Combined Probabilities, $P\left[Speed \cap Direction\right]$, for Oshkosh, Wisconsin for Period January 1998 through December 2007.

		Wind Direction									
		0	**North**	**Northeast**	**East**	**Southeast**	**South**	**Southwest**	**West**	**Northwest**	**SUM**
2 Minute Averaged Wind Speed (mph)	**0**	0.08793	0.00000	0.00000	0.00000	0.00000	0.00000	0.00000	0.00000	0.00000	**0.08793**
	5	0	0.03490	0.02978	0.04416	0.03111	0.07487	0.06452	0.08273	0.03974	**0.40182**
	10	0	0.03704	0.04361	0.03749	0.02148	0.05412	0.05093	0.04993	0.04184	**0.33644**
	15	0	0.01661	0.02260	0.01175	0.00807	0.02180	0.01967	0.01614	0.02239	**0.13903**
	20	0	0.00383	0.00568	0.00179	0.00112	0.00445	0.00322	0.00333	0.00517	**0.02857**
	25	0	0.00092	0.00117	0.00017	0.00007	0.00082	0.00042	0.00073	0.00106	**0.00537**
	30	0	0.00014	0.00010	0	0.00002	0.00018	0.00011	0.00006	0.00014	**0.00074**
	35	0	0.00002	0	0	0	0.00002	0.00003	0	0.00001	**0.00007**
	40	0	0	0	0	0	0	0	0	0.00001	**0.00001**
	45	0	0	0	0	0	0	0.00001	0	0.00001	**0.00002**
	50	0	0	0	0	0	0	0	0	0	**0**
	55	0	0	0	0	0	0	0	0	0	**0**
	60	0	0	0	0	0	0	0	0	0	**0**
	65	0	0	0	0	0	0	0	0	0	**0**
	70	0	0	0	0	0	0	0	0	0	**0**
	75	0	0	0	0	0	0	0	0	0	**0**
	80	0	0	0	0	0	0	0	0	0	**0**
	SUM	**0.08793**	**0.09345**	**0.10294**	**0.09535**	**0.06187**	**0.15626**	**0.13890**	**0.15292**	**0.11037**	**1**

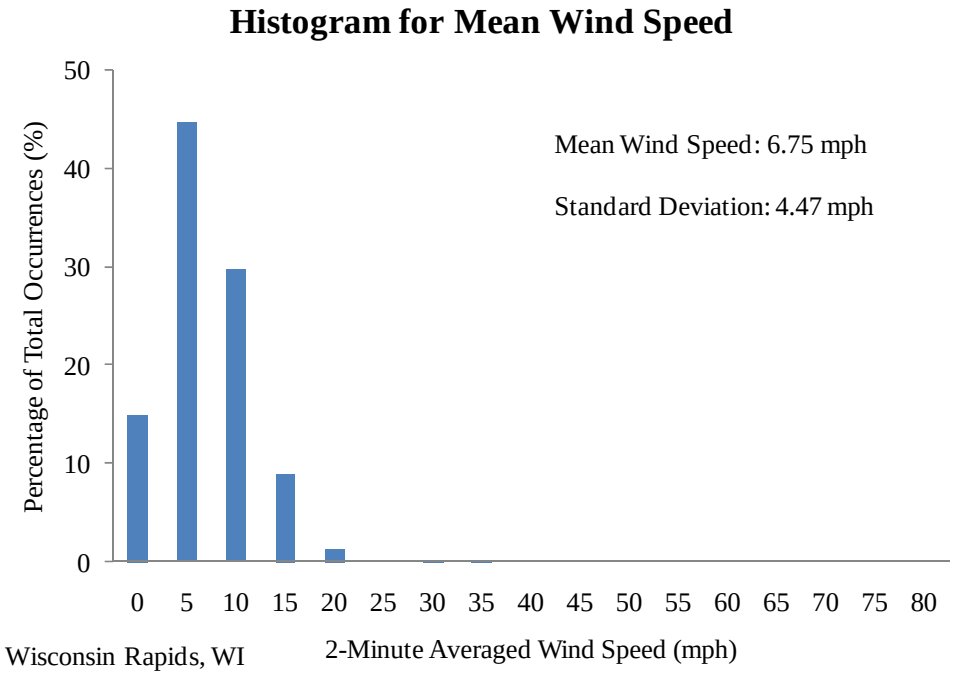

Figure Q.1. Probability Mass Function for Wind Speed Irrespective of Direction for Wisconsin Rapids, Wisconsin for Period January 1998 through December 2007.

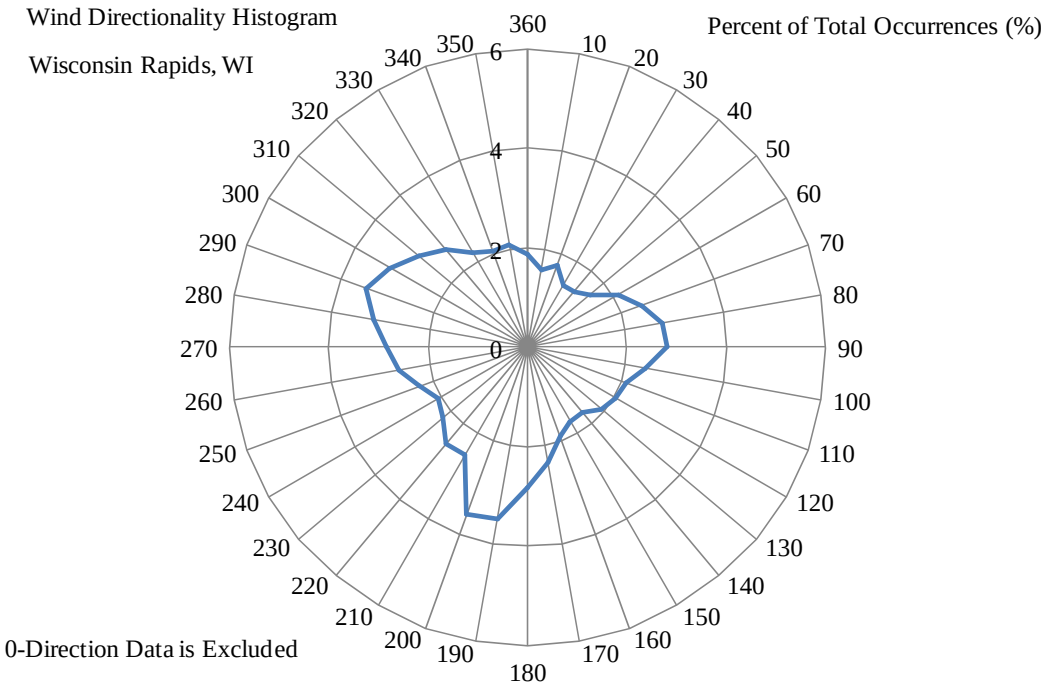

Figure Q.2. Probability Mass Functions for Wind Direction Irrespective of Speed for Wisconsin Rapids, Wisconsin for January 1998 through December 2007.

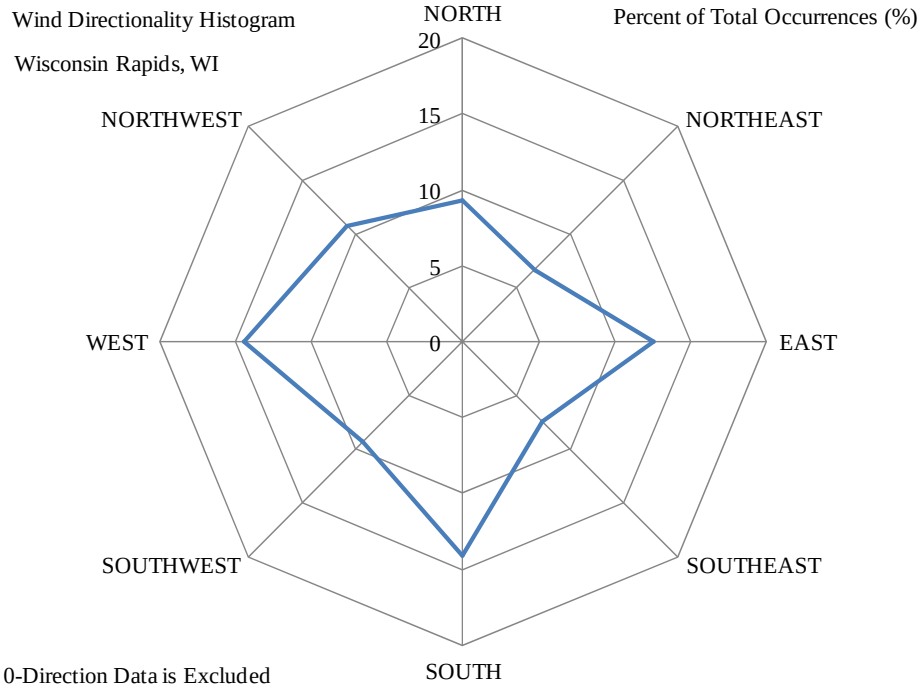

Figure Q.3. Probability Mass Functions for Wind Direction Irrespective of Speed for Wisconsin Rapids, Wisconsin for January 1998 through December 2007.

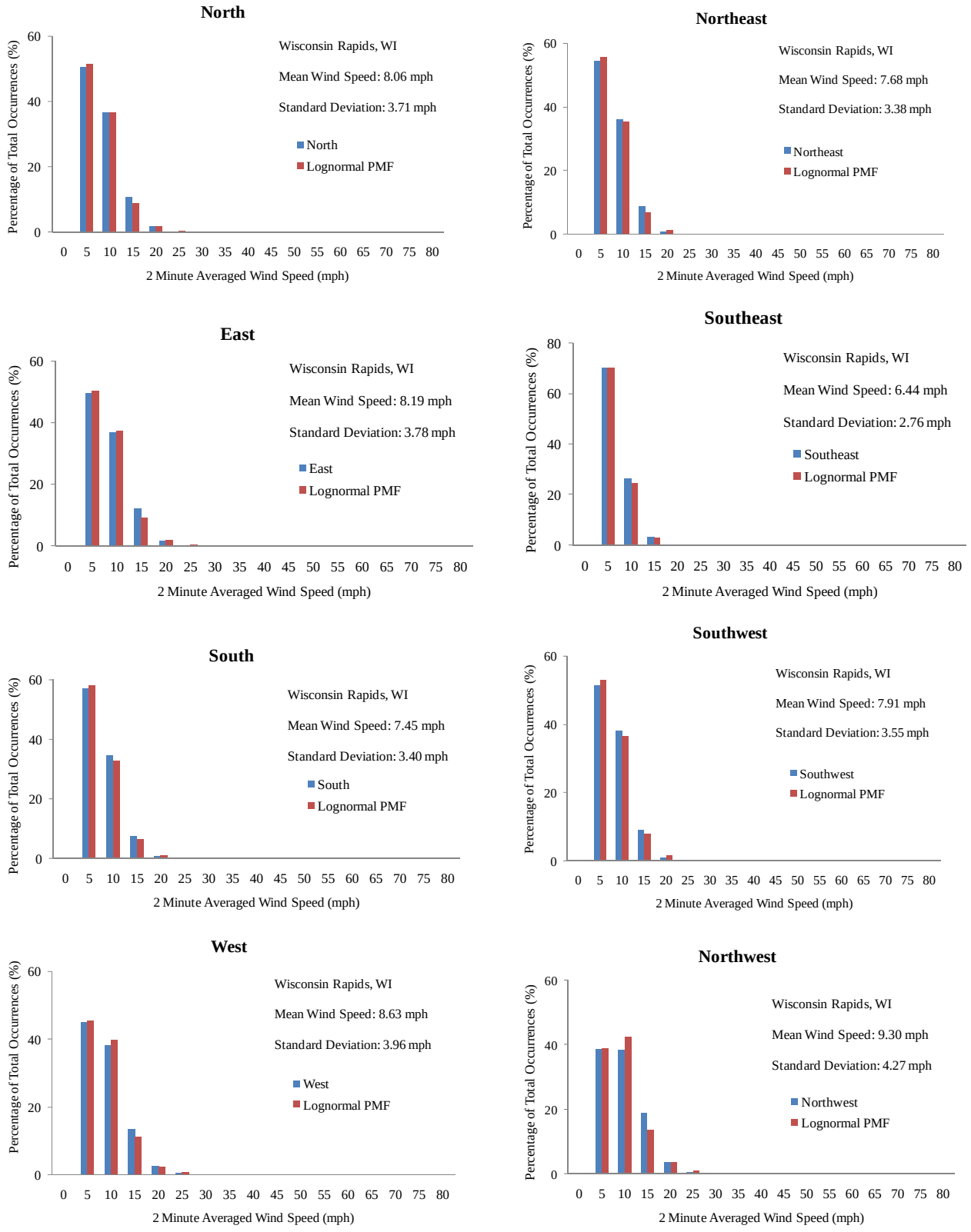

Figure Q.4. Probability Mass Functions for Wind Speeds for Specific Directions for Wisconsin Rapids, Wisconsin for January 1998 through December 2007.

Table Q.1. Combined Probabilities, $P\left[Speed \cap Direction\right]$, for Wisconsin Rapids, Wisconsin for Period January 1998 through December 2007.

		Wind Direction									
		0	**North**	**Northeast**	**East**	**Southeast**	**South**	**Southwest**	**West**	**Northwest**	**SUM**
2 Minute Mean Wind Speed (mph)	**0**	0.15326	0	0	0	0	0	0	0	0	**0.15326**
	5	0	0.04733	0.03612	0.06197	0.05200	0.08064	0.04782	0.06501	0.04186	**0.43274**
	10	0	0.03426	0.02397	0.04596	0.01948	0.04877	0.03549	0.05512	0.04163	**0.30469**
	15	0	0.01010	0.00588	0.01505	0.00261	0.01051	0.00855	0.01958	0.02039	**0.09266**
	20	0	0.00158	0.00050	0.00217	0.00015	0.00126	0.00089	0.00363	0.00382	**0.01400**
	25	0	0.00022	0.00007	0.00034	0	0.00017	0.00028	0.00060	0.00062	**0.00230**
	30	0	0.00003	0.00001	0.00001	0	0.00008	0.00010	0.00006	0.00003	**0.00031**
	35	0	0	0	0	0	0.00001	0.00001	0	0.00001	**0.00003**
	40	0	0	0	0	0	0	0	0	0	**0**
	45	0	0	0	0	0	0	0	0	0	**0**
	50	0	0	0	0	0	0	0	0	0	**0**
	55	0	0	0	0	0	0	0	0	0	**0**
	60	0	0	0	0	0	0	0	0	0	**0**
	65	0	0	0	0	0	0	0	0	0	**0**
	70	0	0	0	0	0	0	0	0	0	**0**
	75	0	0	0	0	0	0	0	0	0	**0**
	80	0	0	0	0	0	0	0	0	0	**0**
	SUM	**0.153257**	**0.0935225**	**0.0665473**	**0.1255025**	**0.0742379**	**0.1414477**	**0.0931286**	**0.1440082**	**0.1083486**	**1**